

**Pharmacological and second  
messenger-mediated modulation  
of heterologously expressed and  
neuronal calcium-dependent  
potassium currents**

Thesis submitted at UCL

by

**Timothy Howe**

for the degree of

**Doctor of Philosophy, PhD**

## DECLARATION

I, Tim Howe can confirm that the work presented in this thesis is my own. where information has been derived from other sources, I confirm that this has been indicated in the thesis.

---

## Abstract

The modulation of calcium-activated and calcium and voltage-dependent potassium channels, by drugs and second messengers, was investigated using the whole cell patch clamp technique in hippocampal slices, primary neuronal cultures, and transiently transfected HEK293 cells.

The voltage and  $\text{Ca}^{2+}$ -sensitive BK channel has emerged as a potential therapeutic target in conditions including multiple sclerosis and Fragile X syndrome.

The Selwood lab have developed a compound, VSN-16R, that can rescue functions in mouse models of these diseases, and preliminary evidence suggested VSN-16R might act as a BK channel activator.. In the first part of the project I tested VSN-16R on heterologously expressed BK channels formed from  $\alpha$ -subunit homomultimers or from coexpression of the alpha subunit with  $\beta$  subunits, and determined that VSN-16R does not act as an activator of these channels. Additionally, I characterised for the first time the effects of the BK activator NS19504 on heterologously expressed channels incorporating beta subunits, and assessed the effects of VSN-16R in the presence of intracellular reducing agents glutathione and dithiothreitol, and under conditions of oxidative stress produced by extracellular application of  $\text{H}_2\text{O}_2$ .

In the second part of my thesis I aimed to discover the location of discrete subcellular signalling domains involved in the regulation of the slow afterhyperpolarising current ( $sI_{\text{AHP}}$ ) in hippocampal pyramidal neurons by monoaminergic transmitters. Various monoamines, including noradrenaline, converge on a pathway involving the activation of PKA by elevated cAMP levels, which leads to the inhibition of the  $sI_{\text{AHP}}$  by an unknown mechanism. The results of my experiments provide evidence of subcellular spatial variation in the degree of  $sI_{\text{AHP}}$  inhibition in response to focal application of the  $\beta$ -adrenergic agonist isoproterenol, and to localised uncaging of cAMP on the inhibition of the  $sI_{\text{AHP}}$ .

## Acknowledgements

I am deeply indebted to Professor Paola Pedarzani, for her near-decade of support in my scientific progress: firstly during my undergraduate degree as a year tutor, and subsequently as my PhD supervisor. Throughout the time I have known her I have benefited from her guidance and suggestions, and as her PhD student I have very much enjoyed my time in her lab. I deeply value the support and encouragement I have received throughout the PhD process, which as anyone who has been through it can attest, has its ups and downs. A good supervisor can help prevent the challenging times from becoming overwhelming, and I was lucky in that respect!

I am also grateful to my second supervisor, Julie Pitcher, for her advice and assistance, and to Martin Stocker for the wealth of advice he brought to my cell culture work, for his deep knowledge of molecular biology, and for our wide ranging discussions on a variety of topics.

Thanks also to my lab colleagues, Dr. Marisol Sampedro-Castañeda, Dr. Angelo Tedoldi, Simon Bennett, Joseph Tebbs-Warner, Martina d'Antoni, Gloria Garcia Negrodo and Laura Fedele, all of whom aided me with discussions on my work, and helped make the experience fun.

I am also indebted to the two undergraduate students that helped me with my work, Francesca Greenstreet and Ruairi Roberts. You were both great students and good company!

Aside from the academic setting, I am unendingly grateful for the love and support I have received from my mother Hilary and my late father Peter. Peter was not a scientist himself, but he was a great appreciator of the importance of lifelong learning, and a great believer in the importance of science as a driver of progress in the world, and it was his hope that I would study "a good hard science subject" at university. I hope he would be pleased with my having seen this education through to its natural end point with the completion of my PhD thesis. Meanwhile Mum has been a rock of support to me throughout my years of study, and I'm hugely grateful to both of them for exposing my young mind to engaging stimuli during my childhood (when your toddler says they like dinosaurs, get them a paleontology textbook not a picturebook!).

Superlative thanks are due to my fiancée Gem, who has endured this little detour in our life plans with stoicism and patience. I look forward to repaying the favour in supporting her goals in the coming years.

Thanks also to my business partner Dan, for understanding the limits of my endurance in the face of a dual workload, and to all of my other fishing buddies: Marc, Jon, Dave W, Andy M, Peter H and the rest of the SCBI, as well as skippers Lyle Stantiford, Paul

Wells and Andrew Alsop. You have all help me get away to a better place during the stressful moments!

Finally a big thankyou to all the Shire crew and other close friends: Dave, Em, Jimbo, Felix, Lizzie, Ian, James, Rosa, Tom, De, Josh, Tiffer and Todd. It's an incredible feeling to have such close friends to help you along the way and share good times with. Who knew it wouldn't be "two years away from finishing" forever?

# Table of Contents

<b>Abstract</b> .....	<b>3</b>
<b>Acknowledgements</b> .....	<b>4</b>
<b>Chapter 1. Preface</b> .....	<b>13</b>
<b>Chapter 2. Materials and Methods</b> .....	<b>15</b>
2.1 Materials and Consumables .....	15
2.2 Methods .....	18
2.2.1 Coverslip preparation.....	18
2.2.2 Maintenance and splitting of HEK293 cells and stable cell lines .....	18
2.2.3 Preparation of acute dorsal hippocampal slices.....	19
2.2.4 Preparation and maintenance of hippocampal cultures.....	20
2.2.5 Transient transfection of HEK 293 cells .....	21
2.2.5.1 Transfection recipes.....	21
2.2.6 Voltage clamp recordings .....	22
2.2.6.1 Series resistance compensation .....	22
2.2.7 Electrophysiological recordings from transfected HEK293 cells.....	23
2.2.7.1 P/n protocol.....	24
2.2.7.2 Recordings from HEK293 cells expressing BK channel subunits .....	24
2.2.7.3 Recordings from HEK293 cells stably expressing rBK $\alpha^0$ .....	25
2.2.7.4 Recordings from HEK293 cells cotransfected with rBK $\alpha^0$ and hBK- $\beta$ 4.....	26
2.2.7.5 Recordings from HEK293 cells cotransfected with rBK $\alpha^0$ and hBK- $\beta$ 3 or BK- $\beta$ 2.....	26
2.2.7.6 Flash photolysis of DM-Nitrophen in cells stably expressing rBK $\alpha^0$ .....	27
2.2.8 Hippocampal acute slice recordings .....	27
2.2.8.1 Hippocampal slice whole cell voltage clamp protocols .....	29
2.2.9 Focal application of isoproterenol .....	32
2.2.10 Recordings from hippocampal cultures .....	33
2.2.10.1 DM-Nitrophen uncaging .....	35
2.2.11 BCMCM-8Br-cAMP uncaging .....	35
2.2.12 Analysis.....	37
2.2.13 Solutions.....	37
2.2.13.1 Cell culture media .....	37
2.2.13.2 Slice preparation media .....	39
2.2.13.3 Extracellular solutions .....	39
2.2.13.4 Intracellular solutions .....	40

## PART ONE

<b>Chapter 3. Introduction</b> .....	<b>43</b>
3.1 BK channels.....	43
3.1.1 BK channel structure: the alpha subunit .....	43
3.1.2 Functional properties of the BK $\alpha$ homotetrameric channel.....	45
3.1.3 BK Channel variants.....	46
3.1.3.1 Beta subunits .....	46
3.1.3.2 Gamma subunits.....	48
3.1.3.3 Stoichiometry of subunits .....	48
3.1.3.4 Alternative splicing .....	49
3.2 Modulation of BK channels.....	50
3.2.1 Reactive Oxygen/Nitrogen Species .....	50
3.3 BK channel pharmacology .....	51
3.3.1 Peptide blockers.....	52
3.3.2 Small molecule blockers .....	52
3.3.3 Activators.....	53
3.4 Physiological role of BK channels .....	53
3.4.1 Role of BK in neurons.....	54
3.5 Role of BK channels in pathology.....	55
3.5.1 Fragile X.....	55
3.6 VSN-16R: a putative BK channel enhancer with therapeutic possibilities .....	56
<b>Chapter 4. Results</b> .....	<b>58</b>
4.1 Expression of rBK- $\alpha^0$ channels in HEK 293 cells, and characterisation of Ca <sup>2+</sup> sensitivity .....	58
4.2 Effects of Paxilline and TEA on the BK current.....	61
4.3 Effect of NS19504 on currents mediated by the heterologously expressed rBK- $\alpha^0$ .....	64
4.4 Effect of VSN-16R on currents mediated by the heterologously expressed rBK- $\alpha^0$ .....	66
4.5 Effect of NS19504 and VSN-16R on currents mediated by heterologously expressed rBK- $\alpha^0$ + $\beta$ 4 channel complexes .....	69
4.6 Effect of intracellular NS19504 and VSN-16R on heterologously expressed rBK- $\alpha^0$ + $\beta$ 4 .....	77
4.7 Effect of NS19504 and VSN-16R on currents mediated by heterologously expressed rBK- $\alpha^0$ + $\beta$ 2 channel complexes .....	79
4.8 Effect of NS19504 and VSN-16R on currents mediated by heterologously expressed rBK- $\alpha^0$ + $\beta$ 3 channel complexes .....	87
4.9 Effect of VSN-16R on currents mediated by heterologously expressed rBK- $\alpha^0$ in the presence of intracellular reducing agents glutathione and dithiothreitol .....	93
4.10 Effect of VSN-16R on currents mediated by heterologously expressed rBK- $\alpha^0$ channels in the presence of extracellularly applied hydrogen peroxide .....	100

<b>Chapter 5. Discussion .....</b>	<b>104</b>
5.1 Whole cell recordings of currents mediated by heterologously expressed rBK $\alpha^0$ .....	104
5.2 Effect of NS19504 on currents mediated by heterologously expressed rBK $\alpha^0$ .....	106
5.3 Effect of VSN-16R on currents mediated by heterologously expressed rBK $\alpha^0$ .....	107
5.4 Effect of VSN-16R on currents mediated by heterologously expressed rBK $\alpha^0$ in combination with $\beta$ subunits.....	108
5.5 Effect of NS19504 on currents mediated by heterologously expressed rBK $\alpha^0$ in combination with $\beta$ subunits.....	110
5.6 Potential alternative mechanisms of action of VSN-16R.....	110
5.7 Conclusions .....	112
 <b>PART TWO</b>	
<b>Chapter 6. Introduction.....</b>	<b>113</b>
6.1 The Afterhyperpolarisation .....	113
6.1.1 fAHP .....	113
6.1.2 mAHP .....	114
6.1.3 sAHP .....	114
6.2 $sI_{AHP}$ channel kinetics and calcium dependence .....	115
6.3 Molecular identity of $sI_{AHP}$ .....	116
6.4 Suppression of $sI_{AHP}$ by neuromodulators.....	119
6.5 Monoaminergic Signalling Domains .....	120
6.6 Evidence for localised signalling domains contributing to monoaminergic suppression of $sI_{AHP}$ .....	121
6.7 Aims of the project .....	123
<b>Chapter 7. Results.....</b>	<b>125</b>
7.1 Optimization of $sI_{AHP}$ current recording conditions in acute hippocampal slices.....	125
7.1.1 Optimal parameters of the stimulus pulse .....	126
7.1.2 Effect of the K <sup>+</sup> channel blocker TEA on $sI_{AHP}$ amplitude.....	129
7.1.3 Pharmacological modulation of $sI_{AHP}$ amplitude .....	130
7.2 Focal application of the $\beta$ -adrenergic agonist isoproterenol in hippocampal CA1 pyramidal cells .....	136
7.3 Is there subcellular compartmentalisation of the cAMP signal? Evidence from photo-uncaging experiments .....	146
7.3.1 Uncaging of DM-Nitrophen in HEK293 cells stably expressing rBK $\alpha$ channels.....	147
7.3.2 Uncaging DM-Nitrophen in hippocampal cultured neurones\ activates a dTC-sensitive conductance.....	150
7.3.3 Localised uncaging of 8Br-cAMP in hippocampal neurons inhibits $sI_{AHP}$ .....	153

<b>Chapter 8. Discussion .....</b>	<b>165</b>
8.1 Optimisation of $sI_{AHP}$ recordings .....	165
8.1.1 Optimal Stimulus parameters.....	166
8.1.2 Effect of TEA on $sI_{AHP}$ amplitude.....	167
8.1.3 Effect of three pharmacological agents on $sI_{AHP}$ .....	169
8.2 Focal application of isoproterenol reveals intercompartmental differences in $\beta$ -adrenergic suppression of $sI_{AHP}$ .....	172
8.3 Evidence of multiple cAMP signalling domains contributing to suppression of $sI_{AHP}$ .....	175
8.3.1 Flash photolysis of DM-Nitrophen in HEK293 cells containing rBK $\alpha$ produces an increase in the BK current .....	175
8.3.2 Flash photolysis of DM-nitrophen in cultured rat hippocampal neurons elicits a current with similar pharmacology to $I_{AHP}$ .....	176
8.3.3 Spatially localised uncaging of BCMCM 8Br-cAMP reveals intercompartmental differences in $sI_{AHP}$ suppression.....	177
8.4 Conclusions .....	186
<b>References .....</b>	<b>188</b>

## List of Figures

Figure 2.0 Rat transverse hippocampal slice.....	20
Figure 2.1. Example of an action potential train from a CA1 pyramidal neuron .....	28
Figure 2.2. Series Resistance Protocol.....	29
Figure 2.3. sIAHP+Rs Protocol.....	31
Figure 2.4. Schematic of the focal application experiment .....	33
Figure 2.5. Schematic showing location and relative size of the dendritic and somatic flash regions.....	36
Figure 3.1. Cartoon of BK $\alpha$ subunit structure. Membrane spanning helices are shown as numbered red cylinders. N and C respectively represent the amino and carboxy termini of the molecule.....	45
Figure 4.1. Recordings from HEK293 cells transfected with rBK- $\alpha^0$ using different concentrations of intracellular $Ca^{2+}$ .....	60
Figure 4.2. Effect of paxilline and TEA on rBK- $\alpha^0$ in HEK293 cells.....	63
Figure 4.3. Effect of NS19504 on rBK- $\alpha^0$ - mediated currents in HEK293 cells.....	65
Figure 4.4. Effect of VSN-16R on rBK- $\alpha^0$ - mediated currents in HEK293 cells.....	67
Figure 4.5. Functional expression of BK channel complexes containing rBK- $\alpha^0$ and hBK- $\beta_4$ subunits.....	70
Figure 4.6. Effect of NS19504 on currents mediated by rBK- $\alpha^0$ + hBK- $\beta_4$ channel complexes in HEK293 cells.....	72
Figure 4.7. Effect of VSN-16R on currents mediated by rBK- $\alpha^0$ + hBK- $\beta_4$ channel complexes in HEK293 cells.....	75
Figure 4.8. Effect of intracellularly applied VSN-16R and NS19504 on rBK- $\alpha^0$ + hBK- $\beta_4$ channel-mediated currents in HEK293 cells.....	78
Figure 4.9. Effect of NS19504 on currents recorded from HEK293 cells coexpressing rBK- $\alpha^0$ + hBK- $\beta_2$ subunits .....	80
Figure 4.10. Effect of VSN-16R on currents mediated from HEK293 cells coexpressing rBK- $\alpha^0$ + hBK- $\beta_2$ subunits .....	84
Figure 4.11. Effect of NS19504 on currents mediated by rBK- $\alpha^0$ + hBK- $\beta_3$ channels in HEK293 cells.....	88
Figure 4.12. Effect of VSN-16R on currents mediated by rBK- $\alpha^0$ +hBK- $\beta_3$ channel complexes in HEK293 cells.....	91
Figure 4.13. Effect of VSN-16R on currents mediated by channels expressed in HEK293 cells expressing rBK- $\alpha^0$ channels in the presence of intracellular glutathione .....	95
Figure 4.14. Effect of VSN-16R on currents in HEK293 cells expressing rBK- $\alpha^0$ channels in the presence of intracellular dithiothreitol.....	98
Figure 4.15. Effect of hydrogen peroxide on the response to VSN-16R of currents in HEK293 cells expressing rBK- $\alpha^0$ channels .....	101

Figure 7.1. $sI_{AHP}$ properties under typical recording conditions .....	126
Figure 7.2. Effect of stimulus properties on $sI_{AHP}$ .....	128
Figure 7.3. Effect of varying TEA concentration on $sI_{AHP}$ amplitude.....	130
Figure 7.4. Effect of EBIO on $sI^{AHP}$ amplitude.....	132
Figure 7.5. Effect of EtOH on $sI_{AHP}$ properties .....	134
Figure 7.6. Effect of Bay-K 8644 on $sI_{AHP}$ amplitude .....	135
Figure 7.7. Representative example cell for control puff experiment.....	138
Figure 7.9. Representative example cell for focal application at soma .....	140
Figure 7.10. Representative example cell for focal application at distal dendrites .....	142
Figure 7.11. Effect of focal application of 20 $\mu$ M isoproterenol at different cellular locations...	145
Figure 7.12. HEK293 whole cell recordings illustrating BK-alpha channel properties and response to uncaging of DM-Nitrophen .....	149
Figure 7.13. Uncaging of DM-Nitrophen in primary culture hippocampal neurons.....	152
Figure 7.14. Effect of flash protocol on control cells (no BCMCM-8Br-cAMP) .....	155
Figure 7.15. Effect on $sI_{AHP}$ of uncaging BCMCM-8Br-cAMP in soma .....	158
Figure 7.16. Effect on $sI_{AHP}$ of uncaging BCMCM-8Br-cAMP in proximal dendrites.....	160
Figure 7.17. Summary of effects of uncaging BCMCM-8Br-cAMP in different subcellular locations .....	163

## List of Tables

Table 3.1. Summary of the effects of different mammalian $\beta$ subunits on channel properties....	47
Table 4.1. Effect of NS19504 on currents mediated by rBK- $\alpha^{\emptyset}$ .....	66
Table 4.2. 2-way repeated measures ANOVA of the effect of VSN16-R on currents mediated by rBK- $\alpha^{\emptyset}$ .....	68
Table 4.3. 2-way repeated measures ANOVA of the effect of NS19504 on currents mediated by rBK- $\alpha^{\emptyset}+\beta_4$ .....	73
Table 4.4. 2-way repeated measures ANOVA of the effect of VSN16-R on currents mediated by rBK- $\alpha^{\emptyset}+\beta_4$ .....	76
Table 4.5. 2-way repeated measures ANOVA of the effect of NS19504 on currents mediated by rBK- $\alpha^{\emptyset}+\beta_2$ . .....	82
Table 4.6. 2-way repeated measures ANOVA of the effect of VSN16-R on currents mediated by rBK- $\alpha^{\emptyset}+\beta_2$ . .....	86
Table 4.7. 2-way repeated measures ANOVA of the effect of NS19504 on currents mediated by rBK- $\alpha^{\emptyset}+\beta_3$ .....	89
Table 4.8. 2-way repeated measures ANOVA of the effect of VSN-16R on currents mediated by rBK- $\alpha^{\emptyset}+\beta_3$ .....	92
Table 4.9. 2-way repeated measures ANOVA of the effect of VSN-16R on currents mediated by rBK- $\alpha^{\emptyset}$ , in the presence of 500 $\mu$ M GSH.....	96
Table 4.10. 2-way repeated measures ANOVA of the effect of VSN-16R on currents mediated by rBK- $\alpha^{\emptyset}$ , in the presence of 500 $\mu$ M GSH.....	99
Table 4.11. 2-way repeated measures ANOVA of the effect of H <sub>2</sub> O <sub>2</sub> and H <sub>2</sub> O <sub>2</sub> + VSN-16R on currents mediated by rBK- $\alpha^{\emptyset}$ . Multiple comparisons were performed using Tukey's multiple comparisons test to control for the familywise error rate. ....	102

## Chapter 1. Preface

Calcium activated potassium channels are a large family of potassium channels that are activated by rises in cytosolic  $\text{Ca}^{2+}$  concentration, usually in response to the activation of voltage gated calcium channels. They are important players in the regulation of neuronal membrane excitability, transmitter release, and shaping of action potentials, and are also expressed in a wide range of non-neuronal tissues. Calcium activated potassium channels are the modulation target of several neurotransmitters, and are implicated in a number of disorders including multiple sclerosis, fragile X syndrome and epilepsy, and as a result are important potential targets for new drugs.

The broad aim of my PhD project was to investigate the modulation of calcium activated potassium channels by drugs and second messengers. Within this broad framework I focused on two separate projects. The first was an attempt to characterise the effect of VSN-16R, a putative activator of the large conductance voltage and calcium activated (BK) channels, on BK channel subunits heterologously expressed in HEK 293 cells.

In the second part of my project, I examined the monoaminergic inhibition of the channels responsible for the slow afterhyperpolarisation in hippocampal pyramidal cells, and attempted to determine whether this process was spatially localised into subcellular signalling domains.

### **Part One: Modulation of heterologously expressed BK channels by VSN-16R and NS19504**

The primary goal of the first part of the project was to determine whether the drug VSN-16R functioned as an activator of BK channels. VSN-16R was synthesized by Prof. David Selwood and colleagues. It is a derivative of the endogenous cannabinoid anandamide, and has been shown to have an antispastic effect in an experimental autoimmune encephalomyelitis (EAE) mouse model of multiple sclerosis (Baker, Pryce, Selwood, 2015 abstract) and to rescue cognitive deficits in behavioural studies involving mice lacking the Fragile X mental retardation protein (FMRP) (Selwood, unpublished data). Electrophysiological experiments in the EA.hy926 endothelial cell line (Bondarenko and Selwood, unpublished data) have shown that extracellular application of VSN-16R activates a current that is sensitive to paxilline, a specific inhibitor of BK channels (Knaus et al 1994).

In order to investigate whether VSN-16R acts as a direct activator of BK channels, whole cell voltage clamp experiments were performed on HEK293 cells transfected with either the BK $\alpha$  subunit, which is sufficient to form functional channels, or with a combination of the alpha subunit and one of several auxiliary  $\beta$  subunits, which when incorporated into channels alter various channel properties including toxin resistance, kinetics, and Ca<sup>2+</sup> sensitivity (Orio 2002).

In addition, I characterised for the first time the effects of an established activator of BK $\alpha$  homomultimeric channels, NS19504 (Nausch et al 2014) on channels containing  $\beta$  subunits.

Lastly I examined whether the effect of the redox state of the cell altered the effects of VSN-16R on BK channels.

## **Part Two: Evidence for spatially localised signalling domains in the monoaminergic inhibition of the $sI_{AHP}$ .**

The Ca<sup>2+</sup>-dependent K<sup>+</sup> current ( $sI_{AHP}$ ) underlying the slow afterhyperpolarisation in hippocampal CA1 pyramidal neurons is inhibited by noradrenaline and other monoamine neurotransmitters (Madison and Nicoll 1982, Benardo and Prince 1982, Andrade and Nicoll 1987, Haas and Konnerth 1983) via a pathway dependent on the activation of adenylyl cyclase by G $\alpha$ S, and subsequent activation of PKA by cAMP (Pedarzani and Storm 1993). However little is currently known about the distribution of these components on a subcellular level, and whether they are organised into spatially localised cAMP signalling domains as has been reported for other processes involving cAMP dependent activation of PKA (Xiao et al 1999).

To this end, whole cell voltage clamp experiments were performed in which the  $\beta$ -adrenergic receptor agonist isoproterenol was applied focally to either the soma or dendrites of CA1 pyramidal neurons using a microinjector pipette, to determine whether the magnitude of  $sI_{AHP}$  inhibition in response to  $\beta$ -adrenergic activation varied according to subcellular location.

A second set of voltage clamp experiments aimed to probe for discrete cAMP signalling domains, by localised photolysis of the caged cAMP analogue BCMCM 8Br-cAMP (Hagen 1998).

## Chapter 2. Materials and Methods

### 2.1 Materials and Consumables

#### Consumables

Coverslips Ø 10 mm :	Menzel-Glazer
Filters: syringe filter (0.22 µm)	Millex-Millipore
Filter paper (mm)	Whatman
Glass capillaries: borosilicate Ø 1.5 mm	
- Slice electrophysiology	Hilgenberg
- Cell culture electrophysiology	Kimble
Glass Pasteur pipettes	VWR
Microcentrifuge tubes	Sarstedt
Plastic tubes: 10 ml, 15 ml, 50 ml	Sarstedt
Screw cap tubes: 12 ml	Greiner
Serological pipettes: 5ml, 10 ml, 25ml	Sarstedt
Syringes: 1 ml, 2 ml, 50 ml	Terumo
Tissue culture flask: T25	Sarstedt
Volumetric pipette tips: 1 ml, 200 µl	Star Lab

#### Equipment

Antivibration table		TMC
Centrifuges	Mistral 1000	MSE
Digital balance:	LA120S	Sartorius
Hood for cell culture:	Biomat 2	
Incubators:	CO-170	Innova
	MCO-17AI	Sanyo
Mercury lamp	EBQ 100	LEJ
Microscopes:	Axioskop 2	Zeiss
	Axiovert 2	Zeiss
Microelectrode puller:	EPC-10	Narishige
Micromanipulators:	SM-1	Luigs & Neumann
	UL-1000i	Scientifica
Oscilloscope:	TDS 1012	Tektronix
Osmometer:	5520	Vapro
Patch Clamp amplifier:	EPC-10	HEKA
pH meter:	pH Meter776	Knick
Pressure microinjector:	Picospritzer III	General Valve Corporation

Pump:	Dymax 30	Charles Austen Pumps
Spectrophotometers:	Nanodrop 3300	Thermo Scientific
Tissue slicer:	VT 1000S	Leica
UV Flash lamp:	UV Flash II	TILL Photonics

## Chemicals

8CPT cAMP-Na	Sigma
ATP-Na	Sigma
Ampicillin	Roche
AP-V	Ascent Scientific
Bovine Serum Albumin	Sigma
Bay-K8644	Sigma
BCMCM-8Br-cAMP	Biolog
CaCl <sub>2</sub>	Fluka
DMEM-F12	Invitrogen
DM-Nitrophen	Life Technologies
DMSO	Sigma
d-Tubocurarine-Cl	Ascent Scientific
EBIO	Sigma
EDTA	IBI technical
EGTA	Sigma
Ethanol	Fisher
Ethidium Bromide (10 mg/ml)	Sigma
G418	Sigma
Glucose (Anyhdrous)	Fisher
GTP-Na	Sigma
H <sub>2</sub> O (cell culture)	Baxter
H <sub>2</sub> O (intracellular solution)	Romil
HBS (HEPES-Buffered Saline)	Sigma
HBSS	Invitrogen
HEPES	Sigma
HEPES (intracellular solution)	Fluka
Isopropanol	Fisher
Isoproterenol	Sigma
KCl	VWR
Gluconic acid (K-gluconate)	Sigma
Methylsulphuric acid (K-Methylsulphate)	ICN Biomedicals

KH <sub>2</sub> PO <sub>4</sub>	Merck
L-Glutamine	Invitrogen
Lucifer Yellow	Sigma
Luria Broth	Invitrogen
MEM	Invitrogen
MgCl <sub>2</sub>	Fluka
NaCl	VWR
NaHCO <sub>3</sub>	VWR
Na <sub>2</sub> HPO <sub>4</sub>	VWR
NaOH	BDH
NBQX	Ascent Scientific
NS-19504	Neurosearch
Neurobasal	Invitrogen
Paxilline	Latoxan, Neurosearch
PBS	Invitrogen
Penicillin/Streptomycin (10000 u/ml)	Invitrogen
Poly-D-Lysine (MW 70,000-150,000)	Sigma
Pyruvate	Invitrogen
Tetraethylammonium (TEA)	Sigma
Tetrodotoxin (TTX)	Latoxan
TRIS	Bio-Rad
Trypan Blue	Sigma
Trypsin-EDTA (HEK cells, 0.05 %)	Invitrogen
VSN-16R	Canbex Therapeutics

## **2.2 Methods**

### **2.2.1 Coverslip preparation**

#### **HEK293 cells**

Glass coverslips (diameter: 10 mm) were washed for 30 minutes in 100% ethanol, then rinsed in 75% ethanol and sterilized by baking for 8-10 hours at 200°C.

Immediately before use, coverslips were coated by immersion in a 100 µg/ml poly-D-lysine solution for 5-10 minutes at 37°C, then washed 3 times with 2 ml sterile H<sub>2</sub>O and stored in the incubator in culture medium until needed.

#### **Hippocampal cultures**

Glass coverslips (diameter: 10 mm) were sterilized and baked as described above for HEK293 cells. Coverslips were then coated with poly-D-lysine 100 µg/ml and incubated for 3 hours at 37°C, then washed 3 times with sterile H<sub>2</sub>O. One coverslip was then transferred to each well of a 4-well plate and covered with 500 µl attachment medium.

### **2.2.2 Maintenance and splitting of HEK293 cells and stable cell lines**

HEK 293 cells were sourced from the German Collection of Microorganisms and Cell Culture and grown to confluency (80-90%) in T25 flasks in an incubator at 37°C and 5 % CO<sub>2</sub>. To split the cells, the medium was removed and the cell layer washed with 4 ml PBS to remove debris and dead cells. Cells were detached by adding 1 ml of 0.05% Trypsin/EDTA solution. The solution was distributed evenly over the cells and any excess removed, before incubation for 1 minute at 37°C. Cells were then resuspended in 3 ml HEK complete medium (for composition, see paragraph 2.2.13 below) and dissociated mechanically. A new culture was seeded using 500 µl of cell suspension in a total volume of 5 ml HEK complete medium.

#### **Stable BK cell line**

A HEK293 cell line expressing the zero-splice alpha subunit of the rat BK channel (rBKα<sup>0</sup>) was kindly provided by Dr Martin Stocker.

BK cells were grown to confluency (80-90%) in T25 culture flasks in the presence of 220 ng/ml G418 at 37°C and 5 % CO<sub>2</sub>. The medium was removed and the cells washed with

4 ml PBS. Cells were detached by incubation in 3 ml of a 1 mM solution of EDTA in PBS at 37°C and 5% CO<sub>2</sub>. The suspension was centrifuged at 200 x g for 1 minute and the supernatant removed. Cells were resuspended in 3 ml HEK complete medium and dissociated mechanically, and a fresh culture was seeded using 1 ml of cell suspension in a total volume of 5 ml.

### **2.2.3 Preparation of acute dorsal hippocampal slices**

Transverse hippocampal slices (350 µm thick) were obtained from P19-24 male Sprague-Dawley rats. All procedures followed the guidelines outlined by the Home Office in the Animals for Scientific Procedures (Act 1987). Animals were anaesthetised by isoflurane inhalation, and decapitated with surgical scissors once adequate depth of anaesthesia had been confirmed by absence of a paw withdrawal reflex. Following decapitation, the skin on the skull was cut open using a scalpel blade. The skull was then cut open in a caudal to rostral direction, and the halves of the cranium peeled back to expose the brain. Ice-cold dissection and maintenance artificial cerebro-spinal fluid (dACSF; for composition, see paragraph 2.2.13 below) was poured over the brain to slow metabolic processes, and the hindbrain and cerebellum removed with a sharp scalpel blade. The hemispheres were then separated with a single longitudinal cut, dissected with two frontal cuts at ~85° with respect to the midline, and stored in ice cold dACSF for ~1 minute while the slicing chamber was prepared. The hemispheres were then glued (rostral end downwards) onto the stage of a Leica VT1000S slicer. Slicing was performed in ice cold ACSF, bubbled with carbogen (95% O<sub>2</sub>, 5% CO<sub>2</sub>). Immediately after separation, slices were transferred to an interface chamber containing dACSF with the wide end of a Pasteur pipette, and left to recover at room temperature (22-24°C) for at least an hour before recording. The atmosphere of the chamber was kept saturated with oxygen by continuous bubbling with carbogen. Slices obtained in this manner remained viable for 6-8 hours following dissection.

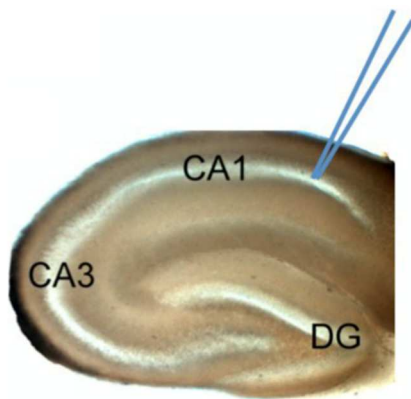


**Figure 2.0. Rat transverse hippocampal slice**

*Locations of dentate gyrus (DG), CA1 and CA3 regions of hippocampus shown by positions of labels. Translucent pyramidal cell layer is indicated by cartoon patch pipette. Diagram adapted from Jin et al (2011).*

#### **2.2.4 Preparation and maintenance of hippocampal cultures**

Hippocampal cultures were prepared from P0 Sprague-Dawley rat pups. Animals were sacrificed by decapitation and the brain hemispheres transferred to a 55 mm Petri dish containing ice cold dissection medium (DM; for composition, see paragraph 2.2.13 below). Under a dissecting microscope, the thalamus was removed from the medial side of each hemisphere to expose the hippocampus, which was then dissected out with forceps and transferred to a 35 mm dish containing ice cold DM. The process was repeated for the number of pups required and the 35 mm dish then transferred to the cell culture hood. Hippocampi were cut into 6-8 equal sections, transferred to a 10 ml tube using a plastic Pasteur pipette and incubated for 10 min at 37°C in 2 ml DM containing 200 µl of 2.5% trypsin/EDTA. The tissue pellet was then transferred to a fresh 10 ml tube and washed 3 times with 5 ml attachment medium (AM; for composition, see paragraph 2.2.13 below). Cells were mechanically dissociated using a glass Pasteur pipette and the supernatant then transferred to a fresh 10 ml tube and centrifuged for 3 min at 120 x g. Following centrifugation, the supernatant was aspirated and the pellet resuspended in 3 ml AM using a serological pipette. Density of living cells was calculated using a haemocytometer to count the cells in 50 µl of solution containing 5 µl Trypan blue. Cells were then transferred to coverslips in 4-well plates at a density of 45000 cells/coverslip and incubated overnight at 37°C / 5% CO<sub>2</sub>. After incubation, the attachment medium was aspirated and replaced with 500 µl maintenance medium (for composition, see paragraph 2.2.13 below).

Cells were maintained in the incubator at 37°C / 5% CO<sub>2</sub> and the maintenance medium was partially changed every 5-7 days, with the volume maintained at 500 µl.

### 2.2.5 Transient transfection of HEK 293 cells

The calcium phosphate method was used for all transfections. HEK 293 cells were plated onto 35 mm dishes 10-24 hours prior to transfection and allowed to grow to 70-80% confluency. For every transfection 4.65 µg plasmid DNA was added to a solution of 11.7 µl CaCl<sub>2</sub> (2 M) and 77.5 µl Tris-HCl (10 mM, pH 7.6). Where DNA was used at less than 1 µg/µl concentration, the volume of Tris-HCl was adjusted to give a total volume of 83.1 µl. This solution was added dropwise to 94 µl HBS (50 mM HEPES, 1.5 mM Na<sub>2</sub>HPO<sub>4</sub>, 280 mM NaCl, pH 7.22) while vortexing. The mixture was incubated for 30 min at room temperature, and added dropwise to the cells. The cells were then returned to the incubator for 6 hours at 37°C and 5% CO<sub>2</sub>. The precipitate was then removed from the cells by aspiration of the medium and washing 3 times with 1 x PBS. The medium was replaced with 2 ml HEK293 complete medium (for composition, see paragraph 2.2.13 below).

Transfected cells were then split onto coverslips 24-48 hours post transfection. Cells were detached by incubation at 37°C with 0.05% trypsin/EDTA for 1 minute as per the section on the passage of HEK293 cells. Cells then were resuspended in 1 ml HEK complete medium and dissociated mechanically. Cell concentration was estimated using a cell counting slide, and cells were plated into 3.5 cm dishes containing 5 coverslips each, at a concentration of approximately 400,000 cells per dish for cells to be recorded within 24 hours, or 200,000 cells per dish for cells to be recorded at 24-48 hours post transfection.

#### 2.2.5.1 Transfection recipes

##### **Rat BK alpha subunit, zero splice variant (rBKα<sup>0</sup>)**

rBKα <sup>0</sup> :	0.5 µg
pBluescript:	3.95 µg
eGFP:	0.2 µg

##### **rBKα<sup>0</sup> plus human BK beta subunits (hBK-β 1-4)**

rBKα <sup>0</sup> :	0.5 µg
hBK-β :	1.5 µg

pBluescript:	2.45 $\mu\text{g}$
eGFP:	0.2 $\mu\text{g}$

## 2.2.6 Voltage clamp recordings

In whole cell voltage clamp recordings, the membrane voltage ( $V_m$ ) of the cell is held at a fixed potential (the holding potential,  $V_{\text{hold}}$ ), specified to the amplifier circuit by the experimenter. The amplifier measures the voltage difference between the extracellular and intracellular volumes, and injects positive or negative current as required in order to maintain the cell at the holding potential. Changes in ion flux across the plasma membrane, which under physiological conditions would alter the membrane potential of the cell, are opposed by the amplifier, and are recorded as variations in the current that the amplifier needs to inject in order to maintain  $V_{\text{hold}}$ .

### 2.2.6.1 Series resistance compensation

In whole cell mode, the circuit formed between the patch and bath electrodes of the voltage clamp amplifier can be thought of as the equivalent of a 1<sup>st</sup> order RC circuit, where the capacitor is the capacitance of the plasma membrane ( $C_m$ ), and the resistance is composed of two resistors in series: the input resistance ( $R_{\text{input}}$ ), which is the resistance to ionic current flow across the plasma membrane, and the series resistance ( $R_s$ ), due to the narrow tip of the pipette and the opening of the membrane through which the connection to the cell is achieved. Since  $R_{\text{input}}$  and  $R_s$  are connected in series, there is a voltage error between the command voltage produced by the amplifier and the potential difference achieved at the cell membrane, due to the voltage drop across  $R_s$ . The series resistance therefore produces two kinds of error in patch clamp recording: a steady state error, in which the command voltage is different to the membrane voltage achieved, and dynamic errors, due to the fact that changes in  $V_m$  lag changes in the command voltage with a time constant ( $\tau$ ) determined by  $\tau = R_s * C_m$ , effectively acting as a low pass filter on the current measurements made.

As a result of the above, in cases where the current under observation is either voltage dependent or having fast kinetics, accurate recordings can only be achieved by compensating for the voltage error due to the series resistance. The amplifier can perform this automatically by first estimating and cancelling  $C_m$ , using the waveform used to cancel  $C_m$  to estimate  $R_s$  and calculate the amount of compensation necessary, then applying that compensation, and finally making fine adjustments to the amount of  $C_m$  cancellation required. As this is an iterative feedback process, high degrees of

compensation can lead to destabilising resonance, which can kill the cell. As a result, series compensation was performed at between 70-80% where its use is indicated. In recordings where the properties of the current being measured meant that it was not necessary to compensate  $R_s$  electronically (i.e. slow currents with little or no voltage dependence), every effort was nonetheless made to maintain constant values of  $R_s$  of between 15-25 M $\Omega$ .

### **2.2.7 Electrophysiological recordings from transfected HEK293 cells**

Recordings were made from transfected HEK293 cells between 12 and 48 hours after transfection. Cells were split onto 10 mm coverslips and maintained in culture medium incubated at 37°C and 5% CO<sub>2</sub>. They were allowed to recover for at least 3-4 hours before recording. During recording, coverslips were transferred to a 10 mm recording chamber that was perfused with HEK293 extracellular solution (H-EC; for composition, see paragraph 2.2.13 below) at a rate of 1-1.5ml/min, using a gravity driven perfusion system. Cells were visualised using an Axiovert 200 inverted microscope (Zeiss) with a 40x objective. Additionally, GFP-transfected cells were visualised using a HAL 100 illuminator, 480/40 nm excitation filter, dichroic dcLPQ 505 nm splitter and HQ 510 nm LP emission filter.

Recordings were made at room temperature, using patch pipettes made of borosilicate glass (Kimble-Chase, outside diameter: 1.5-1.8 mm, wall thickness 0.3 mm), pulled using a 2-stage vertical puller (L/M-3P-A, List Medical or PC-10, Narishige, Japan). Pipette resistances were between 2.5 and 4 M $\Omega$  when filled with a methylsulphate-based intracellular solution (for composition, see paragraph 2.2.13 below). Voltage clamp recordings were made using an EPC10 patch clamp amplifier and either Pulse v8.8 or Patchmaster v2.90, (HEKA Elektronik, Germany).

Cells were initially approached under visual control to select a target cell and position the electrode above it, using a micromanipulator (UL-1000i, Scientifica)VXC44. Cells were chosen based on the presence of green fluorescence, good adhesion to the coverslip and absence of any adjacent or connected cells. Sealing was then accomplished by gradual lowering of the pipette onto the cell and patching based on observation of test pulse resistance. Tip resistance was continually monitored using a voltage pulse on the patch amplifier software, and an increase of tip resistance was taken to indicate contact with a cell membrane. Seal formation was effected by releasing the positive pressure and application of gentle negative pressure. During seal formation, the command voltage was gradually lowered to -90 mV. Once a gigaohm seal was acquired,

the fast capacitative transients due to the glass pipette surrounded by intra- and extra-cellular solutions were compensated for and cancelled, and a 5 ms, 400 mV “zap” stimulus was used to rupture the membrane and enter whole-cell configuration.

On entering whole-cell mode, the slow capacitative transients due to the charging of the cell membrane capacitance were compensated for and cancelled, together with  $R_s$  compensation of 70-80%.

#### *2.2.7.1 P/n protocol*

In experiments involving voltage-dependent currents, leak current was determined and subtracted by using a P/n protocol. From a holding potential outside the active range of the channel under study, a series of n depolarising steps of 1/n times the size of the command voltage was produced. These were summed to produce an estimate of the passive current contribution, which was subtracted from the current response to the pulse protocol. In all experiments on BK channels, leak was subtracted using a P/8 protocol from a holding potential of -120 mV.

#### *2.2.7.2 Recordings from HEK293 cells expressing BK channel subunits*

Recordings from HEK293 cells expressing various combinations of BK channel subunits were made in the whole-cell configuration, in a 10 mm recording chamber bathed in H-EC solution (for composition, see paragraph 2.2.13 below).

For the experiment on the calcium dependence of  $rBK\alpha^0$ , whole cell recordings were made using three different intracellular solutions: HEK-BK-0, HEK-BK-200 and HEK-BK-1, differing in the concentration of  $CaCl_2$  added and the concentration of the calcium buffer EGTA, as detailed in the solutions appendix to this section. The free  $Ca^{2+}$  concentration was calculated for each solution using the MaxChelator web application (Chris Patton, Stanford University, USA).

For each combination of BK subunits, the effect of the known BK channel activator NS19504 was tested by addition of the drug to the bath solution at a concentration of 10  $\mu$ M, and the effect of the putative BK channel enhancer VSN-16R was tested by addition of the drug to the bath solution at a concentration of 20  $\mu$ M. BK channel currents were pharmacologically discriminated from any other voltage activated currents by the subsequent addition of 10  $\mu$ M paxilline or 5 mM TEA.

BK steady state current amplitude was determined by taking the mean average of the final 10 ms of the current response to the voltage step. In the case of the recordings of channels containing the  $\beta 2$  subunit, the peak current amplitude was additionally determined, using the mean average of a 5 ms window centred on the largest current response to the voltage step. I-V relationships were determined by recording current responses to a family of voltage steps (see subsequent paragraphs for details of the protocols), and performing a least-squares fit of the Boltzmann function:

$$y = \frac{A_1 - A_2}{1 + e^{(x-x_0)/dx}} + A_2$$

to averaged current responses. Activation time constants were determined by least squares fit of a single exponential to the current response to the voltage step in the case of recordings of BK alpha homomultimers, and by the least squares fit of a double exponential in the case of recordings of BK  $\alpha / \beta 4$  heteromultimers, taking the longer of the two time constants.

#### 2.2.7.3 Recordings from HEK293 cells stably expressing rBK $\alpha^0$

Recordings from HEK293 cells stably expressing BK were made in the whole-cell configuration using pipettes filled with HEK-BK-0, HEK-BK-200, or HEK-BK1 (for composition, see paragraph 2.2.13 below). In some experiments, either 500  $\mu$ M glutathione or 500  $\mu$ M dithiothreitol (DTT) were added to the HEK-BK-200 intracellular solution. The time course of activation for either VSN-16R or NS19504, or inhibition of the current by TEA or paxilline, was determined by applying 20 ms-long pulses to +90 mV from a holding potential of -80 mV, at 10 second intervals. In every experiment the pulse protocol was applied for a period of at least 5 minutes to establish a stable baseline of current activation before application of drugs. At the end of the baseline period, and upon reaching steady state after each drug application, current-voltage relationships were determined by means of a family of 20 ms-long voltage steps from -100 to +100 mV in 10 mV intervals, again from a holding potential of -80 mV. The time interval between voltage steps was 3 seconds.

In some experiments, following acquisition of the baseline time course, H<sub>2</sub>O<sub>2</sub> (1 mM, 5 mM or 10 mM) was added to the extracellular perfusion, and the current amplitude allowed to stabilise at a new level before application of the drugs.

#### 2.2.7.4 Recordings from HEK293 cells cotransfected with rBK $\alpha^0$ and hBK- $\beta$ 4

HEK-293 cells transfected with rBK $\alpha^0$ , human BK-beta4 (hBK- $\beta$ 4) and eGFP were patched in the whole-cell configuration using pipettes filled with HEK-BK-200 (for composition, see paragraph 2.2.13 below).

The time course of activation for either VSN-16R or NS19504, or inhibition of the current by TEA or paxilline, were determined by applying 200 ms-long pulses to +90 mV from a holding potential of -80 mV, at 10 second intervals. At the end of the baseline period, and upon reaching steady state after each drug application, current-voltage relationships were determined by means of a family of 200 ms-long voltage steps from -100 to +100 mV in 10 mV intervals, again from a holding potential of -80 mV.

The longer pulse duration compared to that used for rBK $\alpha^0$  alone was required to allow for the slower activation kinetics of channels with the  $\beta$ 4 subunit to reach steady state.

An additional set of experiments were performed in which HEK293 cells, transfected with rBK $\alpha^0$ , hBK- $\beta$ 4 and eGFP, were recorded in the whole cell mode using pipettes filled with HEK-BK-200, or HEK-BK-200 containing either 20  $\mu$ M VSN-16R or 10  $\mu$ M NS19504 (for composition, see paragraph 2.2.13 below). After allowing 5 minutes for the intracellular solution to perfuse the cell completely, the same family of voltage steps described above was performed, after which the bath was perfused with Ringer solution containing 10  $\mu$ M paxilline, and the voltage family was repeated.

#### 2.2.7.5 Recordings from HEK293 cells cotransfected with rBK $\alpha^0$ and hBK- $\beta$ 3 or BK- $\beta$ 2

HEK-293 cells, transfected with rBK $\alpha^0$ , hBK- $\beta$ 3 or hBK- $\beta$ 2 and eGFP were recorded in the whole-cell configuration using pipettes filled with HEK-BK-200 intracellular solution (for composition, see paragraph 2.2.13 below). The time course of activation for either VSN-16R or NS19504, or inhibition of the current by TEA or paxilline, was determined by applying a 20 ms-long step to -140 mV from a holding potential of -80 mV, immediately followed by a 50 ms-long step to +90 mV, and then a 20 ms-long step to -120 mV. The entire protocol was repeated at 10 second intervals. At the end of the baseline period, and upon reaching steady state after each drug application, current-voltage relationships were determined by means of a family of 200 ms-long voltage steps from -100 to +100 mV ( $\beta$ 3) or -100 to +120 mV ( $\beta$ 2) in 10 mV intervals, again preceded by a 20 ms-long step to -140 mV and followed by a 20 ms-long step to -120 mV. In both protocols, the purpose of the preceding hyperpolarising step was to remove any tonic inactivation of

the channel by the  $\beta$  subunit, while the -120 mV step following each step in the voltage family permitted the deactivation kinetics to be observed.

#### 2.2.7.6 *Flash photolysis of DM-Nitrophen in cells stably expressing rBK $\alpha^0$*

Recordings from HEK293 cells stably expressing BK were made in the whole-cell configuration using pipettes filled with IC-DM (for composition, see paragraph 2.2.13 below). To determine the effect of flash photolysis, uncaging experiments were performed in which the cell was held at +40 mV for 1 s, while a single UV flash was delivered after 500 ms using an UV Flash II lamp (Till Photonics / FEI Munich GmbH). UV flashes varied between 0.5 and 5 ms in duration by manually varying the 'intensity' dial on the machine, which in reality sets the duration of a constant power UV flash. The effect of repeated flashes on the available pool of unphotolysed DM-Nitrophen was tested by measuring the current response following repeated flashes delivered at 5 second intervals, while the cell was held at +40 mV.

### 2.2.8 Hippocampal acute slice recordings

All recordings from hippocampal acute slice preparations were made from CA1 pyramidal cells in dorsal hippocampal slices using the blind whole-cell patch clamp technique (Blanton et al., 1989). Experiments were performed with a HEKA EPC-10 amplifier controlled by Pulse or Patchmaster software (HeKa Elektronik). Slices were transferred from the interface chamber to the recording chamber on the stage of an upright microscope (Zeiss Axioskop) and immobilised using a "harp" – a net made from a platinum wire frame with nylon fibres stretched across it. During recordings, slices were submerged in the recording chamber and perfused at a rate of 2-2.5 ml/min with ACSF-2 (for composition, see paragraph 2.2.13 below), bubbled with carbogen.

Recordings were made using patch pipettes prepared using a 2-stage vertical puller (Narishige PC-10) and glass capillaries (1.5 mm  $\varnothing$  borosilicate glass, Hilgenberg, Germany). Pipettes were long shanked and had a tip resistance between 4.5-6 M $\Omega$  when filled with K-gluconate (IC-APA1; for composition, see paragraph 2.2.13 below).

Before the pipette tip was placed in the bath, a small amount of positive pressure was applied to prevent clogging of the tip and to clear debris from the surface of the slice. Once in the bath, the pipette was gradually lowered towards the CA1 cell layer using a micromanipulator (Luigs & Neumann, Germany). To achieve a GigaOhm seal, the pipette was lowered gradually into the cell layer, while a test pulse of 5 mV amplitude and 10 ms duration was applied to the electrode and visualised on an oscilloscope. The

test pulse allowed the tip resistance to be monitored as the electrode was lowered, and an increase of tip resistance was used as an indication of contact with a cell membrane. Positive pressure was then released and a small amount of negative pressure applied to induce seal formation. During this process, the command voltage was stepped from 0 to -60 mV to facilitate seal formation.

Once a high resistance ( $>1\text{G}\Omega$ ) seal was formed, the fast capacitive transient of the electrode was cancelled electronically using the amplifier circuitry. To achieve whole cell configuration, the membrane under the pipette was then ruptured using a 5 ms-long, 400 mV zap stimulus and sustained gentle suction. Once the whole cell configuration had been acquired, the patch amplifier was switched to the current clamp mode to acquire a measure of the resting membrane potential. Cells with a resting potential more depolarised than -55 mV were discarded. Additionally, the firing behaviour of the cells was assessed in order to determine that the patched cell was a CA1 pyramidal neuron, as opposed to a glial cell or interneuron. Action potentials were elicited using a 40-100 pA current injection of 1 s duration. Experiments were only performed where action potential shape, duration and spike frequency adaptation were typical for CA1 pyramidal cells (Figure 2.1).

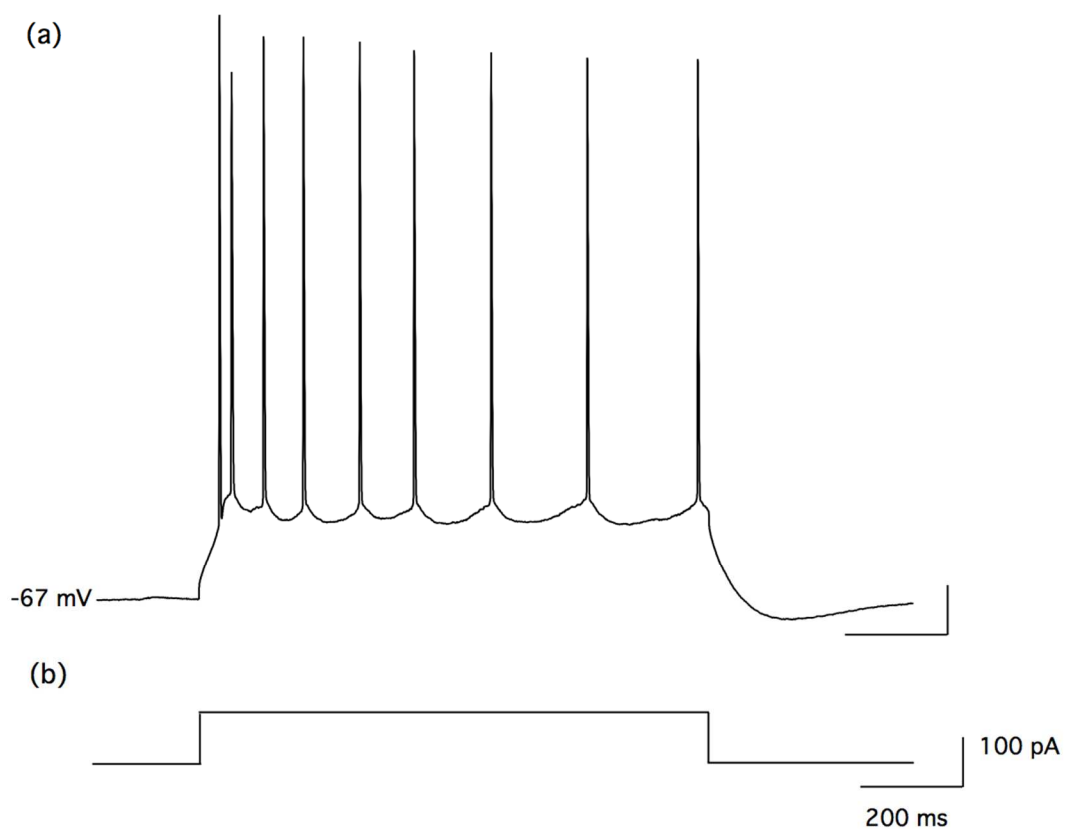


**Figure 2.1. Example of an action potential train from a CA1 pyramidal neuron**

**Action potential train was elicited from a CA1 pyramidal cell using ICAPA-1 intracellular.**

**(a) Voltage response to the current injection in (b). The presence of a late phase adaptation is typical of pyramidal cells as opposed to interneurons.**

**(b) The 1s current injection of 100 pA, used to generate the action potential train.**

### 2.2.8.1 Hippocampal slice whole cell voltage clamp protocols

#### **Series Resistance Protocol**

Series resistance ( $R_s$ ) and input resistance ( $R_{input}$ ) were determined by measuring the current response to a hyperpolarising voltage step of amplitude 5 mV and duration 100 ms from a holding potential of -50 mV (Figure 2.2). This holding potential was used to minimise activation of the mixed-cation current  $I_h$ , which activates between -50 and -70 mV (Luthi and McCormick, 1998). The traces were sampled at 20 kHz and filtered to 4 kHz. The voltage protocol used is displayed in Figure 2.2, together with an example current response. Three consecutive measurements were averaged for each cell.

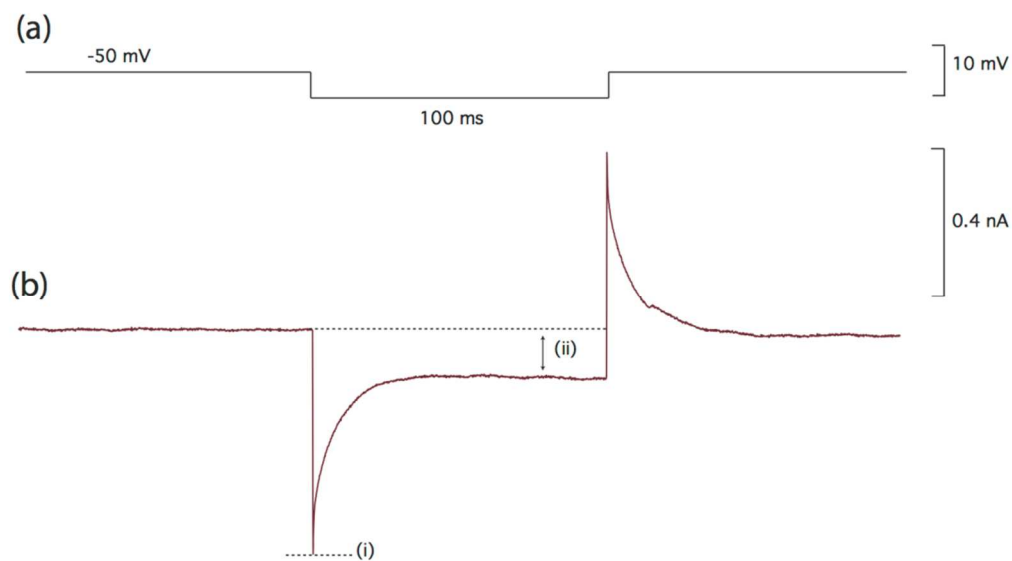


**Figure 2.2. Series Resistance Protocol**

**(a) Voltage protocol, consisting of a 100 ms, -5 mV step from a holding potential of -50 mV.**

**(b) Example current trace in response to (a). Series resistance is calculated by measuring the series current minimum at (i) and converting to resistance via Ohm's law ( $R_s=I_s/\Delta V$ ). Input resistance is calculated by measuring the input current at (ii) and converting to resistance by ( $R_i=I_i/\Delta V$ ).**

### ***sI<sub>AHP</sub> + R<sub>s</sub> protocol***

The  $sI_{AHP}$  was measured following a depolarising step from a holding potential of  $-50$  mV to between  $-10$  and  $+10$  mV for a duration of 50-250 ms. Following the depolarising step, a 12 s-long recording was made of  $sI_{AHP}$  (Figure 2.3). The traces were sampled at 1.25 KHz and filtered to 250 Hz, and the protocol was repeated at intervals of 30 s. A series protocol immediately preceded each stimulus pulse and was used to monitor  $R_s$  throughout the recording. Only experiments in which  $R_s$  varied by less than 15% were used in the analysis. Peak current amplitude was measured by taking the mean average of a window between 500 and 750 ms following the termination of the stimulus voltage step. Decay time constant was calculated by fitting a single exponential function to the trace between 750 ms following the termination of the stimulus step, and the end of the trace.

All acute slice recordings were performed in the presence 0.5  $\mu$ M tetrodotoxin (TTX) to block voltage gated sodium channels, and 50-100  $\mu$ M d-tubocurarine (dTC) to inhibit the SK channel-mediated afterhyperpolarising current ( $I_{AHP}$ ).

Additionally, recordings were made in the presence of tetraethylammonium (TEA), which blocks a subset of voltage-gated  $K^+$  channels. Unless otherwise stated, the concentration of TEA used was 1 mM, at which concentration the  $sI_{AHP}$  is enhanced because VGKC blockade increases the  $Ca^{2+}$  current during the stimulus pulse by removing the contribution of  $K^+$  channels to membrane repolarisation.

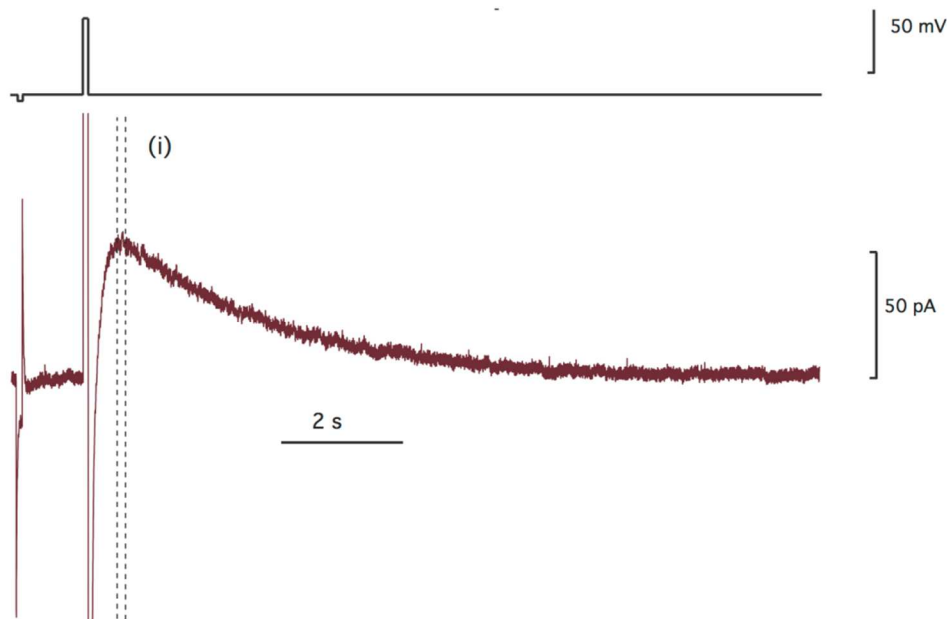


**Figure 2.3. sIAHP+Rs Protocol**

- (a) *Voltage stimulus, consisting of a 100ms, -5 mV hyperpolarising step from holding potential of -50 mV, followed by a depolarising step from -50 mV to +10 mV for 100 ms.*
- (b) *Current trace in response to (a). The Peak amplitude of sIAHP is measured as the mean value of the region between the two dotted lines (i), which are 150 ms apart, the leftmost being 500 ms after the end of the stimulus pulse.*

#### ***Effect of drugs on $sI_{AHP}$***

Following attainment of the whole-cell configuration, the  $sI_{AHP}$  protocol was initiated and the current was allowed to run up to a stable baseline for at least 10 minutes in the presence of TTX, TEA and dTC. After a stable baseline had been achieved, either 1-Ethyl-2-benzimidazolinone (EBIO; 1 mM), ethanol (EtOH; 10 or 20 mM) or Methyl 2,6-dimethyl-5-nitro-4-[2-(trifluoromethyl)phenyl]-1,4-dihydropyridine-

3-carboxylate (Bay-K 8644; 1  $\mu$ M) was dissolved in ACSF and applied extracellularly via bath perfusion until a new stable  $sI_{AHP}$  amplitude was achieved. The drug was then removed and washout attempted.

#### ***Effect of varying concentrations of TEA on $sI_{AHP}$***

The  $sI_{AHP}$  protocol was initiated and the current allowed to run up to a stable baseline for at least 10 minutes in the presence of TTX and dTC. The cell was then bathed in ACSF-

2 (for composition, see paragraph 2.2.13 below) containing increasing concentrations of TEA (1 mM, 5 mM, 10 mM and 20 mM). In the case of the 10 mM and 20 mM concentrations, the NaCl concentration of the ACSF was reduced by an equivalent amount to avoid the possibility of osmolarity changes influencing the behaviour of the cell. In each case the  $sI_{AHP}$  was allowed to reach a stable state before the next concentration of TEA was applied. Following the application of the last concentration, the drug was removed and the recording continued in order to observe a washout.

### **2.2.9 Focal application of isoproterenol**

Hippocampal pyramidal cells were recorded in the whole-cell mode (2.4.2) using IC-APA-1 intracellular solution containing 200  $\mu$ M Lucifer yellow (for composition, see paragraph 2.2.13 below). The cell was allowed to fill with fluorophore for at least 20 minutes, during which time  $R_s$  was monitored, and thereafter  $sI_{AHP}$  was recorded for a further 10 minutes to establish a stable baseline for current amplitude.

ACSF containing 50  $\mu$ M isoproterenol and 1 mM Lucifer yellow was then applied focally to cells using a Picospritzer III microinjector (Parker). The ACSF containing the Lucifer yellow was maintained in a 500  $\mu$ l Eppendorf tube bubbled with carbogen (95% O<sub>2</sub> 5% CO<sub>2</sub>). Immediately before an experiment, 20  $\mu$ M isoproterenol was dissolved in the aliquot and the resultant solution loaded into the microinjector pipette. This procedure was designed to minimize both the potential for oxidization of isoproterenol, which would lead to a change in effective concentration, and de-gassing of the ACSF, which might lead to changes in pH and hypoxic effects being observed in the cell following application.

During the cell-filling, but before the  $sI_{AHP}$  baseline acquisition phase of the experiment, the microinjector pipette was kept some distance above the slice, to prevent any effect on the cell due to leakage of solution from the pipette due to diffusion. The pipette was then moved into the target position and the baseline traces acquired. In each experiment, the puff was applied to one of two distinct regions, chosen to correspond to either the soma/proximal dendritic region or the distal dendritic region. Both target positions were determined by eye, and were defined by positioning the tip approximately 2 soma diameters (i.e. approximately 40  $\mu$ m) from the intersection of the soma with the apical dendrite (soma/proximal) or 5 soma diameters (~100  $\mu$ m) past the first visible branching point of the apical dendrite (distal dendrite).

The microinjector was used as a puffer pipette, and settings were set to 10 ms duration and 10 psi, which produced a cone-shaped puff, in which the fluorescent area was around 20  $\mu\text{m}$  in diameter at a point around 100  $\mu\text{m}$  from the pipette tip.

Due to the laminar flow of ACSF across the surface of the tissue slice, the puff (as indicated by the fluorescent dye) diffused away from the site of application in the direction of the laminar flow. As a result, it was necessary to orient the slice so that the longitudinal axis of the cell being recorded was approximately perpendicular to the direction of flow. The positions of the various elements of the recording setup are shown in figure (Figure 2.4).

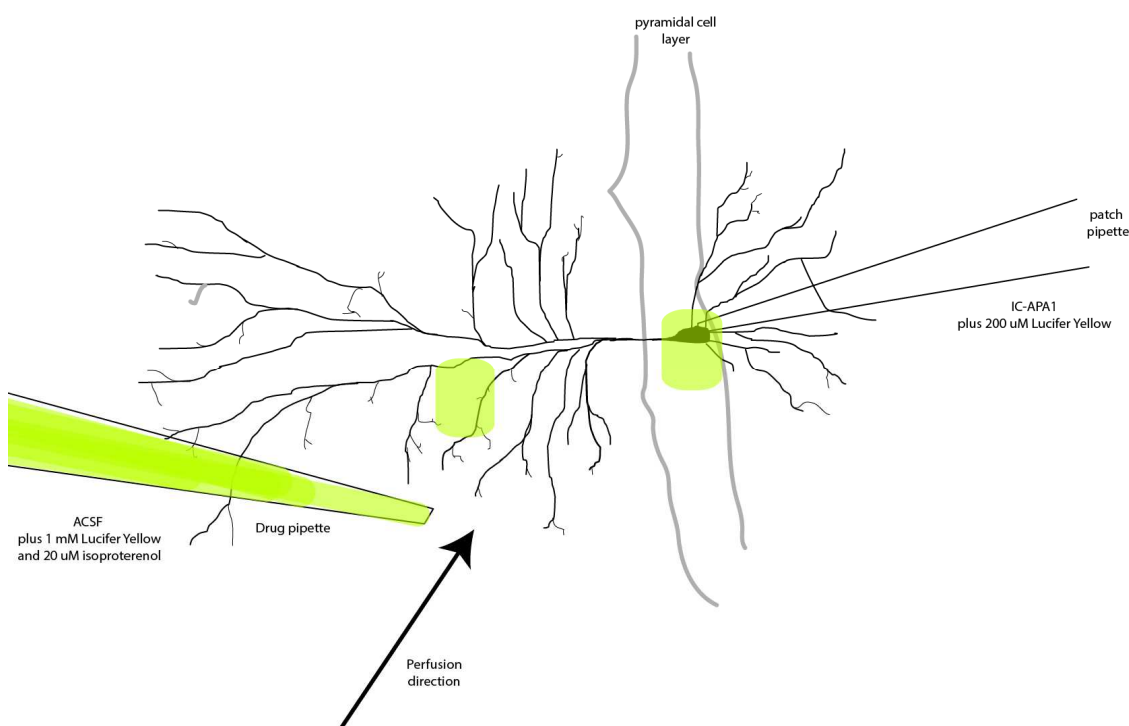


**Figure 2.4. Schematic of the focal application experiment**

*Patch pipette (right) is used to patch soma, microinjector pipette (left) containing lucifer yellow and isoproterenol is used to locally apply isoproterenol to different parts of the neuron.*

### **2.2.10 Recordings from hippocampal cultures**

Recordings were made from cultured hippocampal neurons between DIV 4 to 12 (DM-Nitrophen experiments) and DIV 15 to 24 (BCMCM-8Br-cAMP experiments). Cells were cultured on 10 mm coverslips and maintained in maintenance medium incubated at 37°C and 5% CO<sub>2</sub>. At the start of the recording session, coverslips were transferred to a recording chamber that was perfused with rACSF extracellular solution (for composition, see paragraph 2.2.13 below), bubbled with carbogen, at a rate of 1.5 ml /min using a

pump perfusion system. Cells were visualised using a Zeiss Axioskop microscope with a 60x objective. Additionally the visual field was displayed on a monitor via a camera (VX44, TILL Photonics, Germany).

Recordings were made at room temperature, using patch pipettes (1.5 mm  $\varnothing$  borosilicate glass, Hilgenberg, Germany), pulled using a 2-stage vertical puller (PC-10, Narishige, Japan). Tip resistances were between 3.0 and 4.0 M $\Omega$  in a methylsulphate based intracellular solution (IC-HC or IC-DM; for composition, see paragraph 2.2.13 below). Voltage clamp recordings were made using an EPC10 patch clamp amplifier and Pulse v8.8 (HEKA Elektronik, Germany).

Every attempt was made to record only from pyramidal neurons, and the identity of cells in the culture as pyramidal neurons was determined by observation of the presence of a triangular perikaryon, a large apical dendrite and shorter basal dendrites (Banker and Cowan 1977, Kreigstein and Dichter, 1983). Identification of dendrites was determined based on their length, branching pattern and tapering diameter (Dotti et al 1988).

During seal formation, cells were initially approached by the pipette under visual control in order to select a cell matching the criteria described above, using an SM-1 micromanipulator (Luigs and Neumann, Germany). The pipette was then lowered onto the cell and seal formation was achieved by monitoring changes in the tip resistance in response to a test voltage step on an oscilloscope (Tektronix TDS1012), and an increase in resistance was determined to represent contact of the tip with the cell membrane. The positive pressure was then released and gentle negative pressure applied to facilitate seal formation, and during seal formation the voltage was gradually stepped to -60 mV. Once a GigaOhm seal had been achieved, the fast capacitive transients were compensated for and cancelled on the amplifier software, and the whole-cell configuration was achieved using suction and a zap voltage pulse (10 ms-long step; 400 mV).

Immediately before attempting to achieve the whole cell configuration, 250  $\mu$ M TTX, 25  $\mu$ M (2R)-amino-5-phosphonovaleric acid (APV) and 5  $\mu$ M 2,3-dihydroxy-6-nitro-7-sulfamoyl-benzo[f]quinoxaline-2,3-dione (NBQX) were added via the perfusion system, in order to suppress action potential firing and inhibit glutamatergic synaptic activity. Once the whole cell configuration had been acquired, the patch amplifier was switched to current clamp mode to acquire a measure of the resting membrane potential. Cells with a resting potential more depolarised than -55 mV were discarded.

### 2.2.10.1 DM-Nitrophen uncaging

Pyramidal cells were identified and patched using the method described in 2.10, using IC-DM intracellular solution containing 3 mM of the photolabile calcium buffer DM-Nitrophen, 60% loaded with  $\text{Ca}^{2+}$ . Correct loading of DM-Nitrophen was achieved by making two solution aliquots, one loaded to 100% by adding  $\text{CaCl}_2$  at a concentration calculated using Maxchelator v1 (Chris Patton, Stanford University), and the other containing no  $\text{Ca}^{2+}$ . The solutions were then mixed ratiometrically to achieve correct loading. The soma of the cell to be patched was positioned in the centre of the visual field. Following acquisition of the whole-cell state, the cell was left for a period of at least 10 minutes to permit dialysis of the cell with the intracellular solution and the caged compound.

Flash photolysis of DM-Nitrophen was achieved using a UV Flash II pulsed light source (TILL Photonics), along with a light path that incorporated a sliding lens, permitting the area of the visual field covered by the flash to be altered. The area of the flash was adjusted so that it covered an area approximately twice the diameter of the soma, centred in the middle of the visual field. A series of four flashes was applied, set at the device's maximum duration of 5 ms, with a 2 s interval between flashes. During the flash protocol, the cell was held at -50 mV and current response data were acquired. An  $R_{\text{series}}$  step (2.8.1.1) was included at the start of the data acquisition phase, between the  $R_{\text{series}}$  step and the first flash, and the cell was held at -50 mV and was recorded for a period of 1s before presentation of the flash, in order to establish a current baseline.

### 2.2.11 BCMCM-8Br-cAMP uncaging

Pyramidal cells were identified and patched using the method described at the start of paragraph 2.10, using IC-HC intracellular solution containing 200  $\mu\text{M}$  BCMCM-8Br-cAMP. Prior to patching, the cell was positioned so that the region where the flash was to be centred was in the middle of the visual field.

Once the whole cell configuration was achieved, the cell was recorded for at least 10 min using the  $sI_{\text{AHP}}+R_s$  protocol (2.8.1.2), to establish a baseline for the  $sI_{\text{AHP}}$  amplitude and to permit the diffusion of the caged compound into the cell. Following this period, a train of 5 flashes of duration 5 ms, separated by 800 ms intervals, was delivered, and the  $sI_{\text{AHP}}+R_s$  protocol restarted. In some cells, the flash protocol was delivered at multiple time points in the experiment. In each case, subsequent flashes were delivered once the  $sI_{\text{AHP}}$  amplitude had reached a new stable baseline.

The flash protocol was delivered to one of two subcellular locations. The first covered the cell soma, which was achieved by setting the lens in the light path of the flash such that the flash covered a circular area equal to approximately to  $\frac{1}{8}$  of the visual field of the 60x water immersion lens. Before the start of the experiment, the light source was set to strobe mode, and with the lens immersed and focused on the coverslip, a circle was drawn on the monitor screen around the area covered by the flash. The cell was then positioned so that the soma, but none of the apical dendrite, was inside the inscribed circle, and the cell was then patched at the soma and the experiment performed as described above.

The second region was designed to cover the proximal portion of the apical dendrite, and was set by positioning the light path lens so that the area covered by the flash was equal to approximately to  $\frac{1}{4}$  of the visual field of the 60x lens. The stage was then moved such that the first branch point of the apical dendrite was the edge of the flashed region furthest from the soma (Figure 2.5). In this way it was possible to cover around  $\frac{3}{4}$  of the portion of dendrite between the soma and the first branch point, although the precise proportion varied slightly depending on cell morphology.

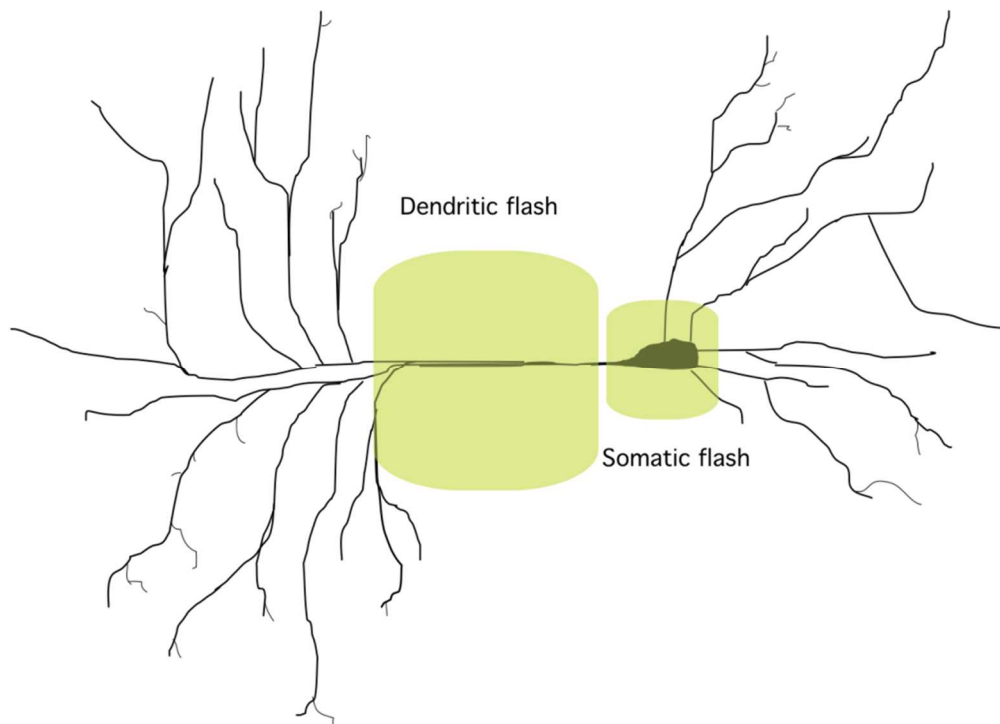


**Figure 2.5. Schematic showing location and relative size of the dendritic and somatic flash regions**

### **2.2.12 Analysis**

All experiments were analysed using IGOR Pro v6.32A (USA) with additional processing in Neuromatic 2 (kindly provided by J. Rothman, UCL). Methods for the measurement of values pertinent to each experimental protocol are detailed in the relevant sections. In all experiments, voltages are reported without correction for liquid junction potential (LJP), which takes values of -11 mV (K-Gluconate) or -5 mV (K-Methylsulphate).

Graphs were produced using IGOR Pro v6.32A and Prism v7 (Graphpad USA), and statistical analysis performed using Prism v7. Throughout this document, error bars on graphs and figures denotes standard error of the mean (SEM). Throughout the text, values are reported as mean  $\pm$  SEM. Normality of sample distributions was determined using the Shapiro-Wilk normality test. Where samples were not normally distributed, the relevant non-parametric test was used, as quoted in the text.

### **2.2.13 Solutions**

#### *2.2.13.1 Cell culture media*

#### **HEK complete medium**

DMEM/F12

Fetal Bovine Serum 10%

L-Glutamine 2 mM

Penicillin/Streptomycin 100 U/ml, 100  $\mu$ g/ml

#### **Dissection Medium**

1 x HBSS

10 mM HEPES

#### **Attachment Medium**

50 ml Aliquot

1 x MEM

1 mM Pyruvate

0.5 ml 100X L-Glutamine

0.66 ml 0.59% Glucose

5 ml 10% Horse Serum

**Maintenance medium**

50 ml Aliquot

1 x Neurobasal

0.33 ml 0.6% Glucose

0.25 ml 100X L-Glutamine

0.25 ml Penicillin/Streptomycin (10000 U/ml)

### 2.2.13.2 Slice preparation media

#### **Dissection and maintenance ACSF (dASCF)**

NaCl	125 mM
KCl	1.25 mM
KH <sub>2</sub> PO <sub>4</sub>	1.25 mM
NaHCO <sub>3</sub>	25 mM
Glucose	16 mM
CaCl <sub>2</sub>	1 mM
MgCl <sub>2</sub>	1.5 mM

pH 7.4 when bubbled to saturation with carbogen.

Solution was prepared as a 5X stock, minus glucose, CaCl<sub>2</sub> and MgCl<sub>2</sub>, using Milli-Q deionised water.

1X solution was prepared on the day by dilution with Milli-Q water and supplemented with glucose, while MgCl<sub>2</sub> and CaCl<sub>2</sub> were added once the solution had been bubbled to saturation with carbogen.

### 2.2.13.3 Extracellular solutions

All extracellular solutions were prepared using Milli-Q deionised water.

#### **HEK 293 Extracellular (H-EC)**

NaCl	145 mM
KCl	4 mM
HEPES	10 mM
Glucose	11 mM
CaCl <sub>2</sub>	1 mM
MgCl <sub>2</sub>	0.5 mM
pH 7.4	

### **Recording ACSF (rACSF)**

NaCl	125 mM
KCl	1.25 mM
KH <sub>2</sub> PO <sub>4</sub>	1.25 mM
NaHCO <sub>3</sub>	25 mM
Glucose	16 mM
CaCl <sub>2</sub>	2 mM
MgCl <sub>2</sub>	1.5 mM

pH 7.4 when bubbled to saturation with carbogen.

Solution was prepared as a 5X stock, minus glucose, CaCl<sub>2</sub> and MgCl<sub>2</sub>, using Milli-Q deionised water.

1X solution was prepared on the day by dilution with Milli-Q water and supplemented with glucose, while MgCl<sub>2</sub> and CaCl<sub>2</sub> were added once the solution had been bubbled to saturation with carbogen.

#### *2.2.13.4 Intracellular solutions*

All intracellular solutions were made with Romil water.

### **HEK-BK-0**

K-Methylsulphate	135 mM
HEPES	10 mM
EGTA	10 mM

MgCl<sub>2</sub> was added in sufficient quantity to give free Mg<sup>2+</sup> of 1 mM, using Maxchelator (C.Patten, Stanford University).

### **HEK-BK-200**

K-Methylsulphate	135 mM
HEPES	10 mM
EGTA	5 mM

CaCl<sub>2</sub> and MgCl<sub>2</sub> were added in sufficient quantity to give free Ca<sup>2+</sup> of 200 nM and free Mg<sup>2+</sup> of 1 mM, using Maxchelator (C.Patten, Stanford University)

### **HEK-BK-1**

K-Methylsulphate	135 mM
HEPES	10 mM
EGTA	5 mM

CaCl<sub>2</sub> and MgCl<sub>2</sub> were added in sufficient quantity to give free Ca<sup>2+</sup> of 1mM and free Mg<sup>2+</sup> of 1 mM, using Maxchelator (C.Patten, Stanford University)

### **IC-APA1: standard neuron intracellular solution (K-Gluconate)**

K-Gluconate	135 mM
KCl	10 mM
HEPES	10 mM
Na <sub>2</sub> ATP	2 mM
Na <sub>3</sub> GTP	0.4 mM
MgCl <sub>2</sub>	1 mM

pH 7.2-7.3

Osmolarity 280-290 mOsm/L

### **IC-APA3: Standard neuron intracellular solution (K-Methylsulphate)**

KMeSO <sub>4</sub>	135 mM
KCl	10 mM
HEPES	10 mM
Na <sub>2</sub> ATP	2 mM
Na <sub>3</sub> GTP	0.4 mM
MgCl <sub>2</sub>	1 mM

pH 7.2-7.3

Osmolarity 280-290 mOsm/L

### **IC-MOPS**

K-Gluconate	100 mM
HEPES	40 mM
MOPS	5 mM
MgCl <sub>2</sub>	2 mM
EGTA	0.1 mM
CaCl <sub>2</sub>	0.05 mM
Na <sub>2</sub> ATP	2 mM
Na <sub>3</sub> GTP	0.4 mM

pH 7.2-7.3

Osmolarity 280-290 mOsm/L

### **IC-DM**

KMeSO <sub>4</sub>	110 mM
HEPES	50 mM
MgCl <sub>2</sub>	0.5 mM
Na <sub>2</sub> ATP	2 mM
Na <sub>3</sub> GTP	0.4 mM
Phosphocreatine	10 mM
DM-Nitrophen	3 mM

pH 7.2

Osmolarity 280-290 mOsm/L

Correct loading of DM-Nitrophen was achieved by ratiometric mixing of IC-DM solution aliquots, one calcium-free, and the other 100% loaded with Ca<sup>2+</sup> using CaCl<sub>2</sub>. Correct load was calculated using Maxchelator (C.Patten, Stanford University).

# **PART ONE: Effect of VSN-16R and NS19504 on heterologously expressed BK channel subunits.**

## **Chapter 3. Introduction**

### **3.1 BK channels**

BK channels, also known as MaxiK, BK<sub>Ca</sub>, Slo1 or KCa1.1, are potassium channels of high unitary conductance that exhibit the unique property of being activated by both intracellular Ca<sup>2+</sup> and voltage. They are ubiquitously expressed throughout the body, performing diverse roles in different tissues, and exhibit variation in their biophysical properties depending on their subunit composition and a variety of alternative splice variants. BK channels have been implicated in a number of pathological conditions, including the monogenic disorder Fragile X syndrome, which is the most common heritable cause of cognitive impairment. They therefore represent an important potential therapeutic target for novel drug therapies.

#### **3.1.1 BK channel structure: the alpha subunit**

The BK $\alpha$  subunit is the necessary and sufficient molecular component for the formation of a functional BK channel. The minimal functional channel is formed from a homotetrameric assembly of this subunit, which is the translation product of the *KCNMA1* gene. Unusually for members of the S4 superfamily of K<sup>+</sup> channels, BK $\alpha$  consists of 7 as opposed to 6 transmembrane segments, known as S0 to S6.

The broad structure of the BK $\alpha$  subunit consists of three functionally distinct regions: a voltage sensitive domain (VSD) comprising transmembrane segments S1-S4, a pore forming region (S5 and S6, plus linker), and a cytosolic C-terminal region which contains two Ca<sup>2+</sup> sensing domains.

As with all other voltage dependent K<sup>+</sup> channels, the positively charged S4 segment is involved in the voltage sensing apparatus, though the extent of the voltage sensing domain (VSD) in Kv channels is defined as the region comprising segments S1 to S4. However in the BK channel, only one of the positively charged residues on S4 has been directly implicated in voltage sensing (Diaz et al 1998). The pore domain of the channel is formed by the S5 and S6 segments, which contain the K<sup>+</sup> channel signature sequence, and mediates pharmacological block by TEA, charybdotoxin and iberiotoxin. A number

of residues forming the inner vestibule of the pore permit the concentration of K<sup>+</sup> ions in the vicinity of the pore via electrostatic mechanisms, leading to the characteristic high conductance of the channel (Brelidze et al 2003), along with a residue (D292) in the external vestibule (Haug 2004).

Tetramerisation of the alpha subunit is mediated by a hydrophilic region linking the transmembrane S6 and intracellular hydrophobic S7 segment (Quirk and Reinhart 2001). This is the only region capable of self-association and formation of stable tetramers in solution, and truncation of the channel at this location produces a dominant negative phenotype.

The presence of an extra transmembrane region at the N terminal end of the molecule leads to the N terminus being located extracellularly (Meera, 1997), and it is this region that mediates association between BK $\alpha$  and the auxiliary beta ( $\beta$ 1- $\beta$ 4) and gamma ( $\gamma$ 1- $\gamma$ 4) subunits (Morrow et al 2006), which confer differences in various properties such as channel kinetics, Ca<sup>2+</sup> sensitivity, and pharmacology.

The region between the S8-S9 linker and the C-terminus is known as the tail. It can be expressed separately from the rest of the protein, and co-expression of the core protein and the tail region produces a functional channel, and both regions are required for the production of functional channels. This intracellular C-terminal portion of the human BK $\alpha$  protein has been successfully crystallised, confirming the prediction that this region contains two Ca<sup>2+</sup>-sensing domains, RCK1 and RCK2 (Yuan et al, 2010), one in the S7-S8 region, and another at the C-terminus comprising the S9-S10 linker and part of the S10 region (Schreiber et al, 1999). The second Ca<sup>2+</sup> sensitive domain also contains the Ca<sup>2+</sup> binding site, a region known as the Calcium bowl, consisting of an Asp-rich sequence.

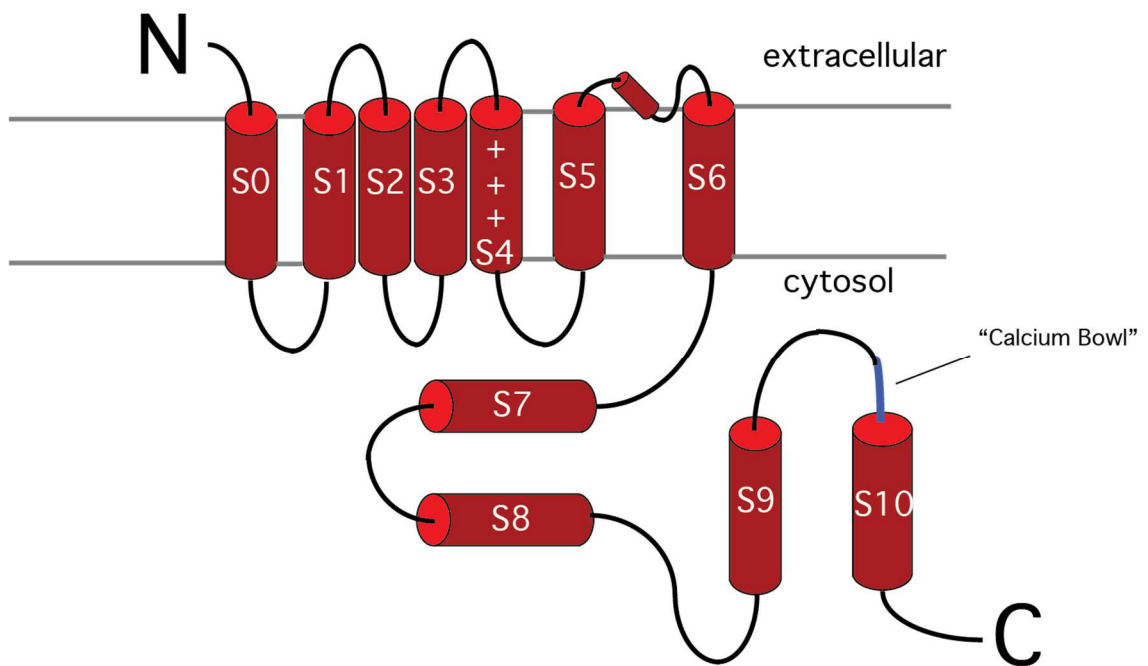


**Figure 3.1. Cartoon of BK  $\alpha$  subunit structure.** Membrane-spanning and intracellular helices are shown as numbered red cylinders. N and C respectively represent the amino and carboxy termini of the molecule.

### 3.1.2 Functional properties of the BK $\alpha$ homotetrameric channel

BK channels display a range of functional properties that make them of particular interest to the biophysicist. Compared to other voltage dependent K<sup>+</sup> channels, they exhibit a very high unitary conductance of around 100-300 pS in 100 mM symmetrical KCl, a property that inspired the channel's nomenclature ("Big" K or MaxiK). As described above, this feature is thought to be due to the capacity of residues in the cytosolic and extracellular vestibule regions of the pore loop to concentrate K<sup>+</sup> ions around the pore entrance via electrostatic attraction. They are also unique in being sensitive to both voltage and intracellular Ca<sup>2+</sup>. Both voltage and calcium are sufficient to activate the channel in the absence of the other (Cui et al 1997, Palotta et al, 1981), though to produce pOpen values in the region of 0.5 in a physiologically relevant membrane potential range requires the presence of around 10  $\mu$ M Ca<sup>2+</sup>. As a result of this, they can be seen as acting as coincidence detectors (Patazis and Olcese 2016), capable of integrating voltage and calcium signalling, as well as providing a homeostatic effect on Ca<sup>2+</sup> entry via voltage gated calcium channels (VGCCs), as increased calcium entry leads to greater BK activation, and hence hyperpolarisation, which in turn reduces VGCC activation. BK channels tend to be colocalised with VGCCs in most tissues (eg. in auditory hair cells (Roberts et al 1990)), with the coupling allowing local elevation of

[Ca<sup>2+</sup>]<sub>i</sub> to the 10 μM range. A similar collocalisation is observed between plasma membrane BK channels and ryanodine receptors in sarcoplasmic reticulum (Orio 2002).

### 3.1.3 BK Channel variants

Mammalian BK channels can be associated with a range of auxiliary subunits of two subtypes, called β and γ, which can greatly alter many properties of the channel: kinetics, resistance to blockade by toxins, and sensitivity to Ca<sup>2+</sup> and voltage. Further functional diversity is conferred by a wide range of alternative splice variants of both the BKα subunit and β subunit RNA, as well as post-translational modifications such as lipidation and phosphorylation.

#### 3.1.3.1 Beta subunits

BK β subunits are a family of small (20-30 KDa) membrane proteins, consisting of two transmembrane regions connected by a 120-residue extracellular loop, with the amino and carboxy termini on the cytoplasmic side of the membrane. At present, four types of β subunit (β1-β4) have been cloned in mammals (Marty 1981, Behrens et al 2000, Brenner, Jegla et al 2000, Ubele et al 2000). Each confers a different set of modifications to the functional properties of the canonical channel.

The first beta subunit to be cloned, now known as β1, was initially identified from smooth muscle preparation as having high affinity for the BK channel blocker charybdotoxin (Ctx). It is found in a range of non-neuronal tissues including hair cell, smooth muscle and endothelium (Orio et al 2002). Co-expression of this subunit with the BKα leads to a leftward shift in the voltage dependence, particularly at intracellular Ca<sup>2+</sup> concentrations greater than 1 μM, as well as slowing the activation and deactivation kinetics of the channel.

A second subunit, β2, was discovered by searching human expressed tag sequence database using β1 as a query sequence (Wallner et al 1999). Coexpression of the resultant peptide with BKα yielded a channel with an inactivating phenotype, reminiscent of the currents previously observed in rat chromaffin cells (Xia et al, 1999), as well as reduced sensitivity to the blocker charybdotoxin (Ctx). Truncation of the cytosolic N-terminus of the β2 subunit produced a mutation lacking the inactivation phenotype, suggesting a mechanism reminiscent of the N-type inactivation model originally described in *Shaker* (Xia et al, 1999). The rate of inactivation was also shown to be calcium-dependent, with the time constant for 10 μM [Ca<sup>2+</sup>]<sub>i</sub> around 5-fold lower than that at 100 nM [Ca<sup>2+</sup>]<sub>i</sub>. The β2 subunit is widely expressed in brain, including in hippocampal

CA1 pyramidal neurons, where it modulates the inter-spike interval in the initial portion of an action potential burst (Shao et al 1999, Faber and Sah 2003), and suprachiasmatic nucleus (Whitt et al, 2016), where circadian changes in  $\beta 2$  expression levels modulate neuronal excitability.

A third beta subunit, named  $\beta 3$ , was also cloned from human EST databases (Xia et al, 2000). It was found to be enriched in various non neuronal tissues, including pancreas, spleen and testis (Orio 2002). Phylogenetically similar to  $\beta 2$ , it confers inactivating properties which are less rapid and pronounced than those of  $\beta 2$ , which are more visible at highly positive voltages. There are three splice variants (a-c), which differ primarily in the speed and completeness of the inactivation properties conferred. In addition, the  $\beta 3$  subunit confer the property of outward rectification on the channel (Behrens et al 2000, Xia et al 2000).

A final subunit,  $\beta 4$ , is expressed primarily in brain, including hippocampus, dentate gyrus, and cortex. It is the most phylogenetically distinct member of the  $\beta$  family, and confers a wide range of properties on the channel, including a reduced  $\text{Ca}^{2+}$  sensitivity, pronounced slow activation and inactivation kinetics, a reduced sensitivity to the specific BK blockers iberiotoxin and charybdotoxin (Meera et al, 2000), and an increased sensitivity to martentoxin (Shi et al, 2008).

**Table 3.1. Summary of the effects of different mammalian  $\beta$  subunits on channel properties**

Subunit	$\text{Ca}^{2+}$ /voltage sensitivity	kinetics	inactivation	Pharmacology
$\beta 1$	Leftward shift	slowed	no	Increased Ctx sensitivity
$\beta 2$	none	No change	rapid	None
$\beta 3$ (a, b, c, d)	none	No change	High voltages only Splice dependent	None
$\beta 4$	Rightward shift	slowed	no	Iberiotoxin resistance Ctx resistance Martentoxin sensitivity

### 3.1.3.2 *Gamma subunits*

In addition to the four members of the beta subunit family, an additional family of BK modulatory subunits, known as  $\gamma$ 1- $\gamma$ 4 have also been identified. The first clue to the existence of this subunit family came from the discovery of an unusual BK-like conductance in lymph node carcinoma cells (Gessener 2005). This conductance displayed most of the characteristics typical of the BK channel, such as a large 200 pS unitary conductance and sensitivity to BK-specific blockers paxilline, iberiotoxin and penitrem A, however the voltage dependence was shifted leftward by as much as 140 mV compared with BK alpha homomultimeric channels in expression systems.

This feature was not readily explicable by any previously known mechanism, and it was subsequently demonstrated that, although the lymph node carcinoma cells expressed the normal splice form of BK $\alpha$ , immunopurification and mass spectrometry of the channel complex revealed a 35 kDa leucine-rich protein, which when knocked down in the tumor cell abolished the leftward shift in the I-V relationship (Yan and Aldrich, 2010). Association of the fragment with BK $\alpha$  was subsequently confirmed via immunoprecipitation following coexpression in HEK293 cells, and its effects on BK $\alpha$  voltage sensitivity were likewise demonstrated by voltage clamp experiments on the same cells (Yan and Aldrich, 2010).

This subunit, and the three others subsequently identified, all share a similar set of structural and functional characteristics. Each has a similar molecular weight, with a single membrane spanning region, an extracellular N-terminus, as evidenced by a cleavable n-terminal extracellular targeting peptide, and a short intracellular C-terminal region (Yan and Aldrich, 2012). All contain a single leucine-rich LRR domain in the extracellular N-terminal region, which in other protein families is implicated in protein-protein interaction. Functionally, all four types of  $\gamma$  subunit appear to have similar effects, differing only in the extent of the hyperpolarising shift conferred. Whilst the expression pattern of these subunits among different tissue subtypes is not yet well known, it is likely that their role is confined primarily to non-excitabile cells, by virtue of this property.

### 3.1.3.3 *Stoichiometry of subunits*

In the initial discovery by immuno-coprecipitation of the  $\beta$ 1 subunit in bovine smooth muscle, the isolated channel complex was found to comprise an octameric assembly of BK $\alpha$  and  $\beta$ 1 subunits in a 1:1 ratio. Thus each alpha subunit can bind to a single  $\beta$  subunit, and the entire assembly can have between 0 and 4  $\beta$  subunits. As a result the

number of  $\beta$  subunits present in each assembly is dependent on the ratio of  $\beta$  to  $\alpha$  expression, and each  $\beta$  present contributes incrementally to the channel properties, as demonstrated in *Xenopus* oocyte by Wang et al (Wang et al 2002), where the beta subunit altered the voltage dependency of the whole cell current in a titration-dependent manner according to the ratio of  $\beta$  to  $\alpha$  mRNA injected. One additional point worthy of consideration in the case of heterologous expression systems is the observation that in the granule cells of dentate gyrus the  $\beta_4$  subunit causes internalisation of the channel assembly from the plasma membrane and sequestration to the endoplasmic reticulum (Shruti et al, 2012). It is not known if this effect is recapitulated in heterologous expression systems, or whether the effect strength is dependent on stoichiometry, but if so it might lead to a bias towards channel complexes containing a lower fraction of beta4 present in the plasma membrane.

The stoichiometry of the more recently discovered  $\gamma$  subunit family is less well characterised, however in terms of contribution to the functional properties of the channel, it has been shown that  $\gamma_1$  exhibits an all-or-none effect: there are no intermediate hyperpolarising shifts dependent on the molar ratio of mRNA injected into *Xenopus* oocytes (Gonzalez-Perez et al, 2014). It is possible that a single  $\gamma_1$  subunit is sufficient to produce the full effect, or it may be that  $\gamma$  subunits form a tetrameric assembly which subsequently associates with the Bk $\alpha$  channel complex.

#### 3.1.3.4 *Alternative splicing*

In addition to the diversity conferred on BK channels by the auxilliary subunits, there is a further source of structural variability in the form of transcriptional modification of the alpha subunit mRNA. A total of 13 alternate exons are present in the human *KCNA1* gene, theoretically leading to thousands of possible splice variants (Beisel et al, 2007). In *C. elegans*, where the combinatorial possibilities number a more manageable 12, all were shown to be expressed endogenously, and under heterologous expression were shown to confer alterations to activation kinetics and calcium sensitivity (Johnson et al, 2011). In mammalian *KCNA1*, a number of studies have shown variations in the properties of the heterologously expressed splice variants, however few have been shown to have much physiological relevance. One exception of note is the STREX exon, which resides at the carboxyl terminus of the BK $\alpha$  molecule. The presence of this exon alters a wide range of channel properties, including enhancement of channel opening (Saito et al, 1997) activation and deactivation kinetics, hormone regulation (Xie and McCobb 1998), and response to cAMP dependent phosphorylation (Tian et al 2001) and oxidation (Erxleben et al 2002). The STREX exon is widely expressed in CNS, and has

been shown to be upregulated in a rat model of temporal lobe epilepsy (Ermolinksy et al 2011), suggesting that the balance of expression between STREX and the zero-splice form might have important physiological consequences in regulating neuronal firing patterns.

## **3.2 Modulation of BK channels**

Aside from voltage and  $\text{Ca}^{2+}$ , BK channels are regulated by a wide range of cellular signalling molecules. These endogenous modulation sources include postranslational modifications such as serine/threonine phosphorylation (Widmer et al, 2003, Yan et al, 2008), palmitoylation (Shipston 2013) and ubiquitination (Liu et al, 2014) as well as direct modulation by small intracellular signals such as  $\text{H}^+$  and  $\text{Mg}^{2+}$  (Brelidze and Magelby, 2004, Zhang et al 2001), CO, membrane lipids (Dopico and Bukiya, 2014), steroids, and haem (Hou et al 2006, Hou et al 2009).

### **3.2.1 Reactive Oxygen/Nitrogen Species**

Reactive oxygen and nitrogen species are generated during normal physiological function, and have been shown to interact with and modulate wide range of cell signalling components including ion channels, and as a result the redox state of the intracellular compartments is under tight homeostatic control. In proteins generally, and ion channels in particular, reactive oxygen and nitrogen species modulate function by reversible oxidation/reduction of the thiol groups on cysteine and methionine residues. Disregulation of such homeostatic mechanisms controlling cellular redox state has been implicated in pathology, including in neurodegenerative disorders such as multiple sclerosis, Parkinsons, and Alzheimers (Pennisi et al 2011). Aside from the importance of redox in pathological conditions, redox-dependent modulation of ion channel function is important for the electrophysiologist, as the artificial intracellular solutions used in patch clamp experiments typically produce a far more oxidising intracellular environment than that of the endogenous cytoplasm.

BK channels in particular have been shown to be affected both by the presence of artificially introduced oxidising and reducing agents, and by oxidative stress. Wang et al (Wang et al 1997) showed that application of the reducing agents glutathione (GSH) and dithiothreitol (DTT) to the cytosolic surface of excised BK macropatches led to an increase in channel activity, whereas sulphhydryl oxidising agents inhibited channel activity, in a manner that persisted following washout, though remained capable of being reversed by reagents that promoted the opposing redox process. DiChiara and Reinhart

(1997) demonstrated that the oxidising agent hydrogen peroxide ( $H_2O_2$ ) caused a reduction in BK channel activity by shifting the voltage dependence to more positive potentials, while DTT produced the opposite effect, and suggested that this phenomenon underlies the 'run-down' effect seen in excised patches. Similar effects on BK channel activity have been observed in rat CA1 pyramidal cells (Soh et al 2001), though other experiments *in vivo* have found an inverted effect, where an oxidising agent DTNB increased BK channel open probability in inside-out patches taken from rat CA1, while GSH had no effect (Gong et al, 2000). A possible explanation for this ambiguity of effect was suggested by Tang et al ( Tang et al, 2001), who showed that the methionine-specific oxidising agent chloramine-T increased BK open probability, whereas cysteine specific reagents such as DNTB decreased channel activity. However this cannot fully explain the *in vivo* results, as DTNB had a facilitative effect on BK channel activity in the experiments described by Gong et al (Gong et al, 2000).

Mammalian neurons are extremely vulnerable to oxidative stress. Hypoxia leads to a variety of effects including depolarisation of the resting membrane potential. It has been hypothesised that this depolarisation is due to oxidative inhibition of  $K^+$  channels, including BK. In support of this hypothesis, Gao and Fung (Gao and Fung, 2002) found that BK channels in hippocampal pyramidal cells of rats exposed to hypoxic conditions for 4 weeks had a lower open probability than those in normal rats, and that this effect was rescued by an oxidising agent, but not by a reducing agent.

Though the precise effects of reactive oxygen/nitrogen species on BK channel function is not fully understood, it remains an important consideration to the researcher, as in other channels redox state has been shown to alter a number of channel properties including kinetics (Ciorba et al, 1999), and could conceivably also affect other properties such as calcium sensitivity and drug binding.

### **3.3 BK channel pharmacology**

A number of pharmacological blockers and activators of BK have been identified, including small molecule blockers such as tetraethylammonium (TEA) and paxilline, scorpion toxins such as charybdotoxin and iberiotoxin, and synthetic activators such as NS1619 and NS19504.

### 3.3.1 Peptide blockers

A number of short-peptide BK channel blockers are known, the majority coming from the  $\alpha$ -kTX family, isolated from the venom of various species of scorpion. These are pore blocking toxins of the cysteine-stabilized  $\alpha/\beta$  family, (C $\alpha/\beta$ ) which reduce K<sup>+</sup> ion flow through the pore by plugging the ion-conducting pathway with a highly-conserved lysine residue (Yu et al 2016). The first blocker used in the characterisation of BK channels was the 37-residue peptide Charybdotoxin (Ctx), isolated from the venom of *Leiurus quinquestriatus*. It possesses an affinity for the BK channel pore in the 50 nM range, but lacks specificity as it also blocks other K<sup>+</sup> conductances including SK (Herman and Erxleben, 1987) and IK (Anderson et al, 1988).

Iberitoxin (Ibtx), another 37-residue peptide with 68% sequence similarity to Ctx, is a specific blocker of BK channels, which also exhibits a higher affinity for BK than Ctx (IC<sub>50</sub> = 2-10 nM). It is also useful in the separation of conductances mediated by  $\beta$ 4 containing channels (eg Brenner et al 2005), as the  $\beta$ 4 subunit confers reduced Ibtx sensitivity (Meera et al, 2000).

There are a number of other toxins with pharmacological utility in the study of BK channels. Limbatustoxin (Lbtx) is very similar in structure to Ibtx, and exhibits similar levels of affinity and selectivity. Slotoxin exhibits differing effects on complexes containing different combinations of alpha and beta subunits as it exhibits different a K<sub>d</sub> depending on the subunit composition (Garcia-Valdez et al 2001). Another  $\alpha$ -KTX peptide, martentoxin, blocks Ibtx-resistant  $\beta$ 4-containing channels with a higher affinity than the BK- $\alpha$  homotetramer (Shi et al, 2008). Additionally a number of toxins from other families can block BK with high specificity and efficacy, including BmP09, a scorpion toxin of a different subfamily of C $\alpha/\beta$ , and natrin, a 220 residue peptide isolated from snake venom (Wang et al, 2005).

### 3.3.2 Small molecule blockers

Aside from the toxins described above, there are a number of small molecular blockers of BK channels, including tetraethylammonium (TEA), a promiscuous K<sup>+</sup> channel blocker which blocks BK channels in a voltage-dependent manner, and a number alkaloids that exhibit BK-specific block, including the indole diterpenes paxilline (Zhou et al 2014) and penitrem A (Asano et al, 2012). which act as allosteric modulators.

### 3.3.3 Activators

A wide range of compounds with BK activating properties have been identified, including steroid hormones such as 17 $\beta$ -estradiol (Valverde et al 1999) and synthetic analogues such as tamoxifen (Dick et al, 2001), arachidonic acid and metabolites of cytochrome P450, epoxygenase, and lipoxigenase (Feletou 2009), and antiepileptic drugs such as chlorzoxazone (Liu et al 2003) and zonisamide (Huang et al 2007). Additionally, a number of synthetic small molecule BK-specific openers have been developed. The first of these was NS004, developed by Neurosearch (Olesen 1994a), but a more recently developed compound NS1619 (Olesen 1994b) is the most widely used in functional studies of the BK channel. NS1619 is not strictly an opener, having no effect in the absence of Ca<sup>2+</sup>, but instead leads to an increase in Ca<sup>2+</sup> sensitivity, producing a leftward shift in the  $V_{1/2}$  of activation of around 25 mV in response to a 10  $\mu$ M concentration. The precise site and of action is not known: the S6/RCK linker is known to be necessary for function (Gessner 2012), but whether this is a binding site or just a portion of the channel necessary for the conformational changes leading to activation is uncertain, though this region has been implicated in transmission of the Ca-dependent conformational changes in the RCK domain to the opening of the gate (Jiang et al, 2002) which would suggest the latter interpretation to be sufficient.

Despite its widespread use, NS1619 exhibits a number of disadvantages as a pharmacological tool, including relatively poor potency, and off-target effects such as inhibition of VGCCs. As a result, a number of analogues have been developed in an attempt to redress these issues, including NS11021 (Bentzen 2007) and NS19504 (Nausch 2014). The latter has been shown to activate BK with an EC<sub>50</sub> of 11  $\mu$ M, with 10  $\mu$ M producing a 60 mV leftward shift of the activation  $V_{1/2}$  in heterologously expressed hBK $\alpha$  channels. These activators have been demonstrated to work in both heterologous expression systems and in a physiological setting (Bentzen et al 2007, Bentzen et al 2009, Kun et al, 2009, Nausch et al 2014), but have yet to be fully characterised, for example in terms of their interaction with channels containing beta subunits.

## 3.4 Physiological role of BK channels

The wide range of BK channel configurations conferred by subunit composition, transcriptional and post-translational modifications leads to a diverse range of physiological functions. In ion transporting cells such as the kidney, BK channels contribute to electrolyte homeostasis by providing a high throughput pathway for K<sup>+</sup> ions (Filosa et al, 2006), and to airway hydration by airway epithelial cells, an effect that relies

on the constitutive activity of the channel, possibly facilitated by gamma subunits (Manzanares et al, 2014). BK channels are especially widely expressed in excitable cells, and are involved in processes such as hormone release in adrenal chromaffin cells (Vergara et al, 1998), vascular smooth muscle (Nelson et al, 1995, Jaggar et al, 2000), and tuning of auditory hair cells (Fettiplace et al, 1999).

### **3.4.1 Role of BK in neurons**

In neurons, BK channels open in response to depolarisation and  $\text{Ca}^{2+}$  influx, leading to  $\text{K}^+$  efflux and hyperpolarisation of the membrane. This general schema is utilised in different ways according to cell type and BK subunit composition, but the main effect categories are contributions to the firing threshold, modulation of action potential (AP) width, and contribution to the fast phase of the afterhyperpolarisation (Adams et al, 1982, Lancaster and Nicoll, 1987). Additionally the above can have further downstream effects on the activity of other channels ( eg. Brenner et al, 2005).

During action potential generation, BK is responsible for tuning the duration of the action potential by altering the rate of membrane repolarisation. Depolarisation leads to the activation of VGCCs, and the coincidence of depolarisation and  $\text{Ca}^{2+}$  entry leads to BK activation and faster repolarisation.

Differing subunit composition of the BK channel population in different neuronal subtypes can lead to different firing behaviour. For example in burst firing in hippocampal CA1 pyramidal cells, BK contributes to the firing rate of the early action potentials in a burst, but not the later ones (Gu et al, 2007). This is because CA1 neurons contain a high proportion of inactivating ( $\beta 2$  containing) BK channels, and channels which initially contribute to the fast phase of the afterhyperpolarisation (fAHP) become inactivated by sustained firing. This in turn affects firing rate, as when BK is active the more pronounced fAHP leads to faster relief of voltage-dependent inactivation in the voltage gated sodium channels, permitting more rapid firing, but as the BK channel population becomes inactivated, the fAHP decreases in amplitude and recovery of voltage gated sodium channels is less rapid.

Conversely, in other cell types, such as the granule cells of the dentate gyrus, the presence of channels containing the  $\beta 4$  subunit lead to slower kinetics of BK activation, effectively inhibiting their participation in rapid membrane repolarisation, as well as inhibiting the activation of other  $\text{Ca}^{2+}$  sensitive conductances.  $\beta 4$  knockout mice displayed epileptiform activity and increased firing rate and reduced inter-spike interval,

as well as reduced spike frequency adaptation, and sharper action potentials (Brenner et al 2005). Additionally, the AHP was smaller in knockouts. Application of 10  $\mu$ M paxilline to the wild type animals had no effect on firing rate, suggesting that BK in this case does not contribute directly to the firing rate. Instead, blockade of SK channels by apamin or UCL1684 in the wild type mice increased firing rate to a level equivalent to that observed in the knockout.

Thus the role of  $\beta$ 4-containing BK channels in DG granule cells is to prevent BK activation during the millisecond timeframe of membrane repolarisation, thereby leading to action potential broadening and a greater degree of SK channel activation, which drives mAHP-mediated adaptation, and an effective low pass filtering of DG granule inputs. This effect makes sense in the context of preventing seizures, as granule cells represent the main site of cortical input to the hippocampal formation.

### **3.5 Role of BK channels in pathology**

BK channels are implicated in a wide variety of pathological conditions. A number of BK channelopathies exist, in which mutations at one or more points in the channel protein lead to dysfunction. Channelopathies of BK underly conditions such as epilepsy and paroxysmal dyskinesia (Lorenz et al 2007, Du et al 2005), and BK dysfunction has also been implicated in conditions as diverse as diabetes, cardiovascular disease (Rusch, 2009), neurological damage following stroke (Koide et al, 2012) and cancer (Ge et al 2014). Recently, a growing body of evidence suggests some involvement of BK in Fragile X syndrome.

#### **3.5.1 Fragile X**

Fragile X syndrome (FXS) is one of the most commonly occurring genetic causes of learning disability and autism. It has a frequency of around 1 in 4000 males, and 1 in 6000 females and around 1 in 250 females are carriers. In approximately 25% of cases it also presents with childhood seizures (Hagerman and Stafstrom, 2009).

Pathology results from the expansion of a CGG repeat sequence in the 5' UTR of the FMR1 gene, leading to hypermethylation of this region which causes the FMR1 gene to be silenced, and the loss of its protein product, FMRP.

FMRP is an mRNA-binding protein that is ubiquitously expressed, with particular abundance in the CNS, where it is present in both neurons and glia. It binds to a wide

variety of mRNA targets and acts as a negative regulator of their translation (Wang et al, 2012). In the central nervous system, much of the work performed in FMR1  $-/-$  mice has focused on widespread alterations to the expression of postsynaptic proteins, but FMRP has also been implicated in presynaptic physiological changes, including elevated levels of  $\text{Ca}^{2+}$  influx and increased neurotransmitter release during stimulation in FMR knockout mice (Deng et al, 2011). Furthermore, recordings from the CA3 region of hippocampus in FMR1  $-/-$  mice has shown a broadening of action potential (AP) width during high frequency spiking, which was rescued by inclusion of FMRP in the pipette, and replicated in WT mice by the introduction of an FMRP antibody (Deng et al 2013). The effect appeared to not be due to modulation of expression level as it persisted in the presence of translation inhibitors. The AP broadening effect caused by the FMRP antibody in wild type mice was suppressed by the introduction of the BK-specific blockers paxilline and iberiotoxin, suggesting that the changes in AP width caused by FMRP are due to a reduction in the BK channel current, and abolished the differences in AP duration between FMRP  $-/-$  and WT mice.

The mechanism for FMRP dependent upregulation of BK activity appears to be that FMRP directly binds the BK channel and modulates the channel's  $\text{Ca}^{2+}$  sensitivity. In the Deng experiment described above, the differences in AP width and fAHP amplitude between FMRP  $-/-$  and WT mice were abolished by the addition of 10 mM BAPTA to the pipette.

A previous study using co-immunoprecipitation of FMRP and FLAG-tagged BK $\alpha$  (Brown et al, 2010) has demonstrated that FMRP does not interact directly with the BK $\alpha$  subunit. However FMRP does coprecipitate with the  $\beta 4$  subunit (Deng et al 2013), the main  $\beta$ -subunit present in CA3 pyramidal cells (Torres et al, 2007). Additionally,  $\beta 4$   $-/-$  mice do not exhibit AP broadening in response to perfusion of FMRP antibody (Deng et al 2013), and FMR1/ $\beta 4$  double knockout mice have phenotypes more similar to WT mice than FMR1 knockouts, in terms of BK channel open probability and action potential duration (Deng and Klyatchko, 2016). It therefore appears that the FMRP-dependent changes to action potential duration observed in FMR1  $-/-$  mice are dependent on interaction with the  $\beta 4$  subunit, leading to an upregulation of BK channel calcium sensitivity.

### **3.6 VSN-16R: a putative BK channel enhancer with therapeutic possibilities**

A compound, VSN-16R, developed by the Selwood Lab (UCL) appears to rescue cognitive deficits in behavioural assays of FMRP  $-/-$  mice (Selwood, unpublished), as

well as having an antispastic effect in the EAE mouse model of multiple sclerosis (Baker, Pryce, Selwood, 2015 abstract). VSN-16R is an anandamide derivative, however it has been shown via in vitro assays to not bind any cannabinoid receptor, save for the predominantly endothelial CBe receptor. Furthermore, in voltage clamp experiments conducted in the EA.hy926 endothelial cell line, VSN-16R induces a large, voltage-dependent whole cell current that is inhibited by 10  $\mu$ M paxilline, a BK-specific blocker. The antispastic effects of VSN-16R in the EAE mouse model are also absent in the presence of paxilline. It is therefore possible that VSN-16R acts as an enhancer of BK channel activity, either via interaction with the alpha subunit, or perhaps more enticingly given its effect on FMRP knockouts, in a beta-4 dependent manner.

### **Aim of the project**

Our project aimed to determine whether VSN-16R acts as a direct enhancer of BK channels, either on the homotetrameric BK $\alpha$  assembly, or in a manner dependent on the presence of one of the  $\beta$  subunits. In order to address this question, we used whole cell recordings of BK channels heterologously expressed in HEK 293 cells. Additionally, we attempted to characterise for the first time the effect of the BK channel activator NS19504 on heterologously expressed BK channels containing  $\beta$  subunits, and investigated whether the effect of VSN-16R on BK channel function was affected by the intracellular redox state.

## Chapter 4. Results

This section of the thesis presents evidence from whole-cell voltage clamp experiments, the primary goal of which was to determine whether the drug VSN-16R functions as an activator of BK channels.

In the EA.hy926 endothelial cell line, VSN-16R applied extracellularly at a concentration of 10  $\mu$ M, led to the activation of a whole-cell current that was inhibited by 10  $\mu$ M paxilline, a specific blocker of BK channels (Bondarenko et al, unpublished data). As a result of this, it was hypothesised that the capacity of VSN-16R to rescue both FMRP  $-/-$  mice behavioural and cognitive deficits and spasticity in an EAE animal model of multiple sclerosis might be due to its action on BK channels. In order to test this hypothesis, it was decided to examine the compound's effect on BK channels formed by the rat BK alpha subunit (rBK- $\alpha^0$ ) in a heterologous expression system, in this case the HEK 293 cell line, by performing whole-cell patch clamp recordings.

### 4.1 Expression of rBK- $\alpha^0$ channels in HEK 293 cells, and characterisation of Ca<sup>2+</sup> sensitivity

The zero-intron splice  $\alpha$  subunit of the rat BK channel (rBK- $\alpha^0$ ) was expressed in HEK 293 cells by transient transfection, using the calcium phosphate method. Transfection efficiency, as estimated by the presence of eGFP expression, varied between 50% and 80%. A large, non-inactivating, voltage-dependent conductance was observed in >95% of green cells patched. A first set of experiments was performed using intracellular solutions containing three different concentrations of free Ca<sup>2+</sup>.

In the whole cell patch clamp configuration, the cell was held at -90 mV, and a family of 40 ms-long voltage steps was delivered, between -100 and +100 mV in 10 mV steps, with an inter-step interval of 8 s. The results are summarised in Figure 4.1. Panel (a) shows current response traces obtained in response to four different voltage pulses from individual representative cells recorded with each of the three calcium concentrations. The currents displayed a number of features typical of BK channels: they exhibited voltage dependency, rapid activation kinetics (time constant = 2.68 ms  $\pm$  0.15 ms, n = 15), and were non-inactivating. Additionally, the high degree of noise observed in the current during the voltage step was likely due to the high unitary conductance of the individual channels, which is the principal characteristic of BK, from which the channel's name is derived. It was more pronounced in the cells recorded with zero (Figure 4.1a, red traces) and 200 nM calcium (Figure 4.1a, blue traces) than with 1  $\mu$ M calcium (Figure

4.1a, yellow traces), presumably because the open probability is lower in the former. The averaged current voltage relationships for cells recorded at each intracellular  $\text{Ca}^{2+}$  concentration is shown in Figure 4.1 (b). At all concentrations tested, the current observed was clearly voltage dependent, but the higher the free  $\text{Ca}^{2+}$  concentration in the intracellular solution, the larger the current produced for a given voltage, and the lower the voltage required to begin activating the current. The fact that a current was elicited at higher voltages even in the absence of intracellular free  $\text{Ca}^{2+}$ , is consistent with the observation that the BK channel is strictly speaking a voltage-gated channel that is modulated by calcium, and is capable of being opened by voltage alone, even in the absence of calcium (Orio 2002).

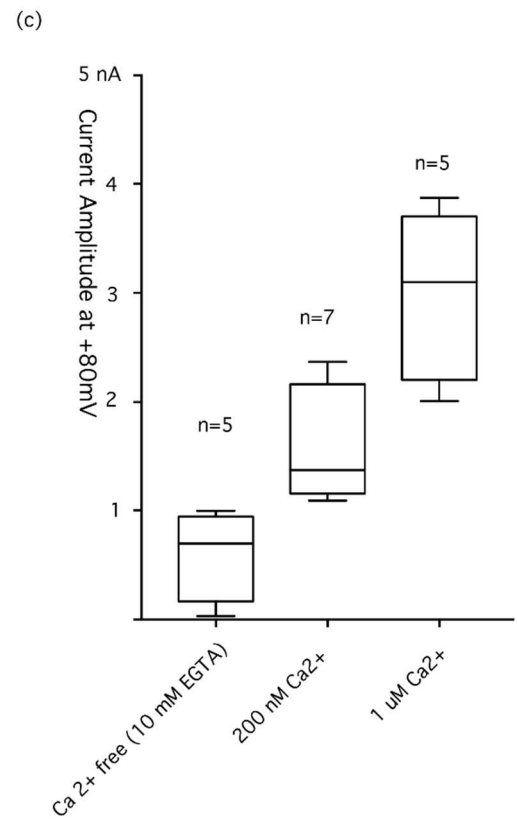
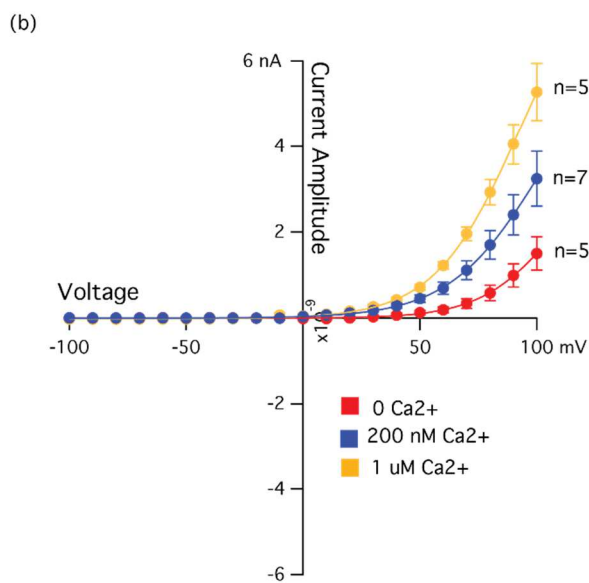
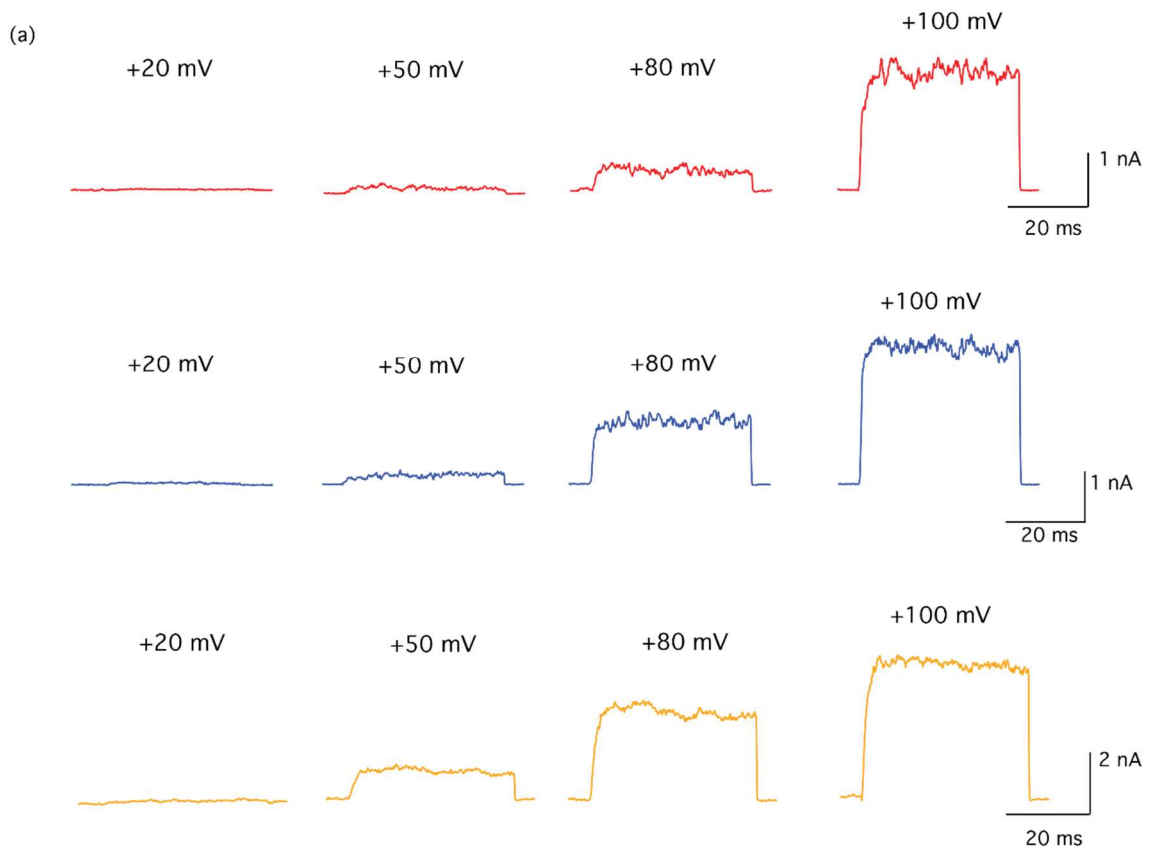


**Figure 4.1. Recordings from HEK293 cells transfected with rBK $\alpha^0$  using different concentrations of intracellular Ca<sup>2+</sup>**

- (a) *Current traces from representative cells recorded in the whole cell patch clamp configuration, using intracellular solution containing 0 (top, red traces), 200 nM (middle, blue traces) and 1  $\mu$ M (bottom, yellow traces) free  $\text{Ca}^{2+}$ . Voltage steps to the values shown above each trace were made from a holding voltage of -90 mV for a period of 40ms.*
- (b) *Averaged I-V curves in response to the voltage families described in (a). Circular markers denote mean current at any given voltage, error bars denote SEM. Trend line is the least-squares fit of the Boltzmann function to the data.*
- (c) *Box-whisker plot of the current amplitudes measured in response to a step to +90 mV for each of the three intracellular  $\text{Ca}^{2+}$  concentrations.*

One of the limitations of the whole cell voltage clamp technique in measuring BK channel activity at low calcium concentrations is that it is not possible to produce a saturating IV curve within a physiologically relevant voltage range. At concentrations of  $\text{Ca}^{2+}$  under 10  $\mu$ M, very high voltages are needed to saturate the I-V relationship, such that the current response to further voltage increases reaches a plateau. This plateau phase is required in order to permit the fitting of the Boltzmann function to the I-V curve in order to determine the voltage of half-maximal activation ( $V_{1/2}$ ). Highly depolarising voltage steps are detrimental to integrity of cell membranes and hence the stability of the gigaOhm seal. Furthermore due to the high degree of overexpression and large unitary conductance, currents recorded at highly depolarising voltages are large, and suffer increasingly from voltage errors, to the point at which they cannot effectively be voltage clamped.

As a result of this, it is difficult to directly quantify the size of the calcium dependent shift in the voltage dependency of the channel population. The standard method for quantifying such a shift is to fit a Boltzmann curve to the  $I/I_{\text{max}}: V$  relationship in order to determine  $V_{1/2}$ : the voltage at which half-maximal activation is achieved. In conditions where the channel does not saturate, this fit cannot be reliably achieved. Therefore although our results imply a leftward shift in the  $V_{1/2}$  of activation with increasing calcium, this cannot be determined quantitatively from the data, except by examining the interaction of voltage and drug effects in the 2-way ANOVA.

## **4.2 Effects of paxilline and TEA on the BK current**

The current produced by the alpha subunit of the BK channel is known to be blocked with a high degree of specificity by the alkaloid paxilline (Knaus et al 1994). In order to confirm the identity of the current produced by the heterologously expressed rBK $\alpha^0$  construct, paxilline was applied to the cells during whole-cell patch clamp recordings. Bath application of 10  $\mu$ M paxilline produced a rapid, non-reversible inhibition of the

current in 10 out of 10 cells tested (Figure 4.2a). The inhibition was almost complete (mean residual current =  $9.1\% \pm 2.2\%$  of baseline; Figure 4.2c), though typically a small, voltage dependent and inactivating conductance remained following application (Figure 4.2b). The mean amplitude of this residual current was  $192 \pm 65$  pA at +90 mV. It is likely that this is a voltage dependent K<sup>+</sup> conductance endogenous to the HEK 293 cell line.

The rBK $\alpha^0$ -mediated current was also fully inhibited by bath application of 5 mM TEA in 7 out of 7 cells tested (mean residual current  $7.2\% \pm 2.9\%$ , Figure 4.2a, b, c), and there was no significant difference between the degree of inhibition by paxilline and that of TEA (2-tailed t-test,  $p=0.65$ , Figure 4.2c). However, unlike paxilline, inhibition by TEA was reversible in 6 out of 7 cells.

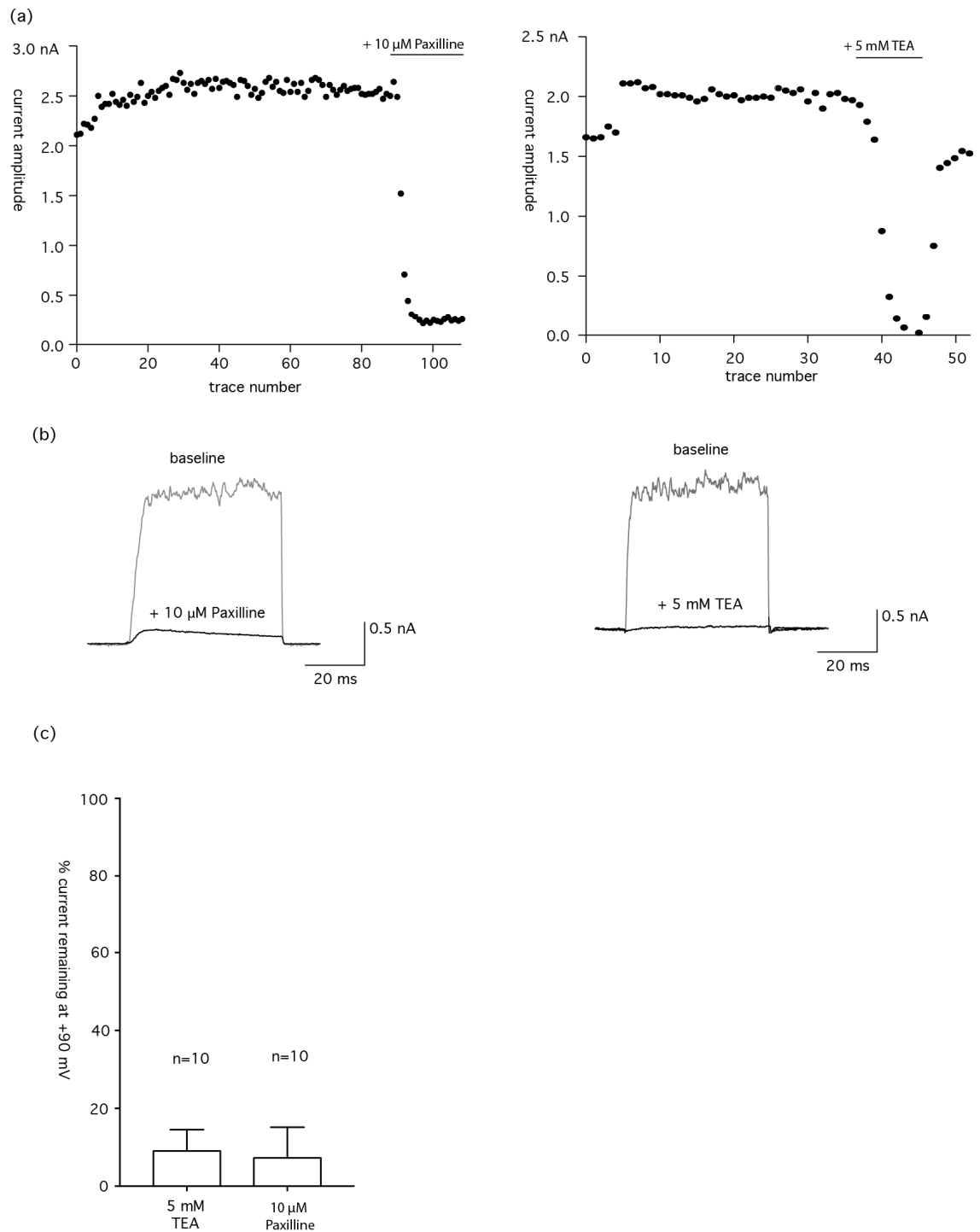


**Figure 4.2. Effect of paxilline and TEA on rBK $\alpha^0$  in HEK293 cells**

- (a)** *Representative timecourses of the steady state current response to a series of 50 ms-long voltage steps to +90 mV from a holding potential of -90 mV. Left hand plot shows the effect of 10  $\mu$ M paxilline on the current, right hand plot shows the effect of 5 mM TEA. Voltage steps were delivered at 10 s intervals.*
- (b)** *Representative traces from the time-course plots shown in (a). Left hand traces show the effect of 10  $\mu$ M paxilline, right hand traces show the effect of 5 mM TEA.*
- (c)** *Bar diagram showing the percentage of the whole cell current remaining in response to a 50 ms-long voltage step to +90 mV, in the presence of 10  $\mu$ M paxilline or 5 mM TEA.*

### 4.3 Effect of NS19504 on currents mediated by the heterologously expressed rBK $\alpha^{\emptyset}$

The compound NS19504 (5-((4-bromophenyl)methyl)-1,3-thiazol-2-amine) is a known activator of the alpha subunit of the current mediated by fully spliced, human BK channel alpha subunits (Nausch et al 2014). It has been shown to produce a leftward shift in the  $V_{1/2}$  of activation at concentrations of 10  $\mu$ M. This property makes it a good candidate for a reference compound for our experimental conditions and for comparison to VSN-16R. To test the effect of NS19504 on HEK 293 cells expressing the rat BK channel isoform, rBK $\alpha^{\emptyset}$ , 10  $\mu$ M of the compound was applied extracellularly, while the time course of any current changes due to the compound was monitored by delivering a 40 ms voltage step to +90 mV from a holding potential of -90 mV, at 10 s intervals. The protocol was run for around 5 minutes in order to permit equilibration of the intracellular solution inside the cell, and to establish a stable baseline current. The compound was then applied continuously until a new stable state was reached, and then 10  $\mu$ M paxilline was applied to abolish the BK current. Additionally, to assess the I-V relationship, families of traces acquired at different voltages, consisting of 40 ms-long steps from -90 mV to between -100 and +100 mV in 10 mV intervals, were obtained at the end of baseline acquisition, at the end of NS19504 application, and following inhibition by paxilline.

Figure 4.3a shows the effect of the compound on the current responses to a family of voltage steps in a typical cell. In 5 out of 5 cells, NS19504 increased the size of the current and the current was largely inhibited by 10  $\mu$ M paxilline. The activation due to NS19504 occurred relatively rapidly, as can be seen from the timecourse (Figure 4.3b). Mean time to plateau was 162 s  $\pm$  16 s (n=5).

The averaged IV curves for all cells, before and after application of NS19504, are shown in Figure 4.3 (d). As with Figure 4.1, in our whole-cell recording conditions, it was not possible to reach saturating values of the current response in the voltage range tested, and it was therefore impossible to measure a shift in  $V_{1/2}$  directly. However, at +90 mV, NS19504 increased current amplitude to 329%  $\pm$  52% of baseline, while at +50 mV the current was increased to 696%  $\pm$  217% of baseline. In the 2-way repeated measures ANOVA, the effect of NS19504 was significant (Table 4.1, p=0.0013, n=5), and there was a significant interaction between the effects of voltage and NS19504 (p=0.002). These results suggest that NS19504 acts as an activator of the currents mediated by the rat homologue of BK- $\alpha$ .

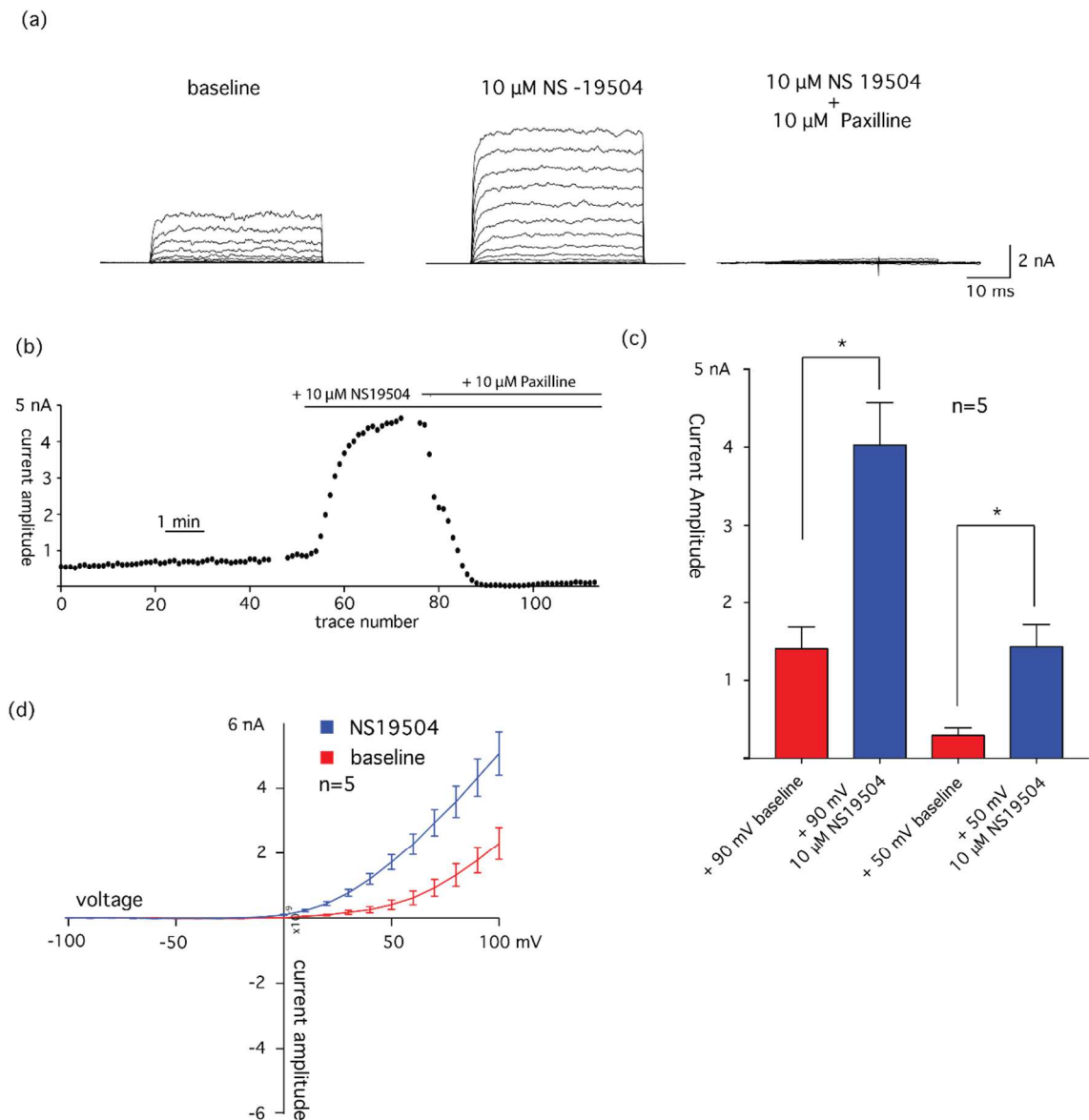


**Figure 4.3. Effect of NS19504 on rBK $\alpha^0$  - mediated currents in HEK293 cells**

- (a) *Current responses from a representative cell to a family of 40 ms-long voltage steps to potentials between -100 and +100 mV, in 10 mV increments, from a holding potential of -90 mV. Leftmost traces shows current responses under baseline conditions, middle traces after application of 10  $\mu$ M NS-19504, right hand traces after co-application of 10  $\mu$ M NS-19504 and 10  $\mu$ M paxilline.*
- (b) *Timecourse of the steady-state current response to a series of 40 ms-long voltage steps to +90 mV from a holding potential of -90 mV for the cell shown in (a). Voltage steps were delivered in 10 s intervals. X-axis shows trace number, Y-axis shows current amplitude in nA. Horizontal bars denote the timing and duration of application of NS-19504 and paxilline.*
- (c) *Bar diagram showing the effect of NS19504 on whole cell current amplitude in response to voltage steps to +90 mV and +50 mV. Error bars show SEM, n=5.*
- (d) *Averaged I-V curves in response to the voltage families described in (a). Bar heights denote mean, error bars denote SEM. Trend line is the least-squares fit of the Boltzmann function to the data.*

**Table 4.1. Effect of NS19504 on currents mediated by rBK $\alpha$** 

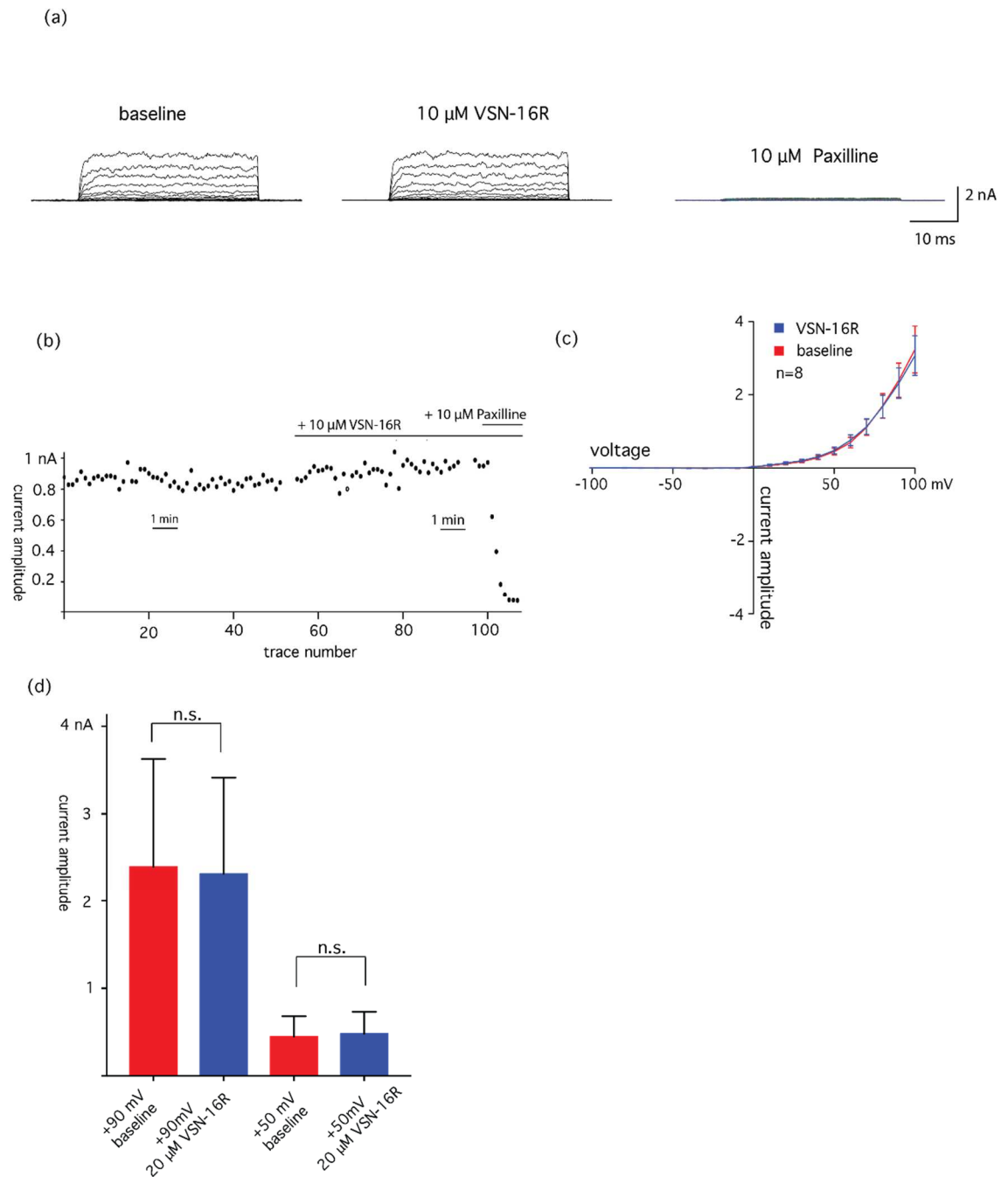
	SS	DF	MS	F (DFn, DFd)	P value
Voltage (50 mV vs. 90 mV)	2.41E-17	1	2.41E-17	F (1, 6) = 57.48	P=0.0003
NS19504	2.48E-17	1	2.48E-17	F (1, 6) = 32.34	P=0.0013
Interaction: voltage x NS19504	3.86E-18	1	3.86E-18	F (1, 6) = 25.21	P=0.0024
	Source of Variation	% of total variation	P value		
	voltage	33.32	0.0003	***	
	NS19504	34.32	0.0013	**	
	Interaction: voltage x NS-19504	5.34	0.0024	**	

Table shows 2-way ANOVA with factors Voltage (+50 vs +90 mV) and NS19504 (baseline vs. + 10  $\mu$ M). Abbreviations: SS= , DF= degrees of freedom, MS= Mean square of treatment effect, F(DFn,DFd)=F statistic based on the degrees of freedom of the treatment (DFn) and error (DFd), values given in parentheses after the F statistic.

#### 4.4 Effect of VSN-16R on currents mediated by the heterologously expressed rBK $\alpha$

To test the hypothesis that VSN-16R acts as an enhancer of BK- $\alpha$  channel activity, experiments were performed in which 20  $\mu$ M of VSN-16R was added extracellularly to HEK 293 cells expressing rBK $\alpha$ . Experiments conducted by Prof. Selwood's collaborators suggested that, in the EA.hy926 cell line, a concentration of 20  $\mu$ M VSN-16R was sufficient to activate a paxilline-sensitive current. The experiments were performed as described above for NS19504. When VSN16-R was applied for 7-15 minutes, no noticeable change in current amplitude was observed, as shown by the time-course of current responses to depolarising steps to +90 mV shown in Figure 4.4b. Figure 4.4a shows the effect of the compound on the current responses to a family of voltage steps in a representative cell. In contrast to the effects seen with NS19504, VSN-16R does not appear to alter the current amplitude or activation kinetics noticeably. Activation time constant for a voltage step to +90 mV at baseline was  $2.36 \pm 0.34$  ms, compared to  $2.65 \pm 0.59$  ms after application of VSN-16R. This difference was not significant (paired 2-tailed t-test  $p=0.41$ ,  $n=7$ ). Comparison of the current responses before and after 7-15 minutes of VSN16-R application shows that at +90 mV, VSN-16R decreased the current to  $97.8\% \pm 2.8\%$  of baseline, while at +50 mV, VSN-16R increased

the current to  $107\% \pm 3.2\%$  of baseline (Figure 4.4c). Neither of these changes were statistically significant (2-Way repeated measures ANOVA, Table 4.2,  $p=0.62$ ,  $n=7$ ). Additionally, the averaged IV curves overlap almost completely (Figure 4.4d). It is therefore apparent that VSN-16R does not act as an enhancer of homomeric channels formed from rBK $\alpha^0$  subunits under our experimental conditions.



**Figure 4.4. Effect of VSN-16R on rBK $\alpha^0$  - mediated currents in HEK293 cells**

(a) *Representative current traces, taken from a single cell in response to a family of 50 ms-long voltage steps to potentials between -100 and +100 mV, in 10 mV increments, from a holding potential of -90 mV. Left traces show current responses under baseline conditions,*

middle traces after application of 20  $\mu\text{M}$  VSN-16R, right hand traces responses to 20  $\mu\text{M}$  VSN-16R and 10  $\mu\text{M}$  paxilline.

- (b) Time-course of current amplitudes from the cell shown in (a) showing response of the whole cell current to a series of 50 ms-long voltage steps, delivered at 10 s intervals, to +90 mV from a resting potential of -90 mV for the cell shown in (a). X-axis shows trace number, Y-axis shows current amplitude in nA. The timing and duration of application of VSN-16R and paxilline are shown by horizontal bars.
- (c) Bar diagram showing the mean effect of VSN-16R on whole cell current amplitudes in response to voltage steps to +90 mV and + 50 mV. Error bars show SEM, n=8.
- (d) Averaged I-V curves in response to the voltage pulse families described in (a). Bar heights denote mean, error bars denote SEM. Trend line is the least-squares fit of the Boltzmann function to the data, n=8.

**Table 4.2. 2-way repeated measures ANOVA of the effect of VSN16-R on currents mediated by rBK $\alpha^{\delta}$**

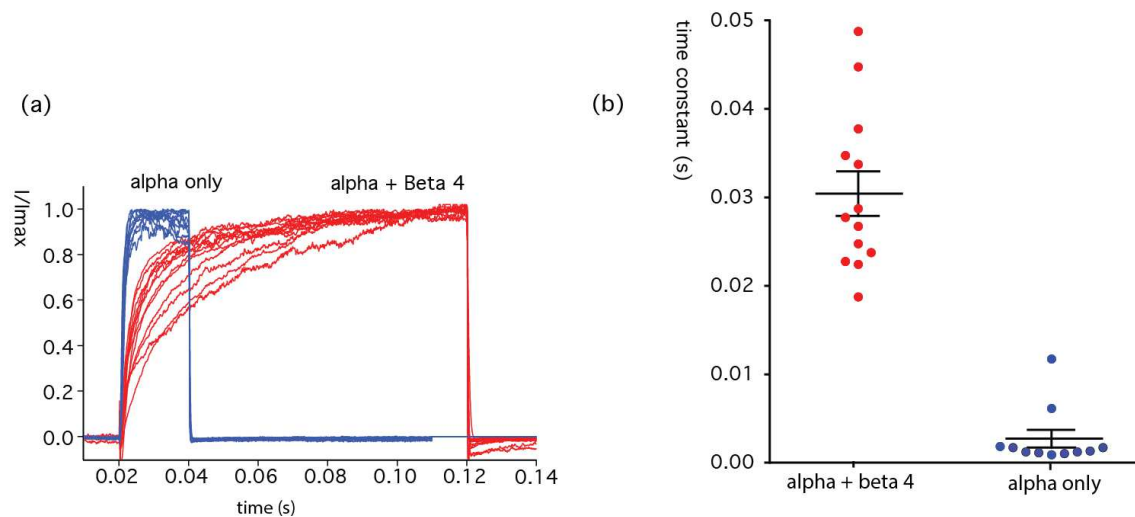
	SS	DF	MS	F (DFn, DFd)	P value
Voltage (50 mV vs. 90 mV)	2.50E-17	1	2.50E-17	F (1, 6) = 25.89	P=0.0022
VSN-16R	4.50E-21	1	4.50E-21	F (1, 6) = 0.2684	P=0.6230
Interaction: voltage x VSN-16R	2.25E-20	1	2.25E-20	F (1, 6) = 0.9601	P=0.3650
	Source of Variation	% of total variation	P value		
	Voltage	59.48	0.0022	**	
	VSN-16R	0.01069	0.623	ns	
	Interaction: voltage x VSN-16R	0.05335	0.365	ns	

Table shows 2-way ANOVA with factors Voltage (+50 vs +90 mV) and VSN-16R (baseline vs. + 10  $\mu\text{M}$ ). Abbreviations: SS= , DF= degrees of freedom, MS= Mean square of treatment effect, F(Dfn,DFd)=F statistic based on the degrees of freedom of the treatment (DFn) and error (DFd), values given in parentheses after the F statistic.

#### **4.5 Effect of NS19504 and VSN-16R on currents mediated by heterologously expressed rBK $\alpha^{\emptyset}$ + $\beta$ 4 channel complexes**

Although VSN-16R appears to have no effect on the currents mediated by homomeric BK- $\alpha$  channels, it is possible that its enhancing effect is dependent on the presence of one or more  $\beta$  subunits as part of the BK channel complex. In particular, the  $\beta$ 4 subunit is not only widely expressed in neurons (Torres 2007) and in the EA.hy926 cell line (Bondarenko et al, unpublished), but also has been implicated as a target for the interaction between FMRP and BK in hippocampal pyramidal cells (Deng et al 2013, Deng and Klyachko 2016). It is therefore possible that the rescue of behavioural and cognitive abnormalities in FMR1  $-/-$  mice by VSN-16R is mediated by interaction of this drug with BK channels containing the  $\beta$ 4 subunit.

In order to test this hypothesis, HEK 293 cells were transfected with both rBK $\alpha^{\emptyset}$  and hBK- $\beta$ 4 subunit cDNA in a ratio of 1:4. Figure 4.5a shows a set of normalised current traces, each averaged from 10 responses to a +90 mV voltage step in a single cell, from cells containing only rBK $\alpha^{\emptyset}$  (n=11) and cells containing rBK $\alpha^{\emptyset}$  and hBK- $\beta$ 4 (n=13). For cells containing  $\beta$ 4, the mean time constant of activation was  $30.6 \pm 2.5$  ms (n = 13), more than an order of magnitude higher than that of cells containing only rBK $\alpha^{\emptyset}$  ( $2.8 \pm 1.0$  ms, n=11, 2-tailed T-test  $p < 0.0001$ ) (Figure 4.5b).



**Figure 4.5. Functional expression of BK channel complexes containing rBK $\alpha^{\emptyset}$  and hBK- $\beta$ 4 subunits**

- (a) *Comparison of normalised current traces from HEK 293 cells expressing rBK $\alpha^{\emptyset}$  and rBK- $\alpha^{\emptyset}$  with hBK- $\beta$ 4. Each trace on the graph represents the averaged current response of a single cell to a series of 10 voltage steps to +90 mV from a holding potential of -90 mV. Duration of step in the rBK $\alpha^{\emptyset}$  traces is 20 ms, that of rBK $\alpha^{\emptyset}$  +hBK- $\beta$ 4 traces is 100 ms. The X-axis denotes time in seconds, the Y axis denotes I/I<sub>max</sub>.*
- (b) *Comparison of the activation time constants ( $\tau$ ) for the cells shown in (a).  $\tau$  was determined for each cell by fitting a double exponential to each averaged trace and treating the longer of the two as the time constant of activation. Y axis shows  $\tau$  in seconds. Bars denote mean and SEM.*

It is therefore apparent that the co-transfection led to the functional expression of BK channels containing the  $\beta$ 4 subunit.

Although NS19504 activates BK- $\alpha$  homomeric channels, there are as yet no data on its effects on BK channels containing any of the  $\beta$  subunits. We therefore conducted experiments to determine the effect of the compound on currents mediated by rBK $\alpha^{\emptyset}$  + hBK- $\beta$ 4 channel complexes in HEK 293 cells.

The effects of bath application of 10  $\mu$ M NS19504 are summarised in Figure 4.6.

Figure 4.6a shows the effect of the compound on the current responses to a family of 200 ms-long voltage steps from -90 mV to between -100 mV and +100 mV in 10 mV steps, in a representative cell. In 4 out of 4 cells, NS19504 increased the amplitude of the current, and the entirety of the current was inhibited by 10  $\mu$ M paxilline (Figure 4.6b). Figure 4.6c summarises the effect on current amplitude at +90 mV and +50 mV. The

mean current amplitude at +90 mV increased to  $410\% \pm 95\%$  of baseline, whereas at +50 mV, NS19504 increased current amplitude to  $682\% \pm 280\%$ . A 2-way repeated measures ANOVA was conducted on the effect of voltage and NS19504 (Table 4.3, n=5). The effect of NS19504 was significant ( $p=0.0007$ ), and there was a significant interaction between voltage and NS19504 ( $p=0.016$ ). These results suggest that the effect of NS19504 on current amplitude in heteromeric channels formed from BK- $\alpha$  and BK- $\beta$ 4 subunits is similar to its effect on the homomeric BK- $\alpha$  channel. Again our results imply some degree voltage dependence in the effect of NS19504, though as before it is impossible to quantify this due to the lack of current saturation across the voltage range tested (Figure 4.6d).

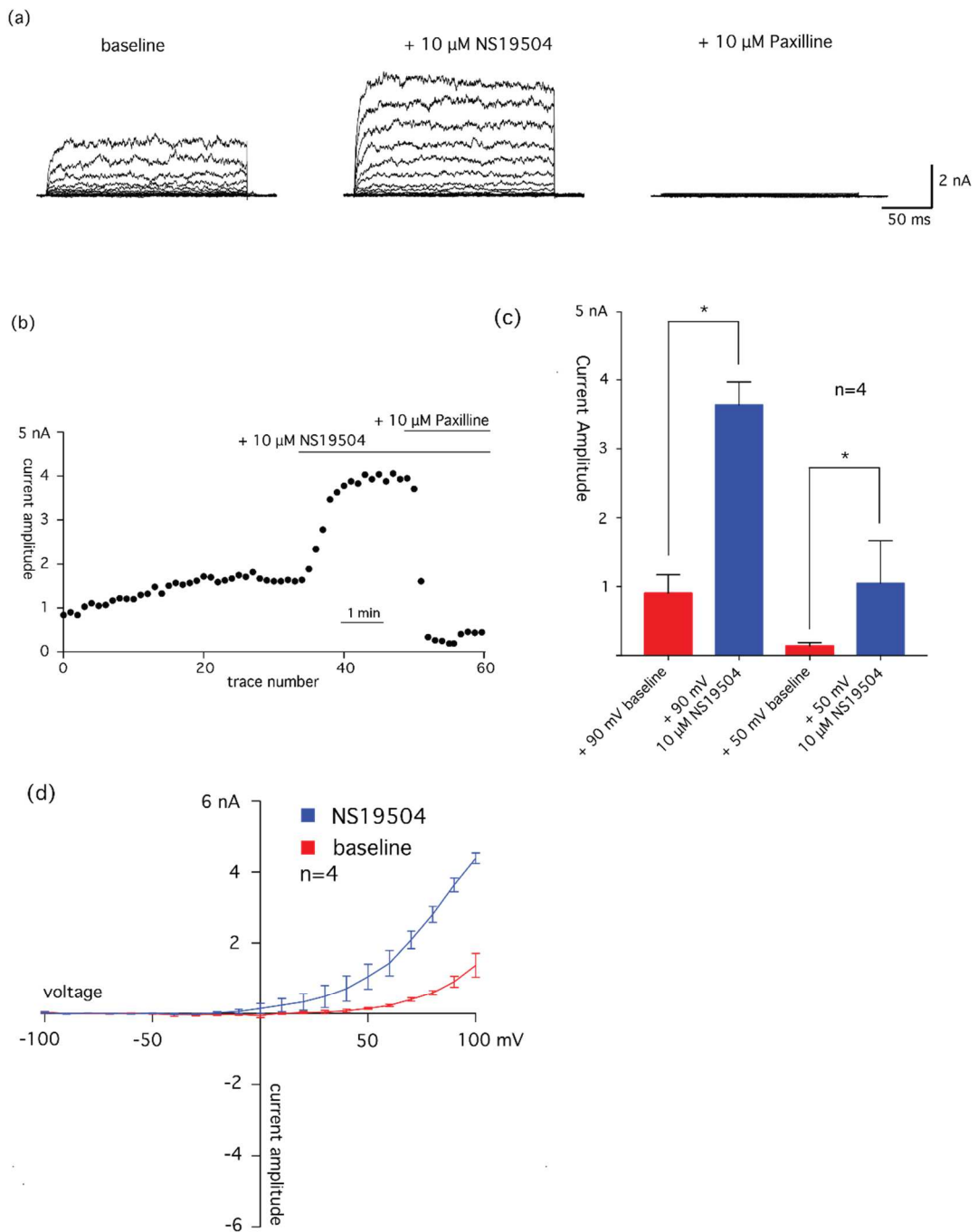


**Figure 4.6. Effect of NS19504 on currents mediated by rBK $\alpha^0$  + hBK- $\beta$ 4 channel complexes in HEK293 cells**

- (a) *Current traces showing the response of a single cell to a family of voltage steps to potentials between -100 and +100 mV, in 10 mV steps, from a resting potential of -90 mV. Duration of the voltage step is 200 ms. Leftmost traces show current responses under baseline conditions, middle traces after application of 10  $\mu$ M NS-19504, right hand traces after co-application of 10  $\mu$ M NS-19504 and 10  $\mu$ M paxilline.*

- (b) *Time-course of currents produced by a series of 100 ms-long voltage steps, at 10 s intervals, to +90 mV from a resting potential of -90 mV. Cell is the same one shown in (a). X-axis shows trace number, Y-axis shows steady state current response in nA. Horizontal bars denote the timing and duration of application of NS-19504 and paxilline.*
- (c) *The bar chart shows the effect of NS19504 on whole cell current amplitude in response to voltage steps to +90 mV and + 50 mV across all cells. Error bars denote SEM, n=4*
- (d) *Averaged I-V curves in response to the voltage families described in (a). Bar heights show mean, error bars denote SEM. Trend line represents the least-squares fit of the Boltzmann function to the data. n=4.*

**Table 4.3. 2-way repeated measures ANOVA of the effect of NS19504 on currents mediated by rBK $\alpha^{\delta}$  + $\beta$ 4**

	SS	DF	MS	F (DFn, DFd)	P value
<b>Voltage (50 mV vs. 90 mV)</b>	1.54E-17	1	1.54E-17	F (1, 4) = 120.2	P=0.0004
<b>NS19504</b>	1.48E-17	1	1.48E-17	F (1, 4) = 89.26	P=0.0007
<b>Interaction: voltage x NS19504</b>	2.36E-18	1	2.36E-18	F (1, 4) = 15.97	P=0.0162
	<b>Source of Variation</b>	<b>% of total variation</b>	<b>P value</b>		
	voltage	40.13	0.0004	***	
	NS19504	38.72	0.0007	***	
	Interaction: voltage x NS19504	6.166	0.0162	*	

*Table shows 2-way ANOVA with factors Voltage (+50 vs +90 mV) and NS19504 (baseline vs. + 10  $\mu$ M). Abbreviations: SS= , DF= degrees of freedom, MS= Mean square of treatment effect, F(Dfn,DFd)=F statistic based on the degrees of freedom of the treatment (DFn) and error (DFd), values given in parentheses after the F statistic.*

The effects of bath application of VSN-16R on currents mediated by BK- $\alpha$  +  $\beta$ 4 heteromeric channels are summarised in Figure 4.7. Figure 4.7a shows the response of a representative cell to a family of 200 ms voltage steps from -90 mV to between -100

mV and + 100 mV in 10 mV steps, before and after the application of 20  $\mu$ M VSN-16R, and following the application of 10  $\mu$ M paxilline, while Figure 4.7b shows the time-course from the same cell in response to a series of 100 ms-long depolarising steps to +90mV, from a holding potential of -90 mV. In 5 of 7 cells tested there was a small increase in current amplitude following application of 10  $\mu$ M VSN-16R, whilst in one cell there was no change in current amplitude, and in one cell the current decreased by 20%. The averaged I/V curves for all cells, before and after application of VSN-16R, is shown in Figure 4.7c. At any given voltage, the mean current was slightly higher following the application of VSN-16R, but the effect was rather small. Comparisons of the current responses at +90 mV and +50 mV, before and after application of 10  $\mu$ M VSN-16R are summarised in Figure 4.7d. Although the current amplitude at both +50 mV and +90 mV is increased following the application of 20  $\mu$ M VSN-16R, the effect of the drug is not significant (Table 4.4,  $p=0.11$ , 2-way repeated measures ANOVA,  $n=7$ ). From these results, it appears that VSN-16R has little or no effect as an activator of heteromeric BK channels containing BK- $\alpha$  and hBK- $\beta$ 4.

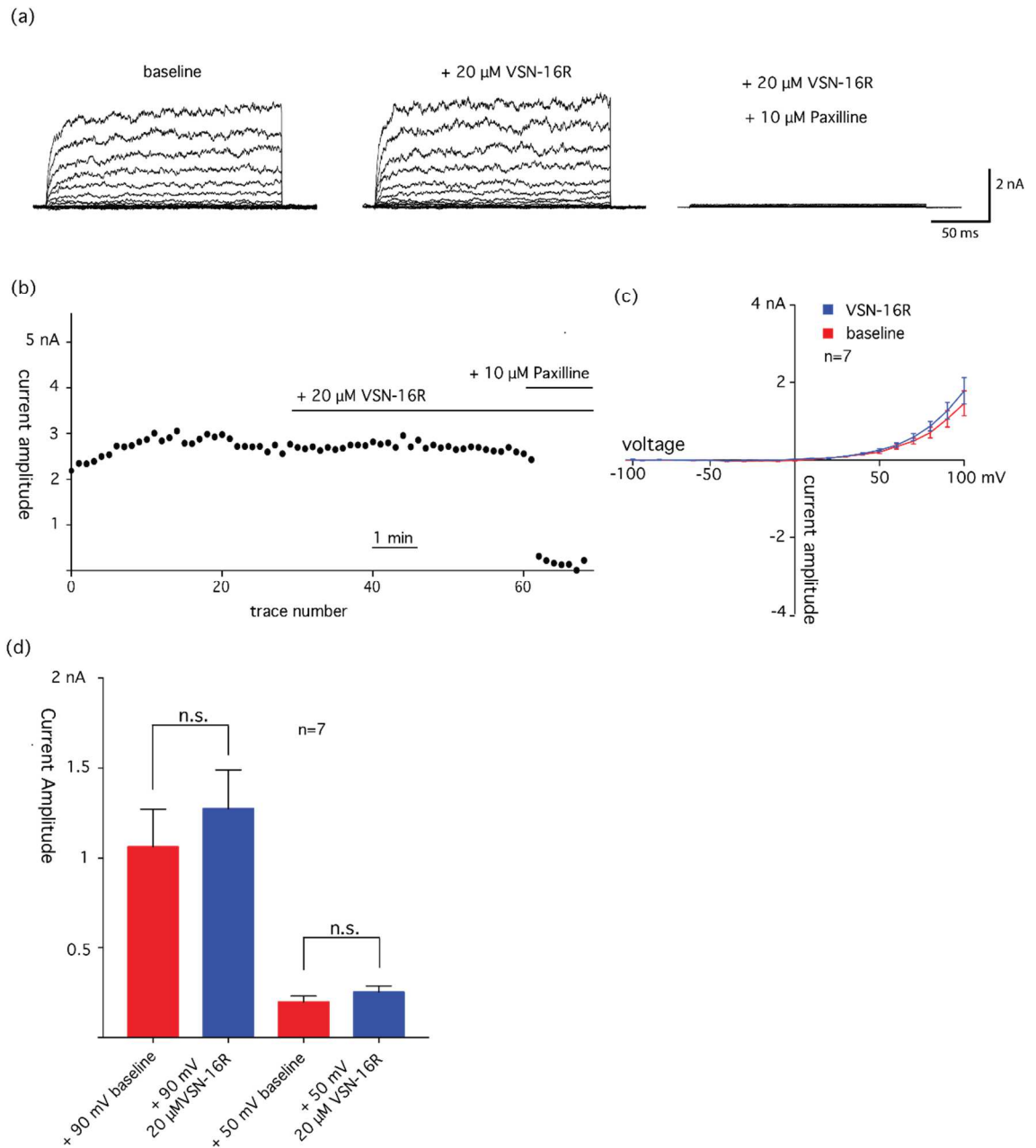


**Figure 4.7. Effect of VSN-16R on currents mediated by rBK $\alpha^0$  + hBK- $\beta$ 4 channel complexes in HEK293 cells**

- (a) *Current responses from a representative cell to a family of 200 ms-long voltage steps to potentials between -100 and +100 mV, in 10 mV increments, from a holding potential of -90 mV. Leftmost traces show current responses under baseline conditions, middle traces after application of 20  $\mu$ M VSN-16R, right hand traces after co-application of 20  $\mu$ M VSN-16R and 10  $\mu$ M paxilline.*
- (b) *Time-course of the steady-state current responses to a series of 100 ms-long voltage steps to +90 mV from a holding potential of -90 mV for the cell shown in (a). Voltage steps were delivered in 10 s intervals. X-axis shows trace number, Y-axis shows current response in nA. Horizontal bars denote the timing and duration of application of VSN-16R and paxilline.*

- (c) Bar diagram showing the effect of VSN-16R on whole cell current amplitude in response to voltage steps to +90 mV and + 50 mV. Error bars show SEM, n=7.
- (d) Averaged I-V curves in response to the voltage families described in (a). Bar heights denote mean, error bars denote SEM. Trend line is the least-squares fit of the Boltzmann function to the data. n=7.

**Table 4.4. 2-way repeated measures ANOVA of the effect of VSN16-R on currents mediated by rBK $\alpha^{\delta}$  + $\beta$ 4**

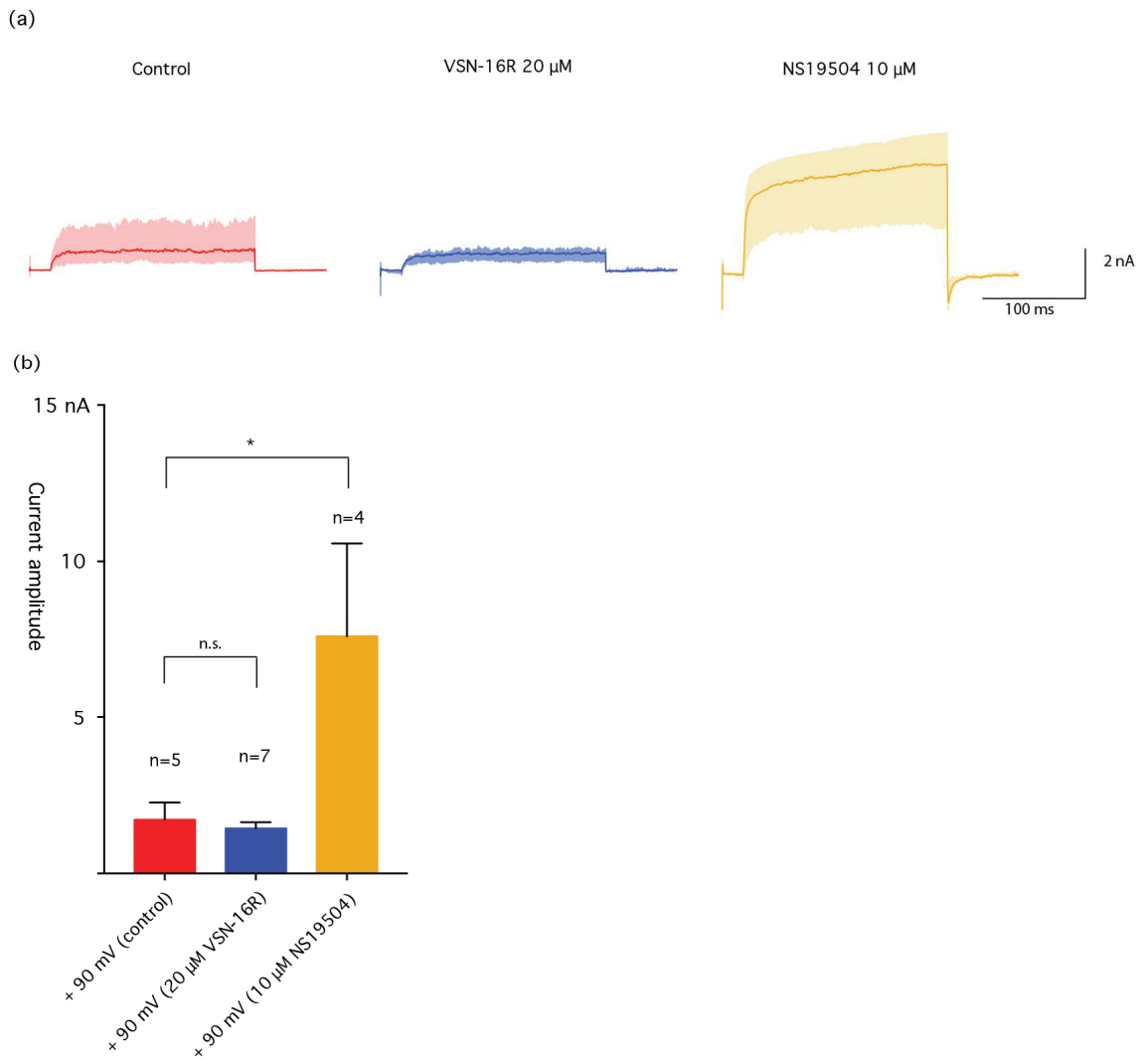
	SS	DF	MS	F (DFn, DFd)	P value
<b>Voltage (50 mV vs. 90 mV)</b>	6.23E-18	1	6.23E-18	F (1, 6) = 25.67	P=0.0023
<b>VSN-16R</b>	6.50E-20	1	6.50E-20	F (1, 6) = 3.438	P=0.1131
<b>Interaction: voltage x VSN-16R</b>	3.74E-20	1	3.74E-20	F (1, 6) = 3.72	P=0.1020
	Source of Variation	% of total variation	P value		
	Voltage	60.76	0.0023	**	
	VSN-16R	0.6331	0.1131	ns	
	Interaction: voltage x VSN-16R	0.3646	0.102	ns	

Table shows 2-way ANOVA with factors Voltage (+50 vs +90 mV) and VSN-16R (baseline vs. + 20  $\mu$ M). Abbreviations: SS= , DF= degrees of freedom, MS= Mean square of treatment effect, F(DFn,DFd)=F statistic based on the degrees of freedom of the treatment (DFn) and error (DFd), values given in parentheses after the F statistic.

#### 4.6 Effect of intracellular NS19504 and VSN-16R on heterologously expressed rBK $\alpha^{\emptyset}$ + $\beta 4$

Given the high solubility of VSN-16R in aqueous solutions, there remains the possibility that its capacity to activate BK channels requires access to the cytosolic region of the channel assembly. Under this hypothesis, it could be that the effects seen in EA.hy926 cells are absent in HEK 293 cells because the latter lack some transporter or other route of uptake into the cytosol. It is also the case that most evidence obtained in EA.hy926 cells was from experiments performed in the inside-out patch clamp configuration, whereby  $\text{Ca}^{2+}$  and VSN-16R were directly applied to the cytosolic side of the membrane. In order to rule out the possibility that VSN-16R might have only a very limited access to the cytosol when it is bath applied and this might limit its effect on BK channels expressed in HEK 293 cells, recordings were made from HEK 293 cells transfected with rBK $\alpha^{\emptyset}$  + hBK- $\beta 4$  subunits, firstly under control conditions using standard intracellular solution in the patch pipette, and subsequently using intracellular solution containing either 10  $\mu\text{M}$  NS19504 or 20  $\mu\text{M}$  VSN-16R.

The results of this experiment are summarised in Figure 4.8. Panel (a) shows traces at +90 mV from the control cells (in red), cells recorded with 20  $\mu\text{M}$  VSN-16R in the pipette (in blue), and cells recorded with 10  $\mu\text{M}$  NS-19504 in the pipette (in yellow). In each case the solid line shows the current trace obtained by averaging recordings from of all cells under each condition, while the shaded area indicates the difference between the smallest and largest currents recorded under each condition. Figure 4.8b shows the mean current sizes recorded in response to a +90 mV step, for each composition of the intracellular solution. Cells recorded using standard intracellular solution exhibited an average current size of  $1.7 \pm 0.5$  nA ( $n=5$ ), whereas cells recorded using an intracellular solution containing 20  $\mu\text{M}$  VSN-16R exhibited an average current amplitude of  $1.4 \pm 0.1$  nA ( $n=7$ ), and those recorded using intracellular solution containing 10  $\mu\text{M}$  NS19504 gave a current of  $7.6 \pm 1.2$  nA ( $n=4$ ). Currents elicited in the NS19504 group were significantly larger than those of the control group, whereas those from the VSN-16R group were not (ANOVA  $p=0.01$ , Sidak's multiple comparisons test  $p=0.01$  (NS19504>control) and  $p=0.98$  (VSN-16R > control)).



**Figure 4.8. Effect of intracellularly applied VSN-16R and NS19504 on rBK $\alpha^0$  + hBK- $\beta$ 4 channel-mediated currents in HEK293 cells**

(a) **Compound traces of responses to a 200 ms-long voltage step to +90 mV, from a holding potential of -90 mV, from cells recorded using standard intracellular solution (red), intracellular solution containing 20  $\mu$ M VSN-16R (blue) and intracellular solution containing 10  $\mu$ M NS19504 (yellow). Solid line shows a current trace obtained by averaging of all cells recorded under the relevant condition, shaded area shows the range between the smallest and largest current traces recorded. Control cells n=5, VSN-16R n=7, NS19504 n=4.**

(b) **Bar diagram showing mean responses to the same +90 mV step using the three different intracellular solutions. Error bars denote SEM. Number of experiments is as stated in (a).**

#### **4.7 Effect of NS19504 and VSN-16R on currents mediated by heterologously expressed rBK $\alpha^0$ + $\beta$ 2 channel complexes**

The other BK channel accessory subunit expressed in the EA.hy926 endothelial cell line is  $\beta$ 2. As with  $\beta$ 4,  $\beta$ 2 is widely expressed in the brain, including the hippocampus (Shao et al 1999, Faber and Sah 2003). Whereas the  $\beta$ 4 subunit confers slow activation kinetics and reduced iberiotoxin sensitivity on the BK current,  $\beta$ 2 produces a distinctive inactivating phenotype.

It is possible that the effects of VSN-16R seen in the endothelial cell line are mediated by an interaction dependent on the presence of the  $\beta$ 2 subunit. In order to test this hypothesis, HEK 293 cells were transfected with both rBK $\alpha^0$  and hBK- $\beta$ 2 cDNAs in a ratio of 1:4.

As with the  $\beta$ 4 experiment, we first examined the effects of NS19504 on currents mediated by BK- $\alpha$  + $\beta$ 2 channels, to assess whether this compound enhances the activity of heterologously expressed channels of this composition.

The effects of bath application of 10  $\mu$ M NS19504 on the BK- $\alpha$  + $\beta$ 2 current are summarised in Figure 4.9. As can be seen from Figure 4.9a, the current produced from cells transfected with BK- $\alpha$  + $\beta$ 2 exhibits an inactivating profile, which becomes increasingly pronounced at more positive voltages. The inactivation is incomplete, with a residual current of around 50% of the peak current present at the end of the trace, even for the most positive voltages tested. As with the experiments with channels formed by BK- $\alpha$  and BK- $\alpha$  + $\beta$ 4 subunits, application of 10  $\mu$ M NS19504 produced a rapid and dramatic increase in current amplitude, as can be seen in the time-course in Figure 4.9b. In 5 of 5 cells tested this increase was greater than 200% of the baseline current amplitude, and in all cells the resultant current was completely inhibited by either 10  $\mu$ M paxilline or 5 mM TEA.

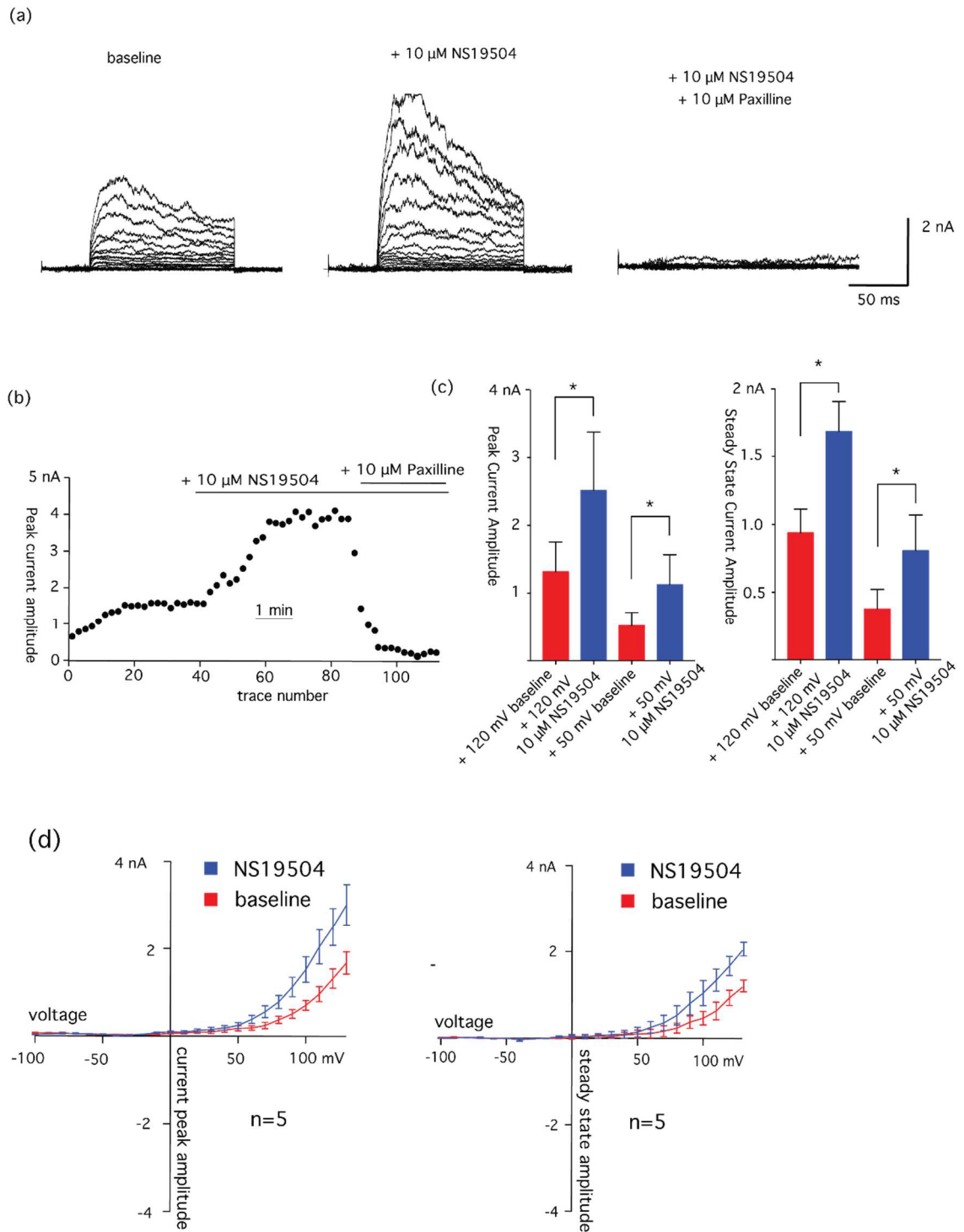


**Figure 4.9. Effect of NS19504 on currents recorded from HEK293 cells coexpressing rBK $\alpha^0$  + hBK- $\beta$ 2 subunits**

- (a) *Current responses from a representative cell to a family of 100 ms-long voltage steps to potentials between -100 and +130 mV, in 10 mV increments, from a holding potential of -90 mV. Leftmost trace shows current response under baseline conditions, middle trace after application of 10  $\mu$ M NS-19504, right hand trace after co-application of 10  $\mu$ M NS-19504 and 10  $\mu$ M paxilline. Following the voltage step, the cell was held at -140 mV for 40 ms in order to remove inactivation, but this portion of the recording is not shown.*

- (b) *The time-course shows the peak current response of the same representative cell to a 100 ms-long step to +100 mV, from a holding potential of -90 mV. Steps were delivered at 10 s intervals. Peak current was determined as the mean current of a 5 ms window either side of the peak value recorded. Horizontal bars show the periods during which NS19504 and paxilline were applied. Y axis shows peak current amplitude, X axis shows trace number.*
- (c) *Bar graphs showing the peak (left) and steady state (right) current amplitude in response to voltage steps to +120 mV and +50 mV steps, taken from the voltage families described in (a). Red bars denote the mean baseline current amplitude, blue bars show the amplitude following application of 10  $\mu$ M NS19504 (n=5). Error bars denote SEM. Y axis shows current amplitude*
- (d) *Averaged I-V relationships for the peak and steady-state current taken from the voltage families described in (a). Bar heights show the mean current amplitude for each voltage step, while error bars show the SEM (n=5). Trend line was generated from a least-squares fit of the Boltzmann function to the data.*

Due to the inactivating nature of the current, the effect of NS19504 on the peak and on the “steady state” component of the current were analysed separately. The preceding scare-quotes are necessary because in 3 of 5 cells, a true steady state had not been reached by the end of the 100 ms-long voltage pulse in the most positive region of the voltage range tested. The “steady state” analysis therefore does not represent a true steady state, but is nonetheless far closer to the inactivated state of the channel population than the peak.

The current-voltage relationship for both peak and steady-state current responses is displayed in Figure 4.9c, and comparisons of specific voltage points are shown in Figure 4.9d. At +120 mV, application of 10  $\mu$ M NS19504 increased peak current amplitude to ~190% of baseline (mean of ratios = 1.90, SEM=0.11), whereas at +50 mV, the peak current amplitude was increased by ~220% (mean of ratios = 2.20, SEM=0.008). The effect of the drug was significant ( Table 4.5a, 2-way repeated measures ANOVA, p=0.0076, n=5) and there was a significant interaction between the effects of NS19504 and that of voltage voltage (p=0.0053).

Application of 10  $\mu$ M NS19504 caused an increase in the steady state current amplitude measured at +120 mV to 182% of baseline (SEM =0.14), while at +50 mV, current amplitude was increased to 222% of baseline (SEM=0.11). Again, both the effect of NS19504 (Table 4.5b, 2-way repeated measures ANOVA, p= 0.0002, n=5) and the interaction between NS19504 and voltage (p=0.0018) were significant.

Taken together, these results suggest that NS19504 functions as an enhancer of heteromeric BK channels composed of BK- $\alpha$  +  $\beta$ 2 subunits.

**Table 4.5. 2-way repeated measures ANOVA of the effect of NS19504 on currents mediated by  $rBK\alpha^{\theta}$  +hBK- $\beta$ 2.** (a) effect of NS19504 on the peak current amplitude. (b) effect of NS19504 on the steady state current amplitude.

<b>(a) Effect of NS19504 (peak)</b>					
	<b>SS</b>	<b>DF</b>	<b>MS</b>	<b>F (DFn, DFd)</b>	<b>P value</b>
<b>voltage</b>	6.02E-18	1	6.02E-18	F (1, 4) = 38.1	P=0.0035
<b>NS19504</b>	4.11E-18	1	4.11E-18	F (1, 4) = 24.82	P=0.0076
<b>Interaction: voltage x NS19504</b>	4.25E-19	1	4.25E-19	F (1, 4) = 30.31	P=0.0053
	<b>Source of Variation</b>	<b>% of total variation</b>	<b>P value</b>		
	Voltage	3.41E+01	0.0035	**	
	NS19504	23.32	0.0076	**	
	voltage x NS19504	2.412	0.0053	**	
<b>(b) Effect of NS19504 (steady state)</b>					
	<b>SS</b>	<b>DF</b>	<b>MS</b>	<b>F (DFn, DFd)</b>	<b>P value</b>
<b>voltage</b>	2.57E-18	1	2.57E-18	F (1, 4) = 2449	P<0.0001
<b>NS19504</b>	1.72E-18	1	1.72E-18	F (1, 4) = 155.3	P=0.0002
<b>Interaction: voltage x NS19504</b>	1.23E-19	1	1.23E-19	F (1, 4) = 54.17	P=0.0018
	<b>Source of Variation</b>	<b>% of total variation</b>	<b>P value</b>		
	voltage	46.62	<0.0001	****	
	NS19504	31.17	0.0002	***	
	voltage x NS19504	2.227	0.0018	**	

*Table shows 2-way ANOVA with factors Voltage (+50 vs +90 mV) and NS19504 (baseline vs. + 10  $\mu$ M). Abbreviations: SS= , DF= degrees of freedom, MS= Mean square of treatment effect, F(Dfn,Dfd)=F statistic based on the degrees of freedom of the treatment (DFn) and error (DFd), values given in parentheses after the F statistic.*

In order to determine whether VSN-16R acts as an enhancer of heteromeric BK- $\alpha$ + $\beta$ 2 channels, 20  $\mu$ M VSN-16R was added under the same conditions as in the NS19504 experiment described above. The results are summarised in Figure 4.10. The time course of current changes in response to drug application for a representative cell is shown in Figure 4.10b, and example traces in response to a family of 100 ms-long voltage pulses is shown in Figure 4.10a. In general, bath application of 20  $\mu$ M VSN-16R had no observable effect on the current, either with reference to the time-course of the response at +100 mV, or with reference to the current families.

Comparisons of specific voltage points are shown in Figure 4.10c and the current-voltage relationship for both peak and steady-state current responses is displayed in Figure 4.10d.. Application of 20  $\mu$ M VSN-16R reduced the peak current amplitude, as measured at +120 mV, to 98% of baseline (mean of ratios= 0.98, SEM=0.01), while at +50 mV, the current was reduced to 94% of baseline (SEM=0.05). The effect of VSN-16R was not statistically significant (Table 4.6a,  $p$ = 0.30, 2-Way Repeated Measures ANOVA ,  $n$ =5).

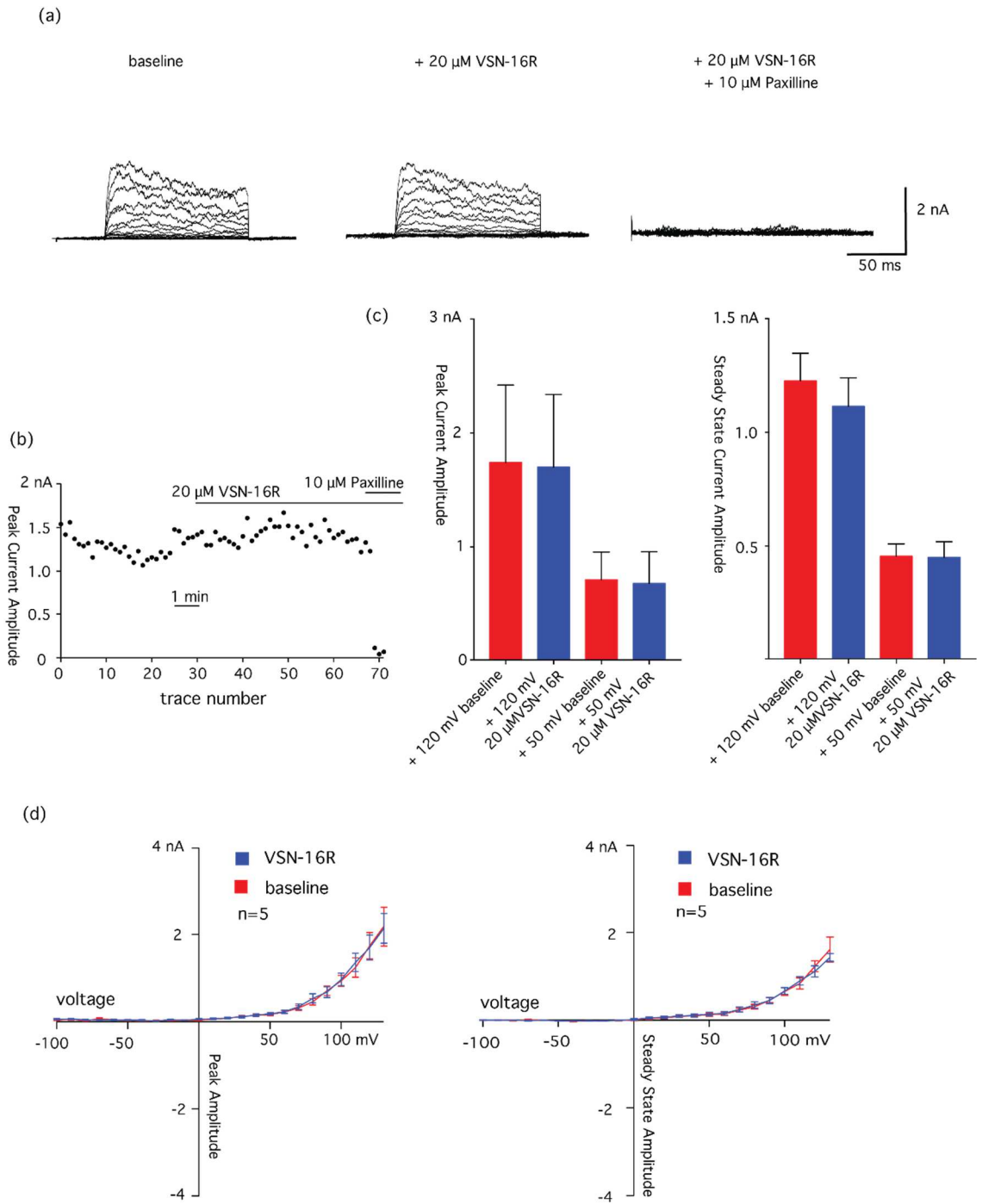


**Figure 4.10. Effect of VSN-16R on currents mediated from HEK293 cells coexpressing rBK $\alpha^0$  + hBK- $\beta$ 2 subunits**

- (a) *The currents measured from a single cell, representative of the dataset, in response to a family of 100 ms-long voltage steps to potentials between -100 and +130 mV, in 10 mV increments, from a holding potential of -90 mV. The cell was held at -140 mV for 40 ms at the end of the main step, in order to remove inactivation. This portion of the recording is not shown. Left-hand traces show baseline current responses to the voltage pulse family, middle traces after application of 20  $\mu$ M VSN-16R, right hand traces responses to 20  $\mu$ M VSN-16R and 10  $\mu$ M paxilline.*

- (b) *Time-course of peak current response of the cell shown in (a) to a series of 120 ms-long steps, delivered at 10 s intervals, to +100 mV, from a holding membrane potential of -90 mV. Peak current was determined as the mean current of a 5 ms window either side of the peak value recorded. Horizontal bars show the periods during which 20  $\mu$ M VSN-16R and 10  $\mu$ M paxilline were applied. Y axis shows peak current amplitude, X axis shows trace number.*
- (c) *Bar graphs showing the peak (left) and steady state (right) mean current amplitude in response to voltage steps to +120 mV and +50 mV steps, taken from the voltage families described in (a). Red bars denote the mean baseline current amplitude, blue bars show the amplitude following application of 20  $\mu$ M VSN-16R (n=5). Error bars denote SEM. Y axis shows current amplitude*
- (d) *Averaged I-V relationships for the peak and steady-state currents obtained in response to the voltage step families described in (a). Bar heights show the mean current amplitude for each voltage step, while error bars show the SEM (n=5). Trend line was generated from a least-squares fit of the Boltzmann function to the data.*

VSN-16R also produced no significant effect on the steady-state amplitude of the current (Table 4.6b,  $p=0.42$ , 2-way Repeated Measures ANOVA  $n=5$ ).

As with the BK- $\alpha$  homomeric and BK- $\alpha+\beta 4$  heteromeric channels, it appears that VSN-16R does not function as a direct enhancer of heteromeric BK- $\alpha+\beta 2$  channels, according to our evidence from heterologous expression in HEK 293 cells.

**Table 4.6. 2-way repeated measures ANOVA of the effect of VSN16-R on currents mediated by  $rBK\alpha^{\delta}$  +hBK- $\beta$ 2.** (a) effect of VSN-16R on the peak current amplitude. (b) effect of VSN-16R on the steady state current amplitude.

<b>(a) effect of VSN-16R (peak)</b>					
	<b>SS</b>	<b>DF</b>	<b>MS</b>	<b>F (DFn, DFd)</b>	<b>P value</b>
<b>Voltage (50 mV vs. 90 mV)</b>	5.25E-18	1	5.25E-18	F (1, 4) = 24.95	P=0.0075
<b>VSN-16R</b>	6.48E-21	1	6.48E-21	F (1, 4) = 1.435	P=0.2971
<b>Interaction: voltage x VSN-16R</b>	8.00E-23	1	8.00E-23	F (1, 4) = 0.03543	P=0.8599
	<b>Source of Variation</b>	<b>% of total variation</b>	<b>P value</b>		
	Voltage	56.57	0.0075	**	
	VSN-16R	0.06986	0.2971	ns	
	Interaction: voltage x VSN-16R	0.0008624	0.8599	ns	
<b>(b) Effect of VSN-16R (steady state)</b>					
	<b>SS</b>	<b>DF</b>	<b>MS</b>	<b>F (DFn, DFd)</b>	<b>P value</b>
<b>Voltage (50 mV vs. 90 mV)</b>	2.58E-18	1	2.58E-18	F (1, 4) = 92.75	P=0.0007
<b>VSN-16R</b>	1.75E-20	1	1.75E-20	F (1, 4) = 0.8123	P=0.4184
<b>Interaction: voltage x VSN-16R</b>	1.43E-20	1	1.43E-20	F (1, 4) = 3.334	P=0.1419
	<b>Source of Variation</b>	<b>% of total variation</b>	<b>P value</b>		
	Voltage	76.51	0.0007	***	
	VSN-16R	0.5177	0.4184	ns	
	Interaction: voltage x VSN-16R	0.4242	0.1419	ns	

**Table shows 2-way ANOVA with factors Voltage (+50 vs +90 mV) and VSN-16R (baseline vs. + 20  $\mu$ M). Abbreviations: SS= , DF= degrees of freedom, MS= Mean square of treatment effect, F(DFn,DFd)=F statistic based on the degrees of freedom of the treatment (DFn) and error (DFd), values given in parentheses after the F statistic.**

#### **4.8 Effect of NS19504 and VSN-16R on currents mediated by heterologously expressed rBK $\alpha^0$ + $\beta$ 3 channel complexes**

The effect of both drugs was additionally tested in HEK 293 cells expressing BK- $\alpha$ + $\beta$ 3 channel subunits. Given that  $\beta$ 3 RNA transcripts were not detected in the EA.hy926 endothelial cell line, a  $\beta$ 3-specific activation effect of VSN-16R would be an unlikely explanation for the results observed in that cell line, however it was decided to test it under our experimental conditions, if only for completeness, and because it would be useful to determine whether the subunit conferred any change in sensitivity to NS19504.

The effects of bath application of 10  $\mu$ M NS19504 on the BK- $\alpha$ + $\beta$ 3 current are summarised in Figure 4.11. The  $\beta$ 3 subunit is reported to confer a fast but incomplete inactivation effect, which is reportedly only visible during large depolarisations (Nausch et al 2014). Our results do not show any inactivation (Figure 4.11a), likely because of the highly voltage-dependent nature of the effect. However, in the previous co-transfection experiments, where the  $\beta$ 2 and  $\beta$ 4 subunits did produce an observable change in the current properties, we saw the change in all of the cells tested. It is therefore reasonable to assume that  $\beta$ 3 was also successfully expressed and incorporated into the channels.

As can be seen from the representative time-course in Figure 4.11b, application of NS19504 produced a distinctive increase in current amplitude, as seen in previous experiments for BK channels with different subunit compositions.

The current-voltage relationships before and after application of 10  $\mu$ M NS19504 are displayed in Figure 4.11c, and comparisons of specific voltage points are shown in Figure 4.11d. Application of NS19504 increased the current amplitude at +90 mV to 200%  $\pm$  13% of baseline, whereas at +50 mV the current increased to 376%  $\pm$  34% of baseline. The effect of NS19504 was significant (Table 4.7,  $p=0.005$ , 2-Way repeated measures ANOVA,  $n=5$ ), and there was an interaction between the drug effect and that of voltage ( $p=0.029$ ).

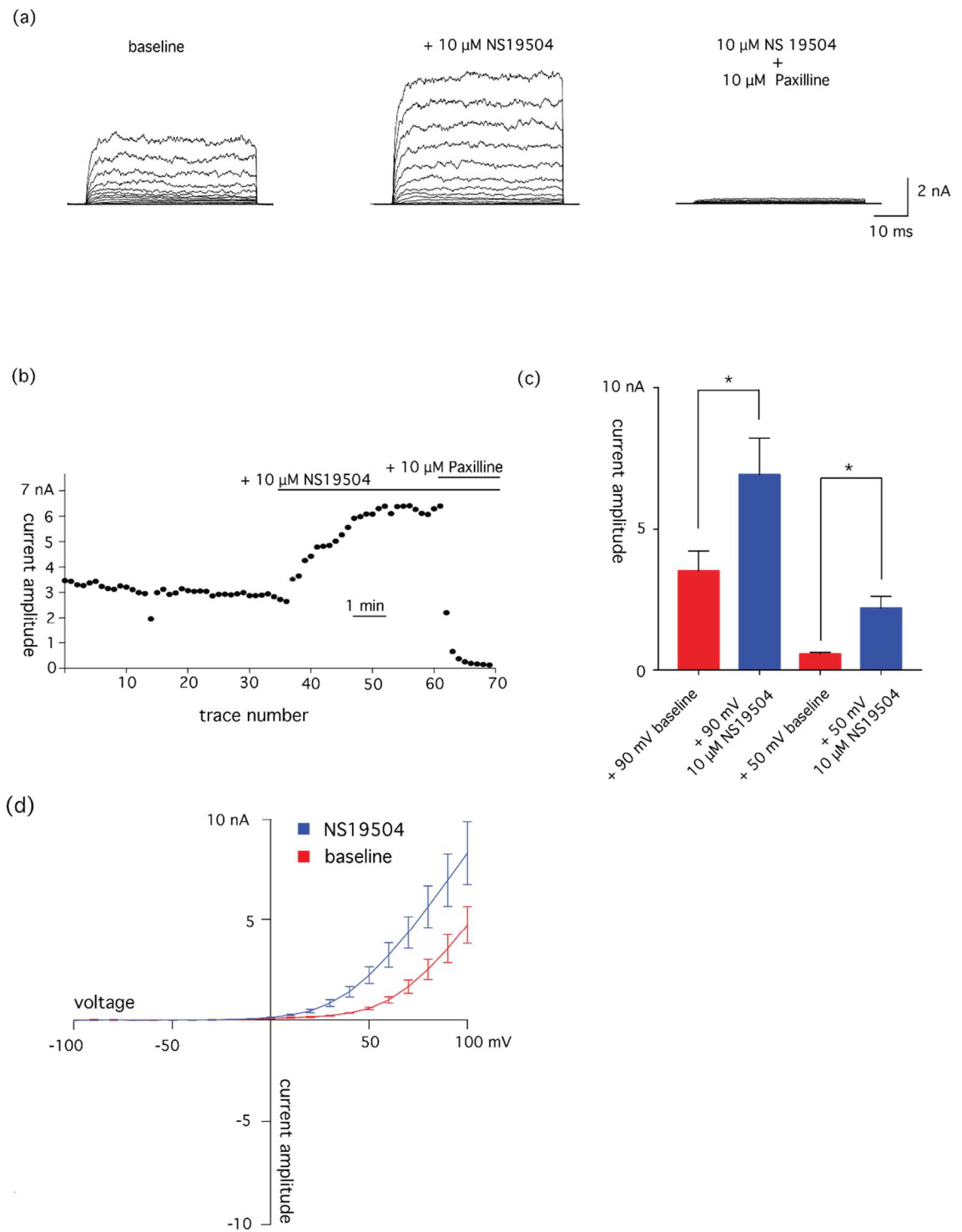


**Figure 4.11. Effect of NS19504 on currents mediated by rBK $\alpha^0$  + hBK- $\beta$ 3 channels in HEK293 cells**

- (a) *Current responses from a representative cell to a family of 50 ms-long voltage steps to potentials between -100 and +100 mV, in 10 mV increments, from a holding potential of -90 mV. Leftmost traces show current responses under baseline conditions, middle traces after application of 10 μM NS-19504, right hand traces after co-application of 10 μM NS-19504 and 10 μM paxilline.*

- (b) *Time-course of the steady-state current response to a series of 50 ms-long voltage steps to +90 mV from a holding potential of -90 mV for the cell shown in (a). Voltage steps were delivered in 10 s intervals. X-axis shows trace number, Y-axis shows current amplitude in nA. Horizontal bars denote the timing and duration of application of NS-19504 and paxilline.*
- (c) *Bar diagram showing the effect of NS19504 on whole cell current amplitude in response to voltage steps to +90 mV and + 50 mV Error bars show SEM, n=5.*
- (d) *Averaged I-V curves in response to the voltage families described in (a). Bar heights denote mean, error bars denote SEM. Trend line is the least-squares fit of the Boltzmann function to the data, n=5.*

This suggests that NS19504 acts as an enhancer of heterologously expressed BK- $\alpha$ + $\beta$ 3 heteromeric channels. Although the lack of saturation of the IV relationship again precludes direct assessment of the  $V_{1/2}$  of activation, the increase in current amplitude at +50 mV is significantly larger than that at +90 mV, which is as would be expected if the  $V_{1/2}$  had been shifted leftward by NS19504.

**Table 4.7. 2-way repeated measures ANOVA of the effect of NS19504 on currents mediated by rBK $\alpha^{\beta}$  +hBK- $\beta$ 3**

	SS	DF	MS	F (DFn, DFd)	P value
<b>Voltage (50 mV vs. 90 mV)</b>	7.37E-17	1	7.37E-17	F (1, 4) = 23.53	P=0.0083
<b>NS19504</b>	3.18E-17	1	3.18E-17	F (1, 4) = 29.62	P=0.0055
<b>Interaction: voltage x NS19504</b>	3.85E-18	1	3.85E-18	F (1, 4) = 10.9	P=0.029
	<b>Source of Variation</b>	<b>% of total variation</b>	<b>P value</b>		
	Voltage	47.26	0.0083	**	
	NS19504	20.39	0.0055	**	
	Interaction: voltage x NS19504	2.47	0.0299	*	

*Table shows 2-way ANOVA with factors Voltage (+50 vs +90 mV) and NS19504 (baseline vs. + 10  $\mu$ M). Abbreviations: SS= , DF= degrees of freedom, MS= Mean square of treatment effect, F(Dfn,DFd)=F statistic based on the degrees of freedom of the treatment (DFn) and error (DFd), values given in parentheses after the F statistic.*

The effects of bath application of 20  $\mu\text{M}$  VSN-16R on the BK- $\alpha$ + $\beta$ 3 currents are summarised in Figure 4.12. As can be seen in Figure 4.12a and 4.12b, VSN-16R does not appear to have any effect on the amplitude of the BK- $\alpha$ + $\beta$ 3 current, either in terms of the time-course at +90 mV or in terms of the amplitude of the current responses to increasing voltage steps before and after drug application. Additionally there is almost complete overlap between the averaged IV curves (Figure 4.12d) At +90 mV, application of 20  $\mu\text{M}$  VSN16R reduced current amplitude to  $99.4\% \pm 7\%$  of baseline, while at +50 mV, the current was increased to  $103\% \pm 14\%$  of baseline. There was no significant difference between the current amplitudes before and after VSN-16R application (Table 4.8,  $p=0.98$ , 2-way repeated measures ANOVA,  $n=5$  ) (Figure 4.12c). It therefore appears that VSN-16R does not function as a direct enhancer of heteromeric BK- $\alpha$  + $\beta$ 3 channels.

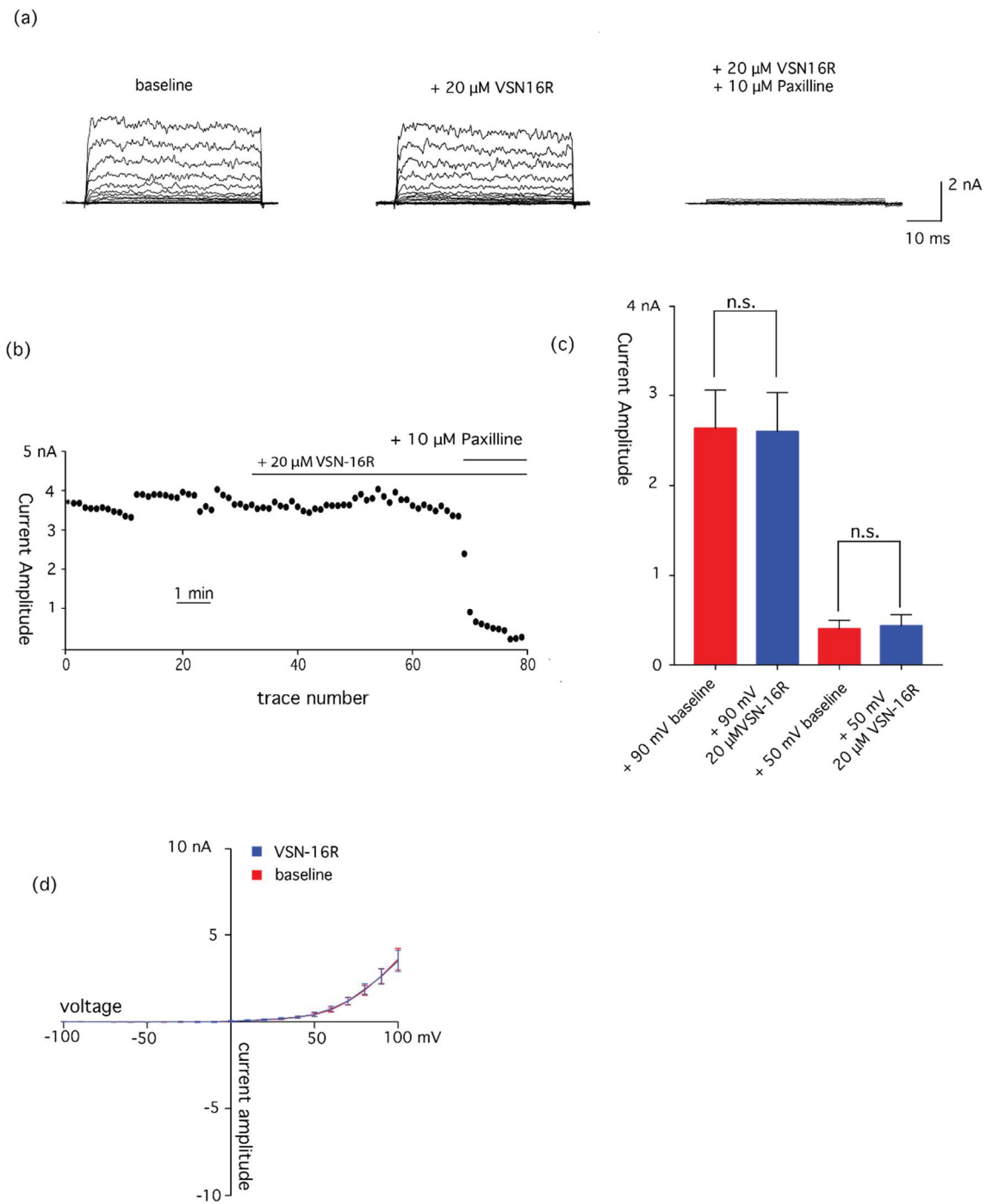


**Figure 4.12. Effect of VSN-16R on currents mediated by  $rBK\alpha^0$  + hBK- $\beta$ 3 channel complexes in HEK293 cells**

- (a) *Current responses from a representative cell to a family of 50 ms-long voltage steps to potentials between -100 and +100 mV, in 10 mV increments, from a holding potential of -90 mV. Leftmost traces show current responses under baseline conditions, middle traces after application of 20  $\mu$ M VSN-16R, right hand traces after co-application of 20  $\mu$ M VSN-16R and 10  $\mu$ M paxilline.*
- (b) *Time-course of the steady-state current response to a series of 50 ms-long voltage steps to +90 mV from a holding potential of -90 mV for the cell shown in (a). Voltage steps are*

delivered in 10 s intervals. X-axis shows trace number, Y-axis shows current amplitude in nA. Horizontal bars denote the timing and duration of application of VSN-16R and paxilline.

- (c) Bar diagram showing the effect of VSN-16R on whole cell current amplitude in response to voltage steps to +90 mV and + 50 mV. Error bars show SEM, n=5.
- (d) Averaged I-V curves in response to the voltage families described in (a). Bar heights denote mean, error bars denote SEM. Trend line is the least-squares fit of the Boltzmann function to the data, n=5.

**Table 4.8. 2-way repeated measures ANOVA of the effect of VSN-16R on currents mediated by rBK $\alpha^{\emptyset}$  +hBK- $\beta$ 3**

	SS	DF	MS	F (DFn, DFd)	P value
Voltage (50 mV vs. 90 mV)	2.42E-17	1	2.42E-17	F (1, 4) = 35.75	P=0.0039
VSN-16R	9.80E-24	1	9.80E-24	F (1, 4) = 0.0002785	P=0.98
Interaction: voltage x VSN-16R	5.99E-21	1	5.99E-21	F (1, 4) = 0.4017	P=0.56
	Source of Variation	% of total variation	P value		
	Voltage	75.59	0.0039	**	
	VSN-16R	3.06E-05	0.98	ns	
	Interaction: voltage x VSN-16R	0.01869	0.56	ns	

Table shows 2-way ANOVA with factors Voltage (+50 vs +90 mV) and VSN-16R (baseline vs. + 20  $\mu$ M). Abbreviations: SS= , DF= degrees of freedom, MS= Mean square of treatment effect, F(Dfn,DFd)=F statistic based on the degrees of freedom of the treatment (DFn) and error (DFd), values given in parentheses after the F statistic.

In summary, the effects of VSN-16R and NS19504 were not noticeably different for currents mediated by BK channels incorporating any of the three  $\beta$  subunits tested, compared to rBK $\alpha^{\emptyset}$ . In the case of VSN-16R, the drug did not appear to have any effect of current amplitude, and in the case of NS19504, it caused an increase in current amplitude for each combination of subunits tested, and the magnitude of the change in

current amplitude was not significantly different in each case (One way ANOVA,  $F(3, 18) = 2.673$ ,  $p=0.08$ ).

#### **4.9 Effect of VSN-16R on on currents mediated by heterologously expressed rBK $\alpha^{\emptyset}$ in the presence of intracellular reducing agents glutathione and dithiothreitol**

VSN-16R failed to enhance currents mediated by channels formed by heterologously expressed rBK $\alpha^{\emptyset}$  and rBK $\alpha^{\emptyset}$  co-expressed with the  $\beta_4$ ,  $\beta_2$ , and  $\beta_3$  subunits, challenging the hypothesis that BK channels could be directly targeted as part of the mechanism by which the compound activated a paxilline-sensitive current in the EA.hy926 cell line. One possibility is that VSN-16R activates BK channels directly in a manner dependent on the redox state of the cell. BK channels are known to be regulated by the redox state of the cell (Herman et al 2015), and endothelial cells are known to utilise redox signalling (Panieri and Santoro, 2015). Furthermore, conventional intracellular solutions for whole cell patch clamp recordings might produce a redox state more oxidised than that of the endogenous cytosol, and we hypothesised that this might affect our results with VSN-16R. We therefore decided to test this hypothesis by conducting experiments on HEK 293 cells expressing channels formed by rBK $\alpha^{\emptyset}$  alone, in which the intracellular solution was augmented with either 500  $\mu\text{M}$  glutathione (GSH) or 500  $\mu\text{M}$  dithiothreitol (DTT) in order to produce a reducing environment in the cell during the whole-cell experiment.

The results for the experiment in which 10  $\mu\text{M}$  VSN-16R was applied to cells expressing rBK $\alpha^{\emptyset}$ , using 500  $\mu\text{M}$  glutathione in the intracellular solution, are shown in Figure 4.13. Panels (a) and (b) show the effects of application of 10  $\mu\text{M}$  VSN-16R on a single representative cell. Glutathione did not significantly alter the kinetics of the currents mediated by BK- $\alpha$  channels (Figure 4.13a as compared with the results described in Figure 4.4). Application of 10  $\mu\text{M}$  VSN-16R did not produce any noticeable effect on the time-course of the BK current amplitude (Figure 4.13b) and, as with previous experiments, the current following application of VSN16-R was abolished by application of 10  $\mu\text{M}$  paxilline or 5 mM TEA. Figure 4.13d shows the I-V relationship before and after the application of 10  $\mu\text{M}$  VSN-16R in the presence of 500  $\mu\text{M}$  intracellular GSH. The two curves overlap almost completely, suggesting that VSN-16R did not affect the voltage dependence of the channel. At +90 mV, application of 10  $\mu\text{M}$  VSN16R reduced current amplitude to  $97\% \pm 7\%$  of baseline, while at +50 mV the current was increased to  $115\% \pm 5\%$  of baseline. The effect of VSN-16R was not significant. (Table 4.9,  $p=0.98$ , 2-Way repeated measures ANOVA,  $n=6$ , Figure 4.13c).

It was therefore concluded that the augmentation of the intracellular solution with 500  $\mu\text{M}$  intracellular GSH was not sufficient to permit the enhancement of BK- $\alpha$ -mediated currents by VSN-16R.

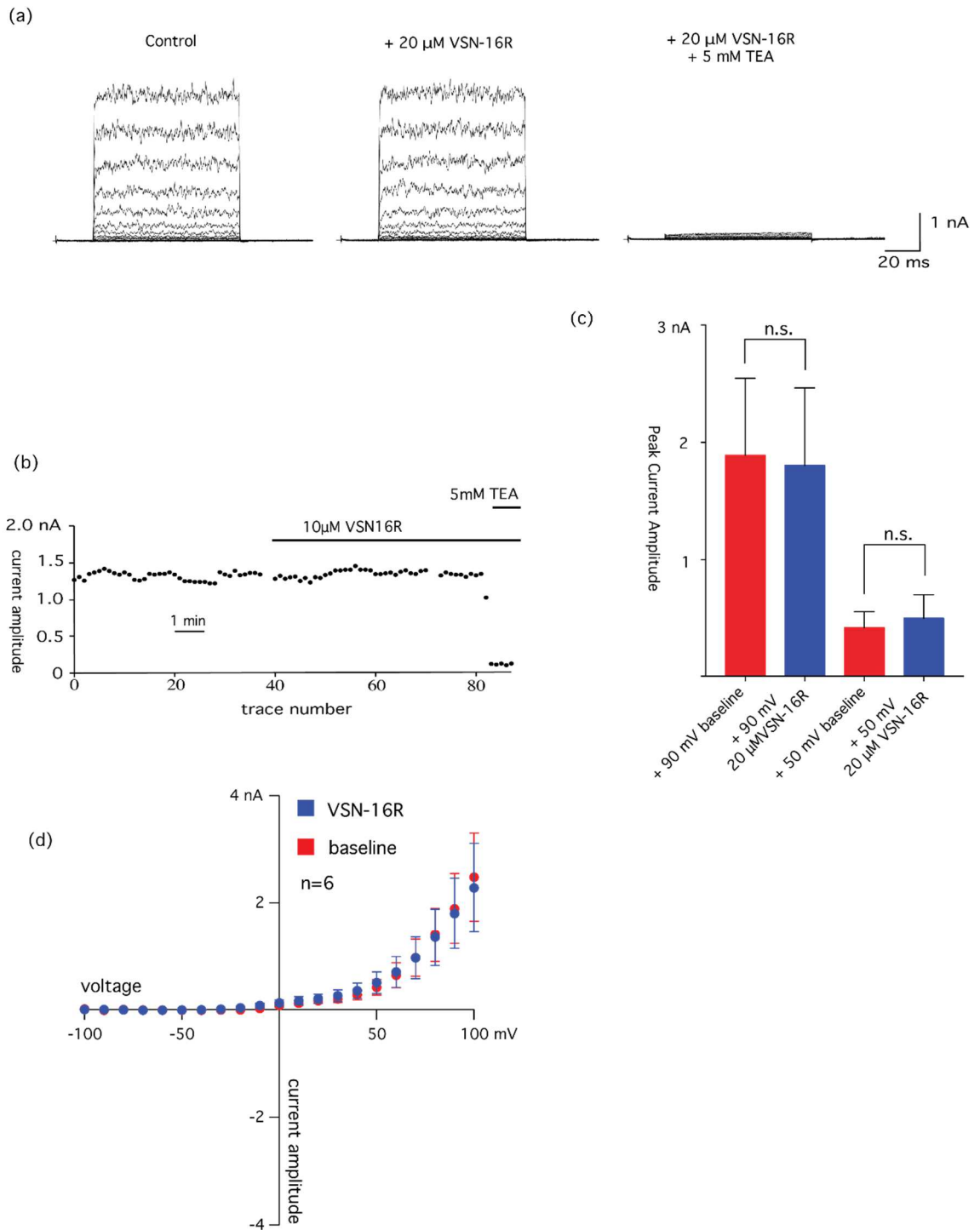


**Figure 4.13. Effect of VSN-16R on currents mediated by channels expressed in HEK293 cells expressing rBK $\alpha^{\theta}$  channels in the presence of intracellular glutathione**

*The experiments summarised in this figure were performed by R. Roberts (undergraduate student), under my supervision.*

- (a) *Current families recorded from a single cell representative of the dataset, in the presence of 500  $\mu\text{M}$  intracellular glutathione (GSH), to a family of 40 ms-long voltage steps to potentials between -100 and +100 mV, in 10 mV increments, from a holding potential of -90 mV. Left traces show baseline current responses of cell, middle traces show responses*

in the presence of 20  $\mu\text{M}$  VSN-16R, and right hand traces show responses following application of 20  $\mu\text{M}$  VSN-16R + 5 mM TEA.

- (b) Time-course of the BK current amplitude in the cell shown in (a). Voltage steps of 50 ms-long to +100 mV were delivered at 10 s intervals, from a holding potential of -90 mV. X-axis shows trace number, Y-axis shows current amplitude at steady state. The periods during which VSN-16R and TEA were applied are denoted by horizontal bars.
- (c) Comparison of the current amplitudes recorded in response to voltage steps to either +90 mV or +50 mV, before and after application of 20  $\mu\text{M}$  VSN-16R. Red bars show the current measured under baseline conditions, blue bars show the response after application of 20  $\mu\text{M}$  VSN-16R. Error bars denote SEM.  $n=7$ .
- (d) Averaged I-V plots for the voltage families described in (a), across all cells ( $n=7$ ). Filled circles show the mean current amplitude for each voltage step, while error bars show the SEM. Trend line was generated from a least-squares fit of the Boltzmann function to the data.

**Table 4.9. 2-way repeated measures ANOVA of the effect of VSN-16R on currents mediated by rBK $\alpha^{\emptyset}$ , in the presence of 500 $\mu\text{M}$  GSH**

	SS	DF	MS	F (DFn, DFd)	P value
Voltage (50 mV vs. 90 mV)	1.16E-17	1	1.16E-17	F (1, 5) = 7.56	P=0.040
VSN-16R	2.67E-24	1	2.67E-24	F (1, 5) = 0.0001847	P=0.98
Interaction: voltage x VSN-16R	4.63E-20	1	4.63E-20	F (1, 5) = 3.019	P=0.14
	Source of Variation	% of total variation	P value		
	Voltage	29.35	0.040	*	Yes
	VSN-16R	6.76E-06	0.98	ns	No
	Interaction: voltage x VSN-16R	0.1173	0.14	ns	No

Table shows 2-way ANOVA with factors Voltage (+50 vs +90 mV) and VSN-16R (baseline vs. + 20  $\mu\text{M}$ ). Abbreviations: SS= , DF= degrees of freedom, MS= Mean square of treatment effect, F(DFn,DFd)=F statistic based on the degrees of freedom of the treatment (DFn) and error (DFd), values given in parentheses after the F statistic.

To corroborate the result obtained using GSH, the same experiment was repeated replacing 500  $\mu\text{M}$  GSH with 500  $\mu\text{M}$  DTT, another reducing agent. The results are summarised in Figure 4.14. As before, there was no observable change in whole-cell current amplitude during either the time-course or the voltage family protocols in response to the bath application of 10  $\mu\text{M}$  VSN-16R (Figure 4.14a, b). The presence of 500  $\mu\text{M}$  DTT also did not appear to alter the kinetics of the observed current (Figure 4.14a). Again, the current was abolished successfully by either 5 mM TEA or 10  $\mu\text{M}$  paxilline. Figure 4.14d shows the effect of 10  $\mu\text{M}$  VSN-16R on the averaged IV relationships across all cells ( $n=7$ ). Qualitatively speaking, it can be seen that there is very little difference in the means  $\pm$  SEM of the two curves, suggesting little change in the I-V relationship following VSN-16R application in the presence of DTT. Additionally, application of 10  $\mu\text{M}$  VSN16R increased current amplitude at +90 mV to  $104\% \pm 4\%$  of baseline, while at +50 mV the current was increased to  $101\% \pm 14\%$  of baseline. However the effect of VSN-16R was not significant (Table 4.10  $p=0.37$ , 2-Way repeated measures ANOVA,  $n=7$ ).

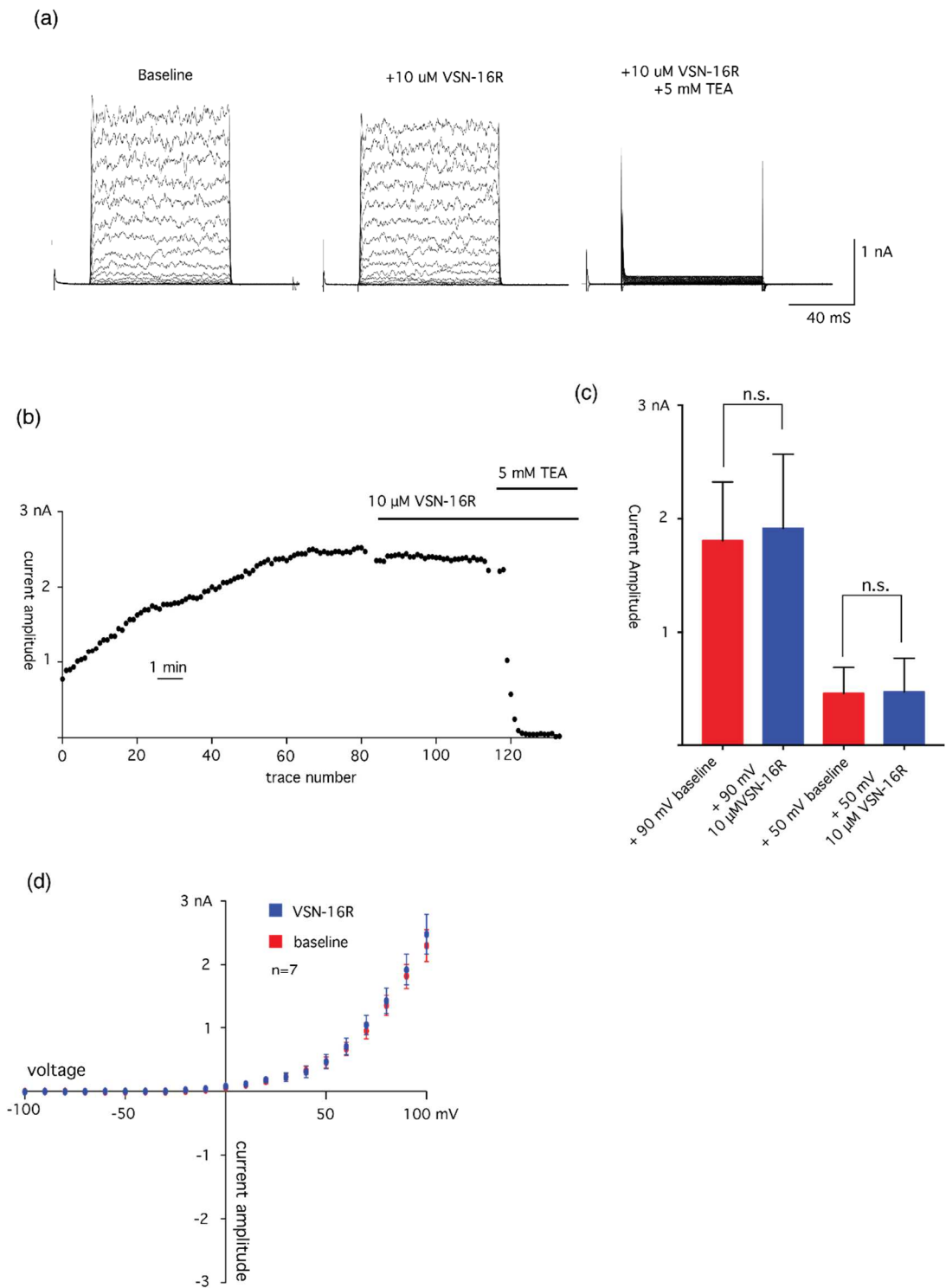


**Figure 4.14. Effect of VSN-16R on currents in HEK293 cells expressing rBK $\alpha^0$  channels in the presence of intracellular dithiothreitol**

*The experiments summarised in this figure were performed by R. Roberts (undergraduate student), under my supervision.*

**(a)** *Current traces in response to a family of 40 ms-long voltage steps to potentials between -100 and +100 mV, in 10 mV increments, from a holding potential of -90 mV, in the presence of 500  $\mu\text{M}$  intracellular dithiothreitol (DTT). Left traces show baseline current responses of*

cell, middle traces show responses in the presence of 20  $\mu\text{M}$  VSN-16R, and right hand traces show responses following application of 20  $\mu\text{M}$  VSN-16R + 5 mM TEA.

- (b) Time-course of the currents recorded from the cell shown in (a). Voltage steps of 50 ms to +100 mV were delivered at 10 s intervals, from a holding potential of -90 mV. X-axis shows trace number, Y-axis shows current amplitude measured at steady state. The periods during which VSN-16R and TEA were applied are denoted by horizontal bars.
- (c) Comparison of the current amplitudes recorded in response to voltage steps to either +90 mV or +50 mV, before and after application of 20  $\mu\text{M}$  VSN-16R. Red bars show the current measured under baseline conditions, blue bars show the response after application of 20  $\mu\text{M}$  VSN-16R. Error bars denote SEM.  $n=7$ .
- (d) Averaged I-V plots for the voltage families described in (a), across all cells ( $n=7$ ). Filled circles show the mean current amplitude for each voltage step, while error bars show the SEM. Trend line was generated from a least-squares fit of the Boltzmann function to the data.

**Table 4.10. 2-way repeated measures ANOVA of the effect of VSN-16R on currents mediated by rBK $\alpha^{\text{D}}$ , in the presence of 500 $\mu\text{M}$  GSH**

	SS	DF	MS	F (DFn, DFd)	P value
Voltage (50 mV vs. 90 mV)	1.37E-17	1	1.37E-17	F (1, 6) = 51.07	P=0.0004
VSN-16R	2.64E-20	1	2.64E-20	F (1, 6) = 0.9254	P=0.37
Interaction: voltage x VSN-16R	1.65E-20	1	1.65E-20	F (1, 6) = 2.465	P=0.17
	Source of Variation	% of total variation	P value		
	Voltage	73.04	0.0004	***	
	VSN-16R	0.1406	0.37	ns	
	Interaction: voltage x VSN-16R	0.08811	0.17	ns	

Table shows 2-way ANOVA with factors Voltage (+50 vs +90 mV) and NS19504 (baseline vs. + 10  $\mu\text{M}$ ). Abbreviations: SS= , DF= degrees of freedom, MS= Mean square of treatment effect, F(DFn,DFd)=F statistic based on the degrees of freedom of the treatment (DFn) and error (DFd), values given in parentheses after the F statistic.

Taken together, the results from the experiments with GSH and DTT in the pipette solution suggest that the presence of a reducing environment does not unmask a redox-dependent enhancing effect of VSN-16R on BK- $\alpha$ -mediated currents.

#### **4.10 Effect of VSN-16R on currents mediated by heterologously expressed rBK $\alpha^{\emptyset}$ channels in the presence of extracellularly applied hydrogen peroxide**

One of the major components in the pathogenesis of multiple sclerosis is oxidative stress, whereby reactive oxygen species emitted by macrophages contribute to the demyelination and axonal damage in both MS itself and the EAE animal model (Syburra and Passi, 1999) (Gilgun-Sherki et al 2004). Given that VSN-16R has been shown to alleviate spasticity in the EAE model, and again given the propensity of BK channel function to be modulated by oxidation states, it was hypothesised that the effects of VSN-16R on BK channels might be dependent on a state of cellular oxidative stress.

In order to test this hypothesis, H<sub>2</sub>O<sub>2</sub> was applied extracellularly to induce a state of oxidative stress in HEK 293 cells transfected with rBK $\alpha^{\emptyset}$  subunits. Initial experiments determined that 10 mM extracellular H<sub>2</sub>O<sub>2</sub> caused a noticeable reduction in the BK current, but proved uncondusive to stable electrophysiological recordings, ultimately causing a breakdown of the seal or the death of the cell. Conversely, at 1 mM H<sub>2</sub>O<sub>2</sub>, there was no discernable reduction in the whole-cell current, and so it would be difficult to argue that the cell was suffering from oxidative stress (data not shown).

Experiments with 5 mM H<sub>2</sub>O<sub>2</sub> provided a satisfactory compromise. The results of experiments performed using H<sub>2</sub>O<sub>2</sub> at this concentration can be seen in Figure 4.15. The time course of the BK current amplitude in Figure 4.15b shows that, once a stable baseline current was established, the cell was exposed to 5 mM extracellular H<sub>2</sub>O<sub>2</sub> until a new stable current level had been obtained. The cell was then perfused with extracellular solution containing 5 mM H<sub>2</sub>O<sub>2</sub> and 10  $\mu$ M VSN-16R, with 5 mM TEA being added at the end of the experiment in order to abolish the BK current (Figure 4.15b). In 5 out of 5 cells tested, extracellular application of 5 mM H<sub>2</sub>O<sub>2</sub> led to a reduction of the whole-cell current, without any visible alteration of the quality of the recordings. Subsequent application of 10  $\mu$ M VSN-16R led to a partial rescue of the current amplitude in 3 out of 5 cells. These effects are summarised in Figure 4.15c. At +90 mV, 5 mM H<sub>2</sub>O<sub>2</sub> reduced the current to 80%  $\pm$  3.4% of baseline, while at +50 mV, the current was largely unchanged at 101%  $\pm$  6.0% of baseline. The current at +90 mV then

increased back to  $98.2\% \pm 6.4\%$  of baseline following the addition of  $10 \mu\text{M}$  VSN-16R on top of the  $5 \text{ mM}$   $\text{H}_2\text{O}_2$ .

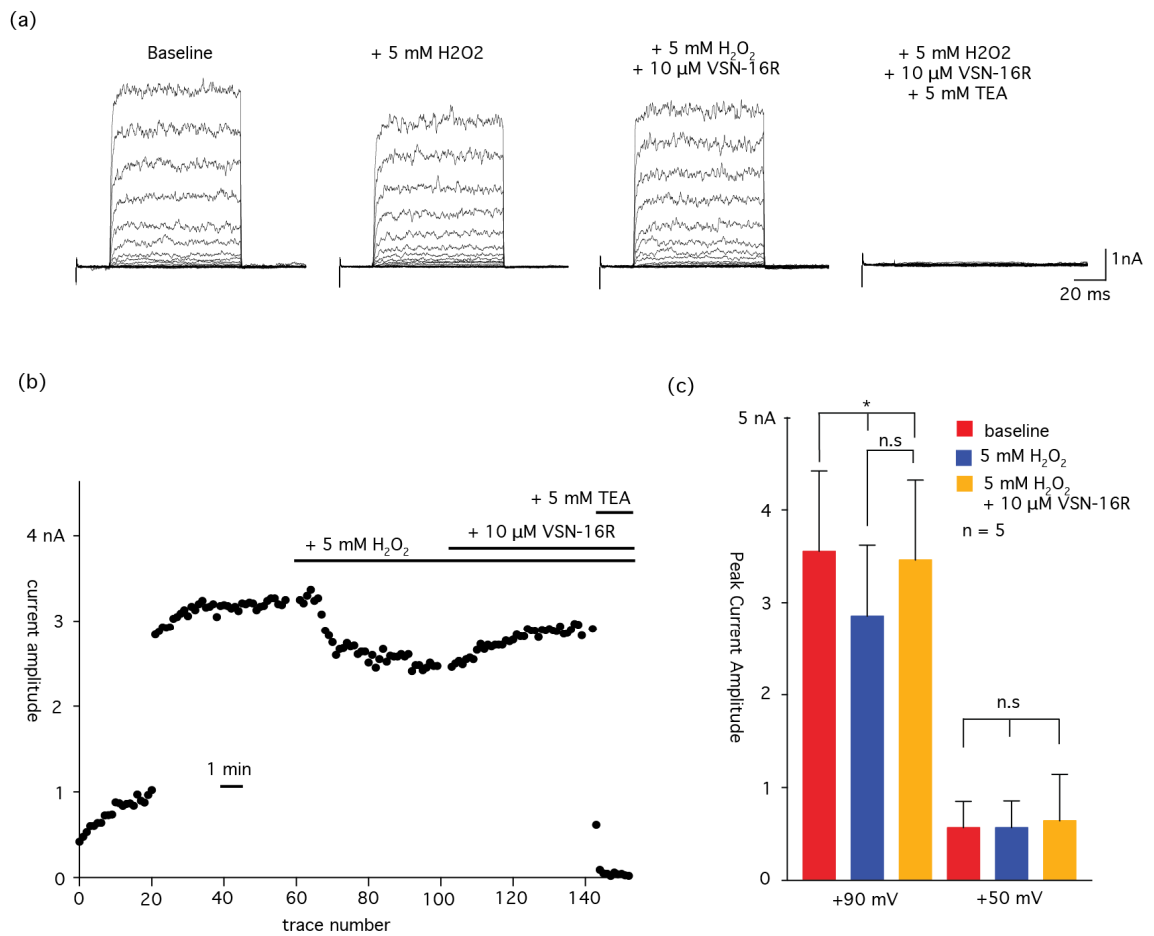


**Figure 4.15. Effect of hydrogen peroxide on the response to VSN-16R of currents in HEK293 cells expressing  $r\text{BK}\alpha^0$  channels**

- (a) *Current traces in response to a family of 40 ms-long voltage steps to potentials between -100 and +100 mV, in 10 mV increments, from a holding potential of -90 mV. All traces come from a single representative cell. From left to right: responses under baseline conditions, in the presence of 5 mM extracellular  $\text{H}_2\text{O}_2$ , following application of 5 mM  $\text{H}_2\text{O}_2$  + 20  $\mu\text{M}$  VSN-16R, and after the addition of 5 mM TEA on top of the aforementioned compounds.*
- (b) *Time-course of the cell shown in (a). Horizontal bars show the periods during which each compound was applied by bath perfusion.*
- (c) *Comparison of the averaged current recorded across all cells ( $n=5$ ) to voltage steps to +50 mV and +90 mV, at baseline (red), following the application of 5 mM  $\text{H}_2\text{O}_2$  (blue) and of 5 mM  $\text{H}_2\text{O}_2$  + 20  $\mu\text{M}$  VSN-16R (yellow). Error bars show SEM.*
- (d) *I-V plots showing the average response at each voltage recorded across all cells ( $n=5$ ). Same colour code as in (b). Filled circles denote the mean current response, while error bars denote the SEM.*

**Table 4.11. 2-way repeated measures ANOVA of the effect of H<sub>2</sub>O<sub>2</sub> and H<sub>2</sub>O<sub>2</sub> + VSN-16R on currents mediated by rBKα<sup>o</sup>.** Multiple comparisons were performed using Tukey's multiple comparisons test to control for the familywise error rate.

	SS	DF	MS	F (DFn, DFd)	P value
<b>voltage</b>	5.35E-17	1	5.35E-17	F (1, 4) = 97.8	P=0.0006
<b>Drug</b>	8.94E-19	2	4.47E-19	F (2, 8) = 8.252	P=0.011
<b>Interaction: voltage x drug</b>	6.27E-19	2	3.14E-19	F (2, 8) = 6.256	P=0.023
	Source of Variation	% of total variation	P value		
	voltage	83.05	0.0006	***	
	VSN-16R	1.388	0.011	*	
	Interaction: voltage x VSN-16R	0.974	0.023	*	
	Mutiple Comparisons				
	<b>90 mV</b>				
	baseline vs. H <sub>2</sub> O <sub>2</sub>	0.0029			
	baseline vs. H <sub>2</sub> O <sub>2</sub> + VSN	0.7977			
	H <sub>2</sub> O <sub>2</sub> vs. H <sub>2</sub> O <sub>2</sub> + VSN-16R	0.0067			
	<b>50 mV</b>				
	baseline vs. H <sub>2</sub> O <sub>2</sub>	>0.9999			
	baseline vs. H <sub>2</sub> O <sub>2</sub> + VSN	0.5316			
	H <sub>2</sub> O <sub>2</sub> vs. H <sub>2</sub> O <sub>2</sub> + VSN-16R	0.5355			

*Table shows 2-way ANOVA with factors Voltage (+50 vs +90 mV) and VSN-16R (baseline vs. + 20  $\mu$ M). Abbreviations: SS= , DF= degrees of freedom, MS= Mean square of treatment effect, F(Dfn, Dfd)=F statistic based on the degrees of freedom of the treatment (DFn) and error (DFd), values given in parentheses after the F statistic.*

The results were compared by a 2-way repeated measures ANOVA (Table 4.11). There was a significant effect of drug treatment ( $p=0.011$ ,  $n=5$ ), and the interaction between voltage and drug effect was also significant ( $p=0.023$ ). Multiple comparisons of the different treatments at each of the two voltage steps yielded a significant difference at +90 mV between baseline and  $H_2O_2$  ( $p=0.0029$ ) and between  $H_2O_2$  and  $H_2O_2 + VSN-16R$  ( $p=0.0067$ ). However at +50 mV, no significant effect of treatment was observed for any comparison pair.

In summary, these data show that 5 mM  $H_2O_2$  causes a decrease in the amplitude of the BK current at +90 mV, and that, following the application of VSN-16R, there does appear to be a recovery of some sort following application of VSN-16R. There does not appear to be any effect of either compound at +50 mV.

## Chapter 5. Discussion

### 5.1 Whole cell recordings of currents mediated by heterologously expressed rBK $\alpha^0$

Whole cell voltage clamp recordings from cells transfected with rBK $\alpha^0$  cDNA elicited currents that displayed characteristics typical of BK $\alpha$  homomultimeric channels. Current amplitude was dependent on both voltage and intracellular [Ca<sup>2+</sup>] (Figure 4.1), and the current was completely blocked by either paxilline (Knaus et al 1994) or low concentrations of TEA (Figure 4.2). Additionally the current recordings exhibited a noisy appearance, typical of currents through channels of large conductance when the open probability is relatively low (Olesen et al 1994). Mean activation time constant was  $1.68 \pm 0.15$  ms, consistent with measurements described elsewhere (Orio et al, 2002, Wang et al 2009, Nausch et al 2014). As a result of these factors, it is clear that the whole cell currents recorded are overwhelmingly mediated by channels formed from the rBK $\alpha^0$  subunit.

In our whole cell recordings, it was not possible to accurately quantify the voltage of half-maximal activation ( $V_{1/2}$ ), a typical measure of changes in voltage dependence. In keeping with previous studies involving whole-cell recordings of BK currents in low intracellular [Ca<sup>2+</sup>] (e.g. Olesen et al, 1994; Strobaek et al 1996, Nausch et al 2014), it was not possible to achieve a voltage at which the current amplitude reached a plateau, which is necessary in order to fit a Boltzmann function to the IV curve and so determine  $V_{1/2}$ . At low intracellular calcium concentrations, the voltage at which saturation is achieved is very high, and the combination of a high unitary conductance and overexpression due to transient transfection lead to very large currents being produced at these high voltages. The large number of open channels of high conductance drastically reduces the membrane resistance, leading to a significant voltage error, which cannot be adequately controlled by  $R_s$  compensation (see methods 2.2.6.1). Additionally, large voltage steps had a destabilising effect on the patched cell.

In their paper on the activation of BK channels by the benzimidazolone NS1619, Olesen and colleagues (Olesen et al 1994) attempted to report voltage shifts using the voltage at which each curve reached an arbitrary current amplitude value. However this seems unreasonably arbitrary, as the recorded curves are essentially fragments of a sigmoidal Boltzmann curve, varying in slope throughout the function. It is therefore not apparent whether any “shift” is due to a genuine voltage shift, or instead due to a generalised

increase in current amplitude in a voltage independent manner, e.g. due to an increase in open probability at all voltages.

As a result of these limitations, it is common to record BK channel currents using excised patches, where the current amplitudes are more manageable. In excised patches, the point at which saturation of the conductance occurs can be observed using a tail current protocol (eg. Strobaek et al 1996). Following the activating voltage step, the cell is stepped to a negative voltage at which the channel is closed, and at which there is an inward driving force on  $K^+$ . At the start of the negative voltage step, current flows through the channel as it closes, allowing observation of channel conductance independent of the driving force on  $K^+$ , which otherwise changes as the voltage is stepped, and adds a linear increase to the observed current amplitude even when the channels are maximally open. This approach allows for an accurate measurement of  $V_{1/2}$ , but again would not work in whole cell experiments in low  $[Ca^{2+}]_i$  as the voltages required to reach maximal activation are still very high (Strobaek et al 1996), such that their application caused the whole cell configuration to become unstable, and led the subsequent loss of the cell.

Excised patch recordings exhibit a number of problems however, which make examining the effect of activators difficult. BK channels are modulated by a wide variety of intracellular signals, and as a result BK currents in excised patches exhibit a number of time-dependent changes in activity following excision, including a prolonged, gradual "run down" of current amplitudes due to a shift in the  $V_{1/2}$  of activation to more depolarised potentials (DiChiara and Reinhart 1997, Lin et al 2004, ). While this is not a serious problem in measuring activators known to have a rapid effect on channel activity, in situations where the timecourse of activation is purely speculative, it is possible that the effect would be masked by the run down. Additionally, BK channels in excised patches can exhibit so-called *Wanderlust* kinetics, in which the channels exhibit large, slow fluctuations in open probability, as well as sensitivity to  $Ca^{2+}$  (Silberberg et al 1996). These features make the interpretation of activation changes in response to drug administration difficult. Additionally, it was considered useful to keep the local environment experienced by the channel as close to physiological relevance as possible. Although heterologous expression systems are necessarily rather less representative of specific physiological contexts than ex vivo preparations, they preserve the presence of cytosolic and membrane-associated intracellular factors that can regulate BK channel function, such as kinases and phosphatases, and membrane phospholipids such as  $PIP_2$ .

It was therefore decided that the whole cell configuration represented a better medium for examining the capacity of VSN-16R to activate BK channels.

## **5.2 Effect of NS19504 on currents mediated by heterologously expressed rBK $\alpha$**

NS19504 produced a pronounced and statistically significant increase in the BK current amplitude when applied extracellularly at a concentration of 10  $\mu$ M (Figure 4.3). The increase in current amplitude due to NS19504 was around 300% of baseline, when measured at +90 mV. The additional application of paxilline once the current had reached a plateau was used to confirm that the observed current was entirely mediated by BK channels.

While the activation observed in our experiments was pronounced, it was only around 15% of that reported by for human BK $\alpha$  as measured in the whole cell configuration in the paper that originally reported the activation effects of NS19504 (Nausch et al 2014). It is possible that this is due to differences in the amount of intracellular free Ca<sup>2+</sup> (their 30 nM vs our 200 nM). Indeed in the same paper, the authors assess the effects of NS19504 in excised patches using a free intracellular [Ca<sup>2+</sup>] of 300 nM, and report a current increase of a similar magnitude to that observed in our experiments. Alternatively the difference could potentially be caused by differences in the response of the rat and human isoforms of the alpha subunit. The time course of the activation effect was similar to that reported in the aforementioned study.

In our experiment there was a larger increase in the current amplitude measured at +50 mV than that measured at +90 mV (Figure 4.3c) and in the 2-way ANOVA there was a significant interaction between the effect of voltage and that of NS19504 (Table 4.1), suggesting there may be some voltage dependence to the effects of NS19504.

Our results represent the first evidence that NS19504 acts as an activator of channels formed by the rat BK $\alpha$  subunit, and are largely in agreement with the observations reported for BK channels formed by the human alpha subunit (Nausch et al 2014). They also act as a benchmark against which to compare the effect of VSN-16R under our experimental conditions.

### 5.3 Effect of VSN-16R on currents mediated by heterologously expressed rBK $\alpha^{\emptyset}$

In experiments conducted by Prof. Selwood's collaborators, VSN-16R produced a large increase in whole cell current amplitude in the EA.hy926 cell line, and this current was inhibited by paxilline (Bondarenko et al, unpublished data). These data suggested that VSN-16R led to the activation of a BK mediated current in the cell line, and so our intention was to determine whether the drug acted by direct activation of BK channels, using the heterologously expressed products of BK cDNA in HEK293 cells. The EA.hy926 cell line (Edgell et al 1983) is derived from the fusion of human umbilical vein endothelial cells with the permanent human cell line A459, and expresses Factor VIII-related antigen, a marker of differentiated endothelial cells. From RNA sequencing data EA.hy926 cells are known to express the BK alpha subunit, and the  $\beta 3$  and  $\beta 4$  subunits (D.Selwood, unpublished data). The presence of the BK alpha subunit has also been independently confirmed in the human umbilical vein endothelial cell by reverse transcriptase PCR (Begg et al, 2003).

In our hands, there was no effect of VSN-16R on currents through channels formed by rBK $\alpha^{\emptyset}$  elicited at either +50 mV or +90 mV. No significant increase in current amplitude was observed during the experiments when the drug was applied for a period of 7-15 minutes (Table 4.2), and there was an almost perfect overlap in the I-V curves produced at the end of the baseline phase of the experiments and at the end of the drug application phase (Figure 4.4). These results largely rule out the possibility of a direct effect of VSN-16R on BK channels purely formed by the pore-bearing rBK $\alpha^{\emptyset}$  subunit. The VSN-16R stock solution used by our lab was tested for purity by Prof. Selwood using high performance liquid chromatography and mass spectrometry (LC-MS), and the compound is highly stable in aqueous solution, making it unlikely that the negative result was observed due to incorrect preparation of the compound. Our results do not rule out the possibility that there is a direct effect of VSN-16R that is specific to the protein product of human *KCNMA1*, and this would need to be examined in future experiments. An additional issue is that there are a total of 13 alternate exons in *KCNMA1*, and together these lead to a combinatorial explosion of thousands of possible splice variants (Beisel et al, 2007). It would therefore be extremely difficult to exclude the involvement of every combination individually. Alternative exons have been shown to affect various aspects of channel function, including voltage and Ca<sup>2+</sup> sensitivity (Shipston et al 2001), and capacity for phosphorylation by PKA (Tian et al 2001, Zhang et al 2004). However as yet no exon-specific change in sensitivity to any small molecule inhibitor or activator, or to any toxin, has been described. Also, given that the VSN-16R effects we are trying to

explain are relatively diverse, including effects from not only individual cell lines but rescue of behavioural and neurological abnormalities in MS and FXS animal models, it seems unlikely that a single splice variant is necessary for all the effects of VSN-16R that have been observed.

An additional possibility that was considered was whether the oxidation state of the intracellular environment had an effect on the efficacy of VSN-16R. The activity of BK channels is modulated by the redox state of the cell (Hermann et al 2015, Wang et al 1997, DiChiara and Reinhardt 1997), and signalling based on redox state changes has been observed in endothelial cells (Panieri and Santoro, 2015). Intracellular solutions used in patch clamp experiments are typically more oxidised than the cytosol, so it was hypothesised that this could mask an effect of VSN-16R. Therefore, under my supervision, Ruairi Roberts performed experiments in HEK 293 cells transfected with rBK $\alpha^0$ , using intracellular solution containing either dithiothreitol (DTT) or glutathione (GSH). Under these conditions, the BK channel-mediated current amplitude was similar to that observed in the presence of standard intracellular solution. Application of VSN-16R again did not produce any change in current amplitude elicited over a whole range of voltages (Figure 4.13, 4.14).

Additional experiments were performed using standard intracellular solution, in which hydrogen peroxide (H<sub>2</sub>O<sub>2</sub>) was applied extracellularly, in order to simulate conditions of oxidative stress, which has been shown to reduce BK channel open probability in rat hippocampal neurons (Gao and Fung, 2002). In keeping with these findings, a reduction in BK current amplitude was observed in response to H<sub>2</sub>O<sub>2</sub>. It was hypothesised that VSN-16R might have an activating effect on BK channels that was dependent on a state of oxidative stress, as reactive oxygen species emitted by macrophages contribute to demyelination in both multiple sclerosis and the EAE mouse model, in which VSN-16R has been shown to have an antispastic effect. However, in our experiments, application of VSN-16R did not have any significant effect on BK current amplitude in the presence of H<sub>2</sub>O<sub>2</sub>.

#### **5.4 Effect of VSN-16R on currents mediated by heterologously expressed rBK $\alpha^0$ in combination with $\beta$ subunits**

As VSN-16R did not appear to have any effect on channels formed by the rBK $\alpha^0$  subunit alone, it was tested on HEK-293 cells transiently transfected with both rBK $\alpha^0$  and one of three different human  $\beta$  subunits, using the same methodology as for the alpha subunit alone. The presence of  $\beta$  subunits is known to affect the sensitivity of the BK channel to

various toxins. For example the  $\beta 4$  subunit confers reduced sensitivity to iberiotoxin (Meera et al 2000) and increased sensitivity to martentoxin (Shi et al 2008). As a result, it is important for any potential BK targeting drug to be tested on channels composed of defined  $\beta$  subunits. Additionally, no  $\beta$  subunit specific opener has yet been found for BK channels, and a compound of this nature would be very valuable, for example being able to activate  $\beta 4$  containing BK channels in neurons, without for example affecting the  $\beta 1$ -containing BK channels responsible for regulation of homeostatic  $K^+$  secretion in renal tubules. As both  $\beta 4$  and  $\beta 3$  had been detected in the RNA sequencing data of the EA.hy926 cell line, both these were tested, as was  $\beta 2$ , which is widely expressed in neurons, and was therefore considered potentially relevant to the reported behavioural and neurological effects in the animal model studies. Currents recorded from cells transfected with rBK $\alpha^0$  and either  $\beta 2$  and  $\beta 4$  displayed a clear electrophysiological phenotype, allowing for easy confirmation that these subunits were being successfully expressed and incorporated into the channel assemblies. When the  $\beta 4$  subunit was co-expressed with rBK $\alpha^0$ , the activation time constant for the current was around an order of magnitude slower than for the currents in cells expressing only the rBK $\alpha^0$  subunit (Figure 4.5), and in the case of the  $\beta 2$  subunit, currents displayed an inactivating phenotype (Figure 4.9, 4.10). Currents from cells transfected with  $\beta 3$  subunit DNA were not noticeably different from those transfected with only rBK $\alpha^0$ , however this was to be expected given that the  $\beta 3$  subunit only confers a very rapid, small inactivation in the presence of low internal free  $Ca^{2+}$ , and even then only at very positive voltages (Xia et al 2000). The ratio of  $\beta$  subunit cDNA to rBK $\alpha$  cDNA used was 4:1 by mass, in order to increase the chances that the expression ratio of  $\beta$  to  $\alpha$  subunits would be high. As the  $\beta$  subunits are only around 20-30 kDa compared to the 60 kDa alpha subunit, the molar ratio is around 6:1. As discussed in the Introduction, the stoichiometry of the BK channel assembly is such that each channel can have between zero and four  $\beta$  subunits, and in a given cell the stoichiometries of the channel population can be described by a Poisson distribution, biased further towards higher numbers the higher the molar ratio of BK $\alpha$  to  $\beta$  RNA transcripts in the cell (Wang et al 2002).

The results of all three sets of experiments were largely identical to those observed in cells expressing channels formed by only the rBK $\alpha^0$  subunit. In all cases, there was no significant effect of VSN-16R on current amplitude, and an almost complete overlap in the averaged I-V curves obtained before and after drug application (Figure 4.7, 4.10, 4.12). In every experiment, currents were almost entirely abolished by paxilline. In additional experiments, the effect on current amplitude of including VSN-16R intracellularly was tested on cells transfected with rBK $\alpha^0$  and h $\beta 4$  subunits (Figure 4.8).

BK current amplitude in cells in which VSN-16R was included in the pipette was not significantly different from currents in the control cells.

From these experiments it seems relatively clear that there is no direct effect of VSN-16R on recombinant BK channels formed from alpha subunits and either  $\beta 2$ ,  $\beta 3$ , or  $\beta 4$  subunits.

## **5.5 Effect of NS19504 on currents mediated by heterologously expressed rBK $\alpha^0$ in combination with $\beta$ subunits**

Extracellular application of NS19504 produced a significant increase in the whole-cell current amplitude for all three of the  $\beta$  subunits tested. The increase in amplitude due to NS19504 was not significantly different between cells expressing only rBK $\alpha^0$ , and cells expressing rBK $\alpha^0$  together with any of the  $\beta$  subunits tested.

In each case, the drug had a larger effect at +50 mV than at +90 mV, and judging from the results of the 2-way ANOVA analysis (Table 4.3, 4.5, 4.7), a small but significant amount of the variance in each case was explained by the interaction between voltage and drug effect. The percentage of variance explained by this interaction was similar in each case, as well as for the alpha subunit alone.

These data are the first to show that NS19504 is effective as an activator of BK channels containing  $\beta$  subunits, though it does not appear that there is much difference between its effect on heteromultimeric channels containing  $\beta$ -subunits, and that observed in BK $\alpha$  homomultimeric channels. The most likely explanation is therefore that the opener acts solely at a site on the alpha subunit, and does not require the beta subunits for its action.

## **5.6 Potential alternative mechanisms of action of VSN-16R**

VSN-16R has been shown to rescue behavioural abnormalities in FMRP $^{-/-}$  mice, and has an antispastic effect in the EAE mouse model of multiple sclerosis, with the effect being prevented by paxilline (Selwood et al, unpublished data). Combined with the activation of a paxilline-sensitive current in the EA.hy926 cell line (Bondarenko and Selwood, unpublished data), these data present a case that the medically useful effects of the compound might be dependent on the activation of a BK current. However, our data do not show any evidence of a direct activation of either recombinant rat BK $\alpha$  homomultimeric channels, or heteromultimers combining rBK $\alpha^0$  and either the beta 3 or beta 4 subunits, which are the only ones expressed in EA.hy926 cells.

One possibility for the lack of effect seen by our lab on heterologously expressed BK channels is that the effect of VSN-16R on a paxilline-sensitive current observed in the EA.hy926 cell line by Bondarenko and Selwood (unpublished data) is not due to a direct activation of BK channels, but instead represents an indirect effect resulting from the interaction of VSN-16R with a different target. The compound has been shown to relax mesenteric artery constriction in rat, and the effect is prevented by the cannabinoid receptor antagonists rimonabant and AM 251 (Hoi et al, 2007), as well as O-1918, a specific inhibitor of a cannabinoid receptor of unknown molecular identity that is present in endothelial cells and activated by anandamide (Offertaler et al, 2003) and atypical cannabidiol (an-cbd). Furthermore, the effect of VSN-16R on vasoconstriction was reduced by inhibiting BK channels using 50 nM charybdotoxin, suggestive of a coupling of cannabinoid receptors to the activation of BK channels as a potential mediator of this effect (Hoi et al, 2007).

VSN-16R has been shown to not bind to either CB<sub>1</sub> or CB<sub>2</sub> cannabinoid receptors (Hoi et al, 2007; D. Selwood, unpublished data). However, a number of groups have proposed the existence of an atypical cannabinoid receptor in endothelial cells, based on evidence that anandamide produces vasodilation in the mesenteric arterial bed (Jarai et al 1999), which is not prevented by CB<sub>1</sub> or CB<sub>2</sub> specific antagonists (Wagner et al 1999) and persists in CB<sub>1</sub>/CB<sub>2</sub> knockout mice (Jarai et al 1999). Abnormal cannabidiol (an-cbd), a structural analog of cannabidiol which does not bind CB<sub>1</sub> or CB<sub>2</sub> receptors, mimicks the vasodilation produced by anandamide in the arterial bed cells (Jarai et al 1999), and both its effects and those of anandamide are inhibited by O-1918, another structural analogue of cannabidiol (Offertaler et al 2003).

Might this atypical cannabinoid receptor be responsible for the effects of VSN-16R on BK channel activation? In human umbilical vein endothelial cells, from which the EA.hy926 cell line is derived, extracellular application of an-cbd has been shown to lead to BK channel activation (Begg et al, 2003). The authors conclude that this effect was independent of intracellular free Ca<sup>2+</sup> concentration, by adding the fast Ca<sup>2+</sup> buffer BAPTA to the intracellular solution. Under these conditions, an-cbd still produced an increase in BK channel activation.

The above results suggest that VSN-16R might indirectly activate the BK current via cannabinoid receptors in the EA.hy926 cell line. Activation of the cannabinoid receptors might lead to activation of BK channels either as a result of a change in intracellular Ca<sup>2+</sup> concentration or of post-translational modifications of BK channels. As the effects of the atypical cannabinoid receptor are inhibited by pertussis toxin (Begg et al 2003), this might

be by direct interaction between  $G_{i/o}$  and the BK channel, or via some downstream second messenger. Alternatively, activation of the receptor could lead to release of  $Ca^{2+}$  from intracellular stores, leading to an increase in BK channel activation due to the  $Ca^{2+}$  dependent shift in the voltage dependence. In support of this latter hypothesis, anandamide has been shown to increase cytoplasmic  $Ca^{2+}$  concentration by mobilisation of calcium from intracellular stores in the EA.hy926 cell line (Mombouli et al, 1999), and this effect was not abolished by the CB1 antagonist SR141716A.

## 5.7 Conclusions

The results presented in this part of the thesis are essentially twofold. First they show that NS19504 is a BK channel activator, capable of activating rat BK $\alpha$  homomeric channels and heteromeric channels comprising the  $\beta$ 2,  $\beta$ 3 and  $\beta$ 4 subunits, extending previous findings obtained on recombinant human BK channels formed by the alpha subunit alone (Nausch et al 2014).

Second, it is concluded that VSN-16R does not act as a direct BK channel activator, either by activation of recombinant channels formed by the alpha subunit alone, or in a manner dependent on any of the three  $\beta$  subunits tested here. Application of VSN-16R is no more effective on BK-mediated currents in cells in a reduced redox state, or under conditions of oxidative stress, than it is under typical whole cell recording conditions.

Given that VSN-16R is a derivative of the endocannabinoid compound anandamide, it remains a reasonable possibility that the effects of VSN-16R observed in the EA.hy926 cell line, the behavioural rescue of FMRP $^{-/-}$  mice, and the compound's antispastic effects in the EAE murine model of multiple sclerosis, are all mediated by the indirect modulation of BK channels via cannabinoid receptors, a hypothesis that needs to be tested in further experiments.

## **PART TWO: Evidence for spatially localised signalling domains in the monoaminergic inhibition of the sI<sub>AHP</sub>.**

### **Chapter 6. Introduction**

#### **6.1 The Afterhyperpolarisation**

In hippocampal pyramidal cells, trains or bursts of action potentials trigger the activation of hyperpolarising K<sup>+</sup> conductances underlying an extended afterhyperpolarisation (AHP) of the membrane potential. Whilst there is some crossover between the currents responsible for the membrane repolarisation phase of an action potential and those responsible for the afterhyperpolarisation, the afterhyperpolarisation represents a delayed opening of K<sup>+</sup> channels that persists beyond the end of spike repolarisation, and is important for controlling neuronal excitability and firing rate.

The AHP in hippocampal pyramidal cells has three components, differing on the basis of their kinetics and the contributing ion channels, and known as the fast AHP (fAHP), medium AHP (mAHP) and slow AHP (sAHP).

##### **6.1.1 fAHP**

The fast afterhyperpolarisation is mediated by a conductance activated by both calcium and voltage, and has a duration of around 2-5 ms (Storm 1989). The associated current, known as I<sub>c</sub>, is absent in the presence of Ca<sup>2+</sup> chelators, is inhibited by tetraethylammonium (TEA) at submillimolar concentrations, and is additionally blocked by the BK-specific inhibitors iberiotoxin and paxilline, as well as by charybdotoxin (Lancaster and Nicoll 1987, Shao et al 1999, Gu et al 2007). It is therefore thought that I<sub>c</sub> is mediated by the large conductance BK channels in hippocampus, which also contribute to the membrane repolarisation phase of the action potential (Adams et al 1982, Lancaster and Nicoll 1987). The fAHP is present after individual action potentials and following the first spikes in a burst, but is absent following the later spikes in a given burst. This is likely due to BK channel inactivation due to the presence of a BK channel subtype containing the β2 subunit (Faber and Sah 2003).

### 6.1.2 mAHP

The mAHP is generated in response to a train or burst of action potentials, and exhibits rapid activation kinetics (<10 ms) and a duration of up to 100 ms. The mAHP is mediated by both  $\text{Ca}^{2+}$  sensitive and voltage sensitive components, and the relative contribution of these varies with cell type. Initial investigations of mAHP in pyramidal cells supported the view that it was mediated by the voltage dependent current,  $I_M$ , which is sensitive to muscarinic receptor activation (Brown and Griffith, 1983). Subsequently, studies in various neuronal subtypes demonstrated the contribution of a separate  $\text{Ca}^{2+}$  dependent component, which was inhibited by the bee venom toxin apamin (Pennefather et al, 1985, Sah and McLachlan 1991, 1992, Schwindt et al, 1988), and this current was ascribed to the small conductance SK channel family. In CA1 pyramidal neurons, a mAHP current ( $I_{AHP}$ ) was described as being largely SK2 mediated in voltage clamp experiments (Stocker et al 1999). However subsequent studies using current clamp argued that the mAHP generated in response to a train of action potentials was exclusively mediated by  $I_M$ , which in CA1 pyramidal cells is mediated by Kv7.3 (Gu et al, 2005). A subsequent study (Chen et al, 2014) resolved the controversy by demonstrating that populations of both channels are present in the soma of CA1 pyramidal neurons, but only Kv7.3 channels normally contribute significantly to mAHP, with SK2 contribution becoming unmasked only when Kv7 channel activity was downregulated.

### 6.1.3 sAHP

The third, and by far the most enigmatic component of the afterhyperpolarisation is the sAHP, mediated by a  $\text{Ca}^{2+}$  dependent  $\text{K}^+$  current ( $sI_{AHP}$ ) with unusually slow kinetics (Alger and Nicoll 1980, Hotson and Prince 1980, Schwartzkroin and Stafstrom 1980, Lancaster and Adams, 1986). The rising phase of the current has a duration of 400-700 ms, with a decay phase lasting several seconds. Channel kinetics are temperature sensitive, but as an example experiments conducted by Lancaster and Adams (1986) give the decay time constant as 1.5 s, though in experiments at room temperature this can be as much as 4 s (Gustafsson & Wigstrom 1981).

The sAHP is generated in response to a train of action potentials or prolonged depolarisation, and plays a prominent role in spike frequency adaptation (Sah and Faber, 2002). The size of the sAHP is directly proportional to the number of action potentials generated in current clamp experiments (Madison and Nicoll 1984, Lancaster and Adams 1986). The property of increasing sAHP activation in a stimulation-dependent

manner acts as a negative feedback control, reducing the neuron's intrinsic excitability in response to further stimulation.

sAHP is pharmacologically separable from the mAHP and fAHP by its insensitivity to apamin and d-tubocurarine (Sah 1996), its lack of sensitivity to TEA up to concentrations of 5 mM (Storm 1990), and its inhibition by a range of neuromodulators, including the monoamines serotonin (5-HT), noradrenaline, dopamine and histamine (Benardo and Prince, 1982; Madison and Nicoll, 1982; Haas and Konnerth, 1983; Andrade and Nicoll, 1987; Colino and Halliwell, 1987; Pedarzani and Storm, 1993, 1995; Torres et al. 1995), as well as acetylcholine (Cole and Nicoll, 1983), and glutamate via metabotropic and NMDA receptors (Charpak et al. 1990; Blitzer et al. 1995).

## **6.2 $sI_{AHP}$ channel kinetics and calcium dependence**

One of the challenges in understanding the sAHP is the relationship between the calcium dependence of the underlying current ( $sI_{AHP}$ ) and its slow kinetics. Whilst it was established early on that  $sI_{AHP}$  activation is dependent on intracellular  $Ca^{2+}$  elevation (Alger and Nicoll 1980, Hotson and Prince 1980, Schwartzkroin and Stafstrom 1980, Lancaster and Adams 1986), it was not clear how the time-course of the  $Ca^{2+}$  signal led to the time-course of the current itself, as the time-course of the  $Ca^{2+}$  signal is around an order of magnitude faster than that of the current (Sah and Clements 1999, Jaffe et al 1992). Given that none of the known potassium channels has single channel kinetics that can directly make sense of this discrepancy, this poses a conundrum, to which several explanations have been proposed:

(1) that the  $sI_{AHP}$  channels are distant from the point of  $Ca^{2+}$  entry and the  $sI_{AHP}$  time-course thus represents the time taken for  $Ca^{2+}$  to diffuse from VGCCs to the  $sI_{AHP}$  channels (Lancaster and Zucker 1994; Zhang et al. 1995); (2) that a second messenger step is needed between  $Ca^{2+}$  influx and  $sI_{AHP}$  channel activation (Schwindt et al. 1992; Lasser-Ross et al. 1997; Abel et al. 2004 ); (3) that the calcium signal activating the channels underlying the sAHP is due to  $Ca^{2+}$  induced  $Ca^{2+}$  release (Sah & McLachlan, 1991; Moore et al. 1998; Tanabe et al. 1998); or (4) that delayed facilitation of the voltage-gated  $Ca^{2+}$  channels is responsible for the activation of  $sI_{AHP}$  (Cloues et al. 1997; Bowden et al. 2001).

### 6.3 Molecular identity of $sI_{AHP}$

The most enigmatic feature of the sAHP current ( $sI_{AHP}$ ) is that as yet there is no conclusive molecular correlate: the identity of the channel responsible for the current in hippocampal neurons remains unknown. It is generally assumed that it is mediated by a single conductance, as its activation and decay kinetics can be fitted adequately by single exponential functions (Sah and Clements 1999). Noise analysis of the whole-cell current (Sah & Isaacson 1995) suggests that the channels underlying the current exhibit a single channel conductance of around 2-7 pS and a mean open time of 2 ms. However this value may represent an underestimate of the unitary conductance if the channels in question are located in the dendrites as opposed to the soma (Valiante et al. 1997; Sah and Bekkers 1996).

Despite the advent of molecular cloning techniques, the channel identity has been difficult to pin down, partly due to conflicting results in different preparations, and also due to a lack of specific pharmacological tools. A number of candidates have been proposed, including SK1 (KCa 2.1; Bowden et al 2001), Kv7.3 (Kv7/M, KCNQ family; Tzingounis and Nicoll 2008, Tzingounis et al 2010, Kim et al 2012), IKCa/SK4 (KCa 3.1; King et al 2015), and the sodium/potassium ATPase (Gulledge et al 2013).

#### **SK1 (KCa2.1)**

It was initially hypothesised that apamin-insensitive SK1 channels were responsible for the  $sI_{AHP}$  (Kohler et al., 1996; Bowden et al 2001), but this was called into question by experiments showing SK1 had a higher sensitivity for apamin than previously thought (Shah and Haylett 2000, Strobaek et al 2000), and by experiments in SK1, SK2, and SK3 knock-out mice, which did not show any reduction in  $sI_{AHP}$  amplitude in CA1 pyramidal cells (Bond et al, 2004). As a result, it is unlikely that SK1 channels are responsible for the  $sI_{AHP}$  in hippocampal pyramidal neurons.

#### **Kv7/KCNQ**

The Kv7 family of potassium channels are the protein products of the KCNQ gene family. Of the five family members, only KCNQ2 (Kv7.2), KCNQ3 (Kv7.3) and KCNQ5 (Kv7.5) are expressed in neurons (Jentsch 2000). A 2008 paper showed that  $I_M$  and  $sI_{AHP}$  were both reduced in the dentate gyrus granule cells of KCNQ2/KCNQ3 double knockout mice, though no change was seen in CA1 pyramidal cells (Tzingounis and Nicoll, 2008). A subsequent paper by the same group proposed that another member of the KCNQ

family, KCNQ5 (Kv7.5) mediates part of the  $sI_{AHP}$  in CA3 pyramidal neurons, as mice transfected with KCNQ5 dominant negative constructs displayed a significantly reduced  $sI_{AHP}$  amplitude compared to controls in CA3, though again not in CA1 neurons (Tzingounis et al, 2010). Another line of evidence comes from the compound UCL2077 which was shown to specifically inhibit  $sI_{AHP}$  in hippocampal neurons in culture (Shah et al, 2006) and also heterologously expressed KCNQ channels, though in a subtype dependent manner, blocking KCNQ1 and KCNQ2 strongly, but not KCNQ5 or KCNQ3 except at positive potentials (Soh et al 2010).

Set against this evidence are a number of objections, including the fact that KCNQ/Kv7 channels are negatively modulated by  $Ca^{2+}$  (Marrion et al, 1991, Selyanko and Brown, 1996), and the fact that UCL2077 is suggested as a blocker of  $sI_{AHP}$  in hippocampal neurons, but has been shown in the heterologously expressed KCNQ channels to only inhibit KCNQ2, the involvement of which has not been experimentally confirmed in CA3 or CA1 pyramidal neurons.

#### **$IK_{Ca}$ / SK4**

Another recently suggested candidate for the  $sI_{AHP}$  in CA1 neurons is  $IK_{Ca}$  / SK4.

The  $IK_{Ca}$  current was initially ruled out as a candidate for the  $sI_{AHP}$  because  $IK_{Ca}$  expression was described as being absent in northern blot experiments of whole-brain lysate (Logsdon et al 1997), but it was subsequently suggested to be present in hippocampal and neocortical pyramidal cells using antibodies against  $IK_{Ca}$  (Turner et al, 2015).

King et al (2015) reported that the selective  $IK_{Ca}$  inhibitor Tram-34 (Wulff et al 2000) reduced spike frequency accommodation and  $sAHP$  amplitude in CA1, and further showed that  $IK_{Ca}$ /SK4 knock out animals exhibited a smaller  $sI_{AHP}$  than control littermates. However this finding conflicts with earlier experiments characterising the pharmacology of  $sI_{AHP}$ , as charybdotoxin, which blocks  $IK_{Ca}$ /SK4 along with BK, Kv1.2 and Kv1.3 channels, did not have any effect on  $sI_{AHP}$  amplitude in rat CA1 pyramidal neurons (Lancaster and Nicoll, 1987, Shah and Haylett 2000). A subsequent study not only failed to recapitulate the Tram-34 result in pyramidal neurons of either CA1 or basolateral amygdala, but also found that SK4 knockout mice exhibited a  $sI_{AHP}$  current that was not significantly different to control animals (Wang et al 2016). As a result of these concerns, the weight of current evidence opposes involvement of SK4 channels in the mediation of  $sI_{AHP}$  in CA1 pyramidal neurons.

## Na<sup>+</sup>/K<sup>+</sup> ATPase

An early paper (Schwindt et al 1989) found evidence of a slow afterhyperpolarisation representing the activation of a pump rather than a channel population in cat neocortical neurons. A 1 s-long depolarising step was used, and activated a long duration hyperpolarisation lasting from a few seconds up to several minutes. This afterpotential was shown to have different characteristics to the sAHP described in CA1 pyramidal neurons (Alger and Nicoll, 1980), as it was insensitive to Ca<sup>2+</sup>, was abolished in the presence of TTX, and was observed even in cells recorded using a Ca<sup>2+</sup>-free extracellular solution. As the underlying current was dependent on Na<sup>+</sup> ions, it was termed I<sub>K(Na)</sub> (Schwindt et al, 1989).

Notwithstanding the obvious differences between this current and the Ca<sup>2+</sup> sensitive sI<sub>AHP</sub> observed in hippocampal pyramidal cells (Alger and Nicoll 1980, Hotson and Prince 1980, Schwartzkroin and Stafstrom 1980, Lancaster and Adams 1986, Storm 1989, Lancaster and Zucker 1994, Zhang et al, 1996, Velumian and Carlen 1999, among others), Gullidge and colleagues (Gullidge et al 2013) speculated that the sodium-potassium ATP-ase was predominantly responsible for the sAHP observed in CA1 pyramidal neurons. They observed a long-lasting (20 s long) afterhyperpolarisation in mouse CA1 pyramidal cells, which was shown to be Na<sup>+</sup> dependent, Ca<sup>2+</sup> insensitive and blocked by TTX and the specific Na<sup>+</sup>/K<sup>+</sup> pump inhibitor ouabain. Their suggestion was that previous experiments attributing the mechanism underlying the sAHP in CA1 pyramidal cell to a Ca<sup>2+</sup> sensitive current represented an inaccurate picture due to focus on conducting experiments at room temperature rather than at a more physiologically relevant temperature, or due to species differences, or due to using predominantly young animals for the experiments. However recent work in the Pedarzani lab (A. Tedoldi 2015, PhD thesis, unpublished) has shown that all of these propositions are not plausible. Experiments in mice of average age 4 months showed a Ca<sup>2+</sup>-dependent sAHP, excluding the possibility that I<sub>K(Na)</sub> involvement had been underestimated due to the age of animals used, while experiments at 35°C showed a sAHP that was insensitive to TTX, and abolished by the application of a membrane-permeable cAMP analogue, 8-CPT-cAMP.

From these results it is clear that the afterpotential described by Gullidge and colleagues (2013) is different from the Ca<sup>2+</sup> dependent, cAMP/PKA modulated afterhyperpolarisation described by previous authors in CA1 pyramidal neurons, and is probably activated by the large amount of current used to elicit the long action potential

trains, which bear similarity to the long (1 s) voltage step used by Schwindt and colleagues in neocortical neurons (Schwindt et al 1989).

## 6.4 Suppression of $sI_{AHP}$ by neuromodulators

The amplitude of  $sI_{AHP}$  is highly modulated by a range of neurotransmitters acting on metabotropic receptors, including glutamate (Charpak et al 1990), acetylcholine (Cole and Nicoll 1983, Cole and Nicoll 1984), and the monoamines serotonin (5-HT) (Andrade and Nicoll, 1987), noradrenaline (Madison and Nicoll 1982), dopamine (Benardo and Prince, 1982), and histamine (Haas and Konnerth, 1983). All of the above transmitters exhibit a similar end effect, namely the inhibition of the sAHP and underlying  $sI_{AHP}$ , and all act via G-protein coupled receptors. However there is some divergence as to their downstream mechanisms of action.

The monoamine transmitters have been shown to act via  $G\alpha_s$  mediated signalling, leading to the activation of adenylyl cyclases, the generation of a cyclic AMP signal and subsequent activation of protein kinase A (PKA). Bath application of the membrane-permeable cAMP analogue 8-CPT-cAMP or the adenylyl cyclase activator forskolin mimics the action of monoaminergic agonists (Pedarzani & Storm, 1993), causing a reversible suppression of sAHP and the underlying  $sI_{AHP}$ . Intracellular application of Rp-cAMPS, a specific inhibitor of the cAMP binding site of PKA, or PKI, a specific peptide inhibitor of the catalytic subunit of PKA, inhibits the suppression of sAHP and  $sI_{AHP}$  by both monoaminergic agonists and 8-CPT-cAMP (Pedarzani & Storm, 1993, 1995). There is therefore strong evidence that all four monoamine neuromodulators act via adenylyl cyclase and PKA to suppress the  $sI_{AHP}$ .

Acetylcholine, acting via M3 muscarinic receptors, and glutamate, acting on mGluR5 and mGluR1 receptors (Ireland and Abraham, 2002), appear to utilise a different pathway, mediated by  $G\alpha_q$  (Krause et al 2002) and independent of PKA (Pedarzani and Storm, 1995). Cholinergic inhibition of the  $sI_{AHP}$  is dependent on  $Ca^{2+}$  /calmodulin-dependent protein kinase II (CaMK-II)(Pedarzani and Storm, 1995), but this is not the case for the glutamatergic pathway.

A common problem in understanding the role played by this large number of apparently redundant neuromodulatory pathways is that in each case, the end actor in the suppression of the  $sI_{AHP}$  is currently unknown. It is possible that the different pathways all converge on the same final step to affect suppression of the current, though it is also plausible that the apparent homogeneity of effect, observed with different modulators

during bath application of pharmacological tools, masks functional diversity mediated by localised signalling domains. There is strong evidence that such domain-limited signalling exists, both as a general principle and in this specific case. For example, the population of CaMK-II that mediates the cholinergic inhibition appears to be insensitive to the rises in bulk  $\text{Ca}^{2+}$  responsible for the activation of the  $\text{sI}_{\text{AHP}}$  during action potential generation (Pedarzani and Storm, 1995). Additionally, there is considerable evidence from a variety of cell types of spatially restricted cAMP signalling domains, which when activated confer different or occasionally even opposing effects.

## 6.5 Monoaminergic Signalling Domains

One of the principal ways in which functional specialisation can be achieved by two signals acting upon a common pathway is by the localisation of signalling components (receptors, kinases and their downstream targets etc.) into discrete, spatially compartmentalised pools or domains. In the case of monoaminergic cAMP-dependent signalling, activation of the receptors produces a spatially localised cAMP signalling domain, leading to the activation of nearby kinases or other targets (Pawson and Nash, 2003). Further tuning and sharpening of the domain boundaries can be achieved by the action of associated phosphodiesterases (Strangherlin et al 2011), and assemblies of the domain components are brought into tight spatial association with the aid of scaffolding proteins.

There is considerable evidence for the existence and functional significance of such domains in PKA-dependent modulation of a variety of cellular processes (reviewed by Zaccolo 2011, Dai and Hell 2009). As a characteristic example, cardiac myocytes contain a population of  $\beta$ -adrenergic receptors of both  $\beta 1$  and  $\beta 2$  subtypes. Stimulation of  $\beta$  receptors by noradrenaline leads to the PKA-dependent activation of L-type voltage gated  $\text{Ca}^{2+}$  channels, and increases pulse rate and contractility. However, whereas the  $\beta 1$  subtype leads to PKA activation throughout the cell, activation of  $\beta 2$  by  $\beta 2$ -specific ligands leads to enhanced kinase activation at the sarcolemma (Xiao et al 1999). This effect is dependent on the assembly of  $\beta 2$  receptors into a signalling complex, along with adenylyl cyclase, PKA and its counteracting phosphatase PP2A, and the L-type channel, held together by structural proteins of the A-kinase anchoring protein family (AKAP) (Shih et al, 1999, Hulme et al, 2003, Dai and Hell 2009). AKAPs are a diverse family of proteins characterised by the presence of an amphipathic helix motif that binds to the PKA regulatory subunit. They also possess a variety of specialised domains, allowing them to bind various other protein partners and facilitate colocalisation and coordination

of action. Additionally, some AKAPs exhibit lipid modifications that permit binding to membrane phospholipids (Davare et al. 2001).

## 6.6 Evidence for localised signalling domains contributing to monoaminergic suppression of $sl_{AHP}$

A currently open question is whether the monoaminergic modulation of  $sl_{AHP}$  by PKA in hippocampal pyramidal cells involves similar localised signalling domains.

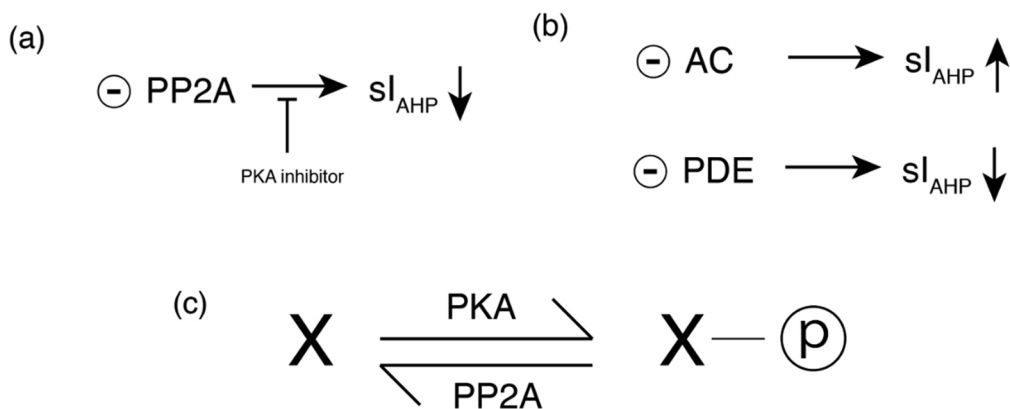


**Figure 6.1 Schematic of signalling relationships implied by evidence in section 6.6**

(a) *Microcystin inhibits PP2A, causing run-down of  $sl_{AHP}$ . This effect is blocked by PKA inhibitors*

(b) *Inhibition of adenylyl cyclase leads to an increase in  $sl_{AHP}$  amplitude, while inhibition of phosphodiesterases leads to a gradual decrease in amplitude of the current.*

(c) *Schematic of the equilibrium between the action of PKA and its associated phosphatase PP2A on the phosphorylation state of the hypothetical target of PKA-mediated inhibition of  $sl_{AHP}$*

One line of evidence that suggests the presence of such mechanisms comes from electrophysiological experiments conducted in the presence of Ht31, a competitive AKAP inhibitor derived from the AKAP binding site of the PKA regulatory subunit (Carr et al 1992), which disrupts the basal tone of PKA signalling in rat hippocampal pyramidal cells.

Intracellular perfusion of microcystin, a serine-threonine protein phosphatase inhibitor, leads to a progressive run-down of  $sl_{AHP}$  amplitude during recordings, and this run-down is abolished by PKA inhibitors (Pedarzani and Storm 1993; Pedarzani et al 1998). Conversely inhibition of adenylyl cyclase leads to an increase in  $sl_{AHP}$  amplitude, while

inhibition of phosphodiesterases leads to its gradual decrease. These findings suggest that there exists a basal tone to PKA-dependent control of  $sI_{AHP}$  amplitude, due to the balance between a constitutively active population and both PKA and phosphatases, most likely PP2A (Pedarzani et al 1998).

It was hypothesised that using Ht31 to inhibit the binding of AKAP to PKA would disrupt this balance, leading to an increase in  $sI_{AHP}$  amplitude. In whole cell voltage clamp recordings of  $sI_{AHP}$ , the current amplitude is small at the beginning of the recordings, but repeated stimulation leads to a typical, gradual increase in the  $sI_{AHP}$  amplitude, a phenomenon known as run-up (Zhang et al., 1995; Borde et al., 2000).

In cells in which Ht31 was included in the intracellular solution, both the increase in  $sI_{AHP}$  amplitude in this run-up phase, and its duration, were enhanced compared with control cells (Pedarzani, unpublished data). This suggests that AKAPs organise a spatially localised pool of PKA in close proximity to the phosphorylation targets that affect the suppression of  $sI_{AHP}$ . It is therefore plausible that  $sI_{AHP}$  channels and their modulating receptors are organised into spatial domains, and that different transmitter systems could act on separate signaling complexes, possibly linked to different populations of  $sI_{AHP}$  channels.

An additional putative mechanism that might produce specificity and divergence of the different PKA-mediated signals is differential activation of isoforms of adenylyl cyclase (AC) by different receptors and their associated G-proteins. A number of different adenylyl cyclases are expressed in hippocampal neurons (Sanabra et al. 2011), which vary in their susceptibility to activation by different G-protein subunits, as well as in their response to  $Ca^{2+}$ . All adenylyl cyclase isoforms are, to some extent, activated by  $G_{\alpha s}$  G-protein subunits, but the AC1 and AC8 isoforms are additionally stimulated by  $Ca^{2+}$ , and inhibited by  $G_{\beta\gamma}$ , and AC8 has a reduced sensitivity to activation by  $G_{\alpha s}$ . Conversely, the AC2 and AC4 isoforms are insensitive to calcium, and activated by  $G_{\beta\gamma}$  (Cooper and Crosshwaite 2006).

Experiments conducted by the Pedarzani lab (R. Taylor, unpublished data) used double knockout mice of AC1 and AC8 to investigate the involvement of these isoforms in the inhibition of  $sI_{AHP}$  by monoamines. No difference was observed between the knockouts and control mice in their response to a non-saturating concentration of either 5-HT or the  $\beta$ -adrenergic agonist isoproterenol. However,  $sI_{AHP}$  is also suppressed in CA1 pyramidal cells in a PKA-dependent manner in response to high frequency stimulation (HFS) of Schaeffer collaterals, mediated by glutamate acting on NMDA receptors (Blitzer et al

1995). The PKA dependency of this process was shown by the fact that it can be abolished by PKI<sub>6-22</sub>, a pseudosubstrate inhibitor of PKA (R. Taylor, unpublished data). In the AC1/AC8 DKO, no significant suppression of the  $sI_{AHP}$  was observed in response to HFS of the Schaffer collaterals. Thus although AC1 and AC8 are not necessary for monoaminergic suppression of  $sI_{AHP}$ , they nonetheless transduce another PKA-dependent pathway leading to the same result. Again this suggests that the general similarities of response, seen in suppression of the sAHP by different neuromodulators during bath application experiments, mask hidden complexities, such as distinct signaling domains, coupled to different receptors, capable of modulating pools of sAHP channels by locally activating the cAMP/PKA pathway.

## **6.7 Aims of the project**

The aim of this project is to investigate the possibility that there are spatially localised cAMP signalling domains in hippocampal pyramidal neurons, comprising monoamine receptors, a population of  $sI_{AHP}$  channels, and the intervening signalling components, such as adenylyl cyclase and PKA. In particular the aim is to acquire the first data on spatial localisation of one of these signalling pathways. Two separate experimental strategies were designed and adopted: focal application of the  $\beta$ -adrenergic agonist isoproterenol via a microinjector, and localised uncaging of BCMCM-8Br-cAMP, a cAMP analogue contained in a photolabile cage (Hagen, 1998).

The first part of this project aims to determine the optimal recording conditions for  $sI_{AHP}$ , such that a large amplitude, stable current can be observed for periods of up to an hour, in order to maximise the dynamic range for the inhibition experiments used in the other two parts. Parts 2 and 3 comprise the focal application experiments and the cyclic nucleotide uncaging, respectively.

### **Focal application technique**

In the extant literature, monoaminergic suppression of  $sI_{AHP}$  has been studied using the application of compounds in the bath perfusion or administered intracellularly via the pipette. Both these approaches are effective at determining the global response of the cell, but lack the spatial or temporal resolution required for the identification of specific effects mediated by localised signalling domains. By utilising techniques that affect only a part of the cell, additional effects can be revealed that are not picked up by bath application.

As an example, Fiorillo and Williams (Fiorillo and Williams 1998) showed that application of mGluR1 agonists to ventral dopaminergic midbrain neurons via the bath perfusion elicited a depolarising potential, whereas transient application of the same agonists, using a microinjector localised to the soma, induced a hyperpolarisation that desensitised in response to prolonged application. Such an approach has not as yet been used for monoamine transmitters and their effects on membrane conductances and excitability.

In the data presented in this project, a microinjector was used to puff the  $\beta$ -adrenergic agonist isoproterenol onto two different compartments of the neuron: the soma / proximal apical dendrite region and the distal apical dendrites. Where differences in the degree of suppression of sI<sub>AHP</sub> between the two regions are observed, this could be interpreted either as a difference in receptor density, or as a change in the degree of coupling between the receptors in that location and the sI<sub>AHP</sub> channel.

### **BCMCM 8Br-cAMP uncaging**

Caged compounds are light sensitive probes, based on the principle that a signalling molecule of interest can be rendered inert from a signalling perspective by the addition of a protecting group that can be cleaved off by irradiation with light (Ellis-Davies 2007). The process thereby allows biological processes to be perturbed with a high degree of spatial and temporal resolution by localised irradiation of an area of interest. Photolabile cages have previously been used to examine the calcium-dependence of sI<sub>AHP</sub> and its relation to the kinetics of the current (Lancaster and Zucker 1994, Sah and Clements, 1999), but thus far a similar approach has not been attempted with caged cyclic AMP. The experiments presented here use a caged form of 8Br-cyclic AMP, (BCMCM 8Br-cAMP) which is resistant to hydrolysis (Hagen 1998). As the Pedarzani lab had not previously worked with caged compounds, preliminary experiments were conducted with DM-Nitrophen (Ellis-Davies et al, 1996), a photolabile calcium buffer, in order to configure our equipment for uncaging and have positive controls for the efficiency of the system.

## Chapter 7. Results

### 7.1 Optimization of $sI_{AHP}$ current recording conditions in acute hippocampal slices

The first set of experiments aimed to determine a set of optimal recording conditions for the slow afterhyperpolarising  $Ca^{2+}$ -dependent  $K^+$  current ( $sI_{AHP}$ ). As subsequent experiments were to investigate the  $sI_{AHP}$  as a target for spatially localised monoaminergic signalling, it was necessary to find experimental conditions in which the current amplitude was stable over a period of between 30 minutes and 1 hour, and also as large as possible, in order to maximise our chances to detect even small changes in response to the activation of the cAMP-dependent signalling pathway.

Whole-cell voltage clamp experiments were performed on CA1 pyramidal cells from acute slice preparations of rat hippocampus, in which the  $sI_{AHP}$  was elicited by the protocol described in the methods (2.2.8.1). In brief, a 100 ms-long depolarising step to +10 mV from a holding potential of -50 mV was used to activate voltage dependent  $Ca^{2+}$  channels, leading to a rise in intracellular  $Ca^{2+}$  concentration, which in turn activated  $sI_{AHP}$ . Immediately following the acquisition of whole-cell configuration, 0.5  $\mu$ M TTX, 1 mM TEA, and 50  $\mu$ M dTC were applied extracellularly in order to block voltage-gated  $Na^+$  channels, some voltage and  $Ca^{2+}$  dependent  $K^+$  channels, and the small conductance  $Ca^{2+}$  activated  $K^+$  (SK) channels that underlie  $I_{AHP}$ . Under these conditions a large, partially unclamped inward  $Ca^{2+}$  current, the calcium action current (Figure 7.1a) was observed during the stimulus pulse, followed by an outward current ( $sI_{AHP}$ ) upon returning to the holding potential of -50 mV (Figure 7.1b). Upon repetition of the depolarising pulse every 30 s, a progressive increase or run-up of the  $sI_{AHP}$  amplitude was observed, reaching a stable level with 5-10 minutes (Figure 7.1c). There was a concomitant run-down of  $I_{AHP}$  over the same time period, due to the effect of dTC.

Cells recorded in this manner displayed a mean resting membrane potential of  $-59.5 \pm 0.5$  mV and a membrane resistance of  $173.7 \pm 8.6$  M $\Omega$  ( $n = 56$ ), as determined at the beginning of each whole-cell recording.

Time courses of  $sI_{AHP}$  peak amplitude and decay time constant from a representative recording can be seen in Figure 7.1c and d). Current amplitude and decay kinetics were stable for over 30 minutes. The intracellular solution used in the recordings was either ICAPA-1 or IC-MOPS, the latter being a modified intracellular solution with increased buffering capacity in the pH 7.0 to 7.2 range (see Methods 2.2.13), which, based on

existing literature, we hypothesised might increase the size and stability of the  $sl_{AHP}$  (Tombaugh 1998). We observed no significant difference between recordings performed with the two intracellular solutions in resting membrane potential ( $V_m$ ), input resistance ( $R_{input}$ ), or peak amplitude and decay time constant of the  $sl_{AHP}$ , so results for the two solutions were combined. The mean  $sl_{AHP}$  amplitude for all cells recorded ( $n=56$ ) was  $39.5 \pm 3.0$  pA, and the mean decay time constant was  $2.8 \pm 0.2$  s. These values were recorded once the current had increased to a stable state in the presence of TTX, TEA and dTC.

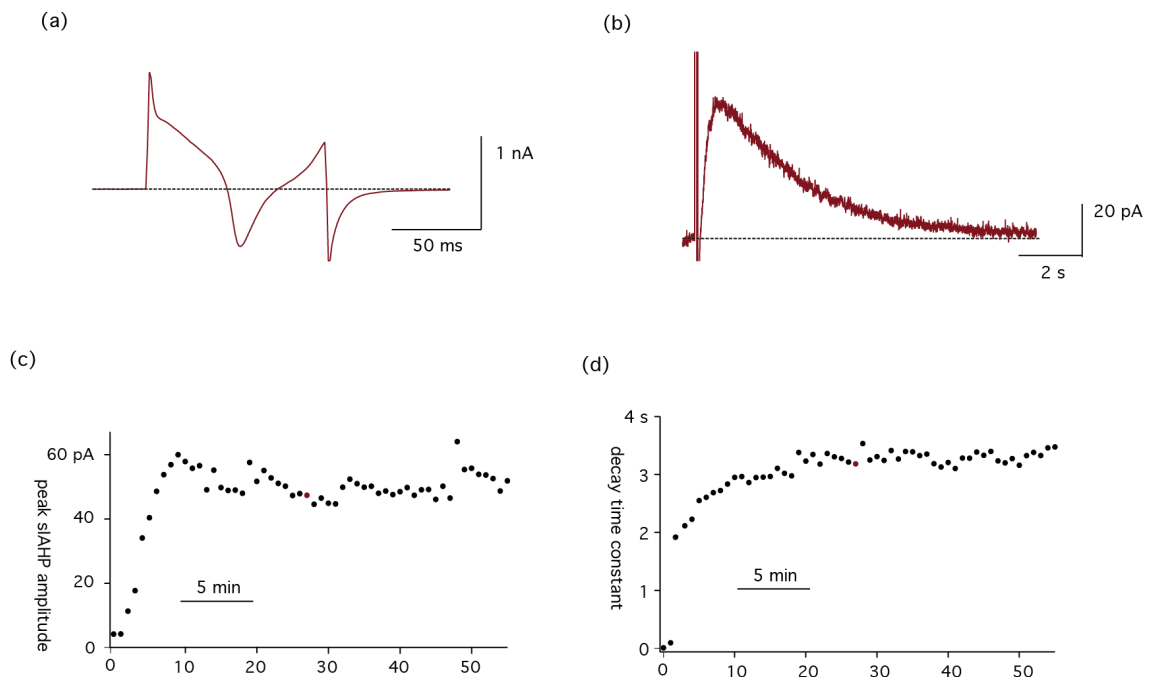


**Figure 7.1.  $sl_{AHP}$  properties under typical recording conditions**

- (a) *Detail of the current response to a 100 ms voltage step to +10 mV from a holding potential of -50 mV from a representative cell, showing the calcium action current. Dashed line denotes baseline current response for cell held at -50 mV.*
- (b) *Example trace from the same recording, showing the outward  $sl_{AHP}$  current following the voltage step. Dashed line denotes the baseline current at -50 mV.*
- (c) *Time course of the  $sl_{AHP}$  peak amplitude for the same representative cell. Traces are acquired at 30s intervals. Note the “run up” phase of the current.*
- (d) *Time course of the  $sl_{AHP}$  decay time constant for the same representative cell.*

### 7.1.1 Optimal parameters of the stimulus pulse

The  $sl_{AHP}$  is a voltage-independent current, which is elicited experimentally using a voltage step to activate voltage-gated  $Ca^{2+}$  channels, which in turn leads to an increase

in cytosolic  $\text{Ca}^{2+}$  that activates the  $sI_{\text{AHP}}$ . In order to determine the optimal parameters for the voltage step, the duration was initially set to 100 ms, while the amplitude was stepped from the holding potential of -50 mV to voltages between -20 and 20 mV in 2 mV steps. Traces from a representative cell are shown in Figure 7.2a. For all cells tested ( $n=5$ ),  $sI_{\text{AHP}}$  increased in amplitude from zero to saturation as the voltage was varied between -10 and +10 mV. In a given cell the current amplitude initially increased gradually with stimulus voltage, and then showed a sharp transition to a near-maximal value. Data from all cells are summarised in Figure 7.2e. In each cell the current amplitude sharply increased from less than 25% of its maximal value to a near-maximal one within a narrow range of voltage steps, suggesting the existence of a threshold voltage at which the  $\text{Ca}^{2+}$  channels driving  $sI_{\text{AHP}}$  are activated. In support of this hypothesis, in each case the unclamped  $\text{Ca}^{2+}$  action current first appeared on the same trace as the  $sI_{\text{AHP}}$  sharply increased in size (Figure 7.2b). The apparent threshold voltage at which the  $sI_{\text{AHP}}$  amplitude showed a sharp increase varied between cells within the range of +2 and +4 mV, hence the large error bars at these voltage values.

To determine optimal stimulus duration, a voltage step from -50 mV to +10 mV was delivered for durations between 50 and 100 ms in 5 ms increments. Example traces from a representative cell are shown in Figure 7.2c, and data from all cells are summarised in Figure 7.2f.  $sI_{\text{AHP}}$  amplitude increased with stimulus duration, reaching saturation between 85 and 100 ms. In contrast to the voltage changes, the current amplitude increased gradually in response to increasing stimulus duration, and did not show any discontinuity. The unclamped  $\text{Ca}^{2+}$  action current also increased gradually with stimulus duration (Figure 7.2d).

From these experiments, optimal parameters for the stimulus pulse in CA1 pyramidal neurons were determined to be a 100 ms-long voltage steps to + 10 mV, as these values were sufficient to saturate the current response to both voltage and duration parameters.

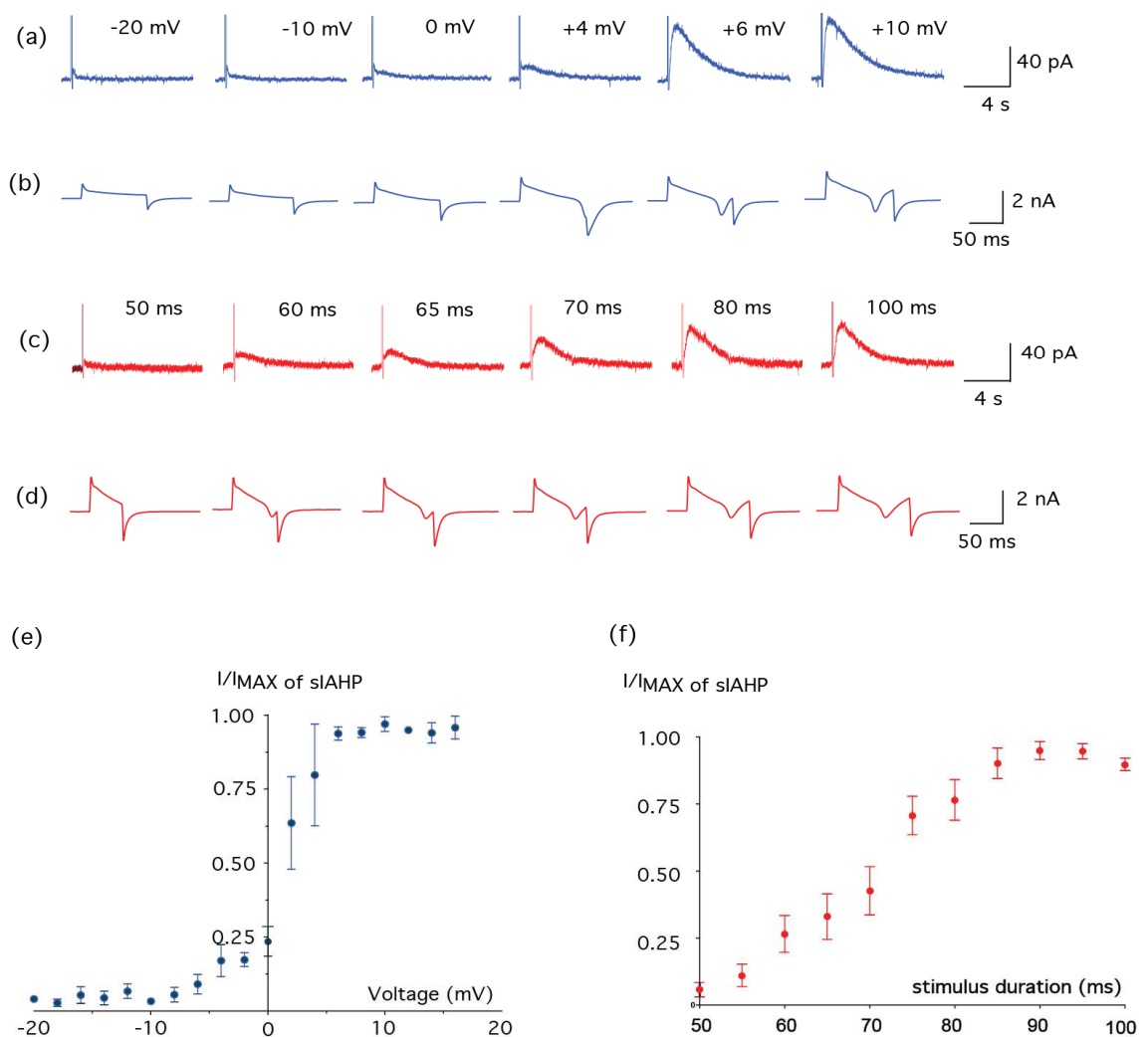


**Figure 7.2. Effect of stimulus properties on sIAHP**

- (a) *sIAHP* response to different sized voltage steps in an example cell. Numbers above each trace represent voltage (mV) to which the cell was stepped, from a resting potential of -50 mV.
- (b) Detail of the stimulus pulses from the traces in (a), showing the development of the calcium action current.
- (c) Traces showing *sIAHP* response to voltage steps of varying duration. Numbers above each trace represent stimulus duration in ms. In each case the cell was stepped from a resting potential of -50 mV to +10 mV.
- (d) Detail of the stimulus pulses from the traces in (c), showing the development of the Ca<sup>2+</sup> action current.
- (e) Graph summarising response of all cells (n=5) to stimulus pulses of varying target voltage. Y axis shows relative activation ( $I/I_{MAX}$ ), filled circles represent the mean, and vertical bars the SEM.
- (f) Graph summarising response of all cells (n=5) to stimulus pulses of varying duration. Y axis shows relative activation ( $I/I_{MAX}$ ), filled circles represent the mean, and vertical bars the SEM.

### 7.1.2 Effect of the K<sup>+</sup> channel blocker TEA on sI<sub>AHP</sub> amplitude

Tetraethylammonium (TEA), a potassium channel blocker, has been shown to increase the Ca<sup>2+</sup> current observed during membrane depolarisation, probably due to its ability to block voltage-gated K<sup>+</sup> channels, which would otherwise contribute to a rapid membrane repolarisation and prevent the generation of regenerative dendritic Ca<sup>2+</sup> spikes (Golding et al. 1999). Application of TEA might therefore be permissive for the Ca<sup>2+</sup> entry necessary for the activation of sI<sub>AHP</sub> and expected to increase sI<sub>AHP</sub> amplitude. However, a reduction in sI<sub>AHP</sub> amplitude following application of TEA at concentrations between 5 and 10 mM has also been reported (Lancaster & Adams, 1986). I therefore tested the sensitivity of sI<sub>AHP</sub> to TEA under our experimental conditions, primarily to find the optimal concentration of TEA to maximise and stabilise sI<sub>AHP</sub> amplitude.

As a secondary objective, recent attempts at identifying the molecular correlate of sI<sub>AHP</sub> have put forward KCNQ channels as potential candidates (Tzingounis et al. 2008, 2010). Depending on their subunit composition, KCNQ channels display sensitivity to TEA in the range of 0.3 to over 50 mM (Hadley et al. 2000; Schroeder et al. 2000). It was therefore additionally useful to compare the degree of potentiation or inhibition of sI<sub>AHP</sub> at different concentrations of TEA to the IC<sub>50</sub> of various KCNQ subunits, in an attempt to assess the validity of the hypothesis that they contribute to the sI<sub>AHP</sub> in CA1 pyramidal neurons.

ACSF containing TEA at four concentrations (1 mM, 5 mM, 10 mM and 20 mM) was applied extracellularly via the perfusion system. In the case of 10 mM and 20 mM, osmolarity was controlled by omission of the equivalent amount of NaCl from the ACSF solution.

The time course of a representative experiment is shown in Figure 7.3a, along with traces from each TEA concentration used in that experiment showing the sI<sub>AHP</sub> (Figure 7.3b) and the partially clamped Ca<sup>2+</sup> transient during the voltage step (Figure 7.3c). Summarised results from all experiments are displayed in Figure 7.3d. Recordings were made from 10 cells but not all concentrations were tested on every cell. The number of trials in which each concentration was tested is indicated above the corresponding bar in the chart. The largest increase in sI<sub>AHP</sub> amplitude occurred in the presence of 1 mM TEA (mean = 167 ± 23% of baseline). At 5 mM TEA also increased the sI<sub>AHP</sub> amplitude, but to a lesser extent, while at 10 mM and 20 mM TEA inhibited the sI<sub>AHP</sub>. In most cases (5/6 cells), at 20 mM TEA abolished the sI<sub>AHP</sub> entirely. As can be seen in Figure 7.3c, the size of the unclamped Ca<sup>2+</sup> current is larger at all TEA concentrations applied than in the

baseline condition, but does not noticeably alter in size between 1 mM TEA and the higher concentrations tested. It therefore appears that TEA facilitates the  $sI_{AHP}$  in the concentration range below 5 mM, by increasing the size of the inward  $Ca^{2+}$  current during the stimulus pulse, but has an inhibitory effect in the 10 - 20 mM range by a mechanism that is independent of the voltage-dependent  $Ca^{2+}$  current and is most likely a block of the channels underlying  $sI_{AHP}$ .

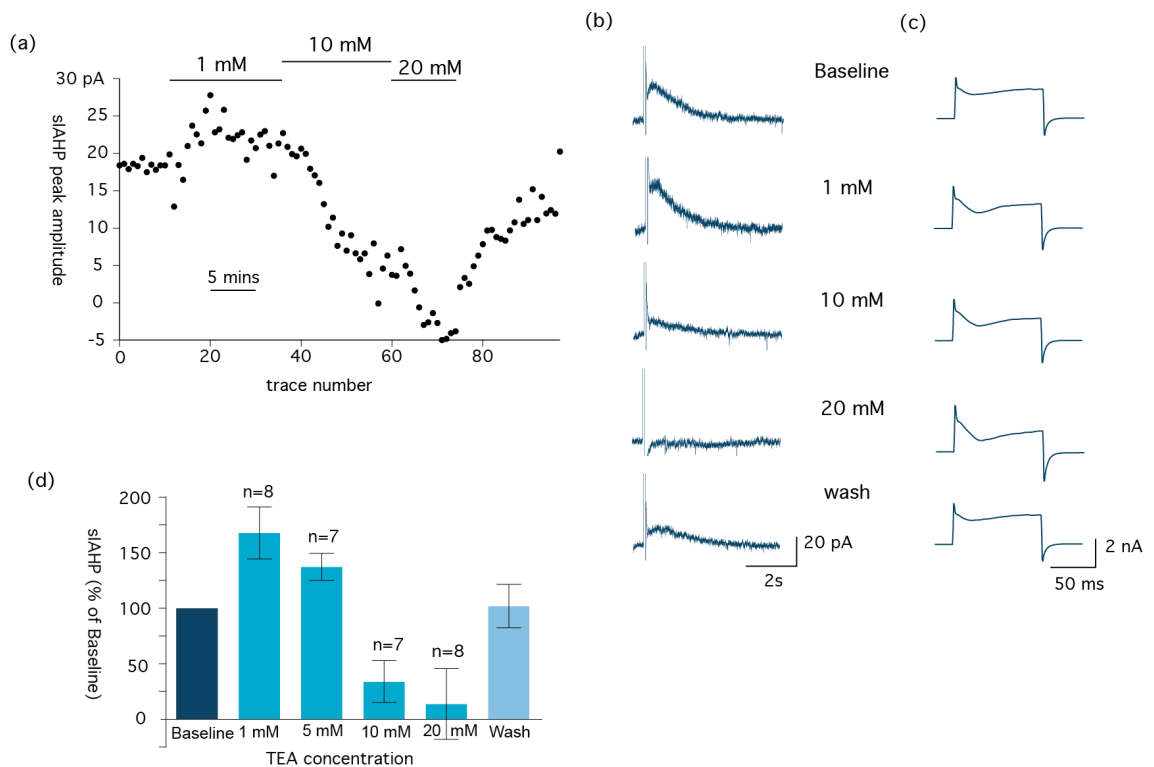


**Figure 7.3. Effect of varying TEA concentration on  $sI_{AHP}$  amplitude**

- (a) *Timecourse of an example cell, in which three concentrations of TEA (1 mM, 10 mM and 20 mM) were applied sequentially. Horizontal lines indicate period during which each concentration was applied.*
- (b) *Representative traces taken from the same cell as the timecourse in (a).*
- (c) *Detail of the stimulus pulses from the traces in (b), showing the  $Ca^{2+}$  action current.*
- (d) *Summarised data for all cells. Y axis shows percentage change in  $sI_{AHP}$  amplitude relative to baseline. Bar height shows mean change for each concentration, Error bars show SEM. The total number of cells in which each concentration was tested is indicated above each column.*

### 7.1.3 Pharmacological modulation of $sI_{AHP}$ amplitude

A number of compounds have been reported to increase  $sI_{AHP}$  amplitude, including EBIO (Pedarzani et al 2001), EtOH (Reynolds et al 1990) and Bay-K 8644 (Tombaugh et al

2005). The possibility of using these compounds to increase the amplitude of  $sI_{AHP}$  in the recordings was therefore explored.

Pedarzani et al (2001) report an increase in  $sI_{AHP}$  amplitude in CA1 pyramidal neurons in response to 1 mM EBIO, applied extracellularly. I therefore tested the effect of 1 mM EBIO by performing voltage clamp recordings in which 1 mM EBIO was added to the bath perfusion for a period of at least 10 minutes, following the establishment of a stable  $sI_{AHP}$  baseline level. The results are summarised in Figure 7.4. In all cells tested ( $n=4$ ), EBIO initially led to an increase in peak  $sI_{AHP}$  amplitude with respect to baseline ( $124\% \pm 8.8\%$  of baseline, Figure 7.4a-d). This increase was significant (Figure 7.4d, one-sample t-test  $p<0.047$ ,  $n=4$ ) at 2 minutes following application. However, the effect of 1 mM EBIO on  $sI_{AHP}$  appeared to be of limited duration, such that at 10 minutes following application the mean current was  $89\% \pm 6.7\%$  of baseline, not significantly different from baseline level (one-sample t-test  $p<0.18$ ,  $n=4$ ). While our recordings did not directly measure the extent of  $Ca^{2+}$  entry during the stimulus pulse, a qualitative impression can be formed by reference to the partially clamped  $Ca^{2+}$  current (Figure 7.4c). EBIO did not appear to substantially alter this current. Also the decay time constant of  $sI_{AHP}$  was not significantly different from baseline at either +2 minutes or +10 minutes following application of EBIO, (Figure 7.4e, one sample t-test  $p=0.37$  (+2 mins) one sample t-test  $p=0.51$  (+10 mins),  $n=4$ ), suggesting that EBIO did not affect current kinetics. It therefore appears that, although EBIO does increase  $sI_{AHP}$  amplitude, the effect is either brief in duration, or else subsequently reversed by an equivalent inhibitory effect. EBIO is therefore not a good candidate for increasing  $sI_{AHP}$  amplitude for the purpose of my experiments.

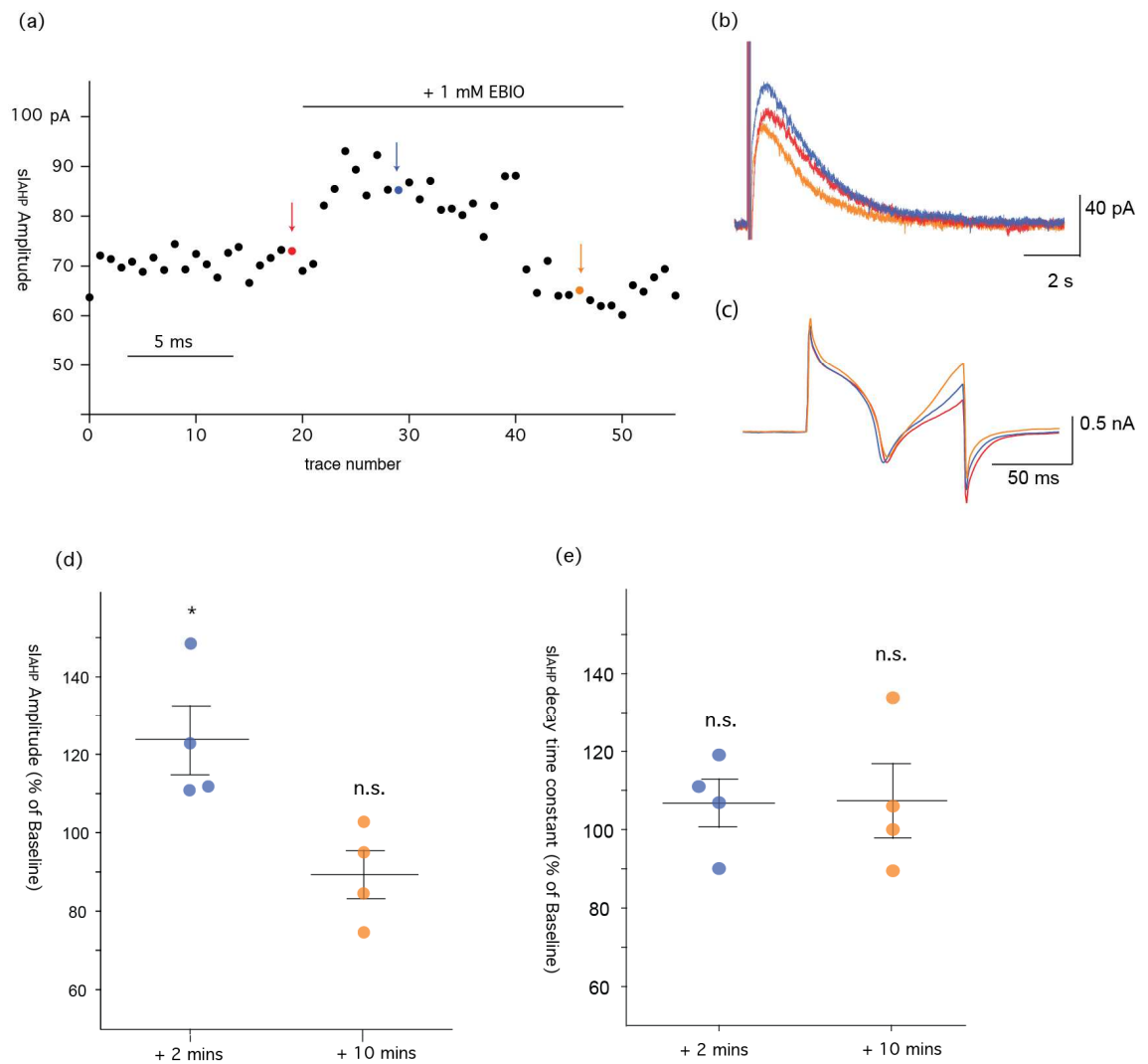


**Figure 7.4. Effect of EBIO on sI<sup>AHP</sup> amplitude**

- (a)** *Example timecourse of sI<sub>AHP</sub> peak amplitude during application of 1 mM EBIO. Time course of drug application is denoted by the horizontal line.*
- (b)** *Individual traces taken from points marked with coloured arrows in (a). Red trace is the baseline amplitude, blue trace is taken from a point 2 minutes after application of 1 mM EBIO, yellow trace is at a point 10 minutes after application of 1 mM EBIO.*
- (c)** *Temporal magnification of the stimulus region of the same traces, showing the calcium action current*
- (d)** *Percentage change of sI<sub>AHP</sub> amplitude relative to baseline, at 2 minutes and 10 minutes following drug application (n=4). Horizontal line indicates mean, vertical bars represent SEM.*
- (e)** *Percentage change of sI<sub>AHP</sub> decay time constant, relative to baseline, at 2 minutes and 10 minutes following drug application (n=4).*

Several studies investigated the effects of ethanol (EtOH) on the afterhyperpolarisation potential in rat CA1 pyramidal cells. Carlen et al (1982) and Reynolds et al (1990) report

an increase in the amplitude and duration of the post-spike afterhyperpolarisation, whereas Siggins et al (1987) observed no increase in either amplitude or duration following EtOH application.

In order to test whether EtOH had any effect on the amplitude of  $sI_{AHP}$  under our experimental conditions, ACSF containing either 10 mM (n=7) or 20 mM (n=5) EtOH was applied to cells and the changes in  $sI_{AHP}$  amplitude and kinetics measured once the current had reached a stable state (Figure 7.5). Neither concentration produced a significant change in the peak amplitude of the current (2-tailed one sample t-test  $p = 0.34$  and  $p = 0.46$  respectively, Figure 7.5 d,e).

Some cells (5 out of 7 at 10 mM and 3 out of 5 at 20 mM) displayed a stable increase in current of up to 42% , however in the others the current decreased by up to 15% (Figure 7.5 d). Exclusion of the non-responding cells from the analysis yields a mean change in  $sI_{AHP}$  amplitude to  $122.7 \pm 8.2\%$  of baseline for 10 mM and  $118.3 \pm 7.6\%$  of baseline for 20 mM ethanol. Ethanol produced a more consistent effect on the kinetics of  $sI_{AHP}$ . Both concentrations caused an increase in the decay time constant of the current in every cell, with a mean change to  $116.9 \pm 5.1\%$  (10 mM) and  $108.7 \pm 3.5\%$  (20 mM) of baseline time constant, though the change was only significant at 10 mM (one-sample t-test  $p = 0.02$ , Figure 7.5 d,e). Neither concentration appeared to alter substantially the size or shape of the partially unclamped  $Ca^{2+}$  current. We therefore conclude that ethanol produced a small, but sizeable and stable increase in current in the majority of cells, however in other cells it appeared to have no effect, or caused a decrease in current amplitude. As a result, there was no significant increase in  $sI_{AHP}$  amplitude for the group as a whole. In the context of the current project, the magnitude of any observed increase in  $sI_{AHP}$  amplitude was outweighed by the inconsistency of the effect. Ethanol was therefore not used as part of the recording conditions for subsequent experiments.

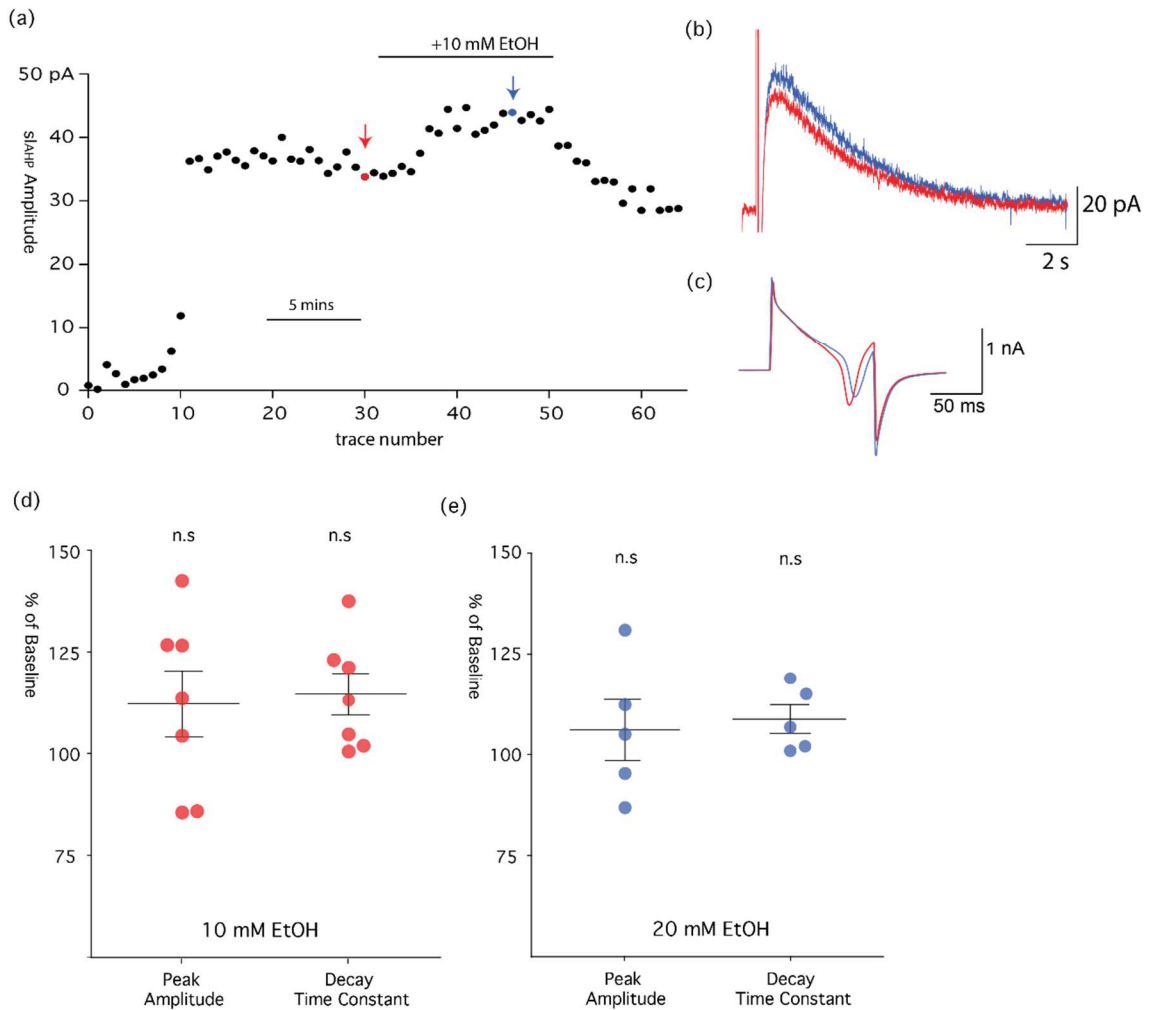


**Figure 7.5. Effect of EtOH on  $sI_{AHP}$  properties**

- (a) **Timecourse of  $sI_{AHP}$  amplitude for a representative cell. Horizontal line indicates duration of EtOH application.**
- (b) **Representative traces from the timecourse in (a). The position of each trace in the timecourse is indicated by a coloured symbol and arrow.**
- (c) **Detail of the current trace in (b) showing the voltage step and calcium action current.**
- (d) **Summarised data for 10 mM EtOH ( $n=7$ ) and (e) 20 mM EtOH. Horizontal lines indicate means, error bars represent SEM. Y axis in each case is percentage of baseline response.**

The dihydropyridine Bay-K8644 is an agonist of L-type  $Ca^{2+}$  channels that has been shown to increase the afterhyperpolarisation and  $Ca^{2+}$  spike amplitude in current clamp recordings (Tombaugh et al. 2005). We applied 1  $\mu$ M Bay-K8644 and measured the change in the amplitude and decay time of  $sI_{AHP}$  once the current had reached a stable state (Figure 7.6a). This usually took between 10 and 20 minutes. The effect of Bay-K8644 on the  $sI_{AHP}$  of a representative cell is shown in Figure 7.6 (a, b, c). Bay-K8644 increased the peak current amplitude in 5 out of 6 cells (mean amplitude  $115.6 \pm 6.9\%$

of baseline,  $n = 6$ , Figure 7.6d), but this increase was not statistically significant (1-sample t-test  $p > 0.05$ ). The  $sl_{AHP}$  decay time constant was significantly increased ( $128.7 \pm 3.5\%$ , 1-sample t-test  $p < 0.02$ ). Bay-K8644 did not appear to affect the partially unclamped  $Ca^{2+}$  current (Figure 7.6c). We could therefore only partly replicate the effect of Bay-K8644 on the afterhyperpolarisation seen by Tombaugh in current clamp recordings, but we did not see any apparent change in the size of the un-clamped  $Ca^{2+}$  current.

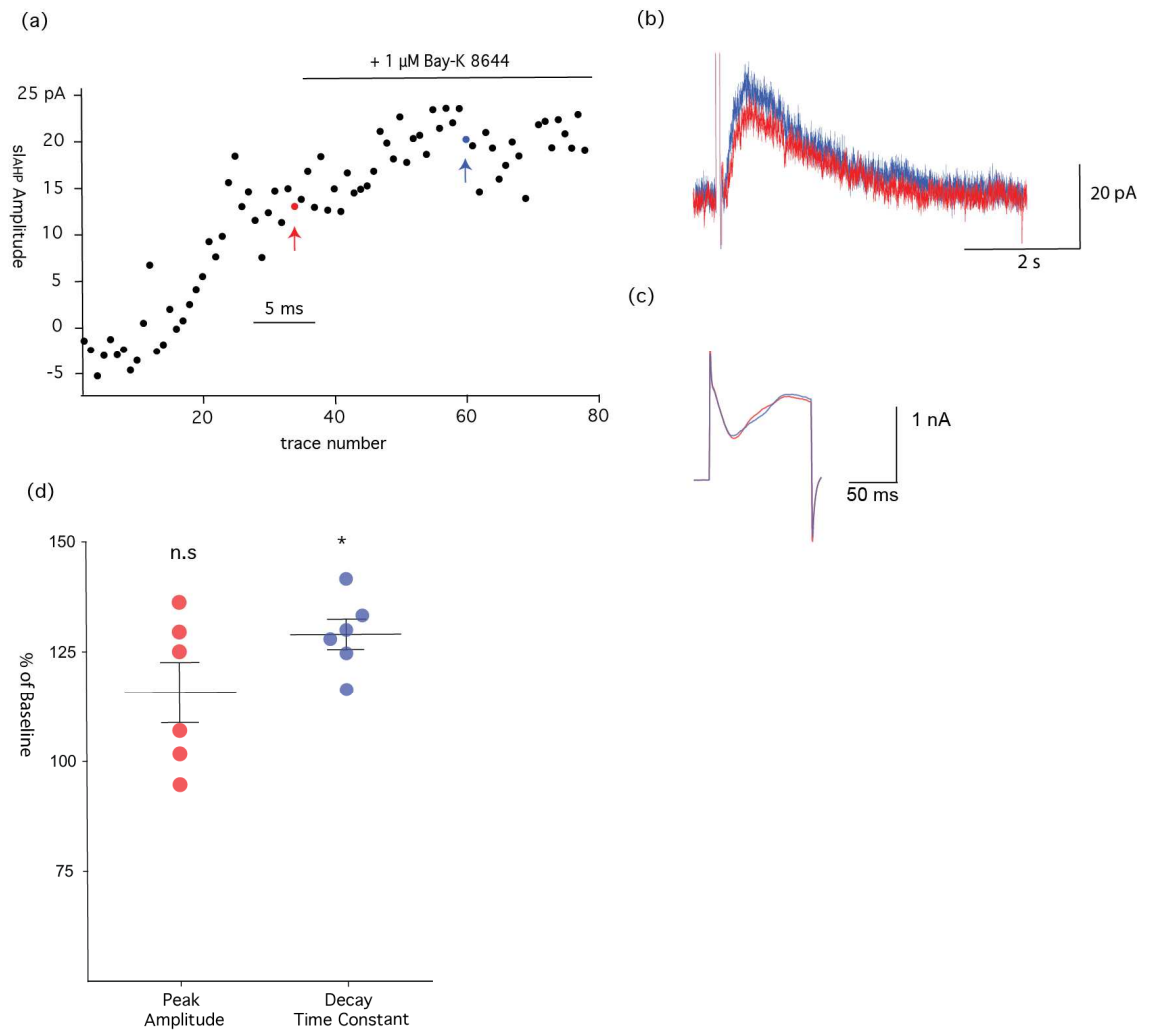


**Figure 7.6. Effect of Bay-K 8644 on  $sl_{AHP}$  amplitude**

(a) *Timecourse of the  $sl_{AHP}$  peak amplitude for a representative cell.*

*Horizontal line indicates duration of Bay-K 8644 applicaiton.*

(b) *Representative traces from the timecourse in (a). The position of each trace in the timecourse is indicated by a coloured circle and arrow.*

(d) *Summarised data for  $1 \mu\text{M}$  Bay-K 8644 ( $n=7$ ). Horizontal line indicates the mean, error bars denote SEM. The Y axis represents percentage of the baseline response.*

Of the three compounds tested, none produced an effect of sufficient magnitude and stability to warrant the compound's inclusion in our experiments. The effect of EBIO on  $sI_{AHP}$  amplitude was initially relatively large, but the enhancement was not persistent. The effects of ethanol varied from cell to cell, and the effect of Bay-K8644 on current amplitude was so small as to be statistically insignificant for our sample size. All three compounds were therefore omitted from the ACSF for subsequent experiments.

## **7.2 Focal application of the $\beta$ -adrenergic agonist isoproterenol in hippocampal CA1 pyramidal cells**

Bath application of the  $\beta$ -adrenergic receptor agonist isoproterenol inhibits  $sI_{AHP}$  in CA1 pyramidal cells via the adenylyl cyclase / PKA pathway (Pedarzani & Storm 1993). At present little is known about the spatial distribution of the receptors responsible for the inhibition of  $sI_{AHP}$ . Considering that cyclic AMP/ PKA signalling is subject to tight spatial control in many cell types (eg .Zaccolo et al 2011), and based on preliminary results of our laboratory on the effect of PKA anchoring proteins on the basal modulation of the  $sI_{AHP}$  amplitude (Pedarzani, unpublished data) and on the involvement of specific subtypes of adenylyl cyclases in the modulation of  $sI_{AHP}$  by different monoamine neurotransmitters (Taylor et al., unpublished data), our working hypothesis is that  $sAHP$  channels might be part of signalling domains organised in the close proximity of specific receptors (i.e. the  $\beta$ -adrenergic receptor) located in distinct subcellular compartments (e.g. soma, axonal initial segment, axon, proximal dendrites, distal dendrites) in CA1 pyramidal neurons. The location of these signalling domains would have important functional consequences for the neuron in terms of signal integration or encoding.

To test the hypothesis that  $\beta$ -adrenergic inhibition of  $sI_{AHP}$  is spatially localised, we used a microinjector to permit focal application of the  $\beta$ -adrenergic agonist isoproterenol onto different subcellular locations in CA1 hippocampal pyramidal neurons. Cells were recorded in whole-cell voltage clamp, using an intracellular solution containing a fluorescent dye (Lucifer yellow) in order to visualise their processes. Following acquisition of the whole-cell configuration, the cell was left for a period of 20 minutes to permit diffusion of the Lucifer yellow of the intracellular solution into the dendritic arbor; ACSF containing 50  $\mu$ M isoproterenol and 1 mM Lucifer yellow was then applied to the dendrites via the microinjector using a 10 ms-long puff at a pressure of 5 psi. To limit the drug application as much as possible to discrete subcellular compartments, the parameters of the microinjector were chosen to produce a puff with an approximate diameter of 2 soma diameters ( $\sim$ 40  $\mu$ m). Because the dendritic arbor of the cell is typically hundreds of microns in length, this was considered sufficient to distinguish

between two major, distinct locations: a region containing the soma and proximal apical dendrite, and another consisting of the distal apical dendrites, distal to the first main branching point of the apical dendritic tree.

In order to demonstrate that the microinjector puff did not directly affect the  $sI_{AHP}$  or the passive membrane properties of the cell, the microinjector tip was positioned adjacent to the soma, and a puff of ACSF containing 1 mM Lucifer yellow, but no isoproterenol, was delivered ( $n = 5$ ). A representative cell from this group is shown in Figure 7.7. The  $sI_{AHP}$  was recorded for a period of 15 minutes in the presence of TTX, TEA and dTC in order to establish a stable baseline for the current amplitude. The puff was then delivered via the pressure system and the recording continued. Figure 7.7a shows the overlay of a traces acquired immediately before (red) and 1 minute after (blue) the puff, and a detail of the same traces showing the partially clamped  $Ca^{2+}$  current can be seen in Figure 7.7b. In both cases, the overlap is almost complete, suggesting that the puff did not either destabilise the whole-cell configuration or have any direct effect on the  $sI_{AHP}$  or the calcium transient. There was likewise no observable change in the time course of either the peak  $sI_{AHP}$  amplitude (Figure 7.7c, e) or input resistance (Figure 7.7d, f). Mean  $sI_{AHP}$  amplitude at 1 minute after the puff was  $99.4\% \pm 2.5\%$  of baseline ( $n = 5$ ), and the change was not significant (Wilcoxon signed rank test  $p = 0.99$ ). Mean input resistance before the puff was  $252\text{ M}\Omega \pm 17\text{ M}\Omega$ . Following the puff, the input resistance was  $259\text{ M}\Omega \pm 21\text{ M}\Omega$ . This change was not statistically significant (Wilcoxon signed rank test  $p = 0.99$ ,  $n=5$ ).

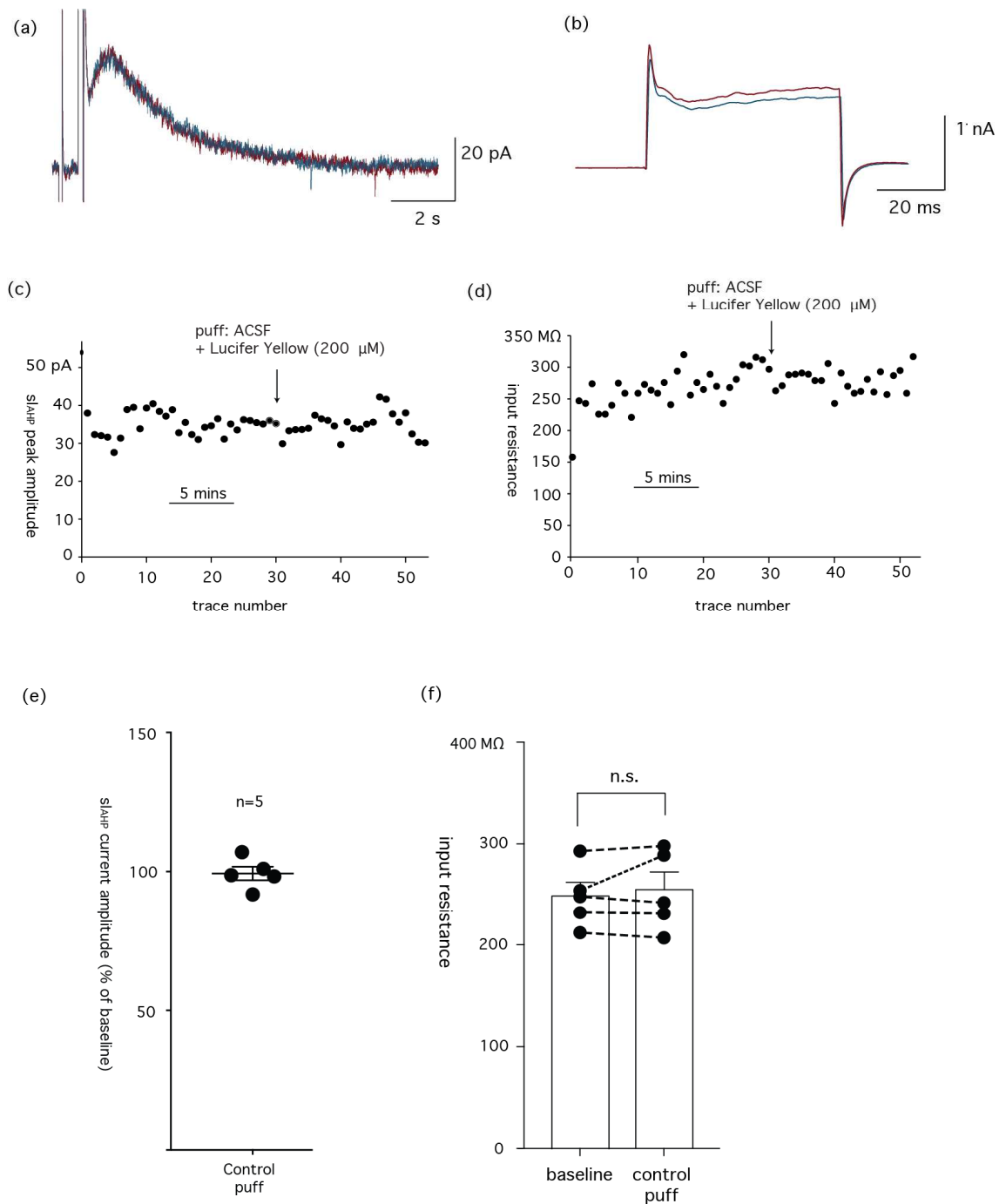


**Figure 7.7. Representative example cell for control puff experiment**

- (a) **Representative traces showing  $sIAHP$  amplitude before (red) and after (blue) application of a 5ms, 5psi puff of ACSF containing 200  $\mu M$  Lucifer yellow only, delivered to the soma of the cell.**
- (b) **Detail of the voltage stimulus from the traces in (a), showing the calcium action current.**
- (c) **Timecourse of the  $sIAHP$  peak amplitude of the same cell. The position of the puff is indicated by the vertical arrow. Traces acquired every 30 s.**
- (d) **Timecourse of the input resistance of the same cell. The position of the puff is indicated by the vertical arrow. Traces acquired every 30 s.**

- (e) **Summary of changes to  $sI_{AHP}$  peak amplitude following the puff protocol. Error bar denotes mean and SEM. Black circles represent responses of individual cells. Y axis denotes percent of baseline current.**
- (f) **Summary of  $R_{input}$  before and after the puff. Individual cell responses are represented by black circles linked by dashed lines. Bar height denotes mean, error bars represent SEM. Y axis shows  $R_{input}$  in  $M\Omega$ .**

Next, puffs of the same size and intensity, but additionally containing 50  $\mu$ M isoproterenol, were delivered to the same somatic location as the control puff. The results of a single representative experiment are shown in Figure 7.8. Puff application of isoproterenol caused a reduction in  $sI_{AHP}$  amplitude in 7/7 cells (Figure 7.8a, c), although a pronounced calcium spike was still visible during the stimulus pulse (Figure 7.8b). The time course of the reduction was rapid, with almost all the reduction occurring within one trace following the puff (Figure 7.8 c).

Application of the puff completely abolished the current in 3/7 cells tested, and in the remaining four the current was reduced to less than 25% of baseline level. Mean residual current was  $6.7\% \pm 2.1\%$  of baseline, and was significantly lower than the baseline current (Wilcoxon signed rank test  $p < 0.03$ , Figure 7.8e). The puff also significantly reduced the input resistance from  $244 \pm 20 M\Omega$  to  $218 \pm 27 M\Omega$  (Wilcoxon Signed Rank Test  $P = 0.03$ , Figure 7.8f). Although the inhibition observed in the  $sI_{AHP}$  would be expected to lead to an increase in input resistance due to the closure of the underlying  $K^+$  channels, the cAMP/PKA pathway activated by isoproterenol is also an important regulator of other neuronal channels (see Discussion).

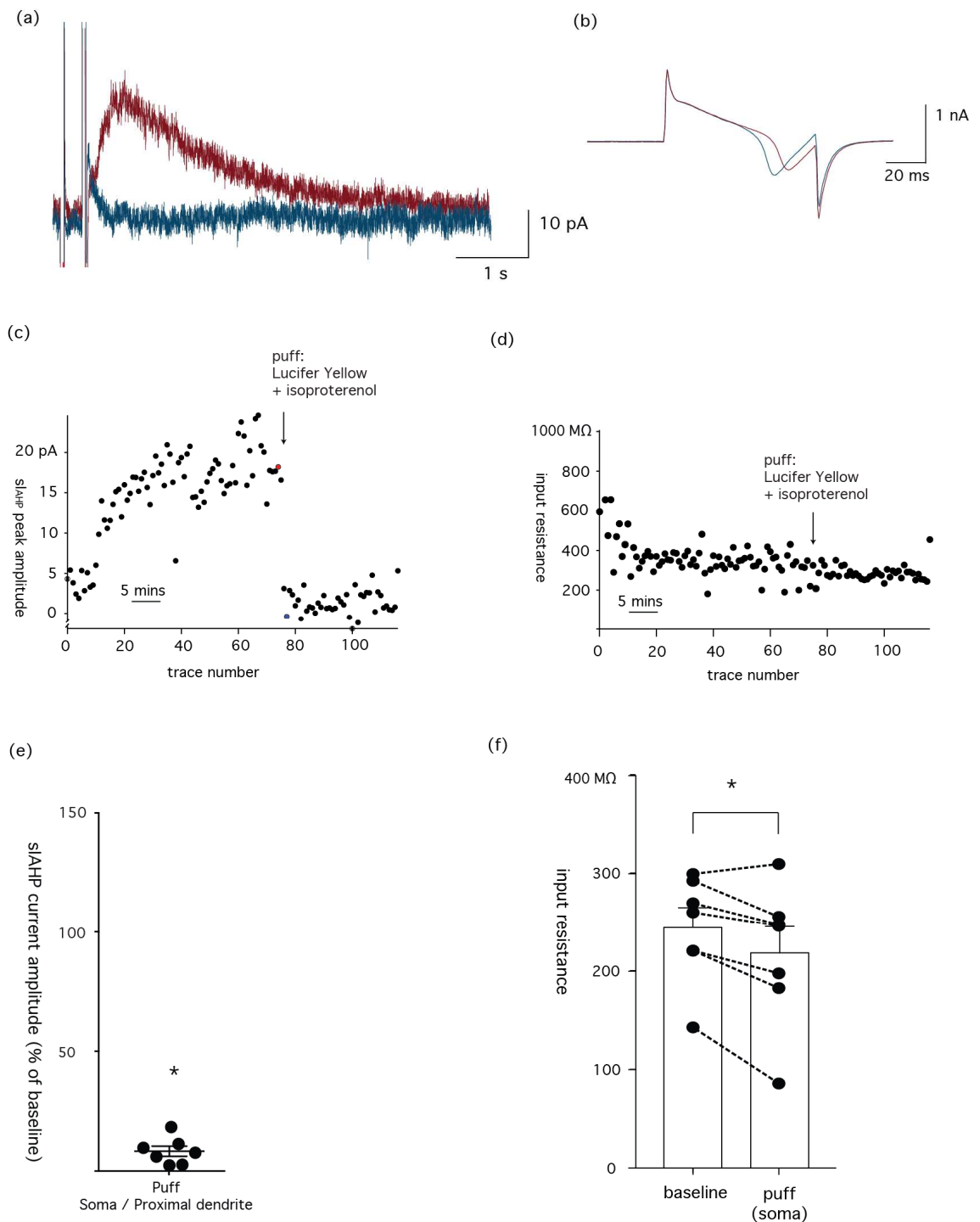


**Figure 7.8. Representative example cell for focal application at soma**

- (a)** *Representative traces showing  $sIAHP$  current response immediately before (red) and immediately after (blue) application of a puff containing 200  $\mu\text{M}$  Lucifer yellow and 20  $\mu\text{M}$  isoproterenol, delivered to the soma of the cell.*
- (b)** *Detail of the voltage step from the traces in (a) and the  $\text{Ca}^{2+}$  current.*
- (c)** *Timecourse of the peak  $sIAHP$  amplitude of the same cell. The position of the puff is indicated by the vertical arrow. Traces acquired every 30 s.*

- (d) *Timecourse of the input resistance for the same cell. The position of the puff is indicated by the vertical arrow. Traces acquired every 30 s.*
- (e) *Summary of change in peak amplitude of  $sI_{AHP}$  following the puff. Error bar denotes mean and SEM. Black circles represent responses of individual cells. Y axis denotes percentage of baseline current.*
- (f) *Summary of  $R_{input}$  before and after the puff protocol. Individual cell responses are represented by black circles linked by dashed lines. Bar height denotes mean, error bars represent SEM. Y axis shows  $R_{input}$  in  $M\Omega$ .*

The same experimental strategy was used to investigate the impact of beta-adrenergic receptor stimulation in the distal dendrites on  $sI_{AHP}$ . To this purpose, the puff pipette was positioned over the distal dendrites, at a location immediately distal to the first observable branch point in the Lucifer yellow filled neuron.

The results of a representative experiment are shown in Figure 7.9. Following the puff, there was a reduction in  $sI_{AHP}$  amplitude in 6/6 cells tested (Figure 7.9 a,e), and again the calcium spike during the stimulus pulse remained pronounced (Figure 7.9b). As with the somatic pulse, the time course of the reduction was rapid, occurring on the trace subsequent to the puff (Figure 7.9c). Mean residual current was  $47.6\% \pm 8.8\%$  of baseline, and the amplitudes after the puff were significantly lower than those before (Wilcoxon signed rank test  $p < 0.03$ , Figure 7.9e). The input resistance also decreased slightly in 6/6 cells following application of the puff, from  $233 \pm 11 M\Omega$  to  $207 \pm 10 M\Omega$ , and this reduction was statistically significant (Wilcoxon Signed Rank Test  $p < 0.03$ , Figure 7.9f).

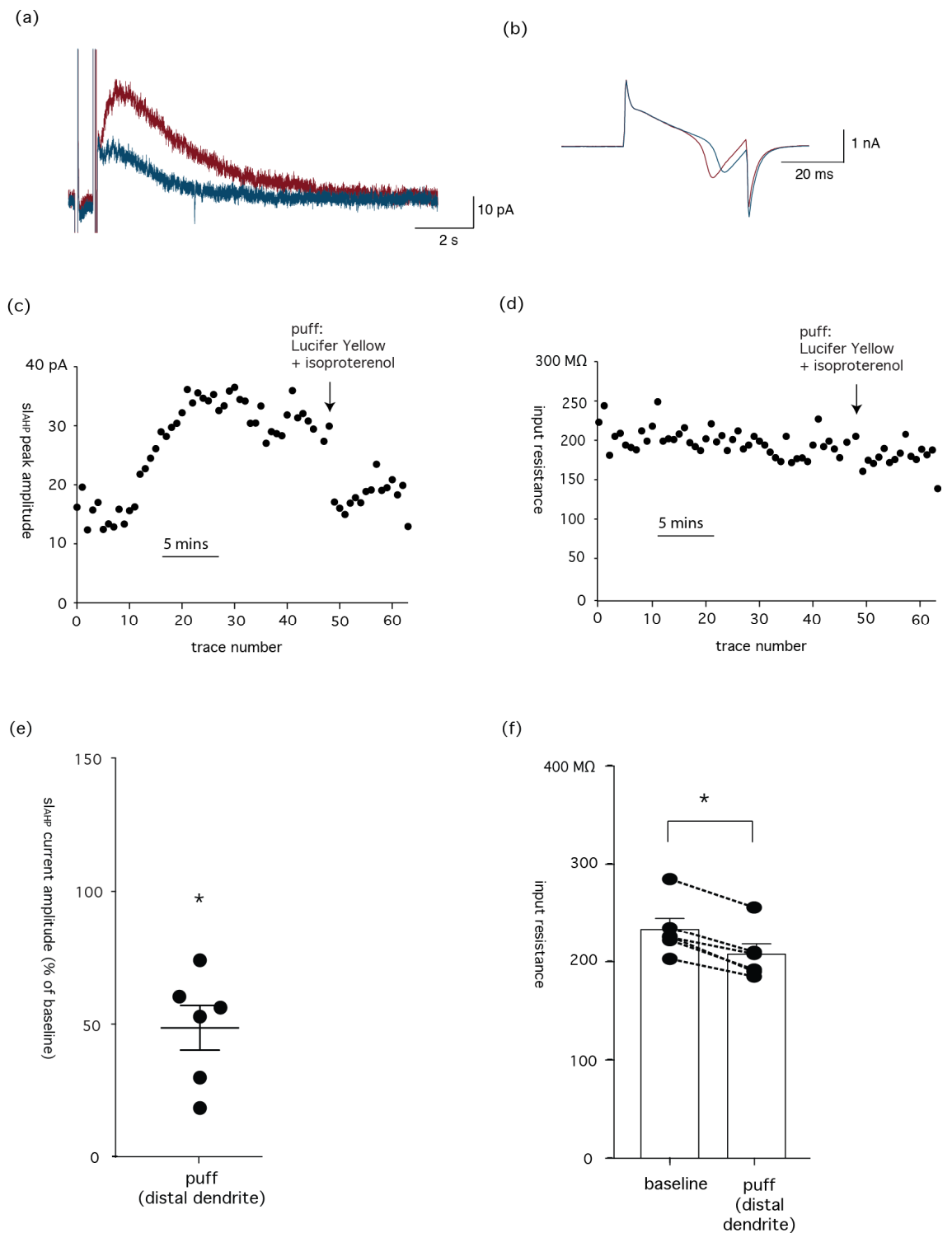


**Figure 7.9. Representative example cell for focal application at distal dendrites**

- (a) *Current traces from a representative cell, showing  $sI_{AHP}$  current immediately before (red) and immediately after (blue) application of a puff containing 200  $\mu\text{M}$  Lucifer yellow and 20  $\mu\text{M}$  isoproterenol, delivered to the distal portion of the apical dendrite.*
- (b) *Detail of the voltage step from the traces in (a), including the  $\text{Ca}^{2+}$  action current.*
- (c) *Timecourse showing the peak amplitude of  $sI_{AHP}$ , taken from the same cell as (a). The position of the puff is indicated by the vertical arrow. Traces acquired every 30 s.*

- (d) *Timecourse of the input resistance for the same cell. The position of the puff is indicated by the vertical arrow. Traces acquired every 30 s.*
- (e) *Summary of change in peak amplitude of  $sI_{AHP}$  following the puff. Error bar denotes mean and SEM. Black circles represent responses of individual cells. Y axis denotes percentage of baseline current.*
- (f) *Summary of  $R_{input}$  before and after the puff protocol. Individual cell responses are represented by black circles linked by dashed lines. Bar height denotes mean, error bars represent SEM. Y axis shows  $R_{input}$  in  $M\Omega$ .*

A comparison of the relative reduction in current amplitude for each experimental group is shown in Figure 7.10a. A 50  $\mu$ M isoproterenol puff delivered to the soma and proximal dendrite region was approximately three times as effective at inhibiting the  $sI_{AHP}$  current as the same puff delivered to the distal dendrite region. The somatic and distal dendrite focal isoproterenol applications both produced reductions that were significantly greater than that of control experiments, performed without isoproterenol, and additionally the reduction due to the somatic puffs was significantly greater than that due to the distal puffs ( ANOVA  $F(2, 15) = 78.2$ ,  $p < 0.0001$ , Sidak's multiple comparisons test:  $p < 0.0001$  (soma vs. control)  $p < 0.0001$  (distal vs. control),  $p < 0.0001$  (distal vs. soma).

The above data provide clear and first evidence that the effect of locally applied isoproterenol on  $sI_{AHP}$  is greater in the soma and proximal dendrite region of the neuron than in the distal dendrite region. It is noted that while the residual current responses to the somatic puff are tightly clustered around the mean, there is a much greater spread of results in response to the puffs delivered to the distal dendrite region. This difference in variability may be due to variability in the spatial spread of the puff, or to the structure of the finer dendritic branches covered by it, compared to the relatively uniform shapes of the soma and the initial segment of the apical dendrite. Another possibility is that in some cells the dendritic tree was not as superficially placed within the slice as the soma. See the Discussion section for a fuller examination of these issues.

Although the absolute reduction in series resistance in response to focal application of isoproterenol was statistically significant in both regions tested, suggestive of a channel opening effect, the magnitude of the change was relatively small. The percentage changes in input resistance for each condition are shown in Figure 7.10 (b). Comparison of the effect sizes for the three experimental conditions yields the result that there is a significant difference between the control condition and each of the conditions where isoproterenol was applied, but no significant difference between the effects of the isoproterenol puff on input resistance at the two locations (Kruskali-Wallace test (3,18)  $p = 0.01$ . Dunn's multiple comparisons test  $p = 0.049$  (soma vs. control),  $p = 0.028$  (distal

dendrite vs. control,  $p=0.99$  (soma vs. dendrite). It therefore appears that isoproterenol acts to open some channels in the neuron, though there is no difference in the magnitude of the input resistance between the two locations. It is possible that this is because the contribution to the change in input resistance made by the channels underlying  $sI_{AHP}$  is outweighed by the opening of unrelated channels by isoproterenol. See the discussion section for possible candidates for the identity of these channels.

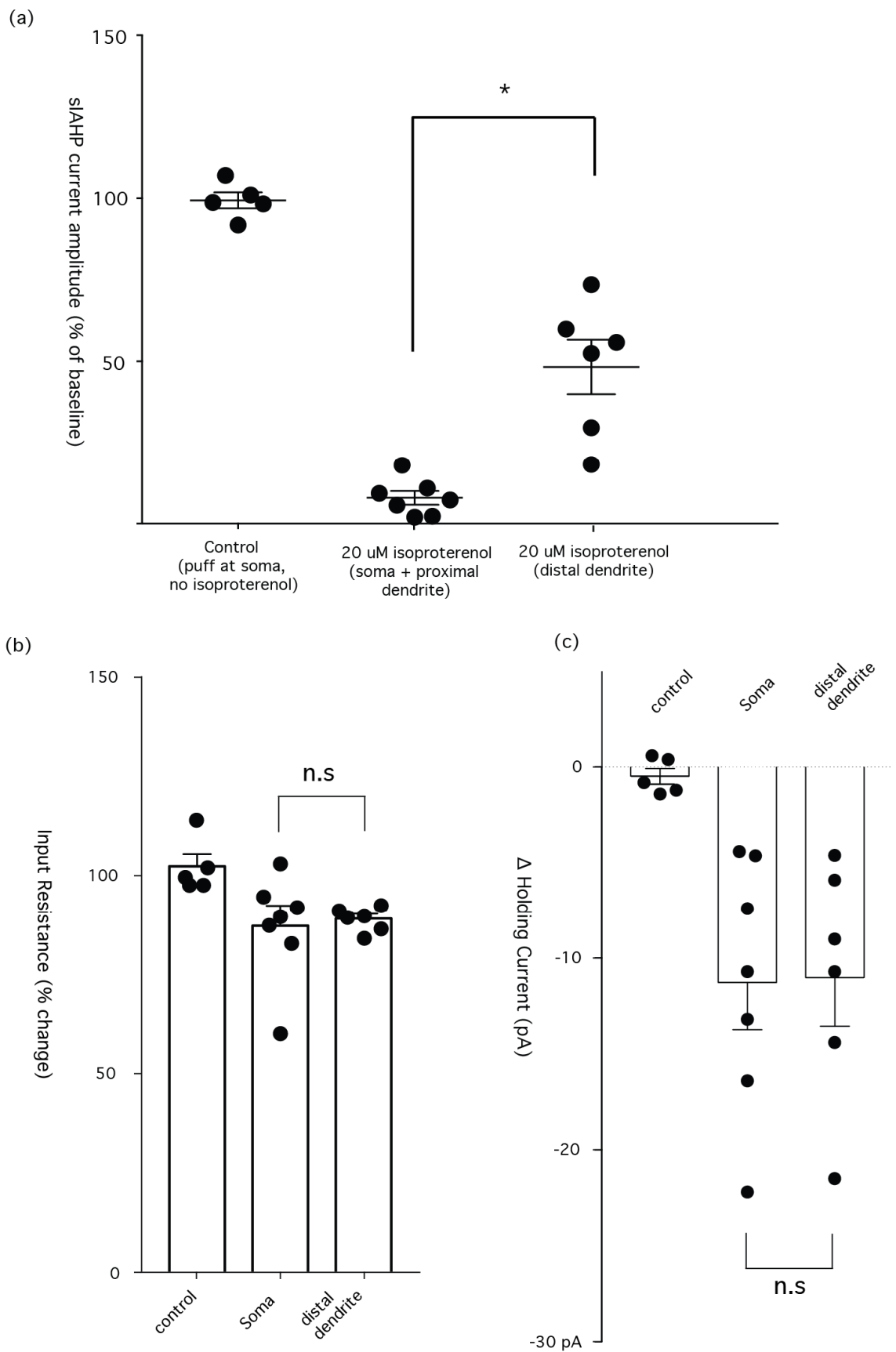


**Figure 7.10. Effect of focal application of 20  $\mu$ M isoproterenol at different cellular locations**

- (a) *Graph showing the change in  $s_{\text{AHP}}$  amplitude, expressed as percentage of baseline amplitude, in response to 5ms, 5 psi puff of ACSF containing 200  $\mu\text{M}$  Lucifer yellow and 20  $\mu\text{M}$  isoproterenol, delivered to the soma or distal dendrite regions of each cell. Also shown is change in  $s_{\text{AHP}}$  amplitude in response to a puff of ACSF containing only 200  $\mu\text{M}$  Lucifer yellow, delivered to the soma of the cell. Individual cell responses are denoted by black circles. Error bars show mean and SEM. Y axis represents percentage of baseline peak  $s_{\text{AHP}}$  amplitude.*
- (b) *Graph summarising the effect of the puff protocol on the input resistance for the control puff experiment and the 20  $\mu\text{M}$  isoproterenol puff at the two subcellular locations. Y axis shows percentage of baseline input resistance. Black circles represent individual cell responses. Error bars denote mean and SEM.*
- (c) *Summary of changes in the holding current at -50 mV before and after the puff protocol, for all three experimental groups. Black circles represent responses of individual cells. Error bars show mean and SEM, Y axis shows change in holding current amplitude in pA.*

### **7.3 Is there subcellular compartmentalisation of the cAMP signal? Evidence from photo-uncaging experiments**

The spatial variation in the extent of  $\beta$ -adrenergic receptor mediated inhibition of  $s_{\text{AHP}}$  observed in the focal application experiments could be due to the number and density of receptors in different subcellular compartments. Alternatively it could be evidence for the existence of distinct localised cAMP signalling domains, such that the cAMP signal produced by pool of adenylyl cyclases activated by the receptors in the distal dendrite is less tightly coupled to the  $s_{\text{AHP}}$  channels than that produced by the receptors and cyclases near the soma. Such domains are limited partly by diffusion, such that the cytoplasmic volume where the cAMP concentration is high enough is within a few micrometres of the cyclases, and partly by the presence of phosphodiesterases which limit the spread of the cAMP signal by hydrolysis (Introduction 6.5).

In order to test whether the coupling of the cAMP signal to the  $s_{\text{AHP}}$  channels is spatially localised, it was decided to use flash photolysis of a caged cyclic AMP analogue, BCMCM-8Br-cAMP, using a flash from a UV lamp focused down the light path of the microscope. By using a lens to vary the area covered by the UV flash, and by patching the somata of cells such that they are offset from the centre of the field of view, it was possible to cause this flash to be focused on two separate subcellular locations: the soma, and the proximal portion of the apical dendrite.

### 7.3.1 Uncaging of DM-Nitrophen in HEK293 cells stably expressing rBK $\alpha$ channels

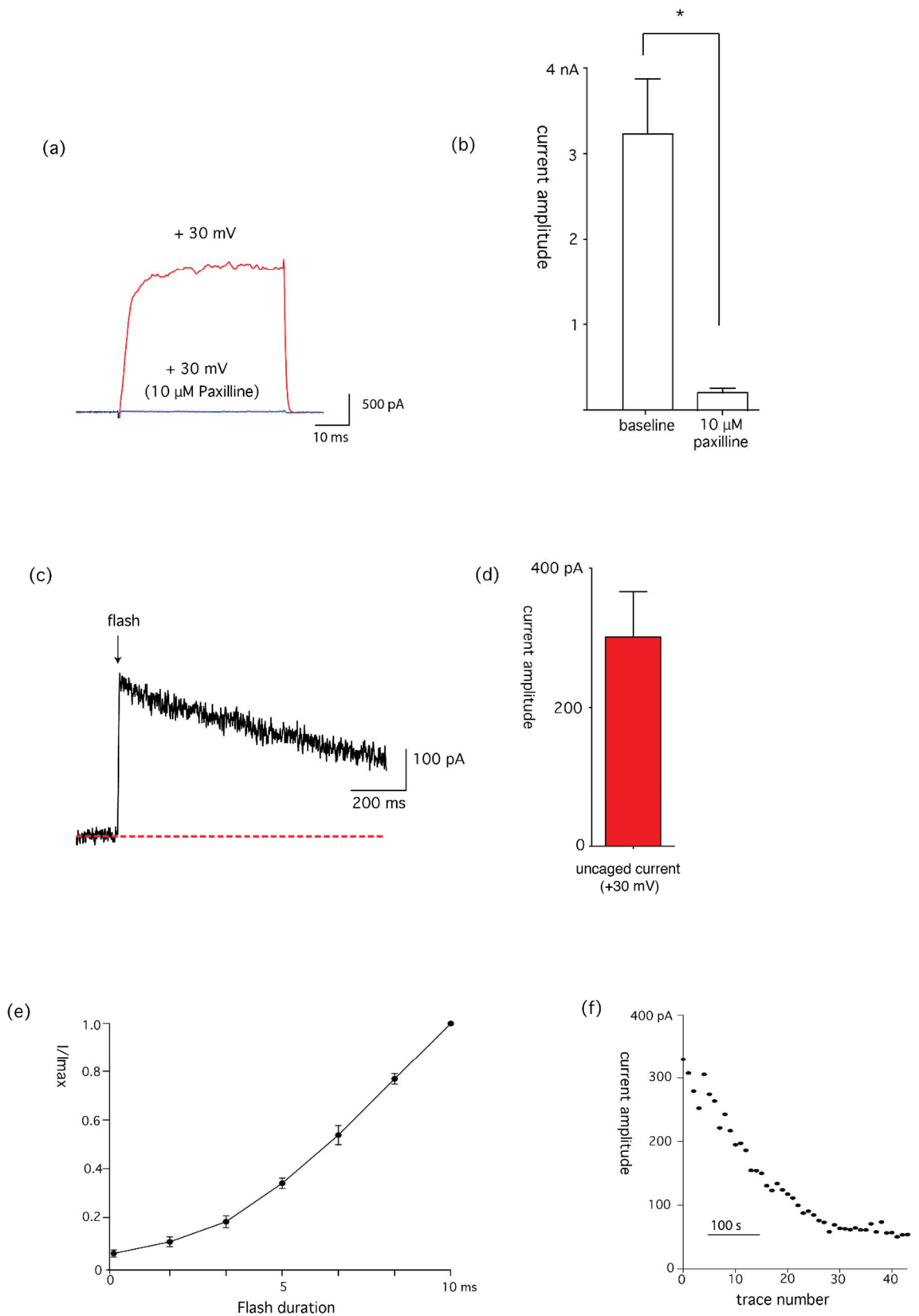
The technique of using flash photolysis via a mercury lamp was new to our lab, and so initially it was decided to set up and test the uncaging apparatus using a simple system and a well characterised caged compound. It was decided to use the calcium cage DM-nitrophen, which is based on the calcium buffer EDTA. Before photolysis, it binds calcium with a  $K_d$  of 5 nM, but following photolysis this increases to 3 mM, allowing the production of a rapid increase in intracellular free  $Ca^{2+}$  in response to a light flash (Kaplan and Ellis-Davies 1988). In order to detect this change in free  $Ca^{2+}$ , recordings were made from HEK293 cells stably expressing the zero-splice alpha subunit of the rat BK channel (rBK $\alpha^0$ ). BK channel activity is modulated by both voltage and  $Ca^{2+}$ , and the half-maximal voltage ( $V_{1/2}$ ) of activation of BK-mediated currents is shifted leftward by increasing intracellular free  $[Ca^{2+}]$ . When expressed in HEK293 cells, channels formed from rBK $\alpha^0$  produce a large whole-cell current, which can act as a sensitive detector of any changes in intracellular free  $[Ca^{2+}]$ .

Figure 7.11a shows a current trace from a representative HEK293-BK cell in response to a 50 ms-long voltage step to +30 mV from a holding potential of -90 mV (red), and in response to the same voltage step in the presence of 10  $\mu$ M paxilline, a specific blocker of BK channels. The mean current recorded in response to the voltage step, before and after the application of paxilline is shown in Figure 7.11b. Application of 10  $\mu$ M paxilline reduced mean current amplitude from  $3.2 \pm 0.6$  nA to  $0.2 \pm 0.04$  nA, mean residual current was  $4.7\% \pm 0.8\%$  of baseline ( $n=7$ ). It is therefore apparent that the current in response to the +30 mV step was predominantly a BK current.

Cells were patched in the whole-cell configuration and left for 10 minutes in order to permit the intracellular solution, including 3 mM DM-Nitrophen, to perfuse the cell. The cell was then held at +30 mV while a 10 ms-long flash was delivered by the mercury lamp. An example trace in response to the flash is shown in Figure 7.11c. The timing of the flash is shown by the arrow. In response to the flash, there was a rapid increase in current amplitude with an onset time of <10 ms, which decayed slowly over the course of several hundred milliseconds. Mean current amplitude in response to a single flash at +30 mV was  $301 \pm 65$  pA (Figure 7.11d,  $n=9$ ). The size of the current response increased with the duration of the flash delivered (Figure 7.11e,  $n = 9$ ). In the lower end of the duration range the increase in current amplitude was supralinear with respect to the increase in flash duration, and this became closer to linear as higher durations were reached. The shape of this relationship suggests that a relatively small proportion of the DM-Nitrophen was uncaged with each flash, as even at maximum duration, there is no sign of a saturation of the response, as would be expected if a flash of shorter duration

was significantly depleting the pool of unphotolysed DM-Nitrophen. Further evidence for this assumption comes from a second experiment, in which a flash at maximum duration was delivered at 10 s intervals while the cell was held at +30 mV. A representative time-course is shown in Figure 7.11f. There is a noticeable run-down of the current response with each additional flash, eventually reaching a stable level. The mean number of flashes required to reduce the current response by half was  $15.8 \pm 1.7$  (n=6).

These results demonstrate that the photolysis system is capable of delivering sufficient energy to photoactivate a subset of the DM-nitrophen in the region covered by the flash, and provided confirmation that our uncaging system was functioning correctly.



**Figure 7.11. HEK293 whole cell recordings illustrating BK- $\alpha$  channel properties and response to uncaging of DM-Nitrophen**

(a) *Example current response to a 50 ms voltage step to +30 mV from a holding potential of -90 mV, under voltage clamp. Red trace shows the current response under baseline conditions, blue trace shows the current response in the presence of 10  $\mu\text{M}$  paxilline.*

- (b) *Effect of 10  $\mu\text{M}$  paxilline on the BK current amplitude (n=7). Error bars denote SEM, bar heights represent mean current response to a voltage step to +30 mV from a holding potential of -90 mV. Y axis denotes current in nA.*
- (c) *Response of a cell to a single flash of 10 ms duration, while held at +30 mV. The position of the flash in the trace is denoted by the vertical arrow. Dashed red line represents the baseline current at +30 mV.*
- (d) *Summary of the response to the flash protocol in (c) across all cells tested (n=9). Bar height denotes the mean current response to the flash when the cells were held at +30 mV. Error bars denote SEM. Y axis shows current amplitude in pA.*
- (e) *Summary of responses from all cells to varying the flash duration. Y axis shows  $I/I_{\text{max}}$ . Error bars show SEM. n=9.*
- (f) *Example timecourse showing the current response to sequential flashes of 10 ms duration, delivered at 10 s intervals, while the cell was held at +30 mV. Each filled circle represents a trace in which one flash was delivered. Y axis shows current amplitude in pA.*

### **7.3.2 Uncaging DM-Nitrophen in hippocampal cultured neurones activates a dTC-sensitive conductance**

Uncaging  $\text{Ca}^{2+}$  in a cell line overexpressing BK channels leads to the generation of a whole-cell current that is likely to be larger than can be seen in most physiologically relevant situations. This might be further enhanced by the lower endogenous calcium buffering capacity of HEK293 cells compared with neurons. We therefore attempted a similar experiment in cultured hippocampal neurons in an attempt to determine the effect of  $\text{Ca}^{2+}$  uncaging under our experimental conditions in a neuronal context.

Rat hippocampal cultured neurons of DIV 7 to 14 were patched in the whole-cell configuration, with an intracellular solution containing 3 mM DM-Nitrophen. Following acquisition of whole-cell state, the cell was left to rest for a period of 10-15 minutes to permit the diffusion of the caged compound into the cell. Two protocols were then used: one, which used a voltage step to elicit an afterhyperpolarising current, as in previous experiments on the  $sI_{\text{AHP}}$ , and another, which delivered 4 consecutive flashes 2 s apart, while holding the cell at -50 mV.

The results of the experiment are summarised in Figure 7.12. Panel (a) shows current traces from a representative cell in response to 4 consecutive flashes. The leftmost trace shows the current under baseline conditions, at a time point ten minutes after whole-cell configuration was first achieved. Successive flashes appear to have an additive effect on the amplitude of the current elicited. Mean current amplitude in response to the fourth flash in the train was  $51.3 \text{ pA} \pm 6.8 \text{ pA}$  (Figure 7.12c, n= 8). Bath application of  $100 \mu\text{M}$

d-tubocurarine (dTC) abolished all but  $10.4\% \pm 3.6\%$  of the current response to flashing (Figure 7.12d). Mean amplitude after application of  $100 \mu\text{M}$  dTC was  $5.1 \text{ pA} \pm 1.6 \text{ pA}$ , and the effect was significant (paired t-test  $p < 0.001$ ,  $n=8$ ). The current produced in response to the flashes was not sensitive to  $1 \text{ mM}$  TEA. Mean residual current after application of  $1 \text{ mM}$  TEA was  $94.9\% \pm 11.3\%$  of baseline (Figure 12e), and this difference was not significant (Wilcoxon matched pairs signed rank test  $p=0.62$ ,  $n = 5$ ). Based on its  $\text{Ca}^{2+}$  sensitivity and pharmacological profile (inhibition by dTC, but not by low TEA concentrations), the flash induced current is likely to be mediated by SK channels.

The current mediated by SK channels,  $I_{\text{AHP}}$ , was further measured in response to a voltage protocol consisting of a  $200 \text{ ms}$ -long depolarising step to  $+20 \text{ mV}$  from a holding potential of  $-50 \text{ mV}$ , interleaved with the flash protocols for each cell. Figure 7.12b shows the  $I_{\text{AHP}}$  elicited in response to the voltage protocol delivered to the same cell as shown in Figure 7.12a.  $I_{\text{AHP}}$  was largely inhibited by  $100 \mu\text{M}$  d-tubocurarine, but was not affected by  $1 \text{ mM}$  TEA, suggesting that the majority of the afterhyperpolarising current in the cells recorded in this experiment, as well as the entirety of that elicited by the flash protocol, is mediated primarily by dTC-sensitive SK channels.

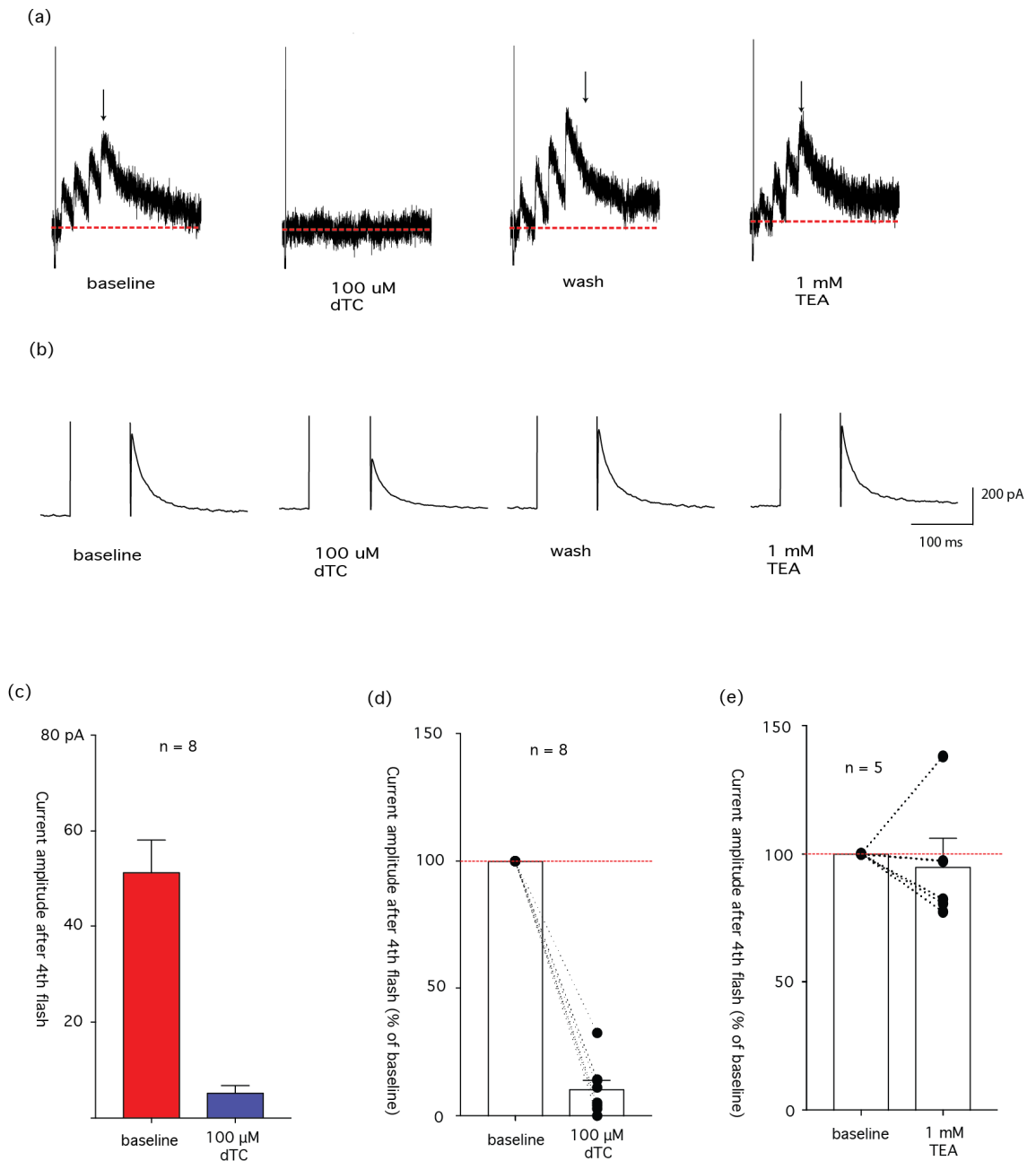


**Figure 7.12. Uncaging of DM-Nitrophen in primary culture hippocampal neurons**

- (a) *Current response of a representative cell to a series of four flashes of 10 ms duration and separation of 800 ms: under baseline conditions, following application of 100  $\mu\text{M}$  d-tubocurarine, following washout of d-tubocurarine, and after subsequent application of 1 mM TEA. The cell was held at -50 mV. Arrow indicates position of the final flash in the series, which provides the values for the graphs in (d) and (e).*
- (b) *Current response under the same cell to a 100 ms voltage step to +10 mV from a holding voltage of -50 mV, under the same conditions as in (a).*
- (c) *Summary of the amplitude of the currents elicited in response to the 4th flash in the train across all cells (n=8), under baseline conditions and following the application of 100  $\mu\text{M}$  dTC. Bar height represents the mean, error bars denote SEM. The Y axis shows current amplitude in response to the 4th flash, in pA.*

- (d) *Relative effect of 100  $\mu$ M dTC on the amplitude of the current response to the 4th flash in the train. Paired responses from an individual cell are denoted by filled circles connected by a dashed line. Y axis denotes percent of baseline current response. Bar height gives the mean response across all cells, error bars denote SEM. Dashed red line indicates the baseline of 100%.*
- (e) *Relative effect of 1 mM TEA on the amplitude of the current response to the 4th flash in the train. Paired responses from an individual cell are denoted by filled circles connected by a dashed line. Y axis denotes percent of baseline current response. Bar height gives the mean response across all cells, error bars denote SEM. Dashed red line indicates the baseline of 100%.*

### **7.3.3 Localised uncaging of 8Br-cAMP in hippocampal neurons inhibits $sI_{AHP}$**

Having established that photolysis of caged compounds in hippocampal cultured neurons was achievable using our apparatus and led to the activation of a  $Ca^{2+}$ -dependent current upon  $Ca^{2+}$  uncaging, we proceeded to use this approach to release a different second messenger and trigger the activation of a signalling pathway known to inhibit  $sI_{AHP}$ . In particular, we used the localised uncaging of a caged cAMP analogue to attempt to determine the existence and location of signalling domains underlying the cAMP-dependent modulation of  $sI_{AHP}$  and compare them to those engaged by monoamine transmitters, as we had investigated by focal activation of  $\beta$ -adrenergic receptors. Whole cell voltage clamp recordings were performed in DIV 14 to 28 hippocampal pyramidal neurons, using a  $KMeSO_4$ -based intracellular solution (IC-4 - see methods) containing 200  $\mu$ M BCMCM-8Br-cAMP. The 8-bromo analogue of cAMP is membrane-permeable and resistant to degradation by phosphodiesterases, and so the signal persists until cleared from the uncaging site by diffusion. This has the advantage that the cAMP signal was likely to be long lasting enough to be detected using the infrequent (30 s interval) sampling frequency required for stable  $sI_{AHP}$  recordings, although, balanced against this, is the capacity for the uncaged 8Br-cAMP to diffuse away from the site of uncaging to other subcellular compartments over time.

As with the DM-Nitrophen experiment described previously, the flash was delivered by focusing the output of a UV flash lamp through the 60x water-immersion objective of the microscope. Using this apparatus, it was possible to vary the size of the area covered by the flash, and by positioning the patch electrode in different parts of the visual field, it was possible to patch the soma whilst flashing a dendritic region at a distance of around 4 to 5 soma diameters away, such that the edge of the flashed area furthest from the soma was set at a point immediately proximal to the first branch point of the apical dendrite. In this way it was possible to create two experimental conditions: in the first one, the flash was centred on the soma, while in the second it was delivered to the

proximal region of the apical dendritic tree. In order to successfully cover the soma while excluding the proximal apical dendrites, the flash aperture was set such that the flash covered a circular area  $\frac{1}{8}$  the area of the visual field of the 60x lens, while in order to cover the proximal dendrite region successfully, it was necessary to increase this to a region equal to  $\frac{1}{4}$  of the area of the visual field. It should be noted that doubling the area in this manner halves the photon density of the flash.

In order to control for any effects of the flash itself on the  $sI_{AHP}$  current, initial control experiments were carried out using an intracellular solution devoid of BCMCM-8Br-cAMP. The current was recorded for an initial period of 15 minutes, in the presence of 0.5  $\mu$ M TTX, 1 mM TEA and 50  $\mu$ M dTC, applied extracellularly, to permit its stabilisation. Following this period, a flash protocol, consisting of a train of 5 flashes of 10 ms duration and 800 ms separation was delivered to the soma, and the current was recorded again for a further 10 minutes immediately following the flash.

The results from a representative cell are shown in Figure 7.13. Panels (a) and (b) show the time-course of the peak  $sI_{AHP}$  amplitude and the input resistance of the cell, with the time point of the flash protocol denoted by an arrow. The current trace immediately preceding the flash protocol (red) and one taken 1 minute after the flash protocol (blue) are superimposed in panel (c). As can be seen from this representative cell, no discernible change was observed in the amplitude or kinetics of the current, and this was true of all cells tested. There was also no obvious change in the partially clamped  $Ca^{2+}$  current during the stimulus pulse (Figure 7.13d).

Following the flash train, mean  $sI_{AHP}$  peak current amplitude increased to  $101.8\% \pm 4.0\%$  of baseline. This change was not statistically significant (Wilcoxon matched pairs signed-rank test  $p=0.06$ ,  $n=5$ , Figure 7.13e). There was likewise no significant change in the decay time constant ( $\tau$ ) of the current. Mean baseline  $\tau$  was  $6.02 \pm 0.83$  s, which rose to  $6.31 \pm 0.9$  s following the flash (Wilcoxon matched pairs signed-rank test  $p=0.18$ , Figure 7.13f). Mean input resistance before the flash was  $159 \pm 14$  M $\Omega$ , while after the flash it increased to  $160 \pm 16$  M $\Omega$ , and this change was also not statistically significant (paired 2-tailed t-test  $p<0.81$ ,  $n=5$ , Figure 7.13g). The flashes also had no significant effect on the holding current of the cell. The mean change in the holding current was  $1.82 \pm 1.22$  pA, and this change was not statistically significant (Wilcoxon signed ranks test  $p=0.21$ , Figure 7.13h).

It was therefore concluded that the flash protocol itself did not affect either the current amplitude and kinetics of the  $sI_{AHP}$  current, or on the holding current or input resistance

of the wider cell. It was therefore concluded that the flash protocol alone did not affect the behaviour of the cell or the current.

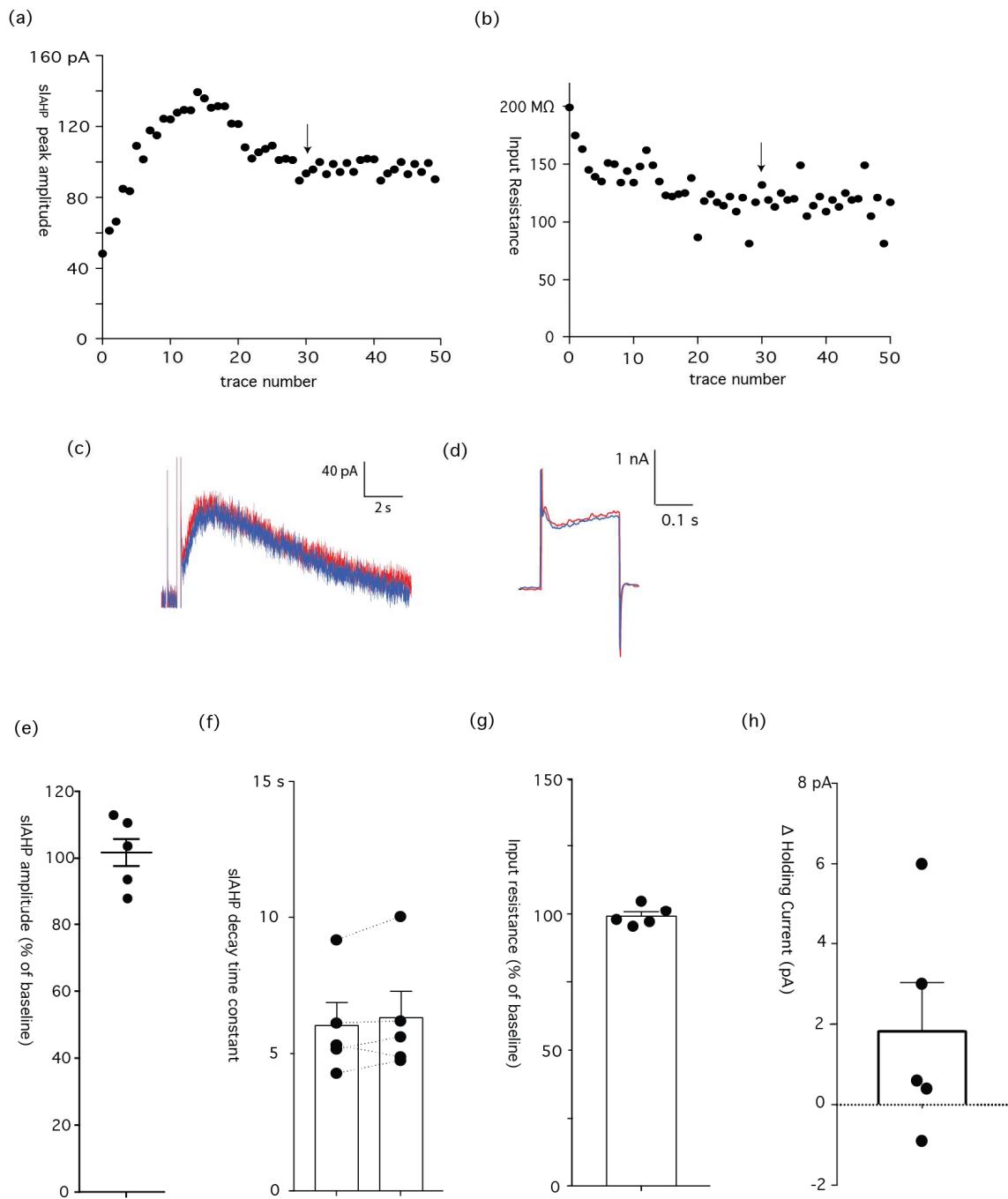


**Figure 7.13. Effect of flash protocol on control cells (no BCMCM-8Br-cAMP)**

- (a) *Timecourse of  $sI_{AHP}$  amplitude for a representative cell in response to a 200 ms voltage step to +20 mV from a holding potential of -50 mV. Vertical arrows show the positions of each flash train protocol, which consisted of 5 flashes of 10 ms duration each, and a separation of 800 ms. Traces were acquired at 30 s intervals.*
- (b) *Timecourse of input resistance for the same cell. Vertical arrows show the positions of each train of flashes.*

- (c) *Example traces showing amplitude of  $sI_{AHP}$  before (red) and after (blue) a flash train protocol. Top traces correspond to first flash, bottom traces correspond to second flash. In each case, “before” traces are the trace immediately before the flash train, and “after” traces are the fourth trace after the flash train.*
- (d) *Detail of the voltage step for the traces in (c), showing the calcium action current.*
- (e) *Summary of the effect of the flash protocol on the peak  $sI_{AHP}$  amplitude. Filled circles show the responses of individual cells. Error bars denote mean and SEM of the responses. Y axis represents percentage of baseline peak amplitude.  $n=5$*
- (f) *Graph summarising the effect of the flash protocol on the decay time constant ( $\tau$ ) of the  $sI_{AHP}$ . Y axis denotes the decay time constant in seconds. Filled circles connected by dashed lines represent the change in  $\tau$  of individual cells. Bars represent the mean  $\tau$  before and after the flash protocol. Error bars show SEM.  $n=5$*
- (g) *Summary of the effect of the flash protocol on the input resistance. Y axis shows input resistance following the flash as a percentage of the baseline input resistance. Filled circles denote individual cell responses. Bar height shows mean response of all cells. Error bars denote SEM.  $n=5$*
- (h) *Summary of the change in holding current in response to the flash protocol. Y axis represents change in holding current in pA. Individual responses are represented as black filled circles. Bar height denotes the mean change in  $I_{hold}$  across all cells. Error bars represent SEM.  $n=5$*

In subsequent experiments, cells were filled with intracellular solution containing 200  $\mu\text{M}$  BCMCM-8Br-cAMP. Following a 15 minute period to allow current run-up and diffusion of the caged compound into the cellular processes, a flash protocol, consisting of a train of 5 flashes of 10 ms duration and 800 ms interval, was delivered to either the soma or the proximal apical dendrite.

The results from a cell representative of the somatic experiments is shown in Figure 7.14. Panel (a) shows the timecourse of the  $sI_{AHP}$  peak amplitude for the cell. In some experiments, such as the one shown, the flash protocol was repeatedly applied, primarily to provide a demonstration of the reproducibility of the flash effect. The time-course of the input resistance is shown in panel (b), again with arrows denoting the timing of the flash protocols. Panel (c) shows the effect of the first two flash trains on the  $sI_{AHP}$  peak current amplitude, as superimpositions of the trace immediately preceding the flashing (red) and one taken 1 minute after the flashing (blue). In both cases the flash protocol led to a noticeable decrease in the current amplitude (left traces), without substantially altering the size of the partially clamped  $\text{Ca}^{2+}$  current (d). Multiple instances of the flash protocol were delivered to 3 of 7 cells, and in each case the third or fourth application led to an irreversible run-down of the  $sI_{AHP}$  current, a concomitant increase in the current required to hold the cell at -50 mV, and a decrease of the input resistance.

Considering only the first flash in each cell, a reduction in the current amplitude and a shortening of current decay kinetics was observed in all cells tested (Figure 7.14e, f). The mean current following the flash was  $54.2 \pm 5.2\%$  of the baseline value, and this change was statistically significant (Wilcoxon signed rank test  $p < 0.01$ ,  $n = 7$ ). Mean decay T was  $6.4 \pm 0.85$  s before the flash, and  $4.2 \pm 0.30$  s after, and this difference was significant (Wilcoxon matched pairs signed rank test 0.015).

Following the flash, the input resistance increased from  $178 \pm 14$  M $\Omega$  to  $194 \pm 12$  M $\Omega$ , a statistically significant increase (paired 2-tailed t-test,  $p < 0.015$ , Figure 7.14g). In percentage terms, the average  $R_{\text{input}}$  increase was  $110\% \pm 5.3\%$ . The flash also produced an inward shift in the holding current by an average of  $17.9 \pm 4.1$  pA (one-sample t-test  $p = 0.005$ , Figure 7.14h).

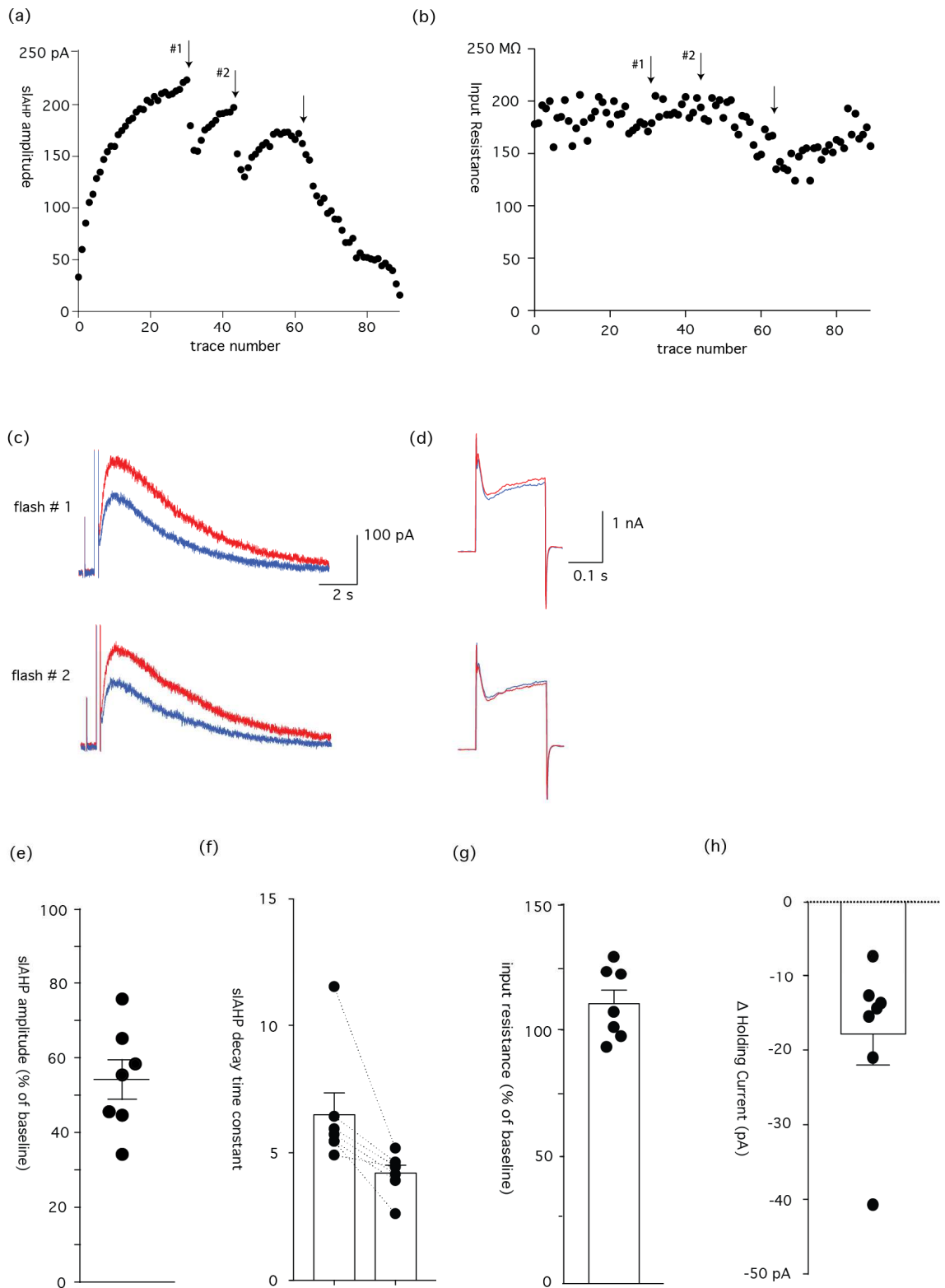


**Figure 7.14. Effect on  $sI_{AHP}$  of uncaging BCMCM-8Br-cAMP in soma**

- (a) *Timecourse of  $sI_{AHP}$  amplitude for a representative cell in response to a 200 ms voltage step to +20 mV from a holding potential of -50 mV. Vertical arrows show the positions of each flash train protocol. Traces were acquired at 30 s intervals.*
- (b) *Timecourse of input resistance for the same cell. Vertical arrows show the positions of each train of flashes.*

- (c) *Example traces showing amplitude of  $sI_{AHP}$  before (red) and after (blue) a flash protocol. Top traces correspond to first flash, bottom traces correspond to second flash. In each case, “before” traces are the trace immediately after the flash train, and “after” traces are the third trace after the flash train.*
- (d) *Detail of the voltage step for the traces in (c), showing the calcium action current.*
- (e) *Summary of the effect of the flash protocol on the peak  $sI_{AHP}$  amplitude. Filled circles show the responses of individual cells. Error bars denote mean and SEM of the responses. Y axis represents percentage of baseline peak amplitude. n=7*
- (f) *Graph summarising the effect of the flash protocol on the decay time constant ( $\tau$ ) of the  $sI_{AHP}$ . Filled circles connected by dashed lines represent the change in  $\tau$  of individual cells. Y axis represents the decay time constant in seconds. Bars represent the mean decay time constant across all cells, before and after the flash protocol. Error bars show SEM. n=7*
- (g) *Summary of the effect of the flash protocol on the input resistance. Y axis shows input resistance following the flash as a percentage of the baseline input resistance. Filled circles denote individual cell responses. Bar height shows mean response of all cells. Error bars denote SEM. n=7*
- (h) *Summary of the change in holding current in response to the flash protocol. Y axis represents change in holding current in pA. Individual responses are represented as black filled circles. Bar height denotes the mean change in  $I_{hold}$  across all cells. Error bars represent SEM. n=7*

In a separate set of experiments the flash was delivered to the proximal apical dendrite instead of the soma. In order to optimally cover this region while omitting the soma itself, the size of the flash area was increased two-fold. Figure 17.5 shows data from a representative cell, with the time-course of the  $sI_{AHP}$  peak amplitude shown in panel (a), while the time-course of the input resistance is shown in panel (b), again with arrows denoting the timing of the flashes. As with the soma group, the train of flashes led to a reduction in the  $sI_{AHP}$  amplitude in 7/7 cells (Figure 7.15 c, e), without noticeably altering the size of the unclamped  $Ca^{2+}$  current observed during the stimulus pulse (Figure 7.15d).

The effect of the flashes on the  $sI_{AHP}$  current was generally larger than that observed in the somatic experiments, with the mean current amplitude following the flash train being  $31.7 \pm 5.6\%$  of the baseline current, a statistically significant change (Wilcoxon matched pairs signed rank test = 0.015, n=7, Figure 7.15e). The flash train also had a stronger effect on current kinetics, as the mean decay time constant reduced from  $5.87 \pm 0.89$  s to  $2.68 \pm 0.55$  s, (Wilcoxon matched pairs signed rank test p=0.015, n=7, Figure 7.15f).

The input resistance after flashing increased from  $161 \pm 15 \text{ M}\Omega$  to  $183 \pm 17 \text{ M}\Omega$  (in percentage terms an increase to  $114 \pm 2.6\%$  of baseline), also statistically significant (paired 2-tailed t-test,  $p=0.001$ , Figure 7.15g). The flash train also produced an inward shift of the holding current of  $14.0 \pm 2.9 \text{ pA}$ , and this change was statistically significant (one sample t-test  $p=0.003$ ,  $n=7$ , Figure 15h).

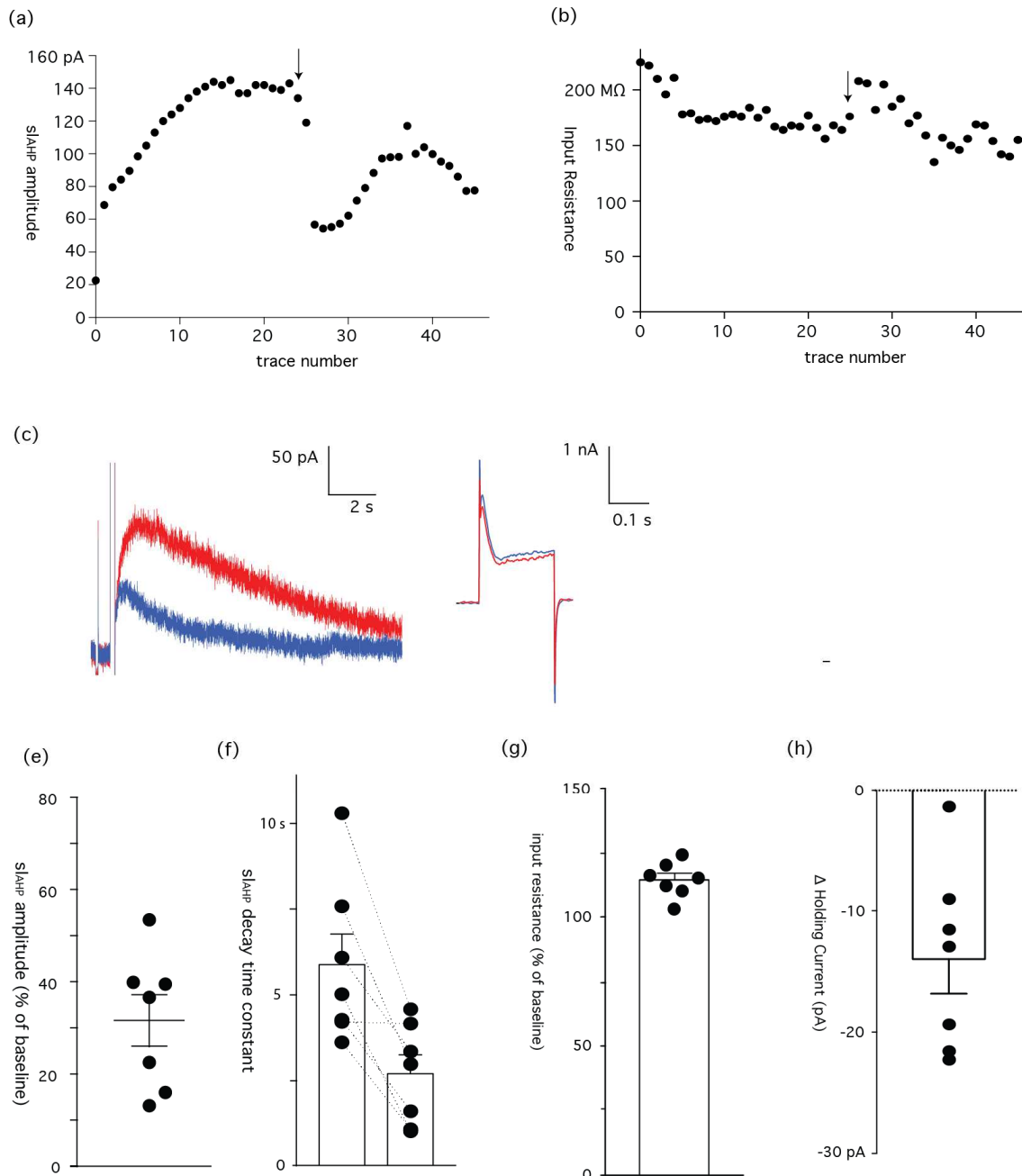


**Figure 7.15. Effect on sIAHP of uncaging BCMCM-8Br-cAMP in proximal dendrites**

(a) *Timecourse of sIAHP amplitude for a representative cell in response to a 200 ms voltage step to +20 mV from a holding potential of -50 mV. Vertical arrows show the positions of each flash train protocol. Traces were acquired at 30 s intervals.*

- (b) *Timecourse of input resistance for the same cell. Vertical arrows show the positions of each train of flashes.*
- (c) *Example traces showing amplitude of  $sI_{AHP}$  before (red) and after (blue) a flash protocol. Top traces correspond to first flash, bottom traces correspond to second flash. In each case, “before” traces are the trace immediately after the flash train, and “after” traces are the third trace after the flash train.*
- (d) *Detail of the voltage step for the traces in (c), showing the calcium action current.*
- (e) *Summary of the effect of the flash protocol on the peak  $sI_{AHP}$  amplitude. Filled circles show the responses of individual cells. Error bars denote mean and SEM of the responses. Y axis represents percentage of baseline peak amplitude.  $n=7$*
- (f) *Graph summarising the effect of the flash protocol on the decay time constant ( $\tau$ ) of the  $sI_{AHP}$ . Filled circles connected by dashed lines represent the change in  $\tau$  of individual cells. Y axis represents the decay time constant in seconds. Bars represent the mean decay time constant across all cells, before and after the flash protocol. Error bars show SEM.  $n=7$*
- (g) *Summary of the effect of the flash protocol on the input resistance. Y axis shows input resistance following the flash as a percentage of the baseline input resistance. Filled circles denote individual cell responses. Bar height shows mean response of all cells. Error bars denote SEM.  $n=7$*
- (h) *Summary of the change in holding current in response to the flash protocol. Y axis represents change in holding current in pA. Individual responses are represented as black filled circles. Bar height denotes the mean change in  $I_{hold}$  across all cells. Error bars represent SEM.  $n=7$*

A comparison of the effects of the flashes at the two different locations is shown in Figure 7.16. The flash protocol had a more pronounced effect on both the amplitude and decay kinetics of the  $sI_{AHP}$  current when delivered at the dendritic location than when delivered to the soma. The percentage residual current following a flash train delivered to the soma was almost twice that following the same flash protocol delivered to the proximal dendrite, and this difference was significant (2-tailed T-test  $p=0.01$ ,  $n=7$ , Figure 7.16a). The effect on the decay time constant of the current was less conclusive. Following a flash protocol delivered to the soma, the decay time constant was  $67.9 \pm 6.0$  % of the baseline duration, versus  $46.5 \pm 9.6$  % following the same protocol delivered to the proximal apical dendrite (Figure 7.16b). However, this effect was not statistically significant (2-tailed T-test  $p=0.08$ ,  $n=7$ ). In the dendritic condition, one cell in particular was an outlier, registering almost no change in decay time constant, while the next smallest effect was a reduction to 55% of baseline, yet this cell responded like the rest in terms of change in current amplitude, so it is difficult to make a case for its exclusion.

In terms of intrinsic membrane properties, the input resistance increased in response to the flash protocol in both locations, though not in the control condition where BCMCM-8Br-cAMP was omitted from the solution. Mean input resistance was  $110 \pm 5.3$  % of baseline for the somatic flash experiments, and  $114.2\% \pm 6.8$  for the dendritic experiments (Figure 7.16c). There was no significant difference between the effect size at the two locations (2-tailed T-test  $p=0.52$ ).

As previously reported, the flash protocol caused an inward shift in the holding current at both locations. However there was no significant difference between the effect size at the two locations (Mann-Whitney test  $p=0.71$ , Figure 7.16d).

These data suggest that a flash train delivered to the proximal apical dendrite has a greater inhibitory effect on the  $sI_{AHP}$  amplitude than one delivered to the soma. The effect is observable despite the fact that the flash covering the dendritic region is effectively at half power in terms of photon density compared to that covering the soma. This result suggests that the signalling machinery responsible for the cAMP-dependent inhibition of  $sI_{AHP}$  may be enriched in the proximal apical dendrite compared to the soma itself.

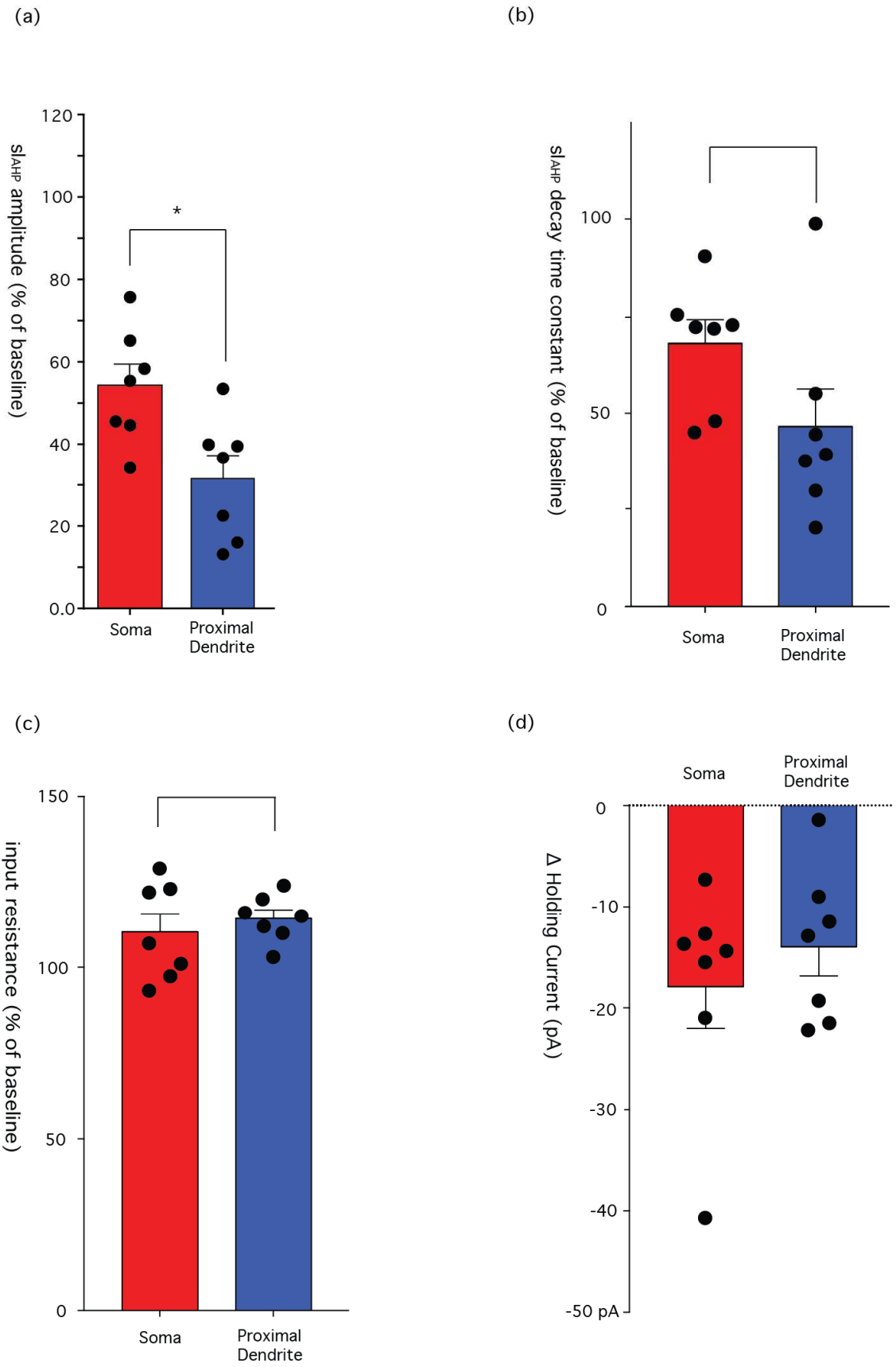


**Figure 7.16. Summary of effects of uncaging BCMCM-8Br-cAMP in different subcellular locations**

- (a) ***Comparison of the change in  $sI_{AHP}$  peak amplitude in response to the flash train protocol at the soma ( $n=7$ ) and at the proximal dendrite ( $n=7$ ). Filled circles denote the responses of individual cells. Y axis shows the percentage of the baseline current present following the flash protocol. Bar heights show the mean of all responses at each location, error bars denote SEM.***
- (b) ***Comparison of the change in the decay  $\tau$  of  $sI_{AHP}$  in response to the flash train protocol at both locations. The response of each individual cell is denoted by a filled circle. Bar height represents mean post-flash decay  $\tau$  expressed as a percentage of the baseline  $\tau$ . Error bars denote SEM. Y axis is percentage of baseline decay time constant.***
- (c) ***Effect of the flash protocol on the input resistance of the cell at the two subcellular locations. Responses of individual cells are indicated by the filled circles. Y axis is  $R_{input}$  following flash train protocol, as percentage of baseline value. Bar height represents mean, error bars denote SEM.***
- (d) ***Summary of changes in  $I_{hold}$  in response to the flash protocol. Filled circles represent the responses of individual cells, bar heights show mean change in  $I_{hold}$  for each region. Error bars denote SEM.***

## Chapter 8. Discussion

The project was divided into three sections. In the first section, experiments were undertaken in order to determine the optimal recording parameters for  $sl_{AHP}$ . For subsequent experiments it was desirable for the  $sl_{AHP}$  to be as large as possible, and to remain at a stable amplitude for a period of approximately one hour. This would allow the greatest possible signal to noise ratio for measurement of any inhibitory responses that might be observed. Optimal parameters of the voltage step protocol were determined, along with the concentration of tetraethylammonium (TEA) that produced the largest facilitatory effect on the  $sl_{AHP}$  amplitude. Additionally, the effects of three drugs (EBIO, ethanol, and Bay-K8644), which had been reported to produce a facilitation of  $sl_{AHP}$ , were tested, though none produced a stable and reliable increase in  $sl_{AHP}$  amplitude under our conditions.

The second section of the project used the focal application of the  $\beta$ -adrenergic agonist isoproterenol to demonstrate that there is spatial variation in the adrenergic inhibition of  $sl_{AHP}$  at a subcellular level. Microinjector application of isoproterenol inhibited a greater proportion of  $sl_{AHP}$  when focused on a region centred on the soma than when focused on the distal portion of the dendritic tree.

The third and final section of the project aimed to determine whether the spatially localised differences in inhibition seen in the isoproterenol experiments might be due to the activation of different spatially localised cAMP signalling domains. The initial experiments in this section involved the setup and testing of a UV flash photolysis (“uncaging”) system, using the photolabile calcium buffer DM-Nitrophen (Kaplan and Ellis-Davies 1988) to demonstrate that uncaging could be achieved using our apparatus both in HEK293 cells and subsequently in hippocampal neuronal cultures. The system was then used to uncage the caged cAMP analogue BCMCM 8Br-cAMP (Hagen et al, 2001) in hippocampal neuronal cultures, and it was demonstrated that a train of UV flashes directed at the proximal dendritic region was more effective at inhibiting  $sl_{AHP}$  than the same protocol delivered to the soma, suggesting the existence of discrete cAMP signalling domains coupled to the channels that underlie  $sl_{AHP}$ .

### 8.1 Optimisation of $sl_{AHP}$ recordings

The aim of the first set of experiments was to find a set of recording conditions for the  $sl_{AHP}$  that maximised both the amplitude and stability of the current over a long period of

time, in order to maximise the sensitivity of the current to modulation by either focally applied isoproterenol or localised uncaging of cAMP analogues.

To this end, a number of parameters were considered. In the first set of experiments, the duration and amplitude the voltage step used to evoke  $s_{\text{AHP}}$  was varied, in an attempt to find the values at which the current response saturated.

Next, a range of concentrations of the  $\text{K}^+$  channel blocker TEA were tested, in order to find the concentration range that produced a facilitation of the  $s_{\text{AHP}}$  amplitude, as well as the range over which the current was inhibited.

Finally we tested the effect on the  $s_{\text{AHP}}$  amplitude of three drugs, which had been previously been reported as having a facilitatory effect on the current.

### **8.1.1 Optimal Stimulus parameters**

The  $s_{\text{AHP}}$  peak amplitude increased from zero to a maximal value as the stimulus voltage was increased between -10 and +10 mV (Figure 7.2). In each cell, a sharp transition was observed, such that the current amplitude jumped from less than 25% of maximal to a near-maximal value, over a single 2 mV increment. The voltage at which this sharp transition occurred varied from cell to cell, but was always in the range of +2 mV to +4 mV, and in each case was accompanied by the appearance of a partially clamped, inward  $\text{Ca}^{2+}$  current on the same trace as the sudden transition in  $s_{\text{AHP}}$  current amplitude (Figure 2a, b).

The result can be explained in two possible ways. The sudden increase in current amplitude could be caused by threshold behaviour of the voltage gated  $\text{Ca}^{2+}$  channel (VGCC) population underlying the calcium transient, perhaps due to the activation of a dendritic calcium spike. Alternatively, the transition could be caused by a non-linear relationship between the command voltage of the stimulus and the number of VGCCs recruited, as could occur if the VGCCs are located in the dendrites and there is only limited space clamp of the dendritic arbor. Simultaneous current clamp of the soma and dendritic compartments of CA1 neurons were used by Golding and colleagues (Golding et al 1999) to determine the factors responsible for calcium spike initiation and repolarisation. Injections of current above a given threshold elicited a calcium spike, and the threshold level was lower for injections to the dendrite than to the soma, though the difference between compartments was abolished when voltage gated sodium channels were inhibited with TTX. This result suggests that, in the presence of TTX, stimulation of the neuron at the soma is as effective at activating  $\text{Ca}^{2+}$  spikes as stimulation at the

dendrite, which would tend to favour the calcium spike explanation of the sudden appearance of the calcium action current and increase in  $sI_{AHP}$  amplitude. However, from our data it is not possible to rule out the potential influence of space clamp limitations.

The relationship between  $sI_{AHP}$  peak amplitude and stimulus duration did not exhibit the same discontinuity as that seen in the case of stimulus voltage. Across the range of durations tested, there was a gradual increase from zero to saturation, with response saturation occurring between 80 and 90 ms (Figure 7.2c). This gradual increase was also reflected in the shape of the calcium action current. It is clear in qualitative terms that the time-to-peak and peak amplitude of the calcium action current are similar for all stimulus durations, but that the duration of the current increases along with the stimulus duration, possibly because at shorter durations, the depolarising stimulus terminates more rapidly than the channels underlying the calcium action current terminated under conditions of sustained stimulation.

For both stimulus voltage and duration, it was possible to find values at which  $sI_{AHP}$  amplitude reached saturation, and it was therefore concluded that a 100 ms step from a holding potential of -50 mV to +10 mV represents the optimal stimulus parameters for use in future experiments. In terms of the survival of the clamped cell and the stability of the recordings, it makes sense to use the minimum sufficient stimulus, as such sustained large depolarisations are probably not experienced during normal physiological function.

The results observed here are broadly consistent with the close relationship between  $Ca^{2+}$  influx and  $sI_{AHP}$  amplitude described by previous studies (eg. Lancaster and Adams 1986, Constanti and Sim 1987).

### **8.1.2 Effect of TEA on $sI_{AHP}$ amplitude**

Low concentrations of TEA have previously been reported to have a potentiating effect on the  $sI_{AHP}$  (Schwartzkroin and Prince 1980, Lancaster and Adams 1986). We therefore examined the effect of varying concentrations of TEA on  $sI_{AHP}$  amplitude. In addition to determining an optimal concentration to add to the extracellular solution, a second motivation for this experiment was that some recent attempts to determine the molecular correlates of  $sI_{AHP}$  have suggested  $K_v7$  (KCNQ) channels as potential candidates (Tzingounis et al 2008, 2010, Soh et al 2010). Depending on their subunit composition, KCNQ channels display varying sensitivity to TEA, ranging from 0.3 mM to over 50 mM. It was therefore instructive to determine the concentration range of TEA over which an inhibitory effect on the  $sI_{AHP}$  was observed.

Our experiments show that at concentrations below 5 mM, TEA has a net facilitatory effect on  $sI_{AHP}$ , whereas at 10 mM and over the effect is inhibitory (Figure 3b, d). Of the concentrations tested, facilitation was highest for 1 mM, and it is likely that between 1 mM and 5 mM there is a point of inflection whereby the inhibitory effects begin to override the facilitation seen at lower concentrations. The number of concentrations used in these experiments was insufficient to determine the  $EC_{50}$  or  $IC_{50}$ , and even with a larger number of concentration steps, the attempt might have been hindered by an overlap of the facilitation and inhibition curves.

It is apparent from our data that the mechanism mediating the inhibitory effect of TEA on  $sI_{AHP}$  is independent of that underlying the facilitatory effect. All concentrations of TEA tested produced a qualitative increase in the amplitude of the calcium action current during the stimulus step, compared to that observed in the absence of TEA. The size of the transient at different TEA concentrations appeared to be similar, and the effect appeared to reverse following washout (Figure 7.3c). This is consistent with the findings of Golding and colleagues (1999), who observed that TEA increases the  $Ca^{2+}$  current observed during membrane depolarisation, probably by blocking various voltage-gated  $K^+$  channels, such as BK and some  $K_V$  channels, which would otherwise contribute to a more rapid repolarisation of the membrane.

The inhibitory effect appears to be independent of the amount of  $Ca^{2+}$  influx, as the transient remains at concentrations that block  $sI_{AHP}$ , suggesting that inhibition occurs by another mechanism, probably by direct block of the  $sI_{AHP}$  channels, as TEA is known to block a wide range of  $K^+$  channel subtypes.

The possibility that the suppression of  $sI_{AHP}$  by TEA may occur due to direct inhibition of the underlying channels has implications for recent work which proposes one or more members of the  $K_V7$  channel family as the molecular correlate of the slow afterhyperpolarisation. Genetic loss of function studies (Tzingounis and Nicoll 2008, Tzingounis et al 2010, Soh et al 2010) have implicated the  $K_V7.2$  (KCNQ2) and  $K_V7.3$  (KCNQ3) subtypes in mediating  $sI_{AHP}$  in dentate gyrus granule cells, and  $K_V7.5$  (KCNQ5) in CA3 pyramidal cells. The remaining family members, encoded by KCNQ1 and 4 are not expressed in the hippocampus (Jentsch et al 2000). Mice transfected with KCNQ5 dominant negative constructs displayed significantly reduced  $sI_{AHP}$  amplitude compared to controls in CA3 pyramidal cells, though not in CA1, while mice co-transfected with dominant negative KCNQ2/KCNQ3 constructs displayed reduced  $sI_{AHP}$  amplitude in dentate gyrus granule cells, though not in hippocampal pyramidal cells.

Assuming that the inhibitory effects of TEA observed in our data occur via direct inhibition of the underlying channels, this argues against the involvement of  $K_V7.3$  or  $K_V7.5$  homomultimers in the CA1  $sI_{AHP}$ , as these have been reported to be inhibited by TEA with  $IC_{50}$  of  $>30$  mM and  $>70$  mM respectively (Hadley et al, 2003, Schroder et al, 2000). Equally, it is unlikely that  $K_V7.2$  is a significant contributor to the current in CA1, as it is inhibited by TEA with an  $IC_{50}$  of 0.3 mM, whereas in our data both 1 mM and 5 mM concentrations of TEA led to an increase in  $sI_{AHP}$  amplitude. The KCNQ3 protein product can also form heteromultimers with KCNQ2. Various estimates of the  $IC_{50}$  of this heteromultimeric channel have been reported in heterologous expression experiments, with the results being somewhat different depending on whether simple co-transfection or transfection of a tandem concatemer was used. Values of  $IC_{50}$  for the co-expressed KCNQ2/3 are reported as 3.5 mM (oocyte, Wang et al 1998), 3.8 mM (CHO, Hadley et al, 2000) and 4.1 mM (HEK-293, Hadley et al, 2003), whereas the  $IC_{50}$  for channels formed of tandem constructs are reported as 6.7 mM (HEK293, Hadley et al, 2003) and 10.2 mM (CHO, Wickenden et al 2000). As a result of this variation, it is not entirely possible to rule out the involvement of such a heteromultimer from our TEA data. However, the fact that double knockouts of KCNQ2 and KCNQ3 did not affect  $sI_{AHP}$  in hippocampal pyramidal cells (R Taylor and P. Pedarzani, unpublished data), coupled with the lack of effect of the  $K_V7$  channel inhibitor XE991 on  $sI_{AHP}$  currents observed by other members of our lab (A. Boehlen, unpublished data), suggests that the  $K_V7$  family members are unlikely to be involved in  $sI_{AHP}$  generation in CA1 pyramidal neurons.

As a result of this experiment, we can conclude that, at low concentrations, TEA has a facilitatory effect on the  $sI_{AHP}$ , probably due to facilitation of  $Ca^{2+}$  influx during the stimulus pulse, while at higher concentrations it has an inhibitory effect, possibly due to blockade of the channels responsible for the  $sI_{AHP}$  current itself. We can therefore use low TEA concentrations (i.e. 1 mM) to enhance the amplitude of the  $sI_{AHP}$  in our recordings.

### **8.1.3 Effect of three pharmacological agents on $sI_{AHP}$**

The effect of three drugs, EBIO, ethanol and Bay-K8644, on the  $sI_{AHP}$  were investigated, based on previous studies that reported an activation effect on the current (Pedarzani et al 2001, Carlen et al 1982, Reynolds et al 1990, Tombaugh et al 1995). In our hands none appeared to increase  $sI_{AHP}$  in a stable and consistent manner.

#### **EBIO**

EBIO has previously been reported to increase the amplitude of  $sI_{AHP}$  in hippocampal neurons (Pedarzani et al, 2001). They reported a ~150% increase in  $sI_{AHP}$  amplitude following bath application of 1 mM EBIO, with the facilitation reaching a maximal value after 2-3 mins. Our data showed a significant but smaller initial increase in  $sI_{AHP}$  amplitude, following a similar timecourse (Figure 4), however an additional gradual run-down of the current amplitude was observed, beginning 5-10 minutes after drug application, and eventually stabilising at a value close to the original baseline. Pedarzani and colleagues do not report this biphasic effect on  $sI_{AHP}$ , though they did observe a gradual run-down of the  $Ca^{2+}$  transient during the voltage step, and this is reported to occur with a similar time course to the run-down of  $sI_{AHP}$  in our data. However in our recordings, the amplitude of the  $Ca^{2+}$  current does not alter noticeably. Regardless, in our hands, EBIO did not appear to increase  $sI_{AHP}$  in a stable manner, and so was not used in subsequent experiments.

## **Ethanol**

Ethanol has been reported to increase both the amplitude and duration of the post-spike afterhyperpolarisation in current clamp recordings (Carlen et al 1982, Reynolds et al 1990). Neither study was conducted in the presence of a compound such as apamin, which could separate the medium and slow phases of the AHP. A similar experiment (Siggins et al 1987) failed to find any increase in AHP amplitude.

Our experiments examined the effects of two concentrations (10 mM and 20 mM) of ethanol on the amplitude of the  $sI_{AHP}$  recorded in voltage clamp mode, with the  $I_{AHP}$  inhibited with dTC. For both concentrations tested, an increase in  $sI_{AHP}$  amplitude was observed in some cells but not in others. At both concentrations,  $sI_{AHP}$  amplitude following application of ethanol is not significantly different from baseline across all experiments, although some cells responded with marked stable increases to as much as 140% of baseline amplitude.

It is possible that in the non-responding cells, a concomitant run-down of the  $sI_{AHP}$ , occurred for reasons unrelated to the drug application, as these experiments were performed early in the first year of my PhD, and  $sI_{AHP}$  is sensitive to the overall health of the patched cell. There were no grounds on which to exclude these cells with regard to changes in input resistance, holding current or resting membrane potential however. An alternative hypothesis is that there is some underlying heterogeneity in the response of CA1 pyramidal neurons to ethanol. There is evidence that distinct subtypes of pyramidal

cell exist in CA1, with regard to intrinsic firing properties (Jensen et al 1996) as well as in their response to neuromodulators (Graves et al 2012).

In agreement with Carlen and colleagues (Carlen et al 1982) we observed an increase in  $sI_{AHP}$  duration, as evidenced by the decay time constant, in every cell tested at both concentrations. In summary, while ethanol does appear to produce an increase in  $sI_{AHP}$  amplitude in some cells, we have not been able to demonstrate that it does so reliably, however it does appear to increase  $sI_{AHP}$  duration in a consistent manner.

### **BAY-K8644**

Bay-K8644 is a dihydropyridine agonist of L-type voltage gated calcium channels (Thomas et al 1985). It has been reported that Bay-K8644 increased the amplitude of the sAHP measured during current clamp experiments in hippocampal pyramidal cells (Tombaugh et al 2005), though the effect was not quantitatively assessed. A change was also reported in the shape of the  $Ca^{2+}$  spike, consistent with the characterised role of Bay-K8644 as an L-type channel agonist.

In our hands, Bay-K8644 appeared to produce a small, gradual increase in  $sI_{AHP}$  amplitude in 5 out of 6 cells tested, but in 3 of 6 cells the magnitude of the increase was under 20% and the effect was overall not statistically significant. There was, however, a significant increase in the duration of the current, as measured by the decay time constant. In our experiments, there was no obvious, qualitative change in the  $Ca^{2+}$  current observed during the voltage step. It is possible that the lack of a dramatic effect on  $sI_{AHP}$  amplitude is due to this lack of change in the  $Ca^{2+}$  current: it may be that our stimulus parameters already are maximally effective at activating the pool of calcium channels that supply the  $Ca^{2+}$  signal that activates  $sI_{AHP}$ . Consistent with this hypothesis, Thomas and colleagues (Thomas et al 1985) report that Bay-K8644 has a stronger facilitative effect at potentials where the open probability of the calcium channels is low.

In conclusion, none of the three drugs tested produced an increase in  $sI_{AHP}$  amplitude that was both reliably reproduced from cell to cell, and stable over a sufficiently long period of time. Of the three, only EBIO produced a statistically significant increase in  $sI_{AHP}$  peak amplitude, but the duration of this effect was too brief for use in long recordings. Ethanol reliably increased  $sI_{AHP}$  duration, but the effect on  $sI_{AHP}$  amplitude was not consistent from cell to cell, and Bay-K8644 did not produce a statistically significant change in  $sI_{AHP}$  amplitude, though it did increase the decay time constant. It

was therefore decided not to add any of the compounds tested to the ACSF during subsequent  $sI_{AHP}$  experiments.

## **8.2 Focal application of isoproterenol reveals intercompartmental differences in $\beta$ -adrenergic suppression of $sI_{AHP}$**

Previous work in our lab has suggested the possibility of spatially localised domains involved in the monoaminergic suppression of  $sI_{AHP}$ . As described in the introduction (6.5), inhibition of PP1/PP2A leads to a run down of  $sI_{AHP}$ , and the run-down is abolished by PKA inhibitors (Pedarzani and Storm, 1993; Pedarzani et al., 1998). Inclusion of the AKAP-inhibitor Ht-31 in the patch pipette caused an increase in the amplitude and duration of the run-up of  $sI_{AHP}$  (Pedarzani, unpublished data). Taken together, these results suggest there is a basal tone of PKA activity, and its associated phosphatases PP1/PP2A, the balance of which is disrupted by the inhibition of AKAPs, anchoring proteins that bind PKA and PP1/PP2A. This suggests that spatial anchoring might be necessary for maintaining the kinase-phosphatase balance, which is in turn suggestive of spatial localisation of the elements of the signalling domains underlying  $sI_{AHP}$  inhibition.

In our experiment, we used focal application of the  $\beta$ -adrenergic agonist isoproterenol, via a microinjector, to test for spatial inhomogeneity in the inhibition of the  $sI_{AHP}$ . Our results show that application of isoproterenol to the soma/proximal dendrite region of rat CA1 pyramidal neurons almost completely abolishes  $sI_{AHP}$ , whereas the same drug concentration applied to the distal dendrite region inhibits only ~50% of the current.

Interpretation of this result hinges to a certain extent on assumptions about the area covered by the microinjector puff. In order to visualise this, Lucifer yellow was included in the puff pipette solution, allowing the spread to be visualised, while the same concentration of Lucifer Yellow was added to the intracellular solution to permit visualisation of the dendritic arbor. The microinjector produced a teardrop-shaped puff, spreading out from the tip of the injection pipette, before diffusing away in the direction of the laminar flow. The slice was positioned in such a way that a puff applied to the dendrite would not diffuse over the soma, and vice versa (Methods Figure 2.4).

The initial spread of the puff was estimated to be ~40  $\mu\text{m}$ . At the somatic location, this was enough to cover both the soma itself and part of the initial segment of the apical dendrite. The same approximate area was covered at the distal dendrite location, which was around 100  $\mu\text{m}$  past the first observable branch point. Due to the larger size of the soma compared to the narrow dendrite, it is likely that a larger absolute surface area of

the cell was covered by the somatic puff than by the one at the distal dendrite. It is also clear that a larger proportion of the somatic membrane was covered by the puff than the proportion of distal dendritic membrane covered by the puff at that location. It could therefore be argued that a larger total surface area of the neuron's plasma membrane was covered by the somatic puff than by the distal dendrite puff, and hence a larger total number of receptors were activated in the soma than in the dendrite, leading to an overstatement of the difference observed between the two regions. However, set against this, the fact that the lumen of the dendritic compartment is far narrower than that of the soma means that for a given number of receptors activated, the subsequent rise in cAMP concentration in response to receptor activation might be expected to be higher. Spatial modelling studies predict that the different geometry of the compartments might alter the shape and dynamics of the cAMP microdomain (Neves et al 2008). Consistent with this, Castro and colleagues measured the activation of PKA by isoproterenol in dendrites compared to the soma, using the fluorescent sensor AKAR2 (Castro et al, 2010). PKA activation in the soma in response to 100 nM isoproterenol was ~60% of that achieved by a saturating concentration of forskolin, an adenylyl cyclase activator. However in the dendrite, the response to the same concentration of isoproterenol was ~95% of that achieved by forskolin. Thus the same concentration of isoproterenol raises PKA activity by a greater amount in the dendrite than in the soma. These differences were abolished by the PDE4 inhibitor rolipram, suggesting that the action of phosphodiesterases is responsible for reducing the spatial spread of the cAMP signal.

Although this suggests that the increase in cytosolic cAMP will be higher in dendrites than in the soma, the increase in cAMP concentration in the vicinity of the membrane may be similar for both compartments. Assuming the channels underlying sAHP are indeed associated with PKA and phosphatases in spatially localised domains at the membrane (Introduction 6.5) then there may not be a difference in the size of the cAMP signal encountered by the relevant PKA population.

Could our results be explained by a different receptor density at the two locations? The subcellular expression pattern of  $\beta$ -adrenergic receptors in hippocampal pyramidal neurons is currently an open question. Davare and colleagues (Davare et al 2001) performed antibody staining of  $\beta_2$ -AR in rat hippocampal sections and reported the presence of  $\beta_2$ -AR in both apical dendritic spines and the somata of pyramidal neurons. A similar study involving both light and electron microscopy to assess  $\beta$ -AR immunoreactivity in dentate gyrus granule cells showed enrichment in the dendrites, though some receptors were also present in the soma (Milner et al, 2000). Given the limited information on  $\beta$ -adrenergic receptor localisation on a subcellular level, it is

impossible to rule out the possibility that the different effect sizes at the two locations simply reflect differences in receptor density, rather than differences in the degree of coupling to the  $sI_{AHP}$  signalling machinery.

One line of evidence against a variation in receptor density, and consequently differences in the number of receptors covered by the puff, is that the puff had a similar effect in both locations on both the input resistance and holding current. Puffs at both locations produced a reduction in both  $R_{input}$  and  $I_{hold}$ , but the effect size was not significantly different between regions (Figure 7.11 b,c) and there was no change in either  $R_{input}$  or holding current following the puff in the control experiments. The reduction in  $I_{hold}$  probably represents the activation of an inward current in response to  $\beta$ -AR activation. This phenomenon has previously been observed in neurons following bath application of noradrenaline as well as serotonin, and is mediated by the cAMP signal (Pedarzani and Storm 1995, Gasparini and DiFrancesco 1999, Chapin et al 2002). The amplitude of the change in holding current observed following the puff is approximately 50% of that reported for the bath application of isoproterenol (Pedarzani and Storm 1995), and also around 50% of that observed in later experiments following the uncaging of 8Br-cAMP in cultured hippocampal neurons (Figure 7.16d). If the number of  $\beta$ -ARs activated was substantially different between the two locations, one might expect a difference in the extent of activation of the inward current mediating the change in  $I_{hold}$ , yet in our experiments the change in  $I_{hold}$  was not significantly different at the soma compared to the distal dendrites. This could be taken as an argument in favour of a relatively uniform distribution of  $\beta$ -ARs, especially given that the measured result is smaller than that reported elsewhere, which would suggest that the homogeneous response of  $I_{hold}$  was not due to maximal activation of the channels responsible for the inward current. This hypothesis would benefit from further experiments in which isoproterenol was bath applied shortly after the puff, to determine whether the puff was sufficient to saturate this response.

However this interpretation suffers from two potential confounds. There could be a gradient of the density of the underlying channels, which might mask that of the  $\beta$ -ARs, and coupling between the  $\beta$ -AR and the channels could vary, either by organisation into subcellular signalling domains, or simply because of the geometry of the compartment, the dendrites having a much higher surface area to volume ratio than the soma. Possible candidates for the channels underlying the change in holding current are discussed in the section on cAMP uncaging (8.3.3).

### **8.3 Evidence of multiple cAMP signalling domains contributing to suppression of $sI_{AHP}$**

The focal application experiments described in the previous section provide evidence of some spatial inhomogeneity in the inhibitory response of  $sI_{AHP}$  to the activation of  $\beta$ -adrenergic receptors. The different effect sizes observed following somatic and dendritic application could potentially be explained either by differences in the density of receptors at the different locations, or by differences in the coupling of those receptors to the population of PKA responsible for the inhibition of  $sI_{AHP}$ . The most obvious way for such coupling to be mediated is by the cAMP signal generated by the activation of adenylyl cyclase by the  $G\alpha_s$  moiety of the G-protein coupled to the  $\beta$ -AR. For this reason we decided to probe the existence of discrete cAMP signalling domains directly, using the localised uncaging of cAMP.

#### **8.3.1 Flash photolysis of DM-Nitrophen in HEK293 cells containing rBK $\alpha^0$ produces an increase in the BK current**

Initial experiments were performed to test the efficacy of the uncaging setup, using the photolabile  $Ca^{2+}$  buffer DM-nitrophen (Kaplan and Ellis-Davies 1988). DM-Nitrophen is one of the most well-established caged compounds, and the calcium signal was readily detectable in a HEK293 cell line stably expressing the rBK $\alpha^0$  channel subunit used in part 1 of the thesis, as the BK whole cell current is large, and the voltage dependence is strongly modulated by intracellular  $Ca^{2+}$ .

Recordings from the stable cell line using an intracellular solution containing 3 mM DM-Nitrophen 50% loaded with  $Ca^{2+}$ , showed a voltage dependent whole-cell current in the nanoampere range that was inhibited by the BK-specific inhibitor paxilline (Figure 11a,b).

When the cell was then held at +30 mV and a single flash was delivered, an increase in whole cell current was observed (figure 11c,d), and the current amplitude varied with the pulse duration (Figure 11e). While it was not possible to quantify the increase in free  $Ca^{2+}$  produced by each flash, repetition of the flash protocol produced a gradual reduction of the amplitude of the current response with each subsequent flash (Figure 11f). The size of the current response decreased with successive flashes before eventually reaching a stable level, presumably because at this level the rate of diffusional exchange of unphotolysed compound through the pipette balanced the rate at which the remaining unphotolysed DM-nitrophen underwent photolysis.

Taken together these data confirm that the flash protocol was competent to effect photolysis of DM-Nitrophen and produce a  $\text{Ca}^{2+}$  signal that led to an increase in the BK current. However, it does not appear that a large fraction of the total DM-nitrophen in the region covered by the flash was photolysed by any given flash.

### **8.3.2 Flash photolysis of DM-nitrophen in cultured rat hippocampal neurons elicits a current with similar pharmacology to $I_{\text{AHP}}$**

Having established that the flash lamp was able to effect photolysis in HEK293 cells, the next set of experiments sought to ensure that a similar effect could be achieved in cultured neurons. Due to the crucial roles played by free  $\text{Ca}^{2+}$  signals and active  $\text{Ca}^{2+}$  currents in neuronal function, neurons have a higher buffering capacity for free  $\text{Ca}^{2+}$  than do HEK293 cells, and hippocampal cultures contain debris and glial cells that might affect the efficiency of the flash photolysis.

DM-Nitrophen was uncaged in cultured rat hippocampal neurons via a series of 4 flashes. This flash protocol elicited a series of short duration outward current responses that grew larger with each flash in the train, with the last and largest response in each recording being of around 30-40 pA amplitude (Figure 12a).

Given that a number of  $\text{Ca}^{2+}$  activated conductances exist in hippocampal neurons, there are several potential candidates for the observed current: specifically, the BK channels that contribute to action potential repolarisation and the fast afterhyperpolarisation, the SK channels thought to underlie  $I_{\text{AHP}}$  (Stocker et al 1999), and the unknown  $\text{Ca}^{2+}$  activated conductance mediating  $sI_{\text{AHP}}$  (Alger and Nicoll 1980, Hotson and Prince 1980, Schwartzkroin and Stafstrom 1980, Lancaster and Adams, 1986).

The current responses elicited by  $\text{Ca}^{2+}$  uncaging were inhibited by d-tubocurarine but not by low concentrations of TEA (Figure 12d,e). d-Tubocurarine inhibits both the SK-mediated medium afterhyperpolarisation ( $I_{\text{AHP}}$ ) (Strøbaek et al 2000) and also BK channels (Smart, 1987). However, BK channels are inhibited by TEA at low concentrations (Vergara et al 1984), so it is unlikely that the observed current is due to their activation. The current responsible for  $sI_{\text{AHP}}$  can likewise be ruled out given that it is insensitive to dTC.

In the same cells, depolarising voltage steps elicited a short outward current of around 400-500 pA. This current was partially inhibited by dTC but not by TEA (Figure 12b), similar to what we observed for the current elicited by  $\text{Ca}^{2+}$  uncaging. It is likely that part of this is the  $I_{\text{AHP}}$ , given its pharmacological profile and that the duration is too short to be

$sI_{AHP}$ . The medium afterhyperpolarisation in hippocampal pyramidal cells is mediated by both the  $Ca^{2+}$  dependent SK channels and the voltage-dependent  $I_M$  (Stocker et al 1999, Gu et al 2007, Chen et al 2014), and it is likely that the partial inhibition of the observed current is due to inhibition of the SK-mediated component.

A similar experiment has been previously performed in rat acute hippocampal slice (Sah and Clements, 1999). In the absence of apamin, flash photolysis of DM-nitrophen produced an outward current that activated rapidly and decayed over several seconds, and in the presence of apamin the activation time constant became an order of magnitude slower. They also observed the  $sI_{AHP}$  in the same cells following a voltage step protocol. Our results differ in that a  $sI_{AHP}$  -like current was not observed either following the voltage step or the uncaging protocol. This may be due to the fact that recordings were made too soon after the neuronal culture preparation, as in acute slices  $sI_{AHP}$  is not visible until around the end of the second postnatal week (L. Cingolani, M. Stocker and P. Pedarzani unpublished results, Costa et al 1991, Spigelman et al 1992). In support of this, during subsequent experiments on cAMP uncaging, large  $sI_{AHP}$  currents of 80-150 pA were observed in response to the same voltage step protocol, using rat hippocampal cultures recorded at DIV 14-28.

### **8.3.3 Spatially localised uncaging of BCMCM 8Br-cAMP reveals intercompartmental differences in $sI_{AHP}$ suppression**

Uncaging of BCMCM 8Br-cAMP in cultured rat hippocampal pyramidal neurons led to a reduction of  $sI_{AHP}$ , amplitude and a shortening of the decay time constant, as well as a small increase in the input resistance of the cell, and an inward shift in the holding current.

These results provide evidence that the  $sI_{AHP}$  exhibits a compartment-specific inhibitory response to cAMP. Uncaging of BCMCM 8Br-cAMP in the proximal dendrite location produced an inhibitory response approximately 1.75 times the size of that observed in the soma (Figure 16a). Evidence from the control experiments excluded the possibility that the flash protocol itself was responsible for any of the observed changes in  $sI_{AHP}$  or intrinsic membrane properties, such as the input resistance or holding current (Figure 13). These results provide a clear indication of the existence of localised signalling domains mediating the cAMP-dependent inhibition of  $sI_{AHP}$ , as discussed in detail below.

**The flash protocol on its own did not affect the cell's intrinsic properties or the amplitude and kinetics of  $sI_{AHP}$ .**

From the lack of effect observed in response to flashes delivered in the absence of the caged compound, it was clear that the flash protocol itself did not affect either the properties of  $sI_{AHP}$  or the intrinsic membrane properties of the neuron. In the traces immediately following application of the flash protocol in the absence of caged compounds, there was no change in either the input resistance or the holding current, suggesting that the flash itself neither led to the opening or closing of membrane channels, nor altered the resting membrane potential (Figure 13 g, h).

There was equally no significant change in the sAHP current amplitude or kinetics in response to the flash train in the absence of caged compounds. While the  $sI_{AHP}$  amplitude altered slightly more in percentage terms than the input resistance or holding current, the direction of change was apparently random, so the mean remained close to 100% and the overall change was not significant (Figure 13d). A rapid change in  $sI_{AHP}$  amplitude was not observed in any cell. Additionally there was no significant alteration in the decay time constant before and after application of the flash protocol.

It is therefore safe to conclude that the effects seen in the subsequent uncaging experiments were due to the effects of the uncaged 8Br-cAMP, and not caused by any non-specific effects of the UV flash on the cell.

#### **Uncaging of BCMCM 8Br-cAMP affects the amplitude and kinetics of $sI_{AHP}$**

$sI_{AHP}$  is known to be modulated by a range of monoamine neurotransmitters, via a pathway involving the activation of adenylyl cyclase by  $G\alpha_s$ , the subsequent production of cAMP and the activation of Protein Kinase A (PKA) (Pedarzani and Storm 1993).

Consistent with these findings, our data shows that uncaging of caged BCMCM 8Br-cAMP leads to a suppression of  $sI_{AHP}$  at both locations tested. This occurred rapidly, with maximal inhibition occurring within 30-60 s of the flash protocol being applied, in every cell tested ( $n=14$ ). This contrasts with the findings of Pedarzani and Storm (1993), which shows maximal effect of bath applied 8CPT-cAMP occurring over a time frame of 3-4 minutes. It is likely that the majority of the observed time difference between the experiments is due to the extra time required for bath-applied 8CPT-cAMP to diffuse through the plasma membrane into the cytosol, however our experiments suggest a new upper bound to the rate of cAMP-dependent inhibition of  $sI_{AHP}$ . It is unfortunate that the voltage protocol used to elicit  $sI_{AHP}$  cannot practicably be delivered with a finer temporal grain, partly because the current duration is so long, and also because an extended period of rest is required to enable clearance of cytoplasmic  $Ca^{2+}$  to prevent deterioration

of the cell. It is therefore not possible to set a lower bound to the inhibition rate below 30 s.

In both the somatic and proximal dendrite locations, a statistically significant shortening of the  $sI_{AHP}$  decay time constant was observed following the flash protocol. It is possible that this change in kinetics is a simple function of the degree of activation of the current. Several studies (Gustafsson and Wigstrom 1981, Madison and Nicoll 1984, Lancaster and Adams 1986) report that the amplitude and kinetics of the sAHP scale in direct proportion to the number of action potentials generated in a neuron.

Following the flash protocol, the  $Ca^{2+}$  action current triggered by the stimulus voltage step remained approximately the same size, so it is not likely that the effect of cAMP was due to any change in the influx of  $Ca^{2+}$  into the cell during the voltage step.

### **Uncaging of BCMCM-8Br-cAMP alters intrinsic membrane properties in a non region-specific manner**

An effect of the flash protocol was also seen in the intrinsic membrane properties of the neurons. Following application of the flash protocol at both locations, the input resistance increased, though in both cases the magnitude of this increase was small: a 10% increase when the flash was applied at the somatic location (Figure 14e) and one of 14% at the dendritic location (Figure 15e). At both locations the effect size was significantly larger than that observed in the control experiment, and there was no significant difference between the effect size at either location (Figure 16c). The input resistance of the cell is inversely proportional to the total membrane conductance, and changes reflect the opening and closing of membrane channel populations. The input resistance increases as channels close. As the inhibition of the sAHP current was stronger in the proximal dendritic location compared to the soma, a larger increase in  $R_{input}$  would be expected in response to the dendritic flash protocol compared with the somatic one. In our data, the change observed in the proximal dendrite is larger than that in the soma, but not significantly so. There are two possible explanations for this. Firstly, if the total pool of channels underlying  $sI_{AHP}$  is relatively small, then it may be that changes in  $R_{input}$  due to their inhibition are dwarfed by intrinsic fluctuations in channel activity unrelated to the uncaging protocol. This explanation does not appear to be supported by the relative stability of  $R_{input}$  in the control cells. Alternatively, the cAMP signal could be acting on other channel populations in a way that partially masks the contribution of the  $sI_{AHP}$  channel population to  $R_{input}$ . The K2P family leak channel TREK-1, for example, is expressed in CA1 pyramidal neurons (Talley et al, 2001), and is inhibited by cAMP via

PKA (Deng et al, 2007). If TREK-1 were enriched at the soma compared to the proximal dendrite, the contribution to  $R_{input}$  due to their inhibition by the cAMP signal could mask that caused by the difference in  $sI_{AHP}$  inhibition.

Other cAMP-modulated channels have been described in hippocampal pyramidal cells. Direct activation of the olfactory cyclic nucleotide gated channel CNGA2 has been suggested as a candidate underlying 5-HT induced membrane depolarisation (Chapin et al, 2002), as has the modulation of the HCN channels underlying  $I_h$  (Gasparini and DiFrancesco, 1999). Activation of  $I_h$  has also been suggested as the mediator of a similar membrane depolarisation in response to noradrenaline (Pedarzani and Storm, 1995).

It is possible that the cAMP signal in response to the flash leads to the activation of a larger fraction of one or both of these channel populations, thereby counteracting the increase in  $R_{input}$  due to the closure of sAHP or TREK-1 channels. In support of this, an inward shift was observed in the holding current following the flash protocol in both regions (Figure 16d), but not in the control experiments (Figure 13h). The magnitude of this shift is similar to that observed by Pedarzani and Storm (1995) following application of isoproterenol or 8-CPT-cAMP. Additionally, there is a well established density gradient of HCN1 and HCN2 channels that underlie  $I_h$  in CA1 pyramidal cells (Lorincz et al 2002, Magee 1998, Notomi and Shigemoto 2004). The density of HCN channels increases with increasing distance along the apical dendrite away from the soma. This would mean that a larger population of HCN channels are available for activation by the cAMP signal at the dendritic location, which might mean that a larger number are activated in response to the flash protocol at this location, counteracting the larger number of sAHP channels closed, and thereby reducing the magnitude of the change in  $R_{input}$ .

## **Uncaging of BCMCM-8Br-cAMP inhibits $sI_{AHP}$ amplitude more in the proximal dendrite than in the soma**

A significantly higher degree of inhibition was observed in response to the flash protocol delivered to the proximal dendrite location than to that delivered to the soma. Following the somatic flash protocol, the mean residual current was 54% of baseline, compared to 31% following the flash protocol delivered to the proximal dendrite (Figure 16a).

One feature of the experimental design that deserves some consideration in the light of this result is the decision to focus the flash on a wider area in the proximal dendrite condition, compared to the soma condition. The reason for this was that the soma presented a more compact target, such that the entire soma could readily be covered by a flash area of a given radius, with little “dead” space: areas where the photons did not hit the target neurons (Figure 2.5). However a flash of the same radius would only hit a small fraction of the proximal dendrite, which would lead to an understatement of the effect size in the dendrite compared to the soma. I therefore decided to use a flash of twice the radius, in order to cover a larger portion of the proximal dendrite. The radius of the flash area is controlled by moving a lens in the light path, and so as a result of this, the photon density of the flash was halved. Any photolytic process has a property known as the quantum yield: a fractional quantity that describes the number of uncaging events that occur per photon absorbed (Lacowicz 2006). Therefore, for a given concentration of the compound, the number of uncaging events is directly proportional to the number of uncaging events, up to the point where the photon density is so high that all most of the caged compound is uncaged at once. The fact that we still observed a significantly stronger inhibition of the  $sI_{AHP}$  in response to the dendritic flash is therefore unlikely to be due to the fact that a larger area was flashed compared to the soma protocol, as the photon density was lower in the proximal dendrite, and this would be expected to reduce the number of uncaging events proportionately, so that approximately the same number of uncaging events would occur in the larger area as the smaller.

One other consideration concerning the differences between the two regions is that the two compartments are different in terms of geometry. The soma has a relatively low surface area to volume ratio compared to the proximal dendrite. As a result, a similar number of uncaging events in the two locations could lead to a proportionately higher concentration of cAMP in the dendritic location compared to the soma. This could potentially contribute to the difference in  $sI_{AHP}$  inhibition seen between the two locations.

In order to correctly interpret the observed differences in  $sI_{AHP}$  inhibition between the two compartments, it is helpful to consider the implications of two hypotheses: one in which the signalling complexes containing PKA and the target channels are distributed throughout the neuron with a uniform density, and one in which there is tight clustering of the complexes at one or more subcellular locations.

If the flash protocol in both were to produce a constant photon density, doubling the area of plasma membrane over which the uncaging occurred would be expected to produce an effect size approaching double the magnitude, given the subsidiary assumptions that the dendritic tree was dense enough that only a small proportion of the photons in either area missed the neuron, and that the signalling complexes are in relatively close association with the plasma membrane. Under such conditions, the larger effect observed at the dendritic location could be simply a function of the area covered by the flash, as opposed to a local enrichment of the cAMP-dependent signalling complex underlying  $sI_{AHP}$  inhibition.

However, in reality two of these assumptions are untenable. Most importantly, the photon density did not remain constant when the flash area was doubled: it halved, as the same number of photons produced by the lamp were distributed over twice the area by the lens array. Also while the somatic flash covered an area approximately equivalent to that of the soma, and hence few photons missed their target, that covering the dendrite was only filled to approximately one third to one half by the dendritic arbor of the patched cell. It is therefore difficult to see how the observed results can be consistent with a uniform distribution of the signalling complex, and it is much more likely that there is some degree of compartmentalisation of the signal.

For the reasons outlined above, it is relatively safe to assume that the results do represent some localisation of the signalling complexes responsible for transducing the cAMP signal into inhibition of  $sI_{AHP}$ . How should the results observed be interpreted in this context?

Uncaging of 8Br-cAMP by the flash protocol produces a local elevation of its concentration in the region where the flash was delivered. The 8Br-cAMP then diffuses away from this initial location towards other compartments of the cell. The rate of this diffusion in a neuron is not fully understood, however estimates of the rate of cAMP diffusion have been produced experimentally in cardiac myocytes (Agarwal et al, 2015). Using a fluorescently labelled cAMP analogue, the diffusion coefficient in cardiac myocytes was estimated to be  $9.7 \mu\text{m}^2/\text{s}$ , significantly slower than that expected under

conditions of free diffusion ( $\sim 300 \mu\text{m}^2/\text{s}$ ). Nonetheless, assuming a similar speed of diffusion, by the start of the second  $s_{\text{I}_{\text{AHP}}}$  trace following the flash protocol, the cAMP signal would be expected to have spread up to  $300 \mu\text{m}$  from the site of uncaging, in other words a greater distance than the separation of the two flash locations.

How then to explain the difference in inhibition between the two regions?

If one were to accurately measure the cAMP concentration at the centre of the flash, and at another point in the neuron outside the flashed region, then the concentration of cAMP would reach a higher level in the centre of the flashed region than in the area outside, and the concentration gradient would subsequently reduce as the cAMP diffused away. It therefore follows that a signalling complex close to the site of uncaging would experience a higher concentration of cAMP immediately following the flash than one at a more distant location. It is likely that the signalling complexes responsible for the inhibition of  $s_{\text{I}_{\text{AHP}}}$  are located closer to the proximal dendritic location than to the soma. Nonetheless, some of the cAMP signal from the somatic flash location would be expected to diffuse to the site occupied by the  $s_{\text{I}_{\text{AHP}}}$  signalling complexes, and hence an effect was seen at both locations.

It is important to remember that 8Br-cAMP has reduced susceptibility to hydrolysis by phosphodiesterases, and it is likely that the real cAMP domains produced by  $\beta$ -adrenergic receptor activation are more tightly spatially tuned as a result of phosphodiesterase activity.

An alternative explanation is that the sAHP channel signalling complexes might be unevenly distributed between the two locations, perhaps with a density gradient that is low at the soma, and increases into the proximal dendrite. These explanations are not mutually exclusive, and the observed result could be due to a mixture of diffusion of the cAMP signal away from the uncaging site, and an uneven distribution of the sAHP/PKA signalling complexes.

The experiments presented in this chapter have provided two separate lines of evidence for spatially localised control over cAMP-dependent suppression of  $s_{\text{I}_{\text{AHP}}}$ . Focal application of isoproterenol in CA1 pyramidal cells in acute slice preparation showed that isoproterenol delivered to the soma/ proximal dendrite region was more effective at inhibiting  $s_{\text{I}_{\text{AHP}}}$  than the same concentration delivered to the distal dendrites, a result that could be explained either by differences in receptor density at the two locations, or by

differences in their coupling to the signalling complexes responsible for inhibition of the sAHP channels by PKA.

The latter explanation assumed the existence of spatially restricted cAMP signalling domains, and in order to determine whether these were present, 8Br-cAMP was uncaged in a spatially localised manner in pyramidal cells of hippocampal neuronal cultures, and it was observed that a train of UV flashes delivered to the proximal portion of the apical dendrite (centred on the first branch point of the dendritic arbor) was more effective at inhibiting  $sI_{AHP}$  than the same protocol delivered to the soma.

It should be noted that the results of these two experiments are not exactly commensurable. In the focal application experiment, the comparison was between the soma/proximal apical dendrite on the one hand, and the distal portion of the apical dendritic arbor on the other. In the flash experiment, the distinction was between the soma and the proximal apical dendrite. This was due to methodological constraints: it was not possible to flash two locations more than a couple of hundred microns apart, due to the requirement of using the 60x objective to focus the UV lamp output sufficiently to produce an uncaging effect. In the focal application experiment, it was necessary to use the 20x objective instead to permit positioning of the microinjector pipette, making it necessary to separate the regions tested further.

Additionally the focal application experiment was performed in acute slice preparations of rat hippocampus, whereas the uncaging experiment was performed in rat hippocampal cultures. This was necessary because it was not possible to achieve the uncaging result, using either DM-Nitrophen or BCMCM-8Br-cAMP, in acute slices, presumably because the layer of debris on the surface of the slice absorbed too great a proportion of the UV photons. The use of these different preparations leads to two potential confounds. The cultured cells are not organised into discrete layers, and so it is necessary to determine whether a cell is pyramidal using its morphology. Our criteria are discussed in methods (2.2.10).

It is not possible to know whether the pyramidal cells recorded in culture were originally from CA1 or CA3, and these cells may have different properties, both in terms of intrinsic membrane properties and in their response to modulatory signals, although similar distinctions have been observed within the CA1 region itself (Graves et al 2012, Jensen et al 1994, 1996). Furthermore, it is not certain that cultured neurons maintain the same subcellular spatial expression patterns of the signalling components of interest, compared to those in acute slice preparations.

As a result of these issues, care needs to be taken in drawing comparisons between the two sets of experiments, as it cannot be assumed that the two systems are identical.

Nonetheless, the results of both experiments are consistent with the hypothesis that the complexes including PKA and the  $sI_{AHP}$  channels are located somewhere in the proximal portion of the apical dendrites. This is in agreement with the result achieved by Sah and Bekkers (1995), who used the time course of relaxation of the membrane current to estimate the location of the sAHP channels. In their experiment, they used the fact that the relaxation of the membrane current in response to a voltage step will occur more slowly, the further the membrane responsible is from the patch pipette, due to the cable properties of the dendritic compartment. By evoking GABA-mediated inhibitory postsynaptic currents (IPSC) at the soma and in the dendrites, they were able to compare the rate of current relaxation for the two currents by stepping the voltage to the reversal potential of the IPSC at the peak of the current. They then compared these estimates to a similar estimate acquired for the  $sI_{AHP}$ , using a compartmental cable model of the CA1 pyramidal neuron, and produced an estimate suggesting that the  $sI_{AHP}$  channels were located in the proximal apical dendrite within 200  $\mu\text{m}$  of the soma.

The results of both of our experiments appear to support this estimate of the location of the  $sI_{AHP}$  channels. In the focal application experiment, a puff of isoproterenol covering the soma and the proximal 20-40  $\mu\text{m}$  of the apical dendrite produced a stronger inhibition of  $sI_{AHP}$  than the same puff delivered to a point 100  $\mu\text{m}$  past the first branch point of the apical dendrite. In the 8Br-cAMP uncaging experiment, a flash delivered to the region immediately proximal to the first branch point of the dendrite was more effective than one delivered directly to the soma. Assuming that the signalling complexes containing PKA are in close proximity to the sAHP channels, these results would support the location of the channels in a proximal dendritic location. It is possible that PKA does not act directly on the channels to effect their inhibition, in which case this assumption would not necessarily hold. An interesting future experiment would be to repeat the cAMP uncaging experiment in the presence of the AKAP inhibitor Ht31, to see if this would abolish the differences in the extent of inhibition observed between the two regions.

## 8.4 Conclusions

The results presented in this section of the thesis provide the first direct evidence for the existence of spatially localised signalling domains mediating the monoaminergic suppression of  $sI_{AHP}$  in hippocampal pyramidal neurons of CA1. Focal application of isoproterenol in acute slice preparation showed that isoproterenol delivered to the soma/proximal dendrite region was more effective at inhibiting  $sI_{AHP}$  than the same concentration delivered to the distal dendrites, and spatially localised uncaging of caged cAMP produced a stronger inhibitory effect on the current in the proximal dendritic region than at the soma. The existence of spatially localised signalling domains in PKA-dependent signalling pathways is well established in other processes, such as the control of L-type calcium channels in cardiac myocytes by B-adrenergic receptors (Xiao et al 1999), but these experiments provide the first evidence of such localised signalling in control of the slow afterhyperpolarisation. This result has particular importance given the difficulties encountered by various experimenters in pharmacologically isolating the  $sI_{AHP}$  current, and hence establishing the molecular identity of the channel or channels that mediate it, as such experiments typically involve bath application of the compounds in question. Such approaches affect the entire cell at once, and are consequently blind to any subcellular differences in the identity of the molecular components mediating the process under scrutiny.

Future experiments should provide greater clarity as to the precise compartmentalisation of the signalling domains underlying the monoaminergic control of  $sI_{AHP}$ , as well as the degree of specialisation among different monoaminergic transmitters and their receptors. It is something of a conceptual puzzle why the current literature shows diverse neuromodulatory systems all converging on the same pathway to suppress  $sI_{AHP}$ . This may be the true picture: that it is functionally advantageous for  $sI_{AHP}$  to be the convergence target of multiple transmitter systems, or it may be that each system actually exerts differential control over subpopulations of the channels underlying  $sI_{AHP}$ . Both these questions might be answered using the more precise spatial targeting made possible by LED-light activation of chimeric optogenetic constructs consisting of the extracellular portion of rhodopsin fused to the intracellular loops of the different monoamine receptors, such as that developed for the B2-adrenergic receptor by the lab of Karl Diesseroth (Airan et al 2009).

Calcium-dependent potassium channels play an important role in setting the intrinsic electrical properties of hippocampal neurons. The first part of my thesis focused on BK channels, which are unique in their ability to respond to both voltage and calcium signals, and therefore play an important role in both signal integration and homeostasis, as well as in tuning the action potential. They therefore represent important potential drug targets for regulation of neuronal function, as evidenced by the fact that differences in BK channel function are observed in the phenotypes of fragile X mouse models. The results described in this thesis were negative in terms of the putative BK opener VSN-16R, but did characterise for the first time the effects of the opener NS19504 on B-subunits of the channel.

The second part of the thesis focused on the slow afterhyperpolarisation  $sI_{AHP}$ , and its regulation by monoaminergic transmitters, and showed the first preliminary evidence of spatial localisation of the noradrenergic control of  $sI_{AHP}$ . As the slow phase of the afterhyperpolarisation is important in the control of firing rate adaptation, and given the continued lack of a clear molecular identity for the channel mediating the current, understanding the precise spatial and temporal dynamics of neuromodulatory influences on the current has important implications for the design of novel drugs that could potentially be of use in treatment of neurological dysfunctions with a high firing rate phenotype, such as epilepsy.

## References

- Abel, H.J., Lee, J.C.F., Callaway, J.C., Foehring, R.C., 2004. Relationships between intracellular calcium and afterhyperpolarizations in neocortical pyramidal neurons. *J. Neurophysiol.* 91, 324–335.
- Adams, P.R., Constanti, A., Brown, D.A., Clark, R.B., 1982. Intracellular Ca<sup>2+</sup> activates a fast voltage-sensitive K<sup>+</sup> current in vertebrate sympathetic neurones. *Nature* 296, 746–749.
- Agarwal, S.R., Clancy, C.E., Harvey, R.D., 2016. Mechanisms Restricting Diffusion of Intracellular cAMP. *Sci Rep* 6, 19577.
- Agre, P., Nielsen, S., 1996. The aquaporin family of water channels in kidney. *Nephrologie* 17, 409–415.
- Airan, R., Thompson, K., Fenno, L., Bernstein, H., and Deisseroth, K., 2009. Temporally precise *in vivo* control of intracellular signalling. *Nature* 458, 1025-1029.
- Alger, B.E., Nicoll, R.A., 1980. Epileptiform burst afterhyperpolarization: calcium-dependent potassium potential in hippocampal CA1 pyramidal cells. *Science* 210, 1122–1124.
- Anderson, A.J., Harvey, A.L., Rowan, E.G., Strong, P.N., 1988. Effects of charybdotoxin, a blocker of Ca<sup>2+</sup>-activated K<sup>+</sup> channels, on motor nerve terminals. *Br. J. Pharmacol.* 95, 1329–1335.
- Andrade, R., Foehring, R.C., Tzingounis, A.V., 2012. The calcium-activated slow AHP: cutting through the Gordian knot. *Front Cell Neurosci* 6, 47.
- Andrade, R., Nicoll, R.A., 1987. Pharmacologically distinct actions of serotonin on single pyramidal neurones of the rat hippocampus recorded *in vitro*. *J. Physiol. (Lond.)* 394, 99–124.
- Asano, S., Bratz, I.N., Berwick, Z.C., Fancher, I.S., Tune, J.D., Dick, G.M., 2012. Penitrem A as a tool for understanding the role of large conductance Ca(2+)/voltage-sensitive K(+) channels in vascular function. *J. Pharmacol. Exp. Ther.* 342, 453–460.
- Begg, M., Mo, F.-M., Offertaler, L., Bátkai, S., Pacher, P., Razdan, R.K., Lovinger, D.M., Kunos, G., 2003. G protein-coupled endothelial receptor for atypical cannabinoid ligands modulates a Ca<sup>2+</sup>-dependent K<sup>+</sup> current. *J. Biol. Chem.* 278, 46188–46194.
- Behrens, R., Nolting, A., Reimann, F., Schwarz, M., Waldschütz, R., Pongs, O., 2000. hKCNMB3 and hKCNMB4, cloning and characterization of two members of the large-conductance calcium-activated potassium channel beta subunit family. *FEBS Lett.* 474, 99–106.
- Beisel, K.W., Rocha-Sanchez, S.M., Ziegenbein, S.J., Morris, K.A., Kai, C., Kawai, J., Carninci, P., Hayashizaki, Y., Davis, R.L., 2007. Diversity of Ca<sup>2+</sup>-activated K<sup>+</sup> channel transcripts in inner ear hair cells. *Gene* 386, 11–23.
- Békésy, G. von, Wever, E.G., 1960. Experiments in hearing. McGraw-Hill, New York.
- Benardo, L.S., Prince, D.A., 1982a. Dopamine modulates a Ca<sup>2+</sup>-activated potassium conductance in mammalian hippocampal pyramidal cells. *Nature* 297, 76–79.

- Benardo, L.S., Prince, D.A., 1982b. Cholinergic excitation of mammalian hippocampal pyramidal cells. *Brain Res.* 249, 315–331.
- Bentzen, B.H., Nardi, A., Calloe, K., Madsen, L.S., Olesen, S.-P., Grunnet, M., 2007. The small molecule NS11021 is a potent and specific activator of Ca<sup>2+</sup>-activated big-conductance K<sup>+</sup> channels. *Mol. Pharmacol.* 72, 1033–1044.
- Bentzen, B.H., Osadchii, O., Jespersen, T., Hansen, R.S., Olesen, S.-P., Grunnet, M., 2009. Activation of big conductance Ca(2+)-activated K (+) channels (BK) protects the heart against ischemia-reperfusion injury. *Pflugers Arch.* 457, 979–988.
- Bienert, G.P., Schjoerring, J.K., Jahn, T.P., 2006. Membrane transport of hydrogen peroxide. *Biochim. Biophys. Acta* 1758, 994–1003.
- Blitzer, R.D., Wong, T., Nouranifar, R., Iyengar, R., Landau, E.M., 1995. Postsynaptic cAMP pathway gates early LTP in hippocampal CA1 region. *Neuron* 15, 1403–1414.
- Bond, C.T., Herson, P.S., Strassmaier, T., Hammond, R., Stackman, R., Maylie, J., Adelman, J.P., 2004. Small conductance Ca<sup>2+</sup>-activated K<sup>+</sup> channel knock-out mice reveal the identity of calcium-dependent afterhyperpolarization currents. *J. Neurosci.* 24, 5301–5306.
- Borde, M., Bonansco, C., Fernández de Sevilla, D., Le Ray, D., Buño, W., 2000. Voltage-clamp analysis of the potentiation of the slow Ca<sup>2+</sup>-activated K<sup>+</sup> current in hippocampal pyramidal neurons. *Hippocampus* 10, 198–206.
- Bowden, S.E., Fletcher, S., Loane, D.J., Marrion, N.V., 2001. Somatic colocalization of rat SK1 and D class (Ca(v)1.2) L-type calcium channels in rat CA1 hippocampal pyramidal neurons. *J. Neurosci.* 21, RC175.
- Brelidze, T.I., Magleby, K.L., 2004. Protons block BK channels by competitive inhibition with K<sup>+</sup> and contribute to the limits of unitary currents at high voltages. *J. Gen. Physiol.* 123, 305–319.
- Brelidze, T.I., Niu, X., Magleby, K.L., 2003. A ring of eight conserved negatively charged amino acids doubles the conductance of BK channels and prevents inward rectification. *Proc. Natl. Acad. Sci. U.S.A.* 100, 9017–9022.
- Brenner, R., Chen, Q.H., Vilaythong, A., Toney, G.M., Noebels, J.L., Aldrich, R.W., 2005. BK channel beta4 subunit reduces dentate gyrus excitability and protects against temporal lobe seizures. *Nat. Neurosci.* 8, 1752–1759.
- Brenner, R., Jegla, T.J., Wickenden, A., Liu, Y., Aldrich, R.W., 2000. Cloning and functional characterization of novel large conductance calcium-activated potassium channel beta subunits, hKCNMB3 and hKCNMB4. *J. Biol. Chem.* 275, 6453–6461.
- Brown, D.A., Griffith, W.H., 1983. Calcium-activated outward current in voltage-clamped hippocampal neurones of the guinea-pig. *J. Physiol. (Lond.)* 337, 287–301.
- Brown, M.R., Kronengold, J., Gazula, V.-R., Chen, Y., Strumbos, J.G., Sigworth, F.J., Navaratnam, D., Kaczmarek, L.K., 2010. Fragile X mental retardation protein controls gating of the sodium-activated potassium channel Slack. *Nat. Neurosci.* 13, 819–821.
- Carlen, P.L., Gurevich, N., Durand, D., 1982. Ethanol in low doses augments calcium-mediated mechanisms measured intracellularly in hippocampal neurons. *Science* 215, 306–309.

- Carr, D. W., Hausken Z. E., Fraser I. D., Stofko-Hahn R. E., Scott J. D., 1992. Association of the type II cAMP-dependent protein kinase with a human thyroid RII-anchoring protein. Cloning and characterization of the RII-binding domain. *J. Biol. Chem.* 267, 13376–13382
- Castro, L.R.V., Gervasi, N., Guiot, E., Cavellini, L., Nikolaev, V.O., Paupardin-Tritsch, D., Vincent, P., 2010. Type 4 Phosphodiesterase Plays Different Integrating Roles in Different Cellular Domains in Pyramidal Cortical Neurons. *J. Neurosci.* 30, 6143–6151.
- Chapin, E.M., Haj-Dahmane, S., Torres, G., Andrade, R., 2002. The 5-HT(4) receptor-induced depolarization in rat hippocampal neurons is mediated by cAMP but is independent of I(h). *Neurosci. Lett.* 324, 1–4.
- Charpak, S., Gähwiler, B.H., Do, K.Q., Knöpfel, T., 1990. Potassium conductances in hippocampal neurons blocked by excitatory amino-acid transmitters. *Nature* 347, 765–767.
- Chen, L., Tian, L., MacDonald, S.H.-F., McClafferty, H., Hammond, M.S.L., Huibant, J.-M., Ruth, P., Knaus, H.-G., Shipston, M.J., 2005. Functionally diverse complement of large conductance calcium- and voltage-activated potassium channel (BK) alpha-subunits generated from a single site of splicing. *J. Biol. Chem.* 280, 33599–33609.
- Chen, S., Benninger, F., Yaari, Y., 2014. Role of small conductance Ca<sup>2+</sup>-activated K<sup>+</sup> channels in controlling CA1 pyramidal cell excitability. *J. Neurosci.* 34, 8219–8230.
- Ciorba, M.A., Heinemann, S.H., Weissbach, H., Brot, N., Hoshi, T., 1999. Regulation of voltage-dependent K<sup>+</sup> channels by methionine oxidation: effect of nitric oxide and vitamin C. *FEBS Lett.* 442, 48–52.
- Cloues, R.K., Tavalin, S.J., Marrion, N.V., 1997. Beta-adrenergic stimulation selectively inhibits long-lasting L-type calcium channel facilitation in hippocampal pyramidal neurons. *J. Neurosci.* 17, 6493–6503.
- Cole, A.E., Nicoll, R.A., 1984. The pharmacology of cholinergic excitatory responses in hippocampal pyramidal cells. *Brain Res.* 305, 283–290.
- Cole, A.E., Nicoll, R.A., 1983. Acetylcholine mediates a slow synaptic potential in hippocampal pyramidal cells. *Science* 221, 1299–1301.
- Colino, A., Halliwell, J.V., 1987. Differential modulation of three separate K<sup>+</sup> conductances in hippocampal CA1 neurons by serotonin. *Nature* 328, 73–77.
- Constanti, A., Sim, J.A., 1987. Calcium-dependent potassium conductance in guinea-pig olfactory cortex neurones in vitro. *J. Physiol. (Lond.)* 387, 173–194.
- Cooper, D.M.F., Crossthwaite, A.J., 2006. Higher-order organization and regulation of adenylyl cyclases. *Trends Pharmacol. Sci.* 27, 426–431.
- Costa, P.F., Ribeiro, M.A., Santos, A.I., 1991. Afterpotential characteristics and firing patterns in maturing rat hippocampal CA1 neurones in in vitro slices. *Brain Res. Dev. Brain Res.* 62, 263–272.
- Dai, S., Hall, D.D., Hell, J.W., 2009. Supramolecular assemblies and localized regulation of voltage-gated ion channels. *Physiol. Rev.* 89, 411–452.
- Davare, M.A., Avdonin, V., Hall, D.D., Peden, E.M., Burette, A., Weinberg, R.J., Horne, M.C., Hoshi, T., Hell, J.W., 2001. A beta2 adrenergic receptor signaling complex assembled with the Ca<sup>2+</sup> channel Cav1.2. *Science* 293, 98–101.

- Deng, P.-Y., Klyachko, V.A., 2016. Genetic upregulation of BK channel activity normalizes multiple synaptic and circuit defects in a mouse model of fragile X syndrome. *J. Physiol. (Lond.)* 594, 83–97.
- Deng, P.-Y., Rotman, Z., Blundon, J.A., Cho, Y., Cui, J., Cavalli, V., Zakharenko, S.S., Klyachko, V.A., 2013. FMRP Regulates Neurotransmitter Release and Synaptic Information Transmission by Modulating Action Potential Duration via BK channels. *Neuron* 77, 696–711.
- De Petrocellis, L., Marini, P., Matias, I., Moriello, A.S., Starowicz, K., Cristino, L., Nigam, S., Di Marzo, V., 2007. Mechanisms for the coupling of cannabinoid receptors to intracellular calcium mobilization in rat insulinoma beta-cells. *Exp. Cell Res.* 313, 2993–3004.
- Díaz, L., Meera, P., Amigo, J., Stefani, E., Alvarez, O., Toro, L., Latorre, R., 1998. Role of the S4 segment in a voltage-dependent calcium-sensitive potassium (hSlo) channel. *J. Biol. Chem.* 273, 32430–32436.
- DiChiara, T.J., Reinhart, P.H., 1997. Redox modulation of hslo Ca<sup>2+</sup>-activated K<sup>+</sup> channels. *J. Neurosci.* 17, 4942–4955.
- Dick, G.M., Rossow, C.F., Smirnov, S., Horowitz, B., Sanders, K.M., 2001. Tamoxifen activates smooth muscle BK channels through the regulatory beta 1 subunit. *J. Biol. Chem.* 276, 34594–34599.
- Dinardo, M.M., Camerino, G., Mele, A., Latorre, R., Conte Camerino, D., Tricarico, D., 2012. Splicing of the rSlo gene affects the molecular composition and drug response of Ca<sup>2+</sup>-activated K<sup>+</sup> channels in skeletal muscle. *PLoS ONE* 7, e40235.
- Dopico, A.M., Bukiya, A.N., 2014. Lipid regulation of BK channel function. *Front Physiol* 5, 312.
- Du, W., Bautista, J.F., Yang, H., Diez-Sampedro, A., You, S.-A., Wang, L., Kotagal, P., Lüders, H.O., Shi, J., Cui, J., Richerson, G.B., Wang, Q.K., 2005. Calcium-sensitive potassium channelopathy in human epilepsy and paroxysmal movement disorder. *Nat. Genet.* 37, 733–738.
- Edgell, C.J., McDonald, C.C., Graham, J.B., 1983. Permanent cell line expressing human factor VIII-related antigen established by hybridization. *Proc Natl Acad Sci U S A* 80, 3734–3737.
- Ellis-Davies, G.C., Kaplan, J.H., Barsotti, R.J., 1996. Laser photolysis of caged calcium: rates of calcium release by nitrophenyl-EGTA and DM-nitrophen. *Biophys. J.* 70, 1006–1016.
- Ermolinsky, B.S., Skinner, F., Garcia, I., Arshadmansab, M.F., Otalora, L.F.P., Zarei, M.M., Garrido-Sanabria, E.R., 2011. Upregulation of STREX splice variant of the large conductance Ca<sup>2+</sup>-activated potassium (BK) channel in a rat model of mesial temporal lobe epilepsy. *Neurosci. Res.* 69, 73–80.
- Erxleben, C., Everhart, A.L., Romeo, C., Florance, H., Bauer, M.B., Alcorta, D.A., Rossie, S., Shipston, M.J., Armstrong, D.L., 2002. Interacting effects of N-terminal variation and strex exon splicing on slo potassium channel regulation by calcium, phosphorylation, and oxidation. *J. Biol. Chem.* 277, 27045–27052.
- Faber, E.S.L., Sah, P., 2003. Ca<sup>2+</sup>-activated K<sup>+</sup> (BK) channel inactivation contributes to spike broadening during repetitive firing in the rat lateral amygdala. *J Physiol* 552, 483–497.

- Féletou, M., 2009. Calcium-activated potassium channels and endothelial dysfunction: therapeutic options? *Br. J. Pharmacol.* 156, 545–562.
- Fettiplace, R., Fuchs, P.A., 1999. Mechanisms of hair cell tuning. *Annu. Rev. Physiol.* 61, 809–834.
- Filosa, J.A., Bonev, A.D., Straub, S.V., Meredith, A.L., Wilkerson, M.K., Aldrich, R.W., Nelson, M.T., 2006. Local potassium signaling couples neuronal activity to vasodilation in the brain. *Nat. Neurosci.* 9, 1397–1403.
- Fiorillo, C.D., Williams, J.T., 1998. Glutamate mediates an inhibitory postsynaptic potential in dopamine neurons. *Nature* 394, 78–82.
- Gao, T.-M., Fung, M.-L., 2002. Decreased large conductance Ca(2+)-activated K(+) channel activity in dissociated CA1 hippocampal neurons in rats exposed to perinatal and postnatal hypoxia. *Neurosci. Lett.* 332, 163–166.
- Garcia-Valdes, J., Zamudio, F.Z., Toro, L., Possani, L.D., Possan, L.D., 2001. Slotoxin, alphaKTx1.11, a new scorpion peptide blocker of MaxiK channels that differentiates between alpha and alpha+beta (beta1 or beta4) complexes. *FEBS Lett.* 505, 369–373.
- Gasparini, S., DiFrancesco, D., 1999. Action of serotonin on the hyperpolarization-activated cation current (I<sub>h</sub>) in rat CA1 hippocampal neurons. *Eur. J. Neurosci.* 11, 3093–3100.
- Ge, L., Hoa, N.T., Wilson, Z., Arismendi-Morillo, G., Kong, X.-T., Tajhya, R.B., Beeton, C., Jadus, M.R., 2014. Big Potassium (BK) ion channels in biology, disease and possible targets for cancer immunotherapy. *Int. Immunopharmacol.* 22, 427–443.
- Gessner, G., Schönherr, K., Soom, M., Hansel, A., Asim, M., Baniahmad, A., Derst, C., Hoshi, T., Heinemann, S.H., 2005. BKCa channels activating at resting potential without calcium in LNCaP prostate cancer cells. *J. Membr. Biol.* 208, 229–240.
- Golding, N.L., Jung, H.Y., Mickus, T., Spruston, N., 1999. Dendritic calcium spike initiation and repolarization are controlled by distinct potassium channel subtypes in CA1 pyramidal neurons. *J. Neurosci.* 19, 8789–8798.
- Gong, L., Gao, T.M., Huang, H., Tong, Z., 2000. Redox modulation of large conductance calcium-activated potassium channels in CA1 pyramidal neurons from adult rat hippocampus. *Neurosci. Lett.* 286, 191–194.
- Gonzalez-Perez, V., Xia, X.-M., Lingle, C.J., 2014. Functional regulation of BK potassium channels by  $\gamma$ 1 auxiliary subunits. *Proc Natl Acad Sci U S A* 111, 4868–4873.
- Graves, A.R., Moore, S.J., Bloss, E.B., Mensh, B.D., Kath, W.L., Spruston, N., 2012. Hippocampal pyramidal neurons comprise two distinct cell types that are countermodulated by metabotropic receptors. *Neuron* 76, 776–789.
- Gulledge, A.T., Dasari, S., Onoue, K., Stephens, E.K., Hasse, J.M., Avesar, D., 2013. A sodium-pump-mediated afterhyperpolarization in pyramidal neurons. *J. Neurosci.* 33, 13025–13041.
- Gu, N., Vervaeke, K., Hu, H., Storm, J.F., 2005. Kv7/KCNQ/M and HCN/h, but not KCa2/SK channels, contribute to the somatic medium after-hyperpolarization and excitability control in CA1 hippocampal pyramidal cells. *J. Physiol. (Lond.)* 566, 689–715.

- Gu, N., Vervaeke, K., Storm, J.F., 2007. BK potassium channels facilitate high-frequency firing and cause early spike frequency adaptation in rat CA1 hippocampal pyramidal cells. *J. Physiol. (Lond.)* 580, 859–882.
- Gustafsson, B., Wigström, H., 1986. Hippocampal long-lasting potentiation produced by pairing single volleys and brief conditioning tetani evoked in separate afferents. *J. Neurosci.* 6, 1575–1582.
- Haas, H.L., Konnerth, A., 1983. Histamine and noradrenaline decrease calcium-activated potassium conductance in hippocampal pyramidal cells. *Nature* 302, 432–434.
- Hadley, J.K., Noda, M., Selyanko, A.A., Wood, I.C., Abogadie, F.C., Brown, D.A., 2000. Differential tetraethylammonium sensitivity of KCNQ1-4 potassium channels. *Br. J. Pharmacol.* 129, 413–415.
- Hadley, J.K., Passmore, G.M., Tatulian, L., Al-Qatari, M., Ye, F., Wickenden, A.D., Brown, D.A., 2003. Stoichiometry of expressed KCNQ2/KCNQ3 potassium channels and subunit composition of native ganglionic M channels deduced from block by tetraethylammonium. *J. Neurosci.* 23, 5012–5019.
- Hagen, V., Bendig, J., Frings, S., Eckardt, T., Helm, S., Reuter, D., Kaupp, U.B., 2001. Highly Efficient and Ultrafast Phototriggers for cAMP and cGMP by Using Long-Wavelength UV/Vis-Activation This work was supported by the Deutsche Forschungsgemeinschaft, the European Union, and the Fonds der Chemischen Industrie. We thank B. Dekowski and J. Loßmann for technical assistance and S. Hecht for proof reading. *Angew. Chem. Int. Ed. Engl.* 40, 1045–1048.
- Hagen, V., Dzeja, C., Bendig, J., Baeger, I., Kaupp, U.B., 1998. Novel caged compounds of hydrolysis-resistant 8-Br-cAMP and 8-Br-cGMP: photolabile NPE esters. *J. Photochem. Photobiol. B, Biol.* 42, 71–78.
- Hagerman, P.J., Stafstrom, C.E., 2009. Origins of Epilepsy in Fragile X Syndrome. *Epilepsy Curr* 9, 108–112.
- Haug, T., Sigg, D., Ciani, S., Toro, L., Stefani, E., Olcese, R., 2004. Regulation of K<sup>+</sup> flow by a ring of negative charges in the outer pore of BKCa channels. Part I: Aspartate 292 modulates K<sup>+</sup> conduction by external surface charge effect. *J. Gen. Physiol.* 124, 173–184.
- Hermann, A., Erxleben, C., 1987. Charybdotoxin selectively blocks small Ca-activated K channels in Aplysia neurons. *J Gen Physiol* 90, 27–47.
- Hermann, A., Sitdikova, G.F., Weiger, T.M., 2015. Oxidative Stress and Maxi Calcium-Activated Potassium (BK) Channels. *Biomolecules* 5, 1870–1911.
- Hoi, P.M., Visintin, C., Okuyama, M., Gardiner, S.M., Kaup, S.S., Bennett, T., Baker, D., Selwood, D.L., Hiley, C.R., 2007. Vascular pharmacology of a novel cannabinoid-like compound, 3-(5-dimethylcarbamoyl-pent-1-enyl)-N-(2-hydroxy-1-methyl-ethyl)benzamide (VSN16) in the rat. *Br J Pharmacol* 152, 751–764.
- Hotson, J.R., Prince, D.A., 1980. A calcium-activated hyperpolarization follows repetitive firing in hippocampal neurons. *J. Neurophysiol.* 43, 409–419.
- Hou, S., Heinemann, S.H., Hoshi, T., 2009. Modulation of BKCa channel gating by endogenous signaling molecules. *Physiology (Bethesda)* 24, 26–35.

- Hou, S., Reynolds, M.F., Horrigan, F.T., Heinemann, S.H., Hoshi, T., 2006. Reversible binding of heme to proteins in cellular signal transduction. *Acc. Chem. Res.* 39, 918–924.
- Huang, C.-W., Huang, C.-C., Wu, S.-N., 2007. Activation by zonisamide, a newer antiepileptic drug, of large-conductance calcium-activated potassium channel in differentiated hippocampal neuron-derived H19-7 cells. *J. Pharmacol. Exp. Ther.* 321, 98–106.
- Hudspeth, A.J., Lewis, R.S., 1988. A model for electrical resonance and frequency tuning in saccular hair cells of the bull-frog, *Rana catesbeiana*. *J Physiol* 400, 275–297.
- Hulme, J.T., Lin, T.W.-C., Westenbroek, R.E., Scheuer, T., Catterall, W.A., 2003. Beta-adrenergic regulation requires direct anchoring of PKA to cardiac CaV1.2 channels via a leucine zipper interaction with A kinase-anchoring protein 15. *Proc. Natl. Acad. Sci. U.S.A.* 100, 13093–13098.
- Ireland, D.R., Abraham, W.C., 2002. Group I mGluRs increase excitability of hippocampal CA1 pyramidal neurons by a PLC-independent mechanism. *J. Neurophysiol.* 88, 107–116.
- Jaffe, D.B., Johnston, D., Lasser-Ross, N., Lisman, J.E., Miyakawa, H., Ross, W.N., 1992. The spread of Na<sup>+</sup> spikes determines the pattern of dendritic Ca<sup>2+</sup> entry into hippocampal neurons. *Nature* 357, 244–246.
- Jaggard, J.H., Porter, V.A., Lederer, W.J., Nelson, M.T., 2000. Calcium sparks in smooth muscle. *Am. J. Physiol., Cell Physiol.* 278, C235–256.
- Járai, Z., Wagner, J.A., Varga, K., Lake, K.D., Compton, D.R., Martin, B.R., Zimmer, A.M., Bonner, T.I., Buckley, N.E., Mezey, E., Razdan, R.K., Zimmer, A., Kunos, G., 1999. Cannabinoid-induced mesenteric vasodilation through an endothelial site distinct from CB1 or CB2 receptors. *Proc. Natl. Acad. Sci. U.S.A.* 96, 14136–14141.
- Jensen, M.S., Azouz, R., Yaari, Y., 1996. Spike after-depolarization and burst generation in adult rat hippocampal CA1 pyramidal cells. *J. Physiol. (Lond.)* 492 ( Pt 1), 199–210.
- Jensen, M.S., Azouz, R., Yaari, Y., 1994. Variant firing patterns in rat hippocampal pyramidal cells modulated by extracellular potassium. *J. Neurophysiol.* 71, 831–839.
- Jentsch, T.J., 2000. Neuronal KCNQ potassium channels: physiology and role in disease. *Nat. Rev. Neurosci.* 1, 21–30.
- Jiang, Y., Lee, A., Chen, J., Cadene, M., Chait, B.T., MacKinnon, R., 2002. Crystal structure and mechanism of a calcium-gated potassium channel. *Nature* 417, 515–522.
- Johnson, B.E., Glauser, D.A., Dan-Glauser, E.S., Halling, D.B., Aldrich, R.W., Goodman, M.B., 2011. Alternatively spliced domains interact to regulate BK potassium channel gating. *Proc. Natl. Acad. Sci. U.S.A.* 108, 20784–20789.
- Jones, E.M., Gray-Keller, M., Fettiplace, R., 1999. The role of Ca<sup>2+</sup>-activated K<sup>+</sup> channel spliced variants in the tonotopic organization of the turtle cochlea. *J. Physiol. (Lond.)* 518 ( Pt 3), 653–665.
- Kaplan, J.H., Ellis-Davies, G.C., 1988. Photolabile chelators for the rapid photorelease of divalent cations. *Proc Natl Acad Sci U S A* 85, 6571–6575.

- Kim, K.S., Kobayashi, M., Takamatsu, K., Tzingounis, A.V., 2012. Hippocalcin and KCNQ channels contribute to the kinetics of the slow afterhyperpolarization. *Biophys. J.* 103, 2446–2454.
- King, B., Rizwan, A.P., Asmara, H., Heath, N.C., Engbers, J.D.T., Dykstra, S., Bartoletti, T.M., Hameed, S., Zamponi, G.W., Turner, R.W., 2015. IKCa channels are a critical determinant of the slow AHP in CA1 pyramidal neurons. *Cell Rep* 11, 175–182.
- Knaus, H.G., McManus, O.B., Lee, S.H., Schmalhofer, W.A., Garcia-Calvo, M., Helms, L.M., Sanchez, M., Giangiacomo, K., Reuben, J.P., Smith, A.B., 1994. Tremorgenic indole alkaloids potently inhibit smooth muscle high-conductance calcium-activated potassium channels. *Biochemistry* 33, 5819–5828.
- Köhler, M., Hirschberg, B., Bond, C.T., Kinzie, J.M., Marrion, N.V., Maylie, J., Adelman, J.P., 1996. Small-conductance, calcium-activated potassium channels from mammalian brain. *Science* 273, 1709–1714.
- Koide, M., Bonev, A.D., Nelson, M.T., Wellman, G.C., 2012. Inversion of neurovascular coupling by subarachnoid blood depends on large-conductance Ca<sup>2+</sup>-activated K<sup>+</sup> (BK) channels. *Proc. Natl. Acad. Sci. U.S.A.* 109, E1387–1395.
- Krause, M., Offermanns, S., Stocker, M., Pedarzani, P., 2002. Functional specificity of G alpha q and G alpha 11 in the cholinergic and glutamatergic modulation of potassium currents and excitability in hippocampal neurons. *J. Neurosci.* 22, 666–673.
- Kun, A., Matchkov, V.V., Stankevicius, E., Nardi, A., Hughes, A.D., Kirkeby, H.J., Demnitz, J., Simonsen, U., 2009. NS11021, a novel opener of large-conductance Ca(2+)-activated K(+) channels, enhances erectile responses in rats. *Br. J. Pharmacol.* 158, 1465–1476.
- Lakowicz, J.R. (Ed.), 2006. *Principles of Fluorescence Spectroscopy*. Springer US, Boston, MA. (p10).
- Lancaster, B., Adams, P.R., 1986. Calcium-dependent current generating the afterhyperpolarization of hippocampal neurons. *J. Neurophysiol.* 55, 1268–1282.
- Lancaster, B., Nicoll, R.A., 1987. Properties of two calcium-activated hyperpolarizations in rat hippocampal neurones. *J. Physiol. (Lond.)* 389, 187–203.
- Lancaster, B., Zucker, R.S., 1994. Photolytic manipulation of Ca<sup>2+</sup> and the time course of slow, Ca(2+)-activated K<sup>+</sup> current in rat hippocampal neurones. *J. Physiol. (Lond.)* 475, 229–239.
- Lang, D.G., Ritchie, A.K., 1987. Large and small conductance calcium-activated potassium channels in the GH3 anterior pituitary cell line. *Pflugers Arch.* 410, 614–622.
- Lasser-Ross, N., Ross, W.N., Yarom, Y., 1997. Activity-dependent [Ca<sup>2+</sup>]<sub>i</sub> changes in guinea pig vagal motoneurons: relationship to the slow afterhyperpolarization. *J. Neurophysiol.* 78, 825–834.
- Liu, G., Shi, J., Yang, L., Cao, L., Park, S.M., Cui, J., Marx, S.O., 2004. Assembly of a Ca<sup>2+</sup>-dependent BK channel signaling complex by binding to beta2 adrenergic receptor. *EMBO J.* 23, 2196–2205.
- Liu, J., Ye, J., Zou, X., Xu, Z., Feng, Y., Zou, X., Chen, Z., Li, Y., Cang, Y., 2014. CRL4A(CRBN) E3 ubiquitin ligase restricts BK channel activity and prevents epileptogenesis. *Nat Commun* 5, 3924.

- Liu, Y.C., Lo, Y.K., Wu, S.N., 2003. Stimulatory effects of chlorzoxazone, a centrally acting muscle relaxant, on large conductance calcium-activated potassium channels in pituitary GH3 cells. *Brain Res.* 959, 86–97.
- Logsdon, N.J., Kang, J., Togo, J.A., Christian, E.P., Aiyar, J., 1997. A novel gene, hKCa4, encodes the calcium-activated potassium channel in human T lymphocytes. *J. Biol. Chem.* 272, 32723–32726.
- Lorenz, S., Heils, A., Kasper, J.M., Sander, T., 2007. Allelic association of a truncation mutation of the KCNMB3 gene with idiopathic generalized epilepsy. *Am. J. Med. Genet. B Neuropsychiatr. Genet.* 144B, 10–13.
- Lörincz, A., Notomi, T., Tamás, G., Shigemoto, R., Nusser, Z., 2002. Polarized and compartment-dependent distribution of HCN1 in pyramidal cell dendrites. *Nat. Neurosci.* 5, 1185–1193.
- Madison, D.V., Nicoll, R.A., 1984. Control of the repetitive discharge of rat CA 1 pyramidal neurones in vitro. *J. Physiol. (Lond.)* 354, 319–331.
- Madison, D.V., Nicoll, R.A., 1982. Noradrenaline blocks accommodation of pyramidal cell discharge in the hippocampus. *Nature* 299, 636–638.
- Magee, J.C., 1998. Dendritic hyperpolarization-activated currents modify the integrative properties of hippocampal CA1 pyramidal neurons. *J. Neurosci.* 18, 7613–7624.
- Manzanares, D., Srinivasan, M., Salathe, S.T., Ivonnet, P., Baumlin, N., Dennis, J.S., Conner, G.E., Salathe, M., 2014. IFN- $\gamma$ -mediated reduction of large-conductance, Ca<sup>2+</sup>-activated, voltage-dependent K<sup>+</sup> (BK) channel activity in airway epithelial cells leads to mucociliary dysfunction. *Am. J. Physiol. Lung Cell Mol. Physiol.* 306, L453–462.
- Marrion, N.V., Zucker, R.S., Marsh, S.J., Adams, P.R., 1991. Modulation of M-current by intracellular Ca<sup>2+</sup>. *Neuron* 6, 533–545.
- Marty, A., Neher, E., 1985. Potassium channels in cultured bovine adrenal chromaffin cells. *J. Physiol. (Lond.)* 367, 117–141.
- McKay, M.C., Dworetzky, S.I., Meanwell, N.A., Olesen, S.P., Reinhart, P.H., Levitan, I.B., Adelman, J.P., Gribkoff, V.K., 1994. Opening of large-conductance calcium-activated potassium channels by the substituted benzimidazolone NS004. *J. Neurophysiol.* 71, 1873–1882.
- Meera, P., Wallner, M., Song, M., Toro, L., 1997. Large conductance voltage- and calcium-dependent K<sup>+</sup> channel, a distinct member of voltage-dependent ion channels with seven N-terminal transmembrane segments (S0-S6), an extracellular N terminus, and an intracellular (S9-S10) C terminus. *Proc. Natl. Acad. Sci. U.S.A.* 94, 14066–14071.
- Meera, P., Wallner, M., Toro, L., 2000. A neuronal beta subunit (KCNMB4) makes the large conductance, voltage- and Ca<sup>2+</sup>-activated K<sup>+</sup> channel resistant to charybdotoxin and iberiotoxin. *Proc. Natl. Acad. Sci. U.S.A.* 97, 5562–5567.
- Miller, E.W., Dickinson, B.C., Chang, C.J., 2010. Aquaporin-3 mediates hydrogen peroxide uptake to regulate downstream intracellular signaling. *Proc Natl Acad Sci U S A* 107, 15681–15686.
- Milner, T.A., Shah, P., Pierce, J.P., 2000. beta-adrenergic receptors primarily are located on the dendrites of granule cells and interneurons but also are found on astrocytes and a few presynaptic profiles in the rat dentate gyrus. *Synapse* 36, 178–193.

- Mombouli, J.-V., Schaeffer, G., Holzmann, S., Kostner, G.M., Graier, W.F., 1999. Anandamide-induced mobilization of cytosolic Ca<sup>2+</sup> in endothelial cells. *Br J Pharmacol* 126, 1593–1600.
- Moore, K.A., Cohen, A.S., Kao, J.P., Weinreich, D., 1998. Ca<sup>2+</sup>-induced Ca<sup>2+</sup> release mediates a slow post-spike hyperpolarization in rabbit vagal afferent neurons. *J. Neurophysiol.* 79, 688–694.
- Morrow, J.P., Zakharov, S.I., Liu, G., Yang, L., Sok, A.J., Marx, S.O., 2006. Defining the BK channel domains required for beta1-subunit modulation. *Proc. Natl. Acad. Sci. U.S.A.* 103, 5096–5101.
- Nausch, B., Rode, F., Jørgensen, S., Nardi, A., Korsgaard, M.P.G., Hougaard, C., Bonev, A.D., Brown, W.D., Dyhring, T., Strøbæk, D., Olesen, S.-P., Christophersen, P., Grunnet, M., Nelson, M.T., Rønn, L.C.B., 2014. NS19504: a novel BK channel activator with relaxing effect on bladder smooth muscle spontaneous phasic contractions. *J. Pharmacol. Exp. Ther.* 350, 520–530.
- Nelson, M.T., Cheng, H., Rubart, M., Santana, L.F., Bonev, A.D., Knot, H.J., Lederer, W.J., 1995. Relaxation of arterial smooth muscle by calcium sparks. *Science* 270, 633–637.
- Neves, S.R., Tsokas, P., Sarkar, A., Grace, E.A., Rangamani, P., Taubenfeld, S.M., Alberini, C.M., Schaff, J.C., Blitzer, R.D., Moraru, I.I., Iyengar, R., 2008. Cell shape and negative links in regulatory motifs together control spatial information flow in signaling networks. *Cell* 133, 666–680.
- Notomi, T., Shigemoto, R., 2004. Immunohistochemical localization of Ih channel subunits, HCN1-4, in the rat brain. *J. Comp. Neurol.* 471, 241–276.
- Offertáler, L., Mo, F.-M., Bátkai, S., Liu, J., Begg, M., Razdan, R.K., Martin, B.R., Bukoski, R.D., Kunos, G., 2003. Selective ligands and cellular effectors of a G protein-coupled endothelial cannabinoid receptor. *Mol. Pharmacol.* 63, 699–705.
- Olesen, S.P., Munch, E., Moldt, P., Drejer, J., 1994. Selective activation of Ca<sup>2+</sup>-dependent K<sup>+</sup> channels by novel benzimidazolone. *Eur. J. Pharmacol.* 251, 53–59.
- Orio, P., Rojas, P., Ferreira, G., Latorre, R., 2002. New disguises for an old channel: MaxiK channel beta-subunits. *News Physiol. Sci.* 17, 156–161.
- Pallotta, B.S., Magleby, K.L., Barrett, J.N., 1981. Single channel recordings of Ca<sup>2+</sup>-activated K<sup>+</sup> currents in rat muscle cell culture. *Nature* 293, 471–474.
- Pantazis, A., Olcese, R., 2016. Biophysics of BK Channel Gating. *Int. Rev. Neurobiol.* 128, 1–49.
- Pawson, T., Nash, P., 2003. Assembly of cell regulatory systems through protein interaction domains. *Science* 300, 445–452.
- Pedarzani, P., Krause, M., Haug, T., Storm, J.F., Stühmer, W., 1998. Modulation of the Ca<sup>2+</sup>-activated K<sup>+</sup> current sIAHP by a phosphatase-kinase balance under basal conditions in rat CA1 pyramidal neurons. *J. Neurophysiol.* 79, 3252–3256.
- Pedarzani, P., Mosbacher, J., Rivard, A., Cingolani, L.A., Oliver, D., Stocker, M., Adelman, J.P., Fakler, B., 2001. Control of electrical activity in central neurons by modulating the gating of small conductance Ca<sup>2+</sup>-activated K<sup>+</sup> channels. *J. Biol. Chem.* 276, 9762–9769.

- Pedarzani, P., Storm, J.F., 1995a. Dopamine modulates the slow Ca(2+)-activated K<sup>+</sup> current IAHP via cyclic AMP-dependent protein kinase in hippocampal neurons. *J. Neurophysiol.* 74, 2749–2753.
- Pedarzani, P., Storm, J.F., 1995b. Protein kinase A-independent modulation of ion channels in the brain by cyclic AMP. *Proc. Natl. Acad. Sci. U.S.A.* 92, 11716–11720.
- Pedarzani, P., Storm, J.F., 1993. PKA mediates the effects of monoamine transmitters on the K<sup>+</sup> current underlying the slow spike frequency adaptation in hippocampal neurons. *Neuron* 11, 1023–1035.
- Pennefather, P., Lancaster, B., Adams, P.R., Nicoll, R.A., 1985. Two distinct Ca-dependent K currents in bullfrog sympathetic ganglion cells. *Proc. Natl. Acad. Sci. U.S.A.* 82, 3040–3044.
- Pennisi, G., Cornelius, C., Cavallaro, M.M., Salinaro, A.T., Cambria, M.T., Pennisi, M., Bella, R., Milone, P., Ventimiglia, B., Migliore, M.R., Di Renzo, L., De Lorenzo, A., Calabrese, V., 2011. Redox regulation of cellular stress response in multiple sclerosis. *Biochem. Pharmacol.* 82, 1490–1499.
- Pluznick, J.L., Sansom, S.C., 2006. BK channels in the kidney: role in K(+) secretion and localization of molecular components. *Am. J. Physiol. Renal Physiol.* 291, F517–529.
- Quirk, J.C., Reinhart, P.H., 2001. Identification of a novel tetramerization domain in large conductance K(ca) channels. *Neuron* 32, 13–23.
- Raffaelli, G., Saviane, C., Mohajerani, M.H., Pedarzani, P., Cherubini, E., 2004. BK potassium channels control transmitter release at CA3-CA3 synapses in the rat hippocampus. *J. Physiol. (Lond.)* 557, 147–157.
- Reynolds, J.N., Wu, P.H., Khanna, J.M., Carlen, P.L., 1990. Ethanol tolerance in hippocampal neurons: adaptive changes in cellular responses to ethanol measured in vitro. *J. Pharmacol. Exp. Ther.* 252, 265–271.
- Roberts, W.M., Jacobs, R.A., Hudspeth, A.J., 1990. Colocalization of ion channels involved in frequency selectivity and synaptic transmission at presynaptic active zones of hair cells. *J. Neurosci.* 10, 3664–3684.
- Rusch, N.J., 2009. BK channels in cardiovascular disease: a complex story of channel dysregulation. *American Journal of Physiology - Heart and Circulatory Physiology* 297, H1580–H1582.
- Sah, P., 1996. Ca(2+)-activated K<sup>+</sup> currents in neurones: types, physiological roles and modulation. *Trends Neurosci.* 19, 150–154.
- Sah, P., Bekkers, J.M., 1996. Apical dendritic location of slow afterhyperpolarization current in hippocampal pyramidal neurons: implications for the integration of long-term potentiation. *J. Neurosci.* 16, 4537–4542.
- Sah, P., Clements, J.D., 1999. Photolytic manipulation of [Ca<sup>2+</sup>]<sub>i</sub> reveals slow kinetics of potassium channels underlying the afterhyperpolarization in hippocampal pyramidal neurons. *J. Neurosci.* 19, 3657–3664.
- Sah, P., Faber, E.S.L., 2002. Channels underlying neuronal calcium-activated potassium currents. *Prog. Neurobiol.* 66, 345–353.

- Sah, P., Isaacson, J.S., 1995. Channels underlying the slow afterhyperpolarization in hippocampal pyramidal neurons: neurotransmitters modulate the open probability. *Neuron* 15, 435–441.
- Sah, P., McLachlan, E.M., 1992. Potassium currents contributing to action potential repolarization and the afterhyperpolarization in rat vagal motoneurons. *J. Neurophysiol.* 68, 1834–1841.
- Sah, P., McLachlan, E.M., 1991. Ca(2+)-activated K<sup>+</sup> currents underlying the afterhyperpolarization in guinea pig vagal neurons: a role for Ca(2+)-activated Ca<sup>2+</sup> release. *Neuron* 7, 257–264.
- Saito, M., Nelson, C., Salkoff, L., Lingle, C.J., 1997. A cysteine-rich domain defined by a novel exon in a slo variant in rat adrenal chromaffin cells and PC12 cells. *J. Biol. Chem.* 272, 11710–11717.
- Sanabra, C., Mengod, G., 2011. Neuroanatomical distribution and neurochemical characterization of cells expressing adenylyl cyclase isoforms in mouse and rat brain. *J. Chem. Neuroanat.* 41, 43–54.
- Schreiber, M., Yuan, A., Salkoff, L., 1999. Transplantable sites confer calcium sensitivity to BK channels. *Nat. Neurosci.* 2, 416–421.
- Schroeder, B.C., Hechenberger, M., Weinreich, F., Kubisch, C., Jentsch, T.J., 2000. KCNQ5, a novel potassium channel broadly expressed in brain, mediates M-type currents. *J. Biol. Chem.* 275, 24089–24095.
- Schwartzkroin, P.A., Prince, D.A., 1980. Effects of TEA on hippocampal neurons. *Brain Res.* 185, 169–181.
- Schwartzkroin, P.A., Stafstrom, C.E., 1980. Effects of EGTA on the calcium-activated afterhyperpolarization in hippocampal CA3 pyramidal cells. *Science* 210, 1125–1126.
- Schwindt, P.C., Spain, W.J., Crill, W.E., 1989. Long-lasting reduction of excitability by a sodium-dependent potassium current in cat neocortical neurons. *J. Neurophysiol.* 61, 233–244.
- Schwindt, P.C., Spain, W.J., Foehring, R.C., Stafstrom, C.E., Chubb, M.C., Crill, W.E., 1988. Multiple potassium conductances and their functions in neurons from cat sensorimotor cortex in vitro. *J. Neurophysiol.* 59, 424–449.
- Selyanko, A.A., Brown, D.A., 1996. Intracellular calcium directly inhibits potassium M channels in excised membrane patches from rat sympathetic neurons. *Neuron* 16, 151–162.
- Shah, M., Haylett, D.G., 2000. Ca(2+) channels involved in the generation of the slow afterhyperpolarization in cultured rat hippocampal pyramidal neurons. *J. Neurophysiol.* 83, 2554–2561.
- Shah, M.M., Javadzadeh-Tabatabaie, M., Benton, D.C.H., Ganellin, C.R., Haylett, D.G., 2006. Enhancement of hippocampal pyramidal cell excitability by the novel selective slow-afterhyperpolarization channel blocker 3-(triphenylmethylaminomethyl)pyridine (UCL2077). *Mol. Pharmacol.* 70, 1494–1502.
- Shao, L.-R., Halvorsrud, R., Borg-Graham, L., Storm, J.F., 1999. The role of BK-type Ca<sup>2+</sup>-dependent K<sup>+</sup> channels in spike broadening during repetitive firing in rat hippocampal pyramidal cells. *J Physiol* 521, 135–146.

- Shelley, C., Whitt, J.P., Montgomery, J.R., Meredith, A.L., 2013. Phosphorylation of a constitutive serine inhibits BK channel variants containing the alternate exon "SRKR." *J. Gen. Physiol.* 142, 585–598.
- Shih, M., Lin, F., Scott, J.D., Wang, H.Y., Malbon, C.C., 1999. Dynamic complexes of beta2-adrenergic receptors with protein kinases and phosphatases and the role of gravin. *J. Biol. Chem.* 274, 1588–1595.
- Shi, J., He, H.Q., Zhao, R., Duan, Y.-H., Chen, J., Chen, Y., Yang, J., Zhang, J.W., Shu, X.Q., Zheng, P., Ji, Y.H., 2008. Inhibition of martenoxin on neuronal BK channel subtype (alpha+beta4): implications for a novel interaction model. *Biophys. J.* 94, 3706–3713.
- Shipston, M.J., 2013. Regulation of large conductance calcium- and voltage-activated potassium (BK) channels by S-palmitoylation. *Biochem. Soc. Trans.* 41, 67–71.
- Shruti, S., Urban-Ciecko, J., Fitzpatrick, J.A., Brenner, R., Bruchez, M.P., Barth, A.L., 2012. The Brain-Specific Beta4 Subunit Downregulates BK Channel Cell Surface Expression. *PLOS ONE* 7, e33429.
- Siggins, G.R., Pittman, Q.J., French, E.D., 1987. Effects of ethanol on CA1 and CA3 pyramidal cells in the hippocampal slice preparation: an intracellular study. *Brain Res.* 414, 22–34.
- Silberberg, S.D., Lagrutta, A., Adelman, J.P., Magleby, K.L., 1996. Wanderlust kinetics and variable Ca(2+)-sensitivity of Drosophila, a large conductance Ca(2+)-activated K+ channel, expressed in oocytes. *Biophys. J.* 70, 2640–2651.
- Smart, T.G., 1987. Single calcium-activated potassium channels recorded from cultured rat sympathetic neurones. *J. Physiol. (Lond.)* 389, 337–360.
- Soh, H., Jung, W., Uhm, D.Y., Chung, S., 2001. Modulation of large conductance calcium-activated potassium channels from rat hippocampal neurons by glutathione. *Neurosci. Lett.* 298, 115–118.
- Soh, H., Tzingounis, A.V., 2010. The specific slow afterhyperpolarization inhibitor UCL2077 is a subtype-selective blocker of the epilepsy associated KCNQ channels. *Mol. Pharmacol.* 78, 1088–1095.
- Spigelman, I., Zhang, L., Carlen, P.L., 1992. Patch-clamp study of postnatal development of CA1 neurons in rat hippocampal slices: membrane excitability and K+ currents. *J. Neurophysiol.* 68, 55–69.
- Stangherlin, A., Zaccolo, M., 2012. Phosphodiesterases and subcellular compartmentalized cAMP signaling in the cardiovascular system. *Am. J. Physiol. Heart Circ. Physiol.* 302, H379–390.
- Stocker, M., Krause, M., Pedarzani, P., 1999. An apamin-sensitive Ca2+-activated K+ current in hippocampal pyramidal neurons. *Proc. Natl. Acad. Sci. U.S.A.* 96, 4662–4667.
- Storm, J.F., 1990. Potassium currents in hippocampal pyramidal cells. *Prog. Brain Res.* 83, 161–187.
- Storm, J.F., 1989. An after-hyperpolarization of medium duration in rat hippocampal pyramidal cells. *J. Physiol. (Lond.)* 409, 171–190.
- Strøbaek, D., Christophersen, P., Holm, N.R., Moldt, P., Ahring, P.K., Johansen, T.E., Olesen, S.P., 1996. Modulation of the Ca(2+)-dependent K+ channel, hsl $\alpha$ , by the

substituted diphenylurea NS 1608, paxilline and internal Ca<sup>2+</sup>. *Neuropharmacology* 35, 903–914.

Strøbaek, D., Jørgensen, T.D., Christophersen, P., Ahring, P.K., Olesen, S.P., 2000. Pharmacological characterization of small-conductance Ca(2+)-activated K(+) channels stably expressed in HEK 293 cells. *Br. J. Pharmacol.* 129, 991–999.

Talley, E.M., Solorzano, G., Lei, Q., Kim, D., Bayliss, D.A., 2001. Cns distribution of members of the two-pore-domain (KCNK) potassium channel family. *J. Neurosci.* 21, 7491–7505.

Tanabe, M., Gähwiler, B.H., Gerber, U., 1998. L-Type Ca<sup>2+</sup> channels mediate the slow Ca<sup>2+</sup>-dependent afterhyperpolarization current in rat CA3 pyramidal cells in vitro. *J. Neurophysiol.* 80, 2268–2273.

Tang, Q.-Y., Zeng, X.-H., Lingle, C.J., 2009. Closed-channel block of BK potassium channels by bbTBA requires partial activation. *J Gen Physiol* 134, 409–436.

Tang, X.D., Daggett, H., Hanner, M., Garcia, M.L., McManus, O.B., Brot, N., Weissbach, H., Heinemann, S.H., Hoshi, T., 2001. Oxidative regulation of large conductance calcium-activated potassium channels. *J. Gen. Physiol.* 117, 253–274.

Thomas, G., Chung, M., Cohen, C.J., 1985. A dihydropyridine (Bay k 8644) that enhances calcium currents in guinea pig and calf myocardial cells. A new type of positive inotropic agent. *Circ. Res.* 56, 87–96.

Tian, L., Duncan, R.R., Hammond, M.S., Coghill, L.S., Wen, H., Rusinova, R., Clark, A.G., Levitan, I.B., Shipston, M.J., 2001. Alternative splicing switches potassium channel sensitivity to protein phosphorylation. *J. Biol. Chem.* 276, 7717–7720.

Tombaugh, G.C., Rowe, W.B., Rose, G.M., 2005. The slow afterhyperpolarization in hippocampal CA1 neurons covaries with spatial learning ability in aged Fisher 344 rats. *J. Neurosci.* 25, 2609–2616.

Torres, G.E., Chaput, Y., Andrade, R., 1995. Cyclic AMP and protein kinase A mediate 5-hydroxytryptamine type 4 receptor regulation of calcium-activated potassium current in adult hippocampal neurons. *Mol. Pharmacol.* 47, 191–197.

Torres, Y.P., Morera, F.J., Carvacho, I., Latorre, R., 2007. A marriage of convenience: beta-subunits and voltage-dependent K<sup>+</sup> channels. *J. Biol. Chem.* 282, 24485–24489.

Turner, R.W., Kruskic, M., Teves, M., Scheidl-Yee, T., Hameed, S., Zamponi, G.W., 2015. Neuronal expression of the intermediate conductance calcium-activated potassium channel KCa3.1 in the mammalian central nervous system. *Pflugers Arch.* 467, 311–328.

Tzingounis, A.V., Heidenreich, M., Kharkovets, T., Spitzmaul, G., Jensen, H.S., Nicoll, R.A., Jentsch, T.J., 2010. The KCNQ5 potassium channel mediates a component of the afterhyperpolarization current in mouse hippocampus. *Proc. Natl. Acad. Sci. U.S.A.* 107, 10232–10237.

Tzingounis, A.V., Nicoll, R.A., 2008. Contribution of KCNQ2 and KCNQ3 to the medium and slow afterhyperpolarization currents. *Proc. Natl. Acad. Sci. U.S.A.* 105, 19974–19979.

Uebele, V.N., Lagrutta, A., Wade, T., Figueroa, D.J., Liu, Y., McKenna, E., Austin, C.P., Bennett, P.B., Swanson, R., 2000. Cloning and functional expression of two families of

- beta-subunits of the large conductance calcium-activated K<sup>+</sup> channel. *J. Biol. Chem.* 275, 23211–23218.
- Valiante, T.A., Abdul-Ghani, M.A., Carlen, P.L., Pennefather, P., 1997. Analysis of current fluctuations during after-hyperpolarization current in dentate granule neurones of the rat hippocampus. *J. Physiol. (Lond.)* 499 ( Pt 1), 121–134.
- Valverde, M.A., Rojas, P., Amigo, J., Cosmelli, D., Orio, P., Bahamonde, M.I., Mann, G.E., Vergara, C., Latorre, R., 1999. Acute activation of Maxi-K channels (hSlo) by estradiol binding to the beta subunit. *Science* 285, 1929–1931.
- Velumian, A.A., Carlen, P.L., 1999. Differential control of three after-hyperpolarizations in rat hippocampal neurones by intracellular calcium buffering. *J. Physiol. (Lond.)* 517 ( Pt 1), 201–216.
- Vergara, C., Alvarez, O., Latorre, R., 1999. Localization of the K<sup>+</sup> Lock-in and the Ba<sup>2+</sup> Binding Sites in a Voltage-Gated Calcium-Modulated Channel. *J Gen Physiol* 114, 365–376.
- Villarroel, A., Alvarez, O., Oberhauser, A., Latorre, R., 1988. Probing a Ca<sup>2+</sup>-activated K<sup>+</sup> channel with quaternary ammonium ions. *Pflügers Arch.* 413, 118–126.
- Wagner, J.A., Varga, K., Járjai, Z., Kunos, G., 1999. Mesenteric vasodilation mediated by endothelial anandamide receptors. *Hypertension* 33, 429–434.
- Wallner, M., Meera, P., Toro, L., 1999. Molecular basis of fast inactivation in voltage and Ca<sup>2+</sup>-activated K<sup>+</sup> channels: a transmembrane beta-subunit homolog. *Proc. Natl. Acad. Sci. U.S.A.* 96, 4137–4142.
- Wang, B., Rothberg, B.S., Brenner, R., 2009. Mechanism of increased BK channel activation from a channel mutation that causes epilepsy. *J. Gen. Physiol.* 133, 283–294.
- Wang, H.S., Pan, Z., Shi, W., Brown, B.S., Wymore, R.S., Cohen, I.S., Dixon, J.E., McKinnon, D., 1998. KCNQ2 and KCNQ3 potassium channel subunits: molecular correlates of the M-channel. *Science* 282, 1890–1893.
- Wang, J., Shen, B., Guo, M., Lou, X., Duan, Y., Cheng, X.P., Teng, M., Niu, L., Liu, Q., Huang, Q., Hao, Q., 2005. Blocking effect and crystal structure of natriin toxin, a cysteine-rich secretory protein from *Naja atra* venom that targets the BKCa channel. *Biochemistry* 44, 10145–10152.
- Wang, K., Mateos-Aparicio, P., Hönigsperger, C., Raghuram, V., Wu, W.W., Ridder, M.C., Sah, P., Maylie, J., Storm, J.F., Adelman, J.P., 2016. IK1 channels do not contribute to the slow afterhyperpolarization in pyramidal neurons. *eLife* 5, e11206.
- Wang, Y.-W., Ding, J.P., Xia, X.-M., Lingle, C.J., 2002. Consequences of the stoichiometry of Slo1 alpha and auxiliary beta subunits on functional properties of large-conductance Ca<sup>2+</sup>-activated K<sup>+</sup> channels. *J. Neurosci.* 22, 1550–1561.
- Wang, Z.-W., Nara, M., Wang, Y.-X., Kotlikoff, M.I., 1997. Redox Regulation of Large Conductance Ca<sup>2+</sup>-activated K<sup>+</sup> Channels in Smooth Muscle Cells. *J Gen Physiol* 110, 35–44.
- Wei, A., Solaro, C., Lingle, C., Salkoff, L., 1994. Calcium sensitivity of BK-type KCa channels determined by a separable domain. *Neuron* 13, 671–681.
- Whitt, J.P., Montgomery, J.R., Meredith, A.L., 2016. BK channel inactivation gates daytime excitability in the circadian clock. *Nat Commun* 7.

- Wickenden, A.D., Yu, W., Zou, A., Jegla, T., Wagoner, P.K., 2000. Retigabine, a novel anti-convulsant, enhances activation of KCNQ2/Q3 potassium channels. *Mol. Pharmacol.* 58, 591–600.
- Widmer, H.A., Rowe, I.C.M., Shipston, M.J., 2003. Conditional protein phosphorylation regulates BK channel activity in rat cerebellar Purkinje neurons. *J. Physiol. (Lond.)* 552, 379–391.
- Wilkins, C.M., Aldrich, R.W., 2006. State-independent block of BK channels by an intracellular quaternary ammonium. *J. Gen. Physiol.* 128, 347–364.
- Wulff, H., Miller, M.J., Hansel, W., Grissmer, S., Cahalan, M.D., Chandy, K.G., 2000. Design of a potent and selective inhibitor of the intermediate-conductance Ca<sup>2+</sup>-activated K<sup>+</sup> channel, IKCa1: a potential immunosuppressant. *Proc. Natl. Acad. Sci. U.S.A.* 97, 8151–8156.
- Xiao, R.P., Cheng, H., Zhou, Y.Y., Kuschel, M., Lakatta, E.G., 1999. Recent advances in cardiac beta(2)-adrenergic signal transduction. *Circ. Res.* 85, 1092–1100.
- Xia, X.M., Ding, J.P., Lingle, C.J., 1999. Molecular basis for the inactivation of Ca<sup>2+</sup>- and voltage-dependent BK channels in adrenal chromaffin cells and rat insulinoma tumor cells. *J. Neurosci.* 19, 5255–5264.
- Xia, X.M., Ding, J.P., Zeng, X.H., Duan, K.L., Lingle, C.J., 2000. Rectification and rapid activation at low Ca<sup>2+</sup> of Ca<sup>2+</sup>-activated, voltage-dependent BK currents: consequences of rapid inactivation by a novel beta subunit. *J. Neurosci.* 20, 4890–4903.
- Xie, J., McCobb, D.P., 1998. Control of alternative splicing of potassium channels by stress hormones. *Science* 280, 443–446.
- Yan, J., Aldrich, R.W., 2012. BK potassium channel modulation by leucine-rich repeat-containing proteins. *Proc. Natl. Acad. Sci. U.S.A.* 109, 7917–7922.
- Yan, J., Aldrich, R.W., 2010. LRRC26 auxiliary protein allows BK channel activation at resting voltage without calcium. *Nature* 466, 513–516.
- Yan, J., Olsen, J.V., Park, K.-S., Li, W., Bildl, W., Schulte, U., Aldrich, R.W., Fakler, B., Trimmer, J.S., 2008. Profiling the phospho-status of the BKCa channel alpha subunit in rat brain reveals unexpected patterns and complexity. *Mol. Cell Proteomics* 7, 2188–2198.
- Yellen, G., 1984. Ionic permeation and blockade in Ca<sup>2+</sup>-activated K<sup>+</sup> channels of bovine chromaffin cells. *J Gen Physiol* 84, 157–186.
- Yuan, P., Leonetti, M.D., Pico, A.R., Hsiung, Y., MacKinnon, R., 2010. Structure of the human BK channel Ca<sup>2+</sup>-activation apparatus at 3.0 Å resolution. *Science* 329, 182–186.
- Yu, M., Liu, S., Sun, P., Pan, H., Tian, C., Zhang, L., 2016. Peptide toxins and small-molecule blockers of BK channels. *Acta Pharmacol. Sin.* 37, 56–66.
- Zaccolo, M., 2011. Spatial control of cAMP signalling in health and disease. *Curr Opin Pharmacol* 11, 649–655.
- Zhang, L., Pennefather, P., Velumian, A., Tymianski, M., Charlton, M., Carlen, P.L., 1995. Potentiation of a slow Ca(2+)-dependent K<sup>+</sup> current by intracellular Ca<sup>2+</sup> chelators in hippocampal CA1 neurons of rat brain slices. *J. Neurophysiol.* 74, 2225–2241.

Zhang, X., Solaro, C.R., Lingle, C.J., 2001. Allosteric regulation of BK channel gating by Ca(2+) and Mg(2+) through a nonselective, low affinity divalent cation site. *J. Gen. Physiol.* 118, 607–636.

Zhang, Y., Joiner, W.J., Bhattacharjee, A., Rassendren, F., Magoski, N.S., Kaczmarek, L.K., 2004. The appearance of a protein kinase A-regulated splice isoform of slo is associated with the maturation of neurons that control reproductive behavior. *J. Biol. Chem.* 279, 52324–52330.

Zhou, M., Morais-Cabral, J.H., Mann, S., MacKinnon, R., 2001. Potassium channel receptor site for the inactivation gate and quaternary amine inhibitors. *Nature* 411, 657–661.

Zhou, Y., Lingle, C.J., 2014. Paxilline inhibits BK channels by an almost exclusively closed-channel block mechanism. *J. Gen. Physiol.* 144, 415–440.